UNIVERSITY OF SOUTHAMPTON

Numerical simulation of nonlinear random noise

Jyothika Narasimha Punekar

Doctor of Philosophy

Aeronautics and Astronautics

December 1996.

ABSTRACT

Numerical simulation of nonlinear random noise

J.N.Punekar

Department of Aeronautics & Astronautics,

University of Southampton, Southampton SO17 1BJ, U.K .

Doctor of Philosophy

Nonlinear acoustics is an important subject area in the aeronautical sciences. Two such areas are (i) the generation of the sonic boom from aircraft travelling at supersonic speeds and (ii) in the generation and propagation of noise from jet propulsion engines. The present work focusses on the problem of the propagation of plane finite amplitude sound waves which evolve from an initial random noise signal. The work is concerned with the numerical solution of Burgers equation, the standard equation of nonlinear acoustics, for the case of high Reynolds number using a new accurate numerical algorithm which we refer to as the Convolution method. The direct numerical method uses the exact solution of Burgers equation based on its reduction to standard linear diffusion equation using Cole-Hopf transformation and where the attenuation is by thermoviscous diffusion only. Comparison of the numerical solutions with known exact inviscid solutions for simple waveforms shows convergence towards the inviscid waveform in each case as the Reynolds number is increased.

The present work is also concerned with waveforms containing a fundamental wave and a superimposed second harmonic. It is shown that for such waveforms, nonlinear interaction give rise to zero crossings in the plots of change in the wavenumber spectrum with time. These zero crossings do not occur after the shock formation time.

Comparisons are also made with Lighthill's analytical model for the one-dimensional propagation of randomly spaced sawtooth shock waves in the inviscid limit. In Lighthill(1994) it was shown that the number of shocks in a long period taken from a given noise sample decreases owing to the phenomenon of 'bunching' whereby the weaker are engulfed in time by the stronger shock waves. From a numerical example Lighthill showed that the average shock strength in the assemblage of sawtoothed waves decreases as $1/\sqrt{t}$ and the same result was found in the present work for large but finite Reynolds number. The result differs from the decay of a regular constant amplitude sawtooth waves which decreases as $1/t$. The changes in time in the energy spectrum from its initial spectrum are studied, and it is shown that the high frequencies are rapidly populated due to nonlinear steepening of the wave distribution and only depopulated by viscous broadening at much later times. Due to nonlinear effects the initial Gaussian statistics are rapidly changed in time to non-Gaussian as the shocks develop from the negative velocity gradients, which increase to near infinite magnitudes compared with the small finite decrease in positive velocity gradients. The resultant changes in the spectrum between a Gaussian signal and a non-Gaussian signal are found to be large.

Acknowledgements

This work was performed at the University of Southampton in the Department of Aeronautics and Astronautics.

The author wishes to thank the Spitfire Mitchell funding for their financial support in this project.

The author would like to thank Dr.G.J.Ball for his guidance and assistance throughout the course of this work.

The author gratefully acknowledges the help of Professor G.M.Lilley and Professor C.L. Morfey for their helpful suggestions and discussions of this work.

Finally the author wishes to thank her family in India for the encouragement throughout the Phd course and her husband for his cooperation without which this work would not have been possible.

Contents

List of Tables

List of Figures

Definitions

ABM	=	Adams Bashforth Method
BE	=	Burgers equation,
CM	=	Convolution method,
CN	=	Crank Nicholson's Method
DFT	=	Discrete Fourier Transform,
FFT	=	Fast Fourier Transform,
KE	=	Kinetic energy
PDF	=	Probability distribution function,
TM	=	Taylor Microscale
TR	=	Trapezoidal rule,

Nomenclature

A	=	ray tube area
c_0	=	local speed of sound
C	=	Courant number
C_p	=	specific heat at constant pressure
C_v	=	specific heat at constant volume
e	=	specific internal energy
$\tilde{E}(k,t)$	=	energy as a function of wavenumber and time
h	=	specific enthalpy
h_s	=	specific total energy
I	=	energy flux per unit volume
$I_0,\ I_1, I_2$	=	zeroth, first and second moments respectively
k	=	thermal conductivity in chapter 2, wavenumber integer
$\tilde{k}$	=	wavenumber
k_p	=	peak wavenumber integer
k_T	=	truncation wavenumber integer
k_λ	=	Taylor microscale integer wavenumber
k_n	=	Nyquist wavenumber integer
L	=	domain length (period)
M	=	number of Fourier components upto to the Nyquist value
n_z	=	number of zero crossings in a random signal
N	=	number of points in the x space

p	=	instantaneous pressure
p'	=	fluctuating pressure
p_0	=	ambient pressure
p_{xx}	=	is the component of the longitudinal stress tensor
Pr	=	Prandtl number
$\mathbf{q}$	=	velocity vector
r	=	distance
R	=	Reynolds number, flow Reynolds number
R_L	=	Reynolds number based on the domain length
R_p	=	Reynolds number based on maximum amplitude
R_T	=	Reynolds number based on Taylor Microscale
s	=	specific entropy
t	=	propagation time
$\bar{t}$	=	non-dimensional time corresponding to t
T_i, T	=	interrupted Non-dimensional time, Non-dimensional time
t_s, T_s	=	dimensional and nondimensional shock formation time
T_a	=	asymptotic time
u	=	instantaneous velocity (particle velocity in sound wave)
u_{ref}, l_{ref}	=	reference velocity and reference length
$U, \dot{U}$	=	non-dimensional velocity and its derivative
u_{ref}	=	reference velocity
v	=	excess signal speed
W	=	acoustic energy per unit volume
x, X	=	spatial distance, Nondimensional spatial coordinate
X_k	=	complex Fourier coefficients of velocity u

β = coefficients describing nonlinear and dispersive properties

δ = effective diffusivity

δ_v = viscous diffusivity

δ_c = diffusivity due to heat conduction

δ_l = contribution from lag due to relaxation effects

ϵ = rate of dissipation

γ = ratio of specific heats for gases

λ = Taylor microscale, in chapter 3 it is the retarded time

ν = kinematic viscosity

μ = dynamic viscosity

ω = angular frequency

$\phi(\tilde{k})$ = wave energy density

ρ_0 = ambient density

ρ = instantaneous density

ρ' = fluctuating density

τ_{xx} = component of the viscous stress tensor for one dimensional flow

θ = solution of the diffusion equation

Chapter 1

1.1 Introduction

Weak disturbances in compressible fluids generate pressure fluctuations which propagate away from the source at the speed of sound. When the disturbance is of finite amplitude the propagation speed exceeds that of sound waves. This latter field of study is referred to as 'Nonlinear acoustics'. A major feature of the propagation of finite amplitude waves is their steepening and consequent distortion, and the formation of shock waves. Applications of nonlinear acoustics are present in many areas as diverse as oceanography, hydraulics, astrophysics and the atmospheric sciences. An important problem is the distortion of nonlinear sound waves in the atmosphere. Such waves are generated by explosions in the atmosphere and from supersonic aircraft. Finite amplitude sound waves are also generated in the vicinity of large jet and rocket propulsion engines. Other problems include applications in underwater acoustics and two phase fluids, but such applications are not considered in the present work. The study of nonlinear wave propagation in fluids is not a new subject. It was first treated by Euler(1755), Lagrange(1759) and Poisson(1808) but the first major advances were made by Earnshaw(1859). This was closely followed by the fundamental work of Riemann (1858). The theory of Riemann shows how non-stationary waves in one dimensional unsteady flow propagate in the x direction as two simple waves, one backwards and one forwards such that along

$$C^+ = \text{constant}, \;\; u + P = \text{constant}$$

$$C^- = \text{constant}, \;\; u - P = \text{constant}$$

where C^+ and C^- each represent one set of characteristic curves. u is the sound particle velocity, c is the local speed of sound and $P = \int dp/\rho c$ [see Lighthill(1978)]. The work of Riemann is fundamental to the work described below.

The work of Riemann and Earnshaw was shown to apply for all smooth variations in pressure and particle velocity. However Whitham(1956) has shown that beyond a given time compression waves converge and the solution becomes multivalued. The practical realisation is that a shock wave is formed with the presssure, density and velocity changing discontinuously across it. Rankine(1870) and Hugoniot(1889) derived the discontinuous changes in pressure, density and velocity across plane shock waves as well as the finite increase in entropy. Thus although continuous, and therefore smooth, variations of pressure, density, temperature and velocity generated by finite amplitude waves are isentropic it was found by Rankine and Hugoniot that discontinuous changes resulted in increases in entropy and it remained unclear as to where the energy associated with this rise in entropy was dissipated. The problem was resolved by Taylor(1909) and Rayleigh(1910) who showed that in real gases no discontinuity was possible and a continuous variation in pressure, density and velocity occured between their upstream and downstream values. However the thickness of the isolated shock wave in air at normal pressures and temperatures is so small, being a few molecular mean free paths in thickness, that the assumption of a discontinuity is a good assumption in many practical cases. For a strong shock wave the thickness is inversely proportional to the shock strength and for a shock of $\Delta p = 100\text{Pa}$ the thickness is $\approx 10^{-7}$ meters. Nevertheless an entropy rise confined to the shock does exist equivalent to the thermoviscous dissipation present within the shock wave. It is noted here that for plane waves the rise in entropy across weak shock waves is $O(\beta^3)$ where $\beta = (p_1 - p_0)/p_0$ is the strength of the shock.

The theory of nonlinear wave propagation was reformulated by Lighthill(1956), and included the Lighthill-Whitham theory for the derivation of the farfield nonlinear corrections to linear theory associated with nonlinear wave distortion. It was shown that if thermo-viscous effects were neglected the exact flow equations reduce to the Riemann equations and thus reduce to the Lighthill-Whitham theory of non-linear wave propagation. Whitham found that linear theory provides a 'good' approximation to the pressure in the far field of a disturbance but showed that the shape of the rays(characteristics) are strongly distorted by the finite amplitude of the waves. The result is the pressure is correct but is assigned to the wrong characteristic. Some aspects of the Lighthill-Whitham theory were developed independently by Landau(1945).

The fundamental equation of nonlinear wave propagation is Burgers equation, which for the nonlinear propagation of waves in the x direction in the one dimensional unsteady

flow case is

$$\frac{\partial u}{\partial t} + u\frac{\partial u}{\partial x} = \nu\frac{\partial^2 u}{\partial x^2},$$

It is known as Burgers equation but was first introduced by Bateman(1915) and later derived independently by Burgers(1951) in connection with Burgers turbulence. The inviscid form was first proposed by Landau(1945) and later independently by Lighthill(1956) and Whitham(1956). It was this theory which was first used to derive the asymptotic shock wave structure for any shape of body travelling through the atmosphere at supersonic speeds. It was also shown that to a good approximation the effects of dissipation and diffusion processes governed by viscosity and thermal conduction can be neglected in deriving the pressure signature from a supersonic aircraft and that the finite thickness of the shock wave could be ignored in many practical cases.

The name Burgers equation was given following the suggestion made by Burgers (1951) to use this equation as a simplification of the Navier-Stokes equations describing the structure of turbulence exhibiting a non-linear transfer of energy across wavenumbers. The Burgers equation is a one-dimensional unsteady quasi-parabolic partial differential equation with ν being the viscosity. In the application to finite amplitude waves, where the amplitude $|u| << c_0$, it provides the exact balance between wave steepening due to nonlinear effects and wave broadening due to thermo-viscous diffusion as well as vibrational relaxation or lag effects. In this model equation in a thermo-viscous medium, the diffusion term guarantees there are no . Its applications to the theory of non-linear acoustics was recognised by Lagerstrom et al(1949). Cole(1951) published an exact solution of the Burgers equation by using what is now known as the Cole-Hopf transformation in which he showed that any waveform in a periodic domain which can be expressed in the form of a sine series will eventually reduce to a sine wave of vanishingly small amplitude. Hopf(1951) independently, discovered this transformation, which is unique in the solutions to nonlinear partial differential equations in that it is the only nonlinear partial differential equation whose solution can be obtained from known solutions to a corresponding linear partial differential equation. Hence the problem of finite amplitude sound waves can be approached through the solution of the nonlinear Burgers equation.

The application of the Burgers equation to multiple dimensional problems in nonlinear acoustics has been covered by Lighthill, Whitham and Guiraud in the 1950's and 1960's. A summary of its application to the sonic boom problem was given by Lilley (1970) in the OECD sonic boom conference. The approximation is made that the particle sound velocity

is propagated along a ray at the local sound speed. This local sound speed is augmented by the amplitude of the sound wave which represents the fundamental change between linear and nonlinear acoustics. Thus the local wave speed $c = u + c_0$, that is it is equal to the ambient speed of sound plus a contribution from the finite amplitude of the wave. Thus when this approximation is introduced into the exact one dimensional flow equations and higher order terms are omitted and the equaations are transformed to coordinates moving with the local speed of sound, they reduce to Burgers equation. The equation in this form may be generalised for 3D waves of small curvature to the equations of geometric acoustics for nonlinear waves. In other words the geometric acoustics approximation is introduced for 3D nonplanar waves which have a similar solution to that of planar waves by accounting for the changes in the ray tube area along the ray. The theory of geometrical acoustics follows the same approximation as used in the theory of geometrical optics. In the case of waves of large radius of curvature locally it may be assumed the wave is pseudo-plane and the wavelength is vanishingly small. In this case sound is propagated along a ray in a medium at rest normal to the wavefront with the normal tracing out the path of the curvilinear ray. The theory is easily modified when the background medium is in motion provided the medium is frozen(stationary) during the passage of the wave.

In an atmosphere without winds the acoustic energy $(p - p_0)^2/\rho_0 c_0^2$ per unit volume is conserved along a ray. In other atmospheres with wind, the ray tube area is curved and the curvature of the wavefront is no longer equal to the distance travelled along the ray. Refraction bends the rays into the direction of decreasing temperature and therefore the rays are bent upwards. In such cases in estimating the magnitude and extent of the disturbances it is usual to assume an atmosphere in which the wind follows some prescribed variation with altitude and the pressure, density and temperature are all functions of altitude. In order to conserve the acoustic energy along rays the above formula is replaced by the Blokhintzev(1946) invariant

$$\frac{A_{ray}(p - p_0)^2 \left| v_{ray}^2 \right|}{\rho_0 c_0^3}$$

where A_{ray} is the ray tube area, v is the wind velocity and c_0 is the local speed of sound. Thus the energy is conserved along the ray tube and flows with the group velocity equal to the ray velocity, $\mathbf{v_{ray}}$, where $\mathbf{v_{ray}} = \mathbf{c_0 \underline{n}} + \mathbf{v}$.

Guiraud(1964) used the exact equations of motion to derive the general equation of non-linear geometrical acoustics for waves propagating along curvilinear rays in an in-

homogeneous medium. These included complex problems of the propagation of shock waves of arbitrary waveform including plane, cylindrical and spherical waves travelling along curvilinear ray paths in an inhomogenuous atmosphere with arbitrary wind. Finally Guiraud showed by a simple transformation that this equation can be reduced to the Burgers equation. His results are shown to be consistent with the work of Blokhintzev(1945), Hayes(1965) and are exactly equivalent to the work of Whitham and Lighthill discussed above. Guiraud's work would be central to an extension of the present work when extended from the properties of the planar finite amplitude waves in a uniform medium without wind, to the general case of curvilinear plane, cylindrical, and spherical waves in an inhomogenuous atmosphere with wind. More general application of solutions to Burgers equation to many nonlinear acoustic problem are given by Crighton(1979), Blackstock(1969), Rudenko and Soluyan(1977), Scott(1982) and by Gurbatov(1991). Gurbatov investigated the propagation of nonlinear random waves, which is a subject Lighthill(1993) has also recently studied in which was introduced the concept of 'bunching'. Lighthill defined 'bunching' as the phenomenon involving the overtaking of weak shocks by stronger shocks and resulting in the reduction of the number of shocks with time. 'Bunching' is a phenomenon when two waves adjacent waves coalesce or unite to form a single wave. The method of matched asymptotic expansions has been used by Crighton and Scott(1979) to derive asymptotically correct solutions to problems of nonlinear propagation in three dimensions which reduce to solutions of a generalised form of Burgers equation.

Progress in the understanding of nonlinear acoustics has been very rapid since the work of Lighthill and Whitham in the 1950's. Reviews of recent progress are given by Blackstock(1969) and Bayer(1960), Rudenko and Soluyan(1977). An extensive theoretical treatment of the problem of the nonlinear plane progressive sound waves is given by Blackstock(1962). Approximate Fourier series solutions have been derived by Blackstock(1966) for the propagation of sinusoidal piston motion. Blackstock(1964)[b] expanded the exact solution of Burgers equation into a Fourier series and obtained its coefficients numerically. Blackstock(1965) also reviewed the well known solutions of Fay(1931) and Fubini(1935) and compared these results and discussed certain properties of these solutions where he showed, in particular, how the boundary value problem, which had previously been studied, could be transformed, by interchanging time and space variables and assuming slow changes of profile into an initial value problem, which is of more immediate interest to

acousticians. In one of his papers, Blackstock(1965) showed that solutions to Burgers equation reduce to the Fubini solution in the limit as the viscosity vanishes. A Fourier series method of solving the Burgers equation to investigate the nonlinear interactions has been given by Fenlon(1971). Mendousse(1953) found pressure fluctuation solutions to the Burgers equation using Cole-Hopf transformation, while Benton(1967) and Benton and Platzmann(1972) discuss for the cases of simple initial waveforms exact analytic solutions.

The importance of using the solutions to the full Burgers equation with viscous terms retained is that for any value of the viscosity ν a continuous solution is obtained with a finite shock thickness. For very low ν, and in the limit $\nu \to 0$, the solution merge exactly with those obtained from the lossless equation ($\nu = 0$) as shown by Whitham and Lighthill(1956) where the multivalued solutions have been replaced by shocks using the 'equal area rule' described below. Thus the solution of the Burgers quasi-parabolic partial differential equation for finite ν reduces exactly to the solution of the nonlinear hyperbolic wave equation as $\nu \to 0$. Hence the nonlinear distortion of a wave can be obtained from the nonlinear inviscid equations either by analysis or directly using geometrical methods. In all these several works relating to Burgers equation it is important to note that the dissipation mechanism, provided by thermo-viscous diffusion, creates the relevant increase in entropy across finite amplitude waves as required by the exact equations of fluid mechanics and given by the Rankine Hugoniot relations. The inviscid solution of Burgers equation has applications to many problems of interest in mathematical physics but when shocks appear the finite increase in entropy can never be ignored. Roman et al(1986) discuss analytic solutions to Burgers equation in a form of Volterra's series in a continuous medium. The kernels of this series enable the probabilistic characteristics of the output signal to be determined under the condition that the input signal is known.

When an initial waveform is described as a Fourier series with known coefficients it is not a straight forward procedure to find how these coefficients change with time and distance from solutions to Burgers equation, even though this has been attempted by a number of workers. An early attempt in this direction was reported by Pernet and Payne (1971). Several theoretical contributions have since been made by Rudenko and Soluyan(1977) and co-workers, although Webster and Blackstock(1977) have commented on difficulties arising in applications of their work to practical problems. Some work on spectral distortion, which accompanies finite amplitude sound propagation, has been reported by Morfey and Howell(1981).

The early history of the analytical treatment of finite amplitude waves and solutions to Burgers equation are discussed by many authors. The history is long and will only briefly be discussed here. Comprehensive reviews in this area have been described in particular by Rayleigh (1910), Lighthill(1956), Blackstock(1969) and Pierce(1981).

The weak shock method represents a direct extension of the lossless theory of the classical era described above. In this theory the shocks which are a result of the wave distortion are treated as discontinuities separating continuous sections of the waveform. The shock propagation velocity U_s moves with a speed in the x direction which is equal to the average of the speed of the wavelets ahead of and behind it. The wave velocity $c_{1,2} = c_0 + \frac{\gamma+1}{2}u_{12}$, on either side of the shock. The shock velocity is thus

$$U_s = c_0 + \frac{\gamma+1}{4}(U_+ + U_-)$$

where $U_\pm$ are the values of the particle velocity, $u(x,t)$, on either side of the shock.

Lighthill showed that the formal procedures used in the weak shock method can be deduced as an approximation of the solution of the Burgers equation. He discussed Burgers equation as an approximation to the exact equation for plane waves in a non-relaxing thermo-viscous fluid. An important feature of the work in nonlinear acoustics is associated with wave trains comprising multiple shocks including their interactions and the effects of dissipation. Lighthill(1993), using inviscid theory, has considered how the number of shocks formed at any particular time can be calculated knowing the number of shocks at an earlier time. A certain 'bunching ' tends to arise, because a union of two adjacent shocks is found to increase the likelihood of further union with other neighbouring shocks. The models studied so far include spatial waveforms formed from a spatial assembly of periodic random 'sawtooth' waves of random amplitudes separated by expansion waves. Existing published work on this area is sparse. Further work is required and the present work, based on a numerical solution of the full Burgers equation, which was commenced in 1992, is devoted towards this end.

It is known that the finite amplitude effects continue to be present at large distances and moreover at great distances the amplitude of the wave becomes independent of the source amplitude. Crighton(1979) in his 'model' equations refers to this as amplitude saturation. The initial amplitude determines the small initial widths of the shocks according

to the Taylor thickness but at large distances viscous broadening occurs and the near discontinuities in the waveform disappear. In Cole's(1951) solution of the Burgers equation with periodic boundary conditions an asymptotic equation is given for large times and predicts that the wave amplitude becomes indepedent of the initial amplitude. At large times the fall in amplitude as a result of nonlinear effects results in the amplitude being less than would be found in the linear diffusion theory. Thus Cole(1951) finds that for any periodic wave it will eventually reduce to a sine wave at a large distance. However an arbitrary pulse of finite length eventually becomes an N wave and continues to remain an N wave of reduced amplitude indefinitely. Figure 1.1 shows the nonlinear distortion for periodic and nonperiodic wave when $\nu \to 0$. An approximate wave equation for sound propagation in an inhomogeneous fluid with arbitrary properties is given by Pierce(1990).

A study on the criteria indicating when it is possible to form a discontinuity in a plane wave in gases is given by Goldberg(1957). Formulas are derived for the absorption coefficient in the case when a discontinuity is impossible, and in the case when a discontinuity is possible. A recent paper by Cox(1994) shows how artificial neural networks can be used to model the nonlinear nature of the propagation of high level nonlinear sound.

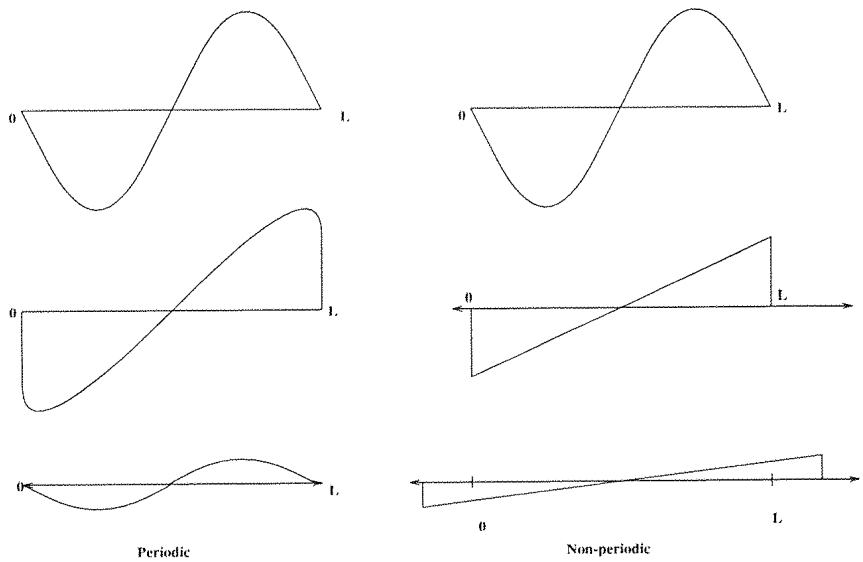

Figure 1.1: Nonlinear distortion with time for periodic and nonperiodic waves

In addition to the numerical solution to Burgers equation, which forms the bulk of the work described in this thesis, a few recent papers have covered particular aspects of the propagation process. For instance Mitome(1989) has discussed a numerical solution of

Burgers equation for the propagation of an initial sine wave which is periodic. Trivett and Van Buren(1981) have numerically treated the generalised form of Burgers equation to calculate the harmonic content in the frequency domain for plane, cylindrical and spherical waves. The non-linear energy exchange and redistribution among the harmonic modes have been investigated by Wu et al(1990) which offer a better means for detecting nonlinear propagation in a medium. From this work Wu has found an optimum periodic signal that will propagate the greatest distance without forming a shock. A finite difference method to solve the general equations of finite amplitude acoustics is used by Sparrow(1991) for simulating the propagation of spark pulses and their interactions. However the finite difference method were less accurate than the spectral methods for waveforms with sharp variations and is discussed by Basevdant et al(1986).

Many theoretical and experimental studies of nonlinear propagation of deterministic signals, such as periodic waves, N waves and sawtooth waves have been performed. Although several studies on finite amplitude noise have been made, there have been very few attempts at the prediction of the finite amplitude changes in a random initial signal with distance from the source. The waveform distortion and the generation of harmonics from finite amplitude sound propagation has been a subject of much interest to acousticians. Solutions to the Burgers equation for nonlinear random waves have recently attracted the attention of a number of authors and is the main subject of the present work.

In many practical problems, the waveform from an acoustic source is a random signal and the requirement is to find not only the changes in waveform arising from any one realization but also the statistical properties averaged over an ensemble of realizations. The properties required include the averaged pressure, its dispersion, the one and two point probability distributions, correlation functions and the power spectrum. Early work on this subject has been reviewed by Rudenko(1977). The spectral and statistical characteristics of sawtooth waves are investigated by Khokhlova et al(1990). Gurbatov(1991) gives details of certain analytical methods used in the statistical theory of nonlinear acoustics[1]. He also investigated the evolution of the high wavenumber spectrum from nonlinear propagation

[1]Gurbatov(1991) showed how solutions to a modified form of Burgers equation with the gravitational constants included could be applied to problems dealing with the distribution of stars and galaxies and a prediction of the distribution of stellar material in the universe.

of random waves. Some statistical properties of solutions to Burgers equation have been given by Jeng et al(1966). Sinai(1992) has discussed the statistics of shocks in solutions of inviscid Burgers equation using She's(1992) numerical work on the inviscid Burgers Equation with initial data of Brownian Type.

Much of the work concerned with the solutions of Burgers equation has been devoted to Burgers 'turbulence'. Although Burgers 'turbulence' is irrotational, since no one-dimensional motion can support vorticity, closeness exists between it and the turbulence derived from the Navier-Stokes equations. In fluid mechanics it is a well known fact that the Burgers equation serves as the simplest model equation of hydrodynamic turbulence. It describes the joint action of the two mechanisms, nonlinear steepening and viscous broadening and hence establishes some of the properties of real hydrodynamic turbulence. Solutions of the Burgers equations exhibit the nonlinear transfer of energy across the wavenumber spectrum with dissipation occuring in the high frequency end of the spectrum. Similarities therefore arise between the physical processes existing in the Burgers turbulence and in the nonlinear propagation of finite amplitude acoustic waves. The literature on Burgers 'turbulence' is too extensive to even single out a few definite references. A reference relevant to the present work on statistics is by Kraichnan(1990), who has given a heuristic model for the evolution of the probability distribution function obtained from Burgers turbulence. He has shown that the changes in the non-Gaussian statistics with time are obtained mainly due to the nonlinear distortion of the negative velocity gradients. This work of Kraichnan is compared with the present results obtained for nonlinear acoustics in chapter 7.

1.2 A further application of nonlinear acoustics to sonic boom

The problem of sonic boom is an important example of aeronautical nonlinear acoustics and cannot be described by linear geometric acoustics. The complete analysis can only be performed by the introduction of the theory of nonlinear acoustics. It is known that an aircraft moving through the atmosphere at supersonic speed emits disturbances in the form of compression and expansion waves which propagate away from the aircraft at the speed of sound. Nonlinear distortion of the compression waves results in a steepening of wavefronts and is referred to as convective or inertial steepening. The propagation of the

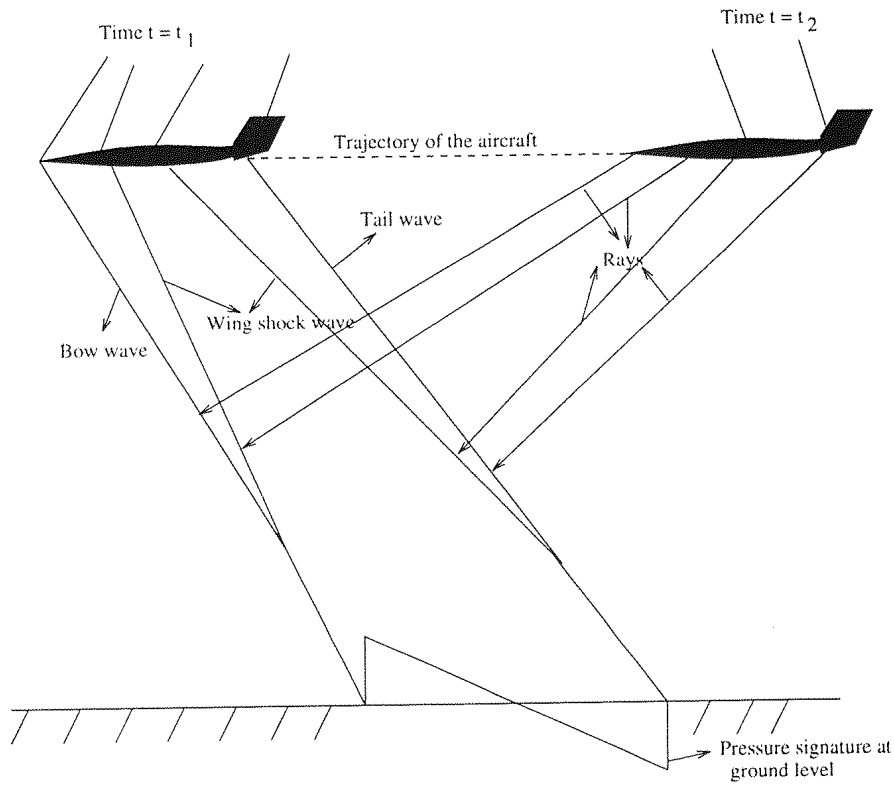

Figure 1.2: Illustration of the sonic boom problem

wave system can be described approximately by linear theory but the cumulative nonlinear effects result in a distortion of the wave signature. The wave distortion results in the generation of shock waves and the general tendency is for the signature to approach an N wave at large distances independent of the aircraft shape. The pressure disturbance it creates by this boom pressure signature near ground level results in a 'bang' or a 'boom' as heard by an observer. The figure below shows the sonic boom pressure signatures where near the aircraft the pressure signature is complex. At large distances the complex pressure signature simplifies into the characteristic far field N wave.

The pressure disturbances created by an aircraft along its flight path are propagated along ray tubes formed by the bundle of neighbouring rays. The variation in the magnitude of the pressure disturbance created can be calculated once the geometry of the rays and wave fronts have been determined. In a steady state atmosphere the ray tube area is proportional to the distance along the ray. The change in the path of a ray and its cross-sectional area, depending on the variation in the atmospheric temperature, sound speed and wind velocity with altitude, is described by Hayes(1965). He showed that for

the cylindrical waves generated by a supersonic aircraft the pressure perturbation varies inversely as the square root of the ray tube area. Figure 1.2 shows the flight path, and the rays approaching the ground eventually forming an N wave. It is shown below that the underlying theory of the sonic boom commences with the theory of nonlinear plane wave distortion, which is the central subject of the work presented below.

1.3 Research Objectives

A gap in the present status of nonlinear acoustics is the non-existence of a general numerical solution to describe the nonlinear propagation of a complex waveform. The present work was undertaken with the main objective to investigate the complete process of the propagation of complex wave propagating in a nondispersive medium at the ambient local speed of sound c_0.

The evolution of the structure of a simple wave was first undertaken in order to develop the numerical method. The simple waves investigated included the sine wave, sawtooth wave and a sine wave with superimposed harmonics. The method was then extended to the case of an assemblage of shock waves that form during nonlinear propagation from an initial complex waveform. Such a waveform soon develops a sawtooth like structure. The case was considered where at $t = 0$ the amplitude and phase of the complex waveform was random. It was then necessary to investigate the fundamental processes governing the formation of shock waves and the resulting populating of higher wavenumbers due to early application of nonlinear effects followed later by depopulating of higher wavenumbers due to viscous dissipation. Nonlinear effects result in the generation of sum and difference frequencies and give rise to higher wavenumber components whereas the effects due to dissipation result in the slow transfer of energy back into the lower wavenumbers. The information obtained from results for simple waveform then led naturally to a deeper understanding of these same processes occurring in more complex waveforms.

The change in the wavenumber spectrum for large propagation times were studied, and in particular the wavenumber interaction processes taking place in the spectral domain corresponding to the wave distortion process in the physical domain. It was therefore possible to investigate the process leading to shock formation and to the prediction of the

shock thickness in the physical domain. The dissipative mechanism present in a damped acoustic wave arising from the viscous forces and their physical interpretation was also investigated both in the spectral and space domains.

To achieve these results it was first necessary to develop an initial waveform at time $t = 0$, which had an energy spectrum, having a prescribed energy $E(k)$ in each wavenumber k, and a dissipation function, ϵ, so as to investigate the changes in spectrum with time. Thus it was possible to describe the energy transfer mechanism both in the low and high wavenumbers resulting in the sum and difference mechanisms. The waveform distortion resulting in the formation of steep gradients in the waveforms, its corresponding changes in the wavenumber part of the spectrum were some of the important physical processes investigated.

All these objectives were realised by the introduction of a new numerical method which here is referred to as, the Convolution Method. This method enables us to study the evolution of an initial complex wave signal at all times over a significant range of Reynolds numbers and especially at high Reynolds numbers.

One of the important objectives was to compare the results obtained for the complex waveform distortion at high Reynolds numbers with Lighthill's(1993) inviscid 'bunching' theory on the propagation of an assemblages of initial plane periodic sawtooth waves. Comparison with Lighthill's inviscid theory enabled a check to be made of the accuracy of the numerical method and to demonstrate as Reynolds number $R \to \infty$, that the numerical method tended to Lighthill's inviscid solution. The work undertaken here on random waves was completed before the work of Lighthill became available.

As a separate study the statistical evolution in time of a complex waveform which is initially Gaussian was investigated. The statistics of the evolving waveform including its probability distribution, the higher moments, the cumulants, and the energy spectrum have been investigated. It is shown how an initial Gaussian signal is transformed into a non-Gausssian signal as a result of nonlinear distortion. The changes resulting from the dissipation rate with time as a function of Reynolds number has been investigated. These results were compared with the results of Kraichnan's(1990) analytical work for Burgers turbulence.

A study was also undertaken to explore the differences in propagating Gaussian and non-Gaussian initial signals. This was undertaken in an attempt to explain some of the anomalies in the comparison between the experiments of Blackstock(1978) and related numerical predictiions.

1.4 Structural layout of the thesis

The thesis consists of 8 chapters. A detailed description of the derivation of the Burgers equation from the exact equations of motion in a lossless medium is given in chapter 2. The chapter also describes the effects due to absorption and the transformation to spherical and cylindrical coordinates.

Chapter 3 gives description of the various numerical methods used in solving the Burgers equation and their limitations. These include the spectral method and the Fast Fourier Transform method. Simple examples using these methods are presented, showing the waveform propagation for large times.

Chapter 4 gives a detail description of the numerical procedure used in solving the Burgers equation using the Gaussian Convolution Method. Full details of the limits of integration, the intergration method and the comparison with exact solution for the sine wave are given for various Renolds numbers. Convergence to the exact inviscid solution for high Reynolds numbers is discussed. This chapter describes how the method developed for simple waves can be generalised to deal with arbitrary initial signals.

A characteristic feature of nonlinear acoustic noise propagation is the growth in the energy of its wavenumber components and their interaction leading to the formation of discontinuities, i.e. the creation of shocks. Chapter 5 gives a step by step study of the problem by first considering the nonlinear distortion of an initial sine wave and then proceeding to cases where the initial waveform was a sine wave modified by the superposition of a number of harmonics of the fundamental. This is compared with Wu's results for the superimposed harmonic. The wave distortion by nonlinear effects at moderately high Reynolds numbers leading to the formation of near shock waves is discussed. The development of 'cusps' in the wavenumber spectral components with time arising from the zeros in the Fourier coefficients of the developing wave are discussed for varying amplitude of the harmonic superimposed on the fundamental. All these results are compared with the

exact solution for the sine wave due to Cole for finite Reynolds number.

Chapter 6 is given the full description of the process of the propagation of the random initial signal for large times both in the physical and spectral domains and their physical interpretations. The method of defining the initial spectrum is described in detail. The dissipative mechanism due to the viscous forces and its physical interpretation both in the spectral and space domain are discussed. Investigation of the statistical evolution of a wave signal with time from the initial waveform for two test cases is described. The study of the probability distribution of the field, the higher moments, the cumulants, and the energy spectrum is given. The bispectrum is presented to show how the initial Gaussian signal becomes non-Gaussian due to the nonlinear effects. The rate of dissipation, Reynolds number effects on the initial Gaussian signal with time has also been studied for several test cases. The changes in the PDF of u and $\partial u/\partial x$ of an initial Gaussian signal are compared with Kraichnan's analytic work.

Chapter 7 gives the effects of re-randomising the signal so as to understand the phase statistics of the signal with time. This method is used to explain the discrepency in Blackstock's(1978) comparison between experiments results using a computational model.

Chapter 8 gives the energy variation with time for plane waves and is compared with the energy decay law found in Lighthill's inviscid calculations for a series of periodic randomly placed sawtooths at high Reynolds number. Hence the chapter shows that the Convolution Method can give results over a wide range of Reynolds numbers, and in particular at very high Reynolds numbers where the solution approaches the inviscid limit.

Chapter 9 discusses the various aspects of the nonlinear propagation of random noise and the conclusion which can be drawn from this work. In addition some recommendations for further work and application are described.

Chapter 2

Finite Amplitude Waves and Burgers Equation

It is well-known that the equations of motion describing nonlinear sound propagation in an absorbing medium reduce to the Burgers equation. In this chapter Burgers equation is derived from the exact equations of one-dimensional fluid flow including the effects of thermo-viscous dissipation, and absorption. It is also shown that the same equation, following a transformation can represent both the propagation of plane waves(one-dimensional), cylindrical waves(two-dimensional) and spherical waves(three-dimensional) in an absorbing medium. The derivation of Burgers equation for one dimensional finite amplitude waves, starting from the exact equations of fluid motion, including the effects of viscous dissipation and heat conduction(absorption), is presented here.

All real fluids are viscous and heat conducting and when in motion the dissipative effects of friction and heat transfer are always present. In the case of fluids such as air the viscous stress and heat conduction are linear in gradients of velocity and temperature respectively. The effects of bulk viscosity are normally neglected. However the effects of absorption and relaxation are important. All these dissipative effects are discussed by Lighthill(1956) and Pierce(1981). In the work presented below it is assumed, for the purpose of simplicity, that all diffusion properties can be lumped together in a single constant diffusion coefficient. The extension of this work to deal with the exact properties of the fluid would involve a modified numerical treatment from that used below. For many problems of fluid flow in which large gradients of velocity and temperature are absent the effects of viscosity and thermal conduction can be ignored and the flow is regarded as

inviscid. However, as will be discussed below, in problems of nonlinear acoustics, which includes the generation of shock waves, the loss of energy and the corresponding increase in entropy can never be neglected, even though for many purposes the presence of the waves may be calculated to good accuracy using the inviscid approximation. (The reason underlying this anomaly is that wave properties are found from solutions to the equations of conservation of mass and momentum where the effects of diffusion are in general small and negligible. On the other hand conservation of energy demands the existence of a dissipation of mechanical energy into heat and in nonlinear acoustics this may be small but is never negligible).

When fluid flow is subjected to small variations of fluid velocity, temperature, pressure, and density, and squares and products of small disturbances are neglected. To this approximation the changes in entropy are small and may be neglected with

$$\frac{p}{\rho^{\gamma}} = \text{constant}.$$

The flow equations may be linearised about the state of the ambient fluid. The equations for these small amplitude disturbances reduce to the acoustic wave equation with the small amplitude disturbance propagating as sound waves at the local speed of sound. However Lighthill(1956) showed that thermo-viscous effects in the propagation of sound waves are never negligible and strictly the flow always remains slightly anisentropic.

Lighthill(1956) reformulated the equations for the propagation of small disturbances in ambient medium at rest when thermo-viscous diffusion and nonlinear effects are included and thus derived the basic equation for the nonlinear propagation of acoustic waves. The resulting equation when viscous terms are absent is known as the Lighthill-Whitham equation but the complete equation including viscous terms is Burgers equation.

In the following section the nonlinear unsteady partial differential equations for finite amplitude sound waves are derived from the exact equations of fluid motion including the effects of viscous dissipation and absorption. Finally Burgers equation is derived for the propagation of nonlinear random waves in a non-dispersive medium.

2.1 The exact equations of fluid flow for one-dimensional unsteady flow

The equations of continuity, momentum and energy in one-dimensional unsteady flow are

Continuity (Conservation of mass):

$$\frac{\partial \rho}{\partial t} + \frac{\partial \rho u}{\partial x} = 0 \tag{2.1}$$

Motion (Conservation of Momentum):

$$\rho \frac{\partial u}{\partial t} + \rho u \frac{\partial u}{\partial x} = -\frac{\partial p}{\partial x} + \frac{\partial \tau_{xx}}{\partial x} \tag{2.2}$$

Energy (Conservation of heat energy equation):

$$\rho \frac{Dh}{Dt} - \frac{Dp}{Dt} = \frac{\partial}{\partial x}\left(\frac{\mu}{Pr}\frac{\partial h}{\partial x}\right) + \tau_{xx}\frac{\partial u}{\partial x} \tag{2.3}$$

where the specify enthalpy $h = e + p/\rho$, e is the specific internal energy.

Total energy equation:

Adding to the heat energy equation, the equation for the kinetic energy found by multiplying equation 2.2 by u,

$$\rho \frac{Dh_s}{Dt} - \frac{\partial p}{\partial t} = \frac{\partial}{\partial x}(\frac{\mu}{Pr}\frac{\partial h}{\partial x} + \tau_{xx}u), \tag{2.4}$$

where the specific stagnation enthalpy is

$$h_s = h + \frac{1}{2}u^2$$

Here ρ, p and u are respectively the density, pressure and velocity. The Prandtl number is

$$Pr = \mu\frac{C_p}{k}$$

where μ, C_p and k are the dynamic viscosity, specific heat at constant pressure and thermal conductivity respectively. The kinematic viscosity $\nu = \mu/\rho$, τ_{xx} is the component of the viscous stress tensor for one-dimensional flow, and in a Newtonian fluid

$$\tau_{xx} = \frac{4}{3}\mu\frac{\partial u}{\partial x} \tag{2.5}$$

To the above equations must be added the equation of state which for a perfect gas is

$$p = \frac{\rho h(\gamma - 1)}{\gamma} \tag{2.6}$$

and

$$c^2 = (\frac{\partial p}{\partial \rho})_s = \frac{\gamma p}{\rho} = (\gamma - 1)h \tag{2.7}$$

is the square of the speed of sound.

Entropy (Conservation of entropy equation): The conservation of entropy equation is found from equation 2.3 for

$$\rho h \frac{D(s/C_p)}{Dt} \left(\equiv \rho \frac{Dh}{Dt} - \frac{Dp}{Dt} \right) = \frac{\partial}{\partial x} \left(\frac{\mu}{Pr} \frac{\partial h}{\partial x} \right) + \tau_{xx} \frac{\partial u}{\partial x} \tag{2.8}$$

The right hand side represents the entropy production per unit volume and s is the specific entropy. In isentropic flow the right hand side is zero and $p/\rho^\gamma = constant$.

2.2 The linearised flow equations for sound waves of small amplitudes

The linearised inviscid flow equations for sound waves of small amplitudes in a compressible inviscid ambient medium at rest are found neglecting squares and products of the small fluctuating quantities ρ', p', and u' and are :

$$\frac{\partial \rho'}{\partial t} + \frac{\rho_0 \partial u'}{\partial x} = 0 \tag{2.9}$$

$$\frac{\partial u'}{\partial t} + \frac{1}{\rho_0} \frac{\partial p'}{\partial x} = 0 \tag{2.10}$$

where ρ_0 is the ambient density. On subtracting from the time derivative of equation 2.9 the x derivative of equation 2.10 and noting $\left(\frac{\partial p}{\partial \rho}\right)_s = c_0^2$, where c_0 is the constant speed of sound, the equation becomes

$$\frac{\partial^2 p'}{\partial t^2} - \frac{c_0^2 \partial^2 p'}{\partial x^2} = 0. \tag{2.11}$$

This is the acoustic wave equation for the pressure disturbance in a medium at rest. Similar equations exist for u' and ρ'.

A sound wave of small amplitude is a longitudinal wave and generates alternatively small compressions and rarefactions in the medium through which it travels at the speed of sound. The small amplitude disturbances $p\prime$ and $\rho\prime$ relative to the constant values p_0

and ρ_0 of the ambient medium are such that $\rho' << \rho_0$ and $p' << p_0$. However, viscous and other dissipative effects are not negligible and the propagation of sound waves over large distances results in a loss of energy. The total energy in a sound wave comprises the sum of its kinetic and potential energies. It follows that the acoustic energy W, per unit volume is

$$W = \frac{1}{2}\rho_0 u'^2 + \frac{1}{2}\frac{c_0^2 \rho'^2}{\rho_0} \tag{2.12}$$

where $\rho' = p'/c_0^2$ and $u' = \rho'/\rho_0 c_0$ giving $W = \rho_0 u'^2$ since the potential and the kinetic energy contributions to W are equal. This is true for plane waves but differs for waves in general. So far the increase in entropy associated with absorption of sound energy by the diffusive medium is ignored. Lighthill(1956) showed that the absorption of sound energy or attenuation arises from

(a) viscous dissipation,

(b) heat conduction and

(c) molecular relaxation. That is, δ is effective diffusivity given by

$$\delta = \delta_v + \delta_c + \delta_l \tag{2.13}$$

where δ_v is the viscous diffusivity, δ_c is the diffusivity due to heat conduction and δ_l is the contribution from lag due to relaxation effects. When lag effects are neglected

$$\delta = \frac{\mu}{\rho_0}\left(\frac{4}{3} + \frac{\gamma - 1}{Pr}\right) \tag{2.14}$$

is the effective thermo-viscous diffusivity, as introduced by Lighthill(1956). Hence in the absence of lag effects, the energy equation for sound waves of small amplitudes is

$$\frac{\partial W}{\partial t} + \frac{\partial I}{\partial x} = -\delta\rho_0 \left(\frac{\partial u'}{\partial x}\right)^2 \tag{2.15}$$

where W is the acoustic energy per unit volume, I is the energy flux per unit volume. Lighthill argued that the linear equations for sound waves must include the viscous stress tensor τ and that the relation between pressure p and density ρ must include the non-isentropic effects in the flow. Lighthill assumed that the component of the stress tensor in the x direction is

$$p_{xx} - p_0 = (p - p_0) - \tau_{xx}$$

But $p - p_0 \approx c_0^2(\rho - \rho_0)$ and

$$\tau_{xx} \approx \rho_0 \delta \frac{\partial u}{\partial x} = -\delta \frac{\partial \rho}{\partial t}$$

Hence

$$p_{xx} - p_0 = c_0^2(\rho - \rho_0) + \delta \frac{\partial \rho}{\partial t} \tag{2.16}$$

2.3 Finite amplitude sound waves

The exact flow equations including the effects of sound attenuation are, following Lighthill (1956) :

$$\frac{\partial \rho}{\partial t} + u\frac{\partial \rho}{\partial x} + \rho\frac{\partial u}{\partial x} = 0 \tag{2.17}$$

$$\rho\frac{\partial u}{\partial t} + \rho u\frac{\partial u}{\partial x} = -\frac{\partial p_{xx}}{\partial x} \tag{2.18}$$

and using equation 2.16 for p_{xx} it is found

$$\frac{\partial u}{\partial t} + u\frac{\partial u}{\partial x} + \frac{c\partial}{\partial x}\int\frac{dp}{\rho c} = \frac{\partial \tau_{xx}}{\rho \partial x} \tag{2.19}$$

where

$$\tau_{xx} = \delta\rho\frac{\partial u}{\partial x}. \tag{2.20}$$

For locally isentropic flow

$$P = \int\frac{dp}{\rho c} = \int\frac{c}{\rho}d\rho \tag{2.21}$$

it is found

$$\frac{\partial u}{\partial t} + u\frac{\partial u}{\partial x} + c\frac{\partial P}{\partial x} = \delta\frac{\partial^2 u}{\partial x^2} \tag{2.22}$$

With P defined by equation 2.21 from equation 2.17 it is found

$$\frac{\partial P}{\partial t} + u\frac{\partial P}{\partial x} + c\frac{\partial u}{\partial x} = 0 \tag{2.23}$$

For the case of isentropic flow equation 2.22 can be written as

$$\frac{\partial u}{\partial t} + u\frac{\partial u}{\partial x} + c\frac{\partial P}{\partial x} = 0 \tag{2.24}$$

and combining equations 2.23 and 2.24 the equations in characteristic form can be derived with the $+$ and $-$ signs representing C^+ and C^- waves respectively giving

$$\frac{\partial(u \pm P)}{\partial t} + (u \pm c)\frac{\partial(u \pm P)}{\partial x} = 0 \tag{2.25}$$

Equation 2.25 is the exact non-linear inviscid equation for plane waves and has a simple physical interpretation in the usual $x - t$ diagram as presented by Lighthill(1978).

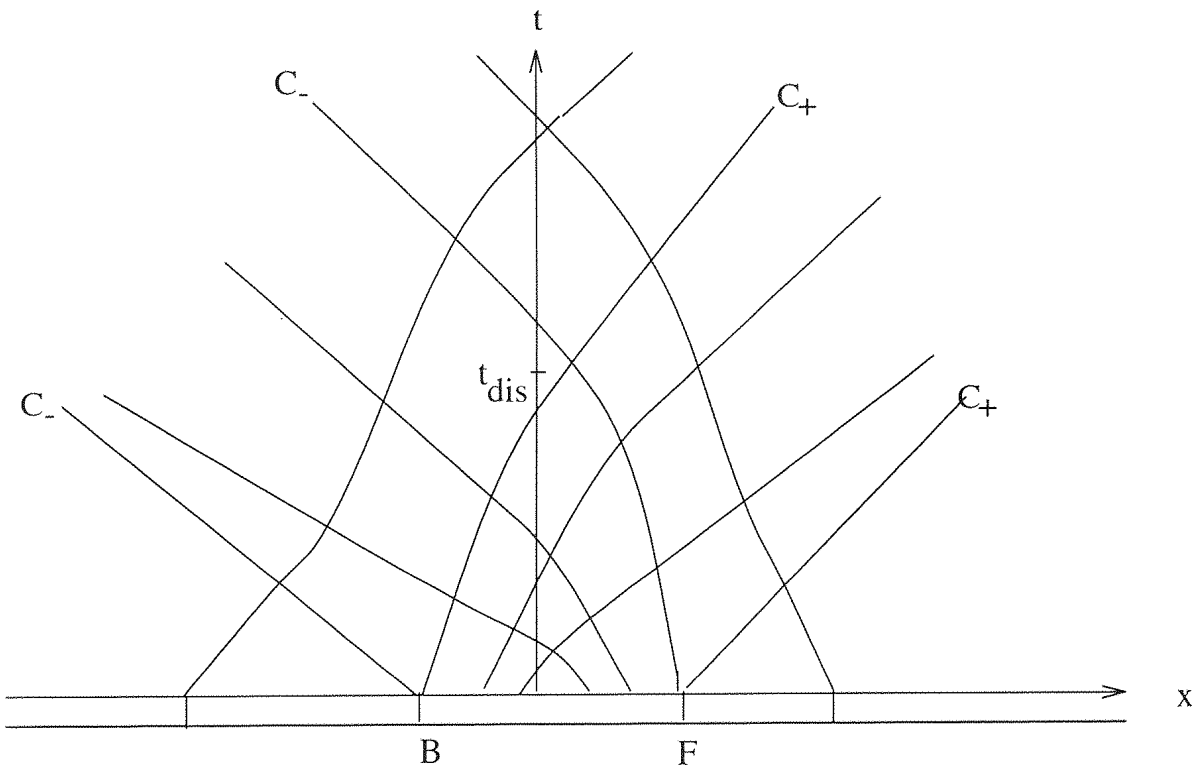

Figure 2.1: Characteristic curves in the $x - t$ plane [after Lighthill(1978)].

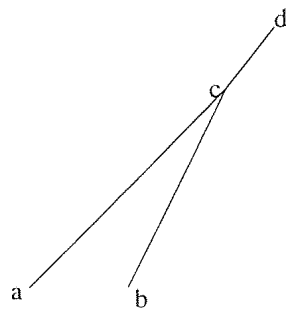

Figure 2.2: Converging characteristics with cd to be the bisector

2.4 One-dimensional Wave theory

In the one-dimensional theory of simple waves the characteristics C^+ and C^- are defined respectively by :

$$\frac{dx}{dt} = (u + c) \quad \text{along} \quad C^+ \tag{2.26}$$

$$\frac{dx}{dt} = (u - c) \quad \text{along} \quad C^- \tag{2.27}$$

where C^+ is the forward propagating wave and C^- is the backward propagating wave and c is the local speed of sound. Equations 2.26 and 2.27 may be called the fundamental relations concerning propagation of simple waves. Along these characteristics

$$u + P = J^+ \quad \text{constant along} \quad C^+$$

$$u - P = J^- \quad \text{constant along} \quad C^-$$

Figure 2.1 shows the characteristic curves in the $x - t$ plane. Along each characteristic u is constant. Hence from the distribution of the characteristics at any time the corresponding change in velocity can be found from its value at $t = 0$. If at $t = 0$ the initial distribution has regions of u increasing and then decreasing as shown in figure 2.1, then the characteristics diverge and converge. In the regions of convergence adjacent characteristics intersect and form one characteristic.

When characteristics intersect and differences in slopes are small, the new characteristic is at an angle bisecting the original converging characteristics. If u changes continuously from a to b then ac (see figure 2.2)will not be a straight characteristic but curved. However in finite difference approximations the curved characteristics are replaced by straight line segments between adjacent intersections.

After integrating equation 2.21 yields

$$P = \frac{2(c - c_0)}{\gamma - 1} \tag{2.28}$$

In a frame of reference moving at the speed c_0, the undisturbed sound speed, the excess signal speed for the C^+ wave is $v = u + c - c_0$, with the space coordinate $X = x - c_0 t$. Thus

$$\left(\frac{\partial}{\partial t}\right)_x = \left(\frac{\partial}{\partial t}\right)_X \left(\frac{\partial t}{\partial t}\right)_x + \left(\frac{\partial}{\partial X}\right)_t \left(\frac{\partial X}{\partial t}\right)_x \tag{2.29}$$

giving

$$\left(\frac{\partial}{\partial t}\right)_x = \left(\frac{\partial}{\partial t}\right)_X - c_0 \left(\frac{\partial}{\partial X}\right)_t \tag{2.30}$$

and

$$\left(\frac{\partial}{\partial x}\right)_t = \left(\frac{\partial}{\partial t}\right)_X \left(\frac{\partial t}{\partial x}\right)_t + \left(\frac{\partial}{\partial X}\right)_t \left(\frac{\partial X}{\partial x}\right)_t \tag{2.31}$$

or

$$\left(\frac{\partial}{\partial x}\right)_t = \left(\frac{\partial}{\partial X}\right)_t \tag{2.32}$$

Hence in a frame of reference moving with speed c_0 it is found

$$\frac{Dv}{Dt} = \frac{\partial v}{\partial t} + \frac{dX}{dt}\frac{\partial v}{\partial X} = 0 \tag{2.33}$$

since $\frac{D}{Dt} \equiv \frac{\partial}{\partial t} + \frac{dX}{dt}\frac{\partial}{\partial X}$. But $\frac{dX}{dt} = v$. Thus the distortion of a simple wave with time can be found from the graph of v against X. $v(x,t)$ is a constant along characteristic line C^+ satisfying $\frac{dX}{dt} = v$. Thus the hyperbolic equation

$$\frac{\partial v}{\partial t} + v\frac{\partial v}{\partial X} = 0 \tag{2.34}$$

Along any characteristic in (t, X) plane

$$\frac{dv}{dt} = \frac{\partial v}{\partial t} + \left(\frac{dX}{dt}\right)\frac{\partial v}{\partial X} = 0 \tag{2.35}$$

Differentiating the above equation with respect to X on a characteristic yields

$$\frac{\partial^2 v}{\partial t \partial X} + \left(\frac{\partial v}{\partial X}\right)^2 + v\frac{\partial^2 v}{\partial X^2} = 0 \tag{2.36}$$

Dividing through out by $(\partial v/\partial X)^2$, and writing $v_X = \frac{\partial v}{\partial X}$,

$$\frac{\partial v_X/\partial t}{v_X^2} + 1 + \frac{v\partial v_X}{v_X^2 \partial X} = 0 \tag{2.37}$$

and therefore

$$\left(\frac{\partial}{\partial t} + v\frac{\partial}{\partial X}\right)\left(\frac{1}{(\partial v/\partial X)}\right) = 1 \tag{2.38}$$

or

$$\frac{D}{Dt}\left(\frac{1}{v_X}\right) = 1 \tag{2.39}$$

Thus on integration

$$\left(\frac{1}{v_X}\right) - \left(\frac{1}{v_X}\right)_0 = \Delta t \tag{2.40}$$

showing that after some finite time an infinite slope v_X will result. This first happens for a given waveform after a time

$$t_0 = \text{Min}\left|\frac{-1}{(\partial v/\partial X)_0}\right| \tag{2.41}$$

Thus in the case of a compressible sine wave where $v = \sin(\pi X)$ the maximum value of $\frac{\partial v}{\partial X}$ is $-\pi$ at time $t = 0$. Thus a shock wave appears after a time $t_0 = 1/\pi$.

2.5 Transformation to the Burgers equation

For a finite amplitude disturbance the propagation speed is

$$c = c_0 + \frac{\gamma - 1}{2} u \tag{2.42}$$

when $|u/c| << 1$. Hence from equation 2.34

$$\frac{\partial u}{\partial t} + \left(\frac{(\gamma + 1)}{2} u\right) \frac{\partial u}{\partial X} = 0 \tag{2.43}$$

This is the fundamental equation for the particle speed in nonlinear acoustics. When the flow is viscous, it is found a similar equation with the viscous term on the right hand side of equation 2.34. This gives

$$\frac{\partial u}{\partial t} + \left(\frac{(\gamma + 1)}{2} u\right) \frac{\partial u}{\partial X} = \frac{\delta}{2} \frac{\partial^2 u}{\partial X^2} \tag{2.44}$$

where δ is the effective viscosity (see equation 2.14). Equation 2.44, following Lighthill (1956), shows the competition between the effects of nonlinear steepening and the diffusive broadening. Thus on introducing $v = \frac{(\gamma+1)u}{2}$ equation 2.44 reduces to the Burgers equation

$$\frac{\partial v}{\partial t} + v \frac{\partial v}{\partial X} = \frac{\delta}{2} \frac{\partial^2 v}{\partial X^2} \tag{2.45}$$

In many problems of nonlinear acoustics, such as boundary value problems it is convenient to transform Burgers equation defined in equation 2.45 into (z, T) coordinates where $X = x - c_0 t$, $z = c_0 t$ and $T = -X/c_0$. Hence $-c_0 T = x - z$ or $T = (z - x)/c_0$ where T is the retarded time.

Substituting $u(z, T) = u(X, t)$ in equation 2.44

$$\frac{\partial u}{\partial z} - \frac{u}{c_0^2} \frac{(\gamma + 1)}{2} \frac{\partial u}{\partial T} = \frac{\delta}{2c_0^3} \frac{\partial^2 u}{\partial T^2} \tag{2.46}$$

where $c_0 T$ is a length (m), and δ has units m^2/sec.

But $p' = \rho_0 c_0 u'$ and since $u = u'$ then

$$\frac{\partial p'}{\partial z} - \beta p' \frac{\partial p'}{\partial T} = \mu \frac{\partial^2 p'}{\partial T^2} \tag{2.47}$$

which is the corresponding equation for the pressure analogous to equation 2.45 which is the equation for the perturbation velocity. The propagation of intense acoustic waves has been described by Gurbatov et al using equation 2.47, where $\beta = (\gamma + 1)/2\rho_0 c_0^3$ and

$\mu = \delta/2c_0^3$ are coefficients describing the nonlinear and dispersive properties of the medium respectively.

If finally by putting $z = c_0\tau$, $c_0 T = -\xi$, $c_0^3\mu = \nu^*$ and $u^* = c_0^3\beta p'/c_0$, then on substitution into equation 2.47

$$\frac{\partial u^*}{\partial \tau} + u^*\frac{\partial u^*}{\partial \xi} = \nu^*\frac{\partial^2 u^*}{\partial \xi^2} \tag{2.48}$$

which is our Burgers equation. Equation 2.48 can be nondimensionalized by putting

$$\bar{u} = u^*/u_{ref}, \qquad \bar{\xi} = \xi/l$$

$$R = u_{ref}l/\nu, \qquad \bar{t} = tu_{ref}/l$$

where l is the characteristic length. Then

$$\frac{\partial \bar{u}}{\partial \bar{t}} + \bar{u}\frac{\partial \bar{u}}{\partial \bar{\xi}} = \frac{1}{R}\frac{\partial^2 \bar{u}}{\partial \bar{\xi}^2} \tag{2.49}$$

which is the nondimensional Burgers equation in terms of a non-dimensional particle velocity and is equivalent to the nondimensional form of equation 2.45.

2.6 Burgers Equation as an initial value problem

The quasilinear parabolic nonlinear partial differential equation known as Burgers equation in its dimensional form is normally written as

$$\frac{\partial u}{\partial t} + u\frac{\partial u}{\partial x} = \nu\frac{\partial^2 u}{\partial x^2} \tag{2.50}$$

The first term describes the time rate of change of the sound particle velocity in a frame moving at the wave speed, while the second term describes its nonlinear distortion [1]. The third term represents linear diffusion mechanisms which include attenuation, dispersion and relaxation by replacing ν by its more general form $\delta/2$, described in equation 2.45. In one dimensional unsteady flow Burgers equation is also an equation for unsteady irrotational flow where $u = \partial\phi/\partial x$ is finite. Since it is an equation in u only there is no need for an additional equation of continuity. The pressure is absent from this equation.

[1] In applications to acoustics solutions to Burgers equation, given in the form of equation 2.50, it should be noted that the sound particle velocity is $2u/(\gamma+1)$ and the effective viscosity, ν is $\delta/2$

2.6.1 Cole-Hopf Transformation

The Cole-Hopf transformation(1951) reduces the nonlinear Burgers equation to the linear diffusion equation. The transformation is valid only for one-dimensional propagation. If $u(x,t)$ is the solution to Burgers equation for given initial conditions then it may be obtained from the corresponding solution to the linear diffusion equation by using the Cole-Hopf transformation(1951) in one-dimension as follows:

$$u(x,t) = \frac{-2\nu\partial\theta/\partial x}{\theta} \tag{2.51}$$

where $\theta(x,t)$ is the solution of the linear diffusion equation,

$$\frac{\partial\theta}{\partial t} = \nu\frac{\partial^2\theta}{\partial x^2}. \tag{2.52}$$

Thus $u(x,t)$ is the solution of the Burgers equation for given initial conditions. If $u(x,0) = u_0(x)$ is its initial value, then the initial value

$$\theta_0 = \theta(x,0) = \exp(-\frac{1}{2\nu}\int_0^x u_0(\xi)d\xi) \tag{2.53}$$

which gives the value of $\theta_0(0) = 1$. It should be noted that u_0 may be positive or negative but θ_0 is a positive function only and similarly $\theta(x,t)$ is a positive function.

2.6.2 Exact Solution of the Burgers equation

For an initial wave in the domain $0 \leq x \leq l$, $u(x,0) = u_0(x) = \sin(x/l)$, at $t = 0$.
An exact solution for this $u_0(x)$ was found by Cole (1951) for periodic boundary conditions with $u(0,t) = u(l,t) = 0$ for all t. The exact solution due to Cole is

$$u(x,t) = \frac{4\nu\pi\sum_{n=1}^{\infty} n\exp(-\nu n^2\pi^2 t/l^2)nI_n(u_0 l/2\pi\nu)\sin(n\pi x/l)}{I_0(u_0 l/2\pi\nu) + 2\sum_{n=1}^{\infty}\exp(-\nu n^2\pi^2 t/l^2)I_n(u_0 l/2\pi\nu)\cos(n\pi x/l)} \tag{2.54}$$

where $I_n's$ are the Bessel functions. Equation 2.54 reduces to the velocity distribution u_0 at time $t = 0$. Thus for small times $u(x,t)$ is dependent on the initial distribution, u_0. However at larger times $u(x,t)$ becomes independent of u_0. The solution reduces to a simpler form for such times which are also large compared with the shock formation time.

$$u(x,t) = -\frac{2\nu\pi}{l}\sum_{n=1}^{\infty}\frac{(-)^n\sin(n\pi x/l)}{\sinh\nu(n\pi^2 t/l^2)} \tag{2.55}$$

The equation 2.55 can be used to obtain the spectra at all large times. It is independent of the initial amplitude and the spectrum damps exponentially with the first power of

the wavenumber for large n. For small n, such that $\nu n^2 t/l^2 << 1$ Cole shows that the coefficients depend on $1/n$. For large times the solution, becomes independent of the Bessel functions which involve the initial value u_0. Hence at large times the solution depends universally on its local time. Thus the solution for large time predicts the wave amplitude becomes independent of its initial amplitude. There are a number of other exact solutions to Burgers equation each being a solution for a given $u_0(x)$ (see footnote [2]). All solutions demonstrate the balance between the competing effects of nonlinear steepening and viscous broadening for all time $t > 0$ and for all $Re > 0$.

2.6.3 Exact Solution of the diffusion equation

The solution of the diffusion equation 2.52 for a given distribution in $\theta_0(x)$, corresponding to $u_0(x)$, is given by Carslaw(1941) in the form

$$\theta(x,t) = \frac{1}{2\pi}\int_{-\infty}^{\infty}\left(\exp(ikx - k^2\nu t)\int_{-\infty}^{\infty}\exp(-ik\xi)\theta_0(\xi)d\xi\right)dk \tag{2.56}$$

The details of this solution is given in Appendix B.

2.6.4 Shock formation time

From the method of characteristics as discussed above in section 2.4 the shock formation time for the inviscid Burgers equation is given by the minimum value of the derivative of u at time $t = 0$ as obtained in equation 2.41 above.

$$T_s = \left|-\frac{1}{(\partial u/\partial x)_{\min}}\right| \tag{2.57}$$

where T_s is the shock formation time.

2.7 Burgers equation as a boundary value problem

In other applications in nonlinear acoustics, where the the boundary value problem is used, u is prescribed as a function of t at some location and with the waveform evolving as a function (X,t). For these problems with distance X and retarded time $\tau = t - x/c_0$ as independent variables, the following equation, first used by Mendousse (1953) for nonlinear acoustics is obtained

$$\frac{\partial u}{\partial X} - \frac{\beta}{c_0^2}u\frac{\partial u}{\partial \tau} = \frac{\delta_0}{2c_0^2}\frac{\partial^2 u}{\partial \tau^2} \tag{2.58}$$

[2]See Benton's solution in reference (1967)

2.8 The 3-dimensional Burgers equation

The one-dimensional Burgers equation described above (equation 2.48) can be generalised to three dimensions by changing the velocity $u(X,t)$ to the vector velocity $\mathbf{q}(X,t)$. The 3D Burgers equation is then

$$\frac{\partial \mathbf{q}}{\partial t} + \mathbf{q}\nabla.\mathbf{q} = \nu\nabla^2\mathbf{q} \tag{2.59}$$

which is an approximation to the Navier-Stokes equation in which the pressure is omitted. The Cole- Hopf transformation is

$$\mathbf{q} = -2\nu\nabla(\log\theta) \tag{2.60}$$

where θ is the solution of the diffusion equation

$$\theta_t = \nu\nabla^2\theta \tag{2.61}$$

Equation 2.60 is thus a solution to equation 2.59. The Cole's solution for the above equation is only valid when $\mathbf{q}$ is irrotational. However for acoustic waves the vorticity is zero and this condition is satisfied.

2.9 Generalised Burgers equation

It is possible to extend the derivation of Burgers equation to cover other one-dimensional progressive waves. For progressive waves with cylindrical or spherical symmetry a generalised Burgers equation has been derived by Blackstock(1964) (a). This is

$$\frac{\partial u}{\partial x} + \frac{ju}{2x} - u\frac{\partial u}{\partial t} = \nu\frac{\partial^2 u}{\partial t^2} \tag{2.62}$$

In equation 2.62 the integer j is determined by the number of dimensions in which the wave can spread. $j = 0, 1, 2$ refers to plane, cylindrical and spherical spreading. The assumption introduced by Blackstock is similar to the farfield approximation made by Lighthill(1956) and requires that changes related to linear geometrical spreading effects should be slow on a wavelength scale.

2.10 Transformation to non-planar waves

In case of atmospheric propagation, the finite amplitude wave undergoes spherical and cylindrical spreading with time in a ray tube which results in the change in the wave

intensity. The wave shape is amplitude dependent and hence non-linear effects will be reduced earlier along the ray path. To solve this numerically the integration along a ray is no more difficult than integrating along a plane wave ray tube. The absorption is defined as a known function of the propagation distance along the ray and again would not add greatly to the time of computation. Over short distances the absorbtion coefficient can be assumed constant. Over long distances however the appropriate absorption correction as a function of distance should be applied. The sound ray velocity in linear acoustics is $\mathbf{w} + e_1 c_0$, where $\mathbf{w}$ is wind velocity, c_0 is the ambient speed of sound and e_1 is the unit vector normal to the wavefront. Figure 2.3 shows a curvilinear ray. An elemental distance along its path s is ds, and the wavefront of the wave distribution is at a position at $t = \Lambda$, say. The distortion of the wave distribution relative to the wavefront from from $t = 0$ to $t = \Lambda$ can be studied.

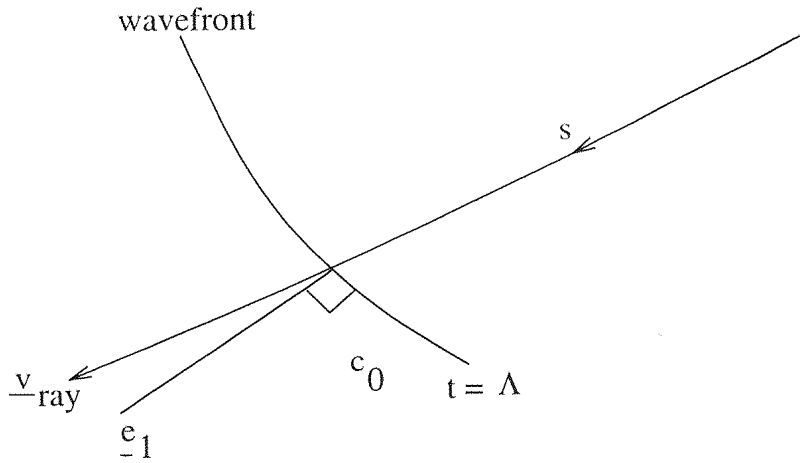

Figure 2.3: Sound ray with a wavefront

To a good approximation the position of the wavefront can be found by linear acoustics, where $\mathbf{v_{ray}} = \mathbf{w} + \mathbf{e_1} c_0$, $\mathbf{v_{ray}}$ is the velocity along the curvilinear ray.

In many problems the ray is a straight line as in a homogeneous atmosphere without wind. In plane wave propagation our coordinates are such that $v_1(x_1, t)$ can be plotted and assume the wave structure is periodic and is the same for all 'periods' of length L. Here x_1 has its origin a distance L behind the wavefront.

The properties of this complex waveform at $t = 0$ as shown in figure 2.4 and the subsequent times are dependent on the amplitude and phase distribution and the number of zero crossings. With increase in time beyond the shock formation time the number of zero crossings decrease as a result of nonlinear distortion.

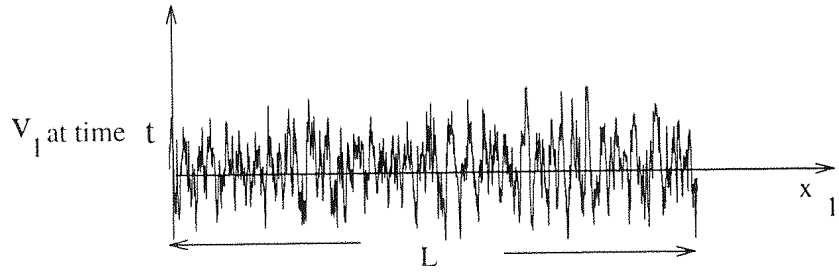

Figure 2.4: Initial signal with period L.

It can be shown, following Guiraud(1964), that the exact nonlinear acoustic wave equations for the sound particle velocity along a ray at time $t = \Lambda$ in a coordinate frame at the local speed of sound reduce to the Burgers equation(and where $t = \Lambda$ corresponds to the position of the wavefront as shown in figure 2.3). The fundamental nonlinear ray acoustic equation for the particle sound velocity as a function of time along the ray $t = \Lambda$ and moving coordinate x_1 (at the ray velocity along the ray) is

$$\frac{\partial v_1}{\partial \Lambda} + \frac{\gamma+1}{2} v_1 \frac{\partial v_1}{\partial x_1} = -\frac{v_1}{2}\left\{ K c_0 + \frac{\partial \ln \rho_0 c_0}{\partial \Lambda} + r\nabla.\mathbf{w} + e_1.\nabla\mathbf{w}.e_1 \right\} + \frac{\delta}{2}\nabla^2 v_1 \qquad (2.63)$$

where following Guiraud (1964),

$$A = \exp\left\{ \frac{1}{2}\int_0^{\Lambda} \left(K c_0 + \frac{\partial \ln \rho_0 c_0}{\partial \Lambda'} + r\nabla.\mathbf{w} + e_1.\nabla\mathbf{w}.e_1 \right) d\Lambda' \right\} \qquad (2.64)$$

For the plane wave case equation 2.63 reduces to Burgers equation as given in equation 2.50. There is a factor $1/2$ in the definition of A, the effective ray tube area and it is

	$K(r)$
Plane	0
Cylindrical	r
Spherical	r^2

Table 2.1: The curvature as a function of r for planar and nonplanar waves

defined without the $1/2$ as used by many authors (see Pierce (1981). In an inhomogeneous atmosphere without wind where $s \approx r$ all quantities in equation 2.64 for the effective ray tube area, A, are functions of time along the ray. K is twice the average curvature of the wavefront at time $\Lambda = t$. σ is the curvilinear coordinate through the centre of the ray tube. In the case of spherical wave propagation and zero wind velocity the direction normal

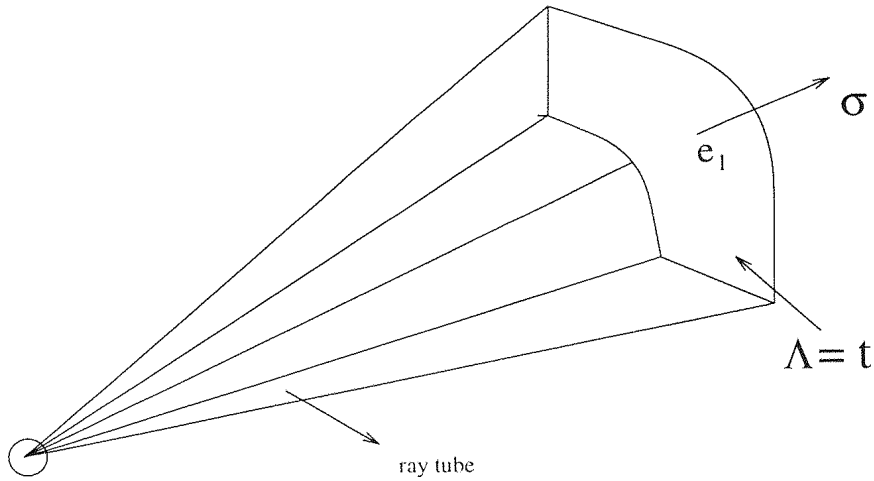

Figure 2.5: Spherical wave propagation

to the wave front coincides with the ray direction as shown in figure 2.5. In Guiraud's notation equation 2.63 reduces to

$$\frac{\partial v_1}{\partial \Lambda} + \frac{\gamma+1}{2} v_1 \frac{\partial v_1}{\partial x_1} + v_1 \frac{\partial \ln A}{\partial \Lambda} = \frac{\delta}{2} \nabla^2 v_1 \tag{2.65}$$

is true for multidimensional problems in nonlinear ray acoustics. A and δ are assumed functions of time (distance) along the ray only and are independent of x_1. Thus the equivalent plane wave problem is with $W = v_1 A$, which is the effective particle velocity,

$$\frac{\partial W}{\partial \lambda} + W \frac{\partial W}{\partial X_1} = \nu_e \nabla^2 W \tag{2.66}$$

where

$$\nu_e = \frac{2\delta A}{\gamma+1}$$

is the effective kinematic viscosity, and

$$\lambda = \int^{\Lambda} \frac{\gamma+1}{2A} d\Lambda'$$

is an age variable and A is the ray tube area function which is a function of the age variable Λ. A depends on the properties of the atmosphere and not on the amplitude of the sound waves. The equivalent distance for plane waves is then

$$x_1 = \sigma - (c_0 + \mathbf{w}.\mathbf{e_1})\, t \tag{2.67}$$

Equation 2.66 presents an equivalent plane wave problem with λ the ' age variable', the distance along the ray, and needs to be calculated from the given distribution of A along the ray tube. In other words K is found to be a function of r (or Λ) for the given wave

(ray) geometry from geometrical linear acoustics, and ν_e varies with Λ. In most cases this effect can be ignored and usually can be replaced by some average value. Thus equations 2.66 and therefore 2.65 can be solved for given initial conditions of $W(x_1, \lambda = 0)$, at $t = 0$ or from some reference time $t = t_1$, where $v_1(x, t_1)$ and $A(t_1)$ are known. Normally the law $A(t)/A(t_1)$ will be known from linear acoustics. Thus when $W(x_1, \lambda)$ is found by solving Burgers equation it can be found $v_1(x_1, t)$ from $W(x_1, \lambda)/A(\lambda)$ where

$$t = \Lambda = \int^{\lambda} \frac{2}{\gamma + 1} A(\xi) d\xi \tag{2.68}$$

Thus the one dimensional solution for $W(x_1, \lambda)$ can give the three dimensional solution $v_1(x_1, t)$ as a function of x_1 and is unchanged provided the wave distortion is located at the correct (transformed) time t corresponding to λ.

Equation 2.66 was first derived by Guiraud (1964), and is a generalised form of the Burgers equation. It is a generalised form of the theory of Lighthill and Whitham. For practical problems the solution of equation 2.66 must be performed numerically. The solution is simplified when following Lighthill(1956) it is assumed a 'good' approximation is found by considering the shocks to be discontinuous and that dissipation only occurs at the shocks. Another approach is to assume the shock to approximately steady over a short distance and hence replace the discontinuity by the continuous function described by Nalaugol'nykh, Soluyan and Khokhlov (1963). However, these methods fail at great distances, when considering the asymptotic solutions to the equation 2.66.

2.11 Conclusion

This Chapter has shown the importance of Burgers equation in modelling nonlinear acoustics. It has been derived from the exact flow equation for a thermo-viscous medium. One-dimensional simple wave theory has been described as the basis for the derivation of Burgers equation. The equation is derived for both as an initial value problem and a boundary value (pressure equation) problem. A key aspect is the time for shock formation and this has been derived for the one-dimensional case. The exact solution of Burgers equation using the Cole-Hopf transformation for an initial sine wave is described. Guiraud's generalised equation for plane, cylindrical and spherical waves is derived together with the inclusion of the effects on sound propagation due to the presence of wind. Even in these complex cases it is shown that the generalised equation for the effective sound particle velocity along a ray reduces to Burgers equation by a simple transforma-

tion. Thus in all these various cases the Cole-Hopf transformation can be used to find the solution in physical space by solving the corresponding linear diffusion problem. In a later section it will be shown that this approach leads to solutions of the physical problem of high accuracy and is superior to the standard numerical approaches of solving Burgers equation directly.

Chapter 3

Numerical Methods

It was shown in chapter 2 that the fundamental equation of nonlinear acoustics, the Burgers equation, has few analytic solutions. The need is therefore to develop a robust numerical method to find solutions to Burgers equation for an arbitrary specified complex waveform at some initial time. In this chapter numerical solutions to Burgers equation are presented to study the distortion processes of simple waveforms. This was necessary since it would give an idea of a complex wave consisting of all such wave geometries.

The problem to be investigated involves a periodic waveform in which the amplitude and phase(velocity) distribution are specified at $t = 0$ where the wavelength equals L. For validation purposes the numerical solutions are compared with known solutions obtained by other workers. The first approach considers the case when the function $u = 0$ at $t = 0$ is expanded in terms of an infinite sequence, or a truncated series from $-N \leq k \leq N$ where N is large.

$$u = \sum_{k=-\infty}^{\infty} \phi(k) \exp(ikx)$$

The method discussed use periodic functions expanded as Fourier series. Corresponding methods for nonperiodic functions are not discussed. The convergence of a truncated Fourier series limits the accuracy of any method which uses the Fast Fourier transform.

Two methods are presented here and are based on the Fourier series expansion. They are the Spectral Method and the Fast Fourier transform method (FFT). The Spectral Method solves the nonlinear Burgers equation by time marching in the spectral domain. Thus the nonlinear term and the linear diffusion term are solved in the spectral domain. The FFT method uses the Cole-Hopf transformation and solves the linear diffusion equa-

tion in the spectral domain. Thus the spectral method solves for $u(x,t)$ in the spectral domain which is the solution of the BE and the FFT method solves for $\theta(x,t)$ in the spectral domain which is the solution of the diffusion equation. The advantages and disadvantages of these methods, when compared with each other, are described. Examples of numerical solutions using these methods are presented and the limitations of each method and their accuracy are discussed. The computations was performed on a Sun Sparc Workstation and the algorithm were written in Fortran. In all the cases presented, periodic boundary conditions are employed.

Spectral methods use the truncated Fourier series expansion which is known to converge rapidly for smooth variations in the dependent variable. Although this method has already been used extensively, it was considered necessary to investigate its advantages and disadvantages when compared with the FFT method. First of all the Spectral Method to solve Burgers equation is described for an initial sine wave since other numerical and analytical results are available, and a detailed comparison was therefore possible.

3.1 Spectral Method

In the present numerical work the spectral method is used to obtain the solution of the nonlinear Burgers equation in the spectral domain. Thus the spectral method will have to deal with discontinuities since it has to compute the nonlinear term as well as the viscous term of the Burgers equation in the spectral domain.

It is well known that spectral methods applied to problems with smooth solutions offer an excellent rate of convergence upto the shock formation time as shown by Canuto et al(1987). The accuracy depends on the Fourier coefficients, which involve Bessel functions J_n. These have asymptotic properties which converge. Hence any truncated Fourier series such as

$$u(x,t) = \sum_{k=-N/2}^{N/2} a_k(t) e^{ikx}$$

converges faster than any finite power of 1/N. In other words the convergence of the spectral method for smooth solutions is more rapid than any finite power of $1/N$. In most practical applications the benefit of the spectral method is not the great accuracy for large values of N but rather the small size of N necessary for a moderately accurate

solution. However it is known that the Spectral Method loses accuracy near discontinuities and therefore it was necessary to investigate how the Spectral Method compared with other schemes such as the Finite Difference Method. The Finite Difference method was introduced by Basevdant et al(1986) and was adopted to solve Burgers equation.

Basevdant et al(1986) also developed a Fourier spectral method for solving Burgers equation in the spectral domain. The results obtained below using the spectral method were compared with the results obtained by Basevdant et al(1986) using both the Finite Difference methods and the Fourier Spectral method. The nonlinear terms are solved using third order Adams-Bashforth method and the implicit second order Crank-Nicholson method is used to solve the linear diffusion term. A pseudo-spectral scheme is used to evaluate the nonlinear term in which the differential, $\partial u/\partial x$, is derived in wavenumber space whereas the multiplication of u and $\partial u/\partial x$ is carried out in the physical domain as proposed by Canuto et al(1987). The Fourier coefficients are obtained using the Fast Fourier Transform . The Fast Fourier transform is a recursive algorithm for evaluating the discrete transform and its inverse. It is defined in Appendix A. Thus the method is spectral in $\bar{u}$, which is the solution of the Burgers equation.

3.1.1 Numerical scheme

In this section the discretization of the Burgers equation is discussed. The nondimensional Burgers equation is

$$\frac{\partial u}{\partial t} + u\frac{\partial u}{\partial x} = \nu\frac{\partial^2 u}{\partial x^2} \tag{3.1}$$

To avoid confusion, introduce

$$\bar{u} = u/U, \qquad \bar{x} = x/L, \qquad \bar{t} = tU/L, \qquad R = UL/\nu$$

where U is the maximum amplitude of the wave and L is the domain length. so that equation 3.1 becomes

$$\frac{\partial \bar{u}}{\partial \bar{t}} + \bar{u}\frac{\partial \bar{u}}{\partial \bar{x}} = \frac{1}{R}\frac{\partial^2 \bar{u}}{\partial \bar{x}^2} \tag{3.2}$$

where $\bar{u}(\bar{x}, \bar{t})$ is the velocity and R_L is the Reynolds number based on the sample length L and the maximum amplitude U of the wave. $\bar{u}$ is periodic in $\bar{x}$, with period $0 \leq \bar{x} \leq 1$. The initial wave distribution $\bar{u}(0, \bar{x}) = \sin(2\pi\bar{x})$ was specified. The solution of equation 3.2 is found using a truncated Fourier series. N is the number of spatial points which

describes the $\bar{x}$ domain. The number of spatial points is 2^N as is required by the FFT Method. The time step $\Delta\bar{t}$, is selected according to the stability conditions, which will be discussed below. The first forward time step uses the Euler method. The second and all other time steps use the second order Adam-Bashforth scheme for the convective term and the second order Crank-Nicholson scheme for the linear diffusion term. Details of the Spectral Method are given in Appendix A. In this method differentiation is performed in the spectral domain, and consists of multiplying each Fourier coefficient by $(-i)$ times the corresponding wavenumber. Thus the first derivative $\partial\bar{u}/\partial\bar{x}$ is carried out in the spectral space as

$$\left(\frac{\partial\tilde{u}}{\partial\bar{x}}\right)_k = -ik\tilde{u}_k \tag{3.3}$$

and the second derivative which is required later for the evaluation of the diffusion term is

$$\left(\frac{\partial^2\tilde{u}}{\partial\bar{x}^2}\right)_k = k^2\tilde{u}_k \tag{3.4}$$

when an inverse transform is performed the derivative in equation 3.3 becomes $\partial\bar{u}/\partial\bar{x}$. Multiplication of the nonlinear term, $\bar{u}\partial\bar{u}/\partial\bar{x}$ is carried out in the physical domain.

3.1.2 Stability Criteria

The stability of the numerical method concerns the growth of errors at every time step. In other words any difference scheme must not allow errors to grow indefinitely, that is amplified without bound when progressed from one time step to another. Thus it is important to chose the time step and the space step such that the error E_n^i involved between the computed solution, v_n^i and its exact solution, u_n^i, is bounded. This is expressed mathematically as

$$E_i = u_n^i - v_n^i$$

with

$$\lim E_n^i \leq K \quad \text{at fixed} \quad \Delta t$$

where the suffixes i and n are points of time and space respectively.

It is known that the scheme of discretisation of a differential equation is based on the CFL number and is described below. The stability requirement for the discretized time

and space steps for the explicit method depend on the CFL number

$$C = \frac{a\Delta t}{\Delta x} \leq \frac{1}{2} \tag{3.5}$$

where C is called the Courant- Friedrichs- Levy (CFL), stability criterion and is fully described by Hirsh(1986) where Δt is the time step and Δx is the space step. The CFL criterion is based on the linearised Burgers equation with the nonlinear term being replaced by $a\partial u/\partial x$, where a is a constant characteristic velocity. In the present case a is given by its maximum value equal to unity and so

$$C = \frac{\Delta t}{\Delta x} \leq \frac{1}{2}$$

This condition has to be satisfied for all time and space coordinates for the explicit third order Adams-Bashforth method. The time step for the implicit second order Crank-Nicholson scheme is adjusted according to the explicit scheme. The explicit method is conditionally stable when $C \leq 1/2$. Hence there is a restriction on Δt to be small. The implicit method does not impose restrictions on the time step Δt as it is unconditionally stable as shown by Sod (1985). This does not mean that Δt can be chosen arbitrarily large since the CFL condition must be maintained. Hence in Burgers equation, absolute stability can be obtained depending on the stability limit of the convective term only.

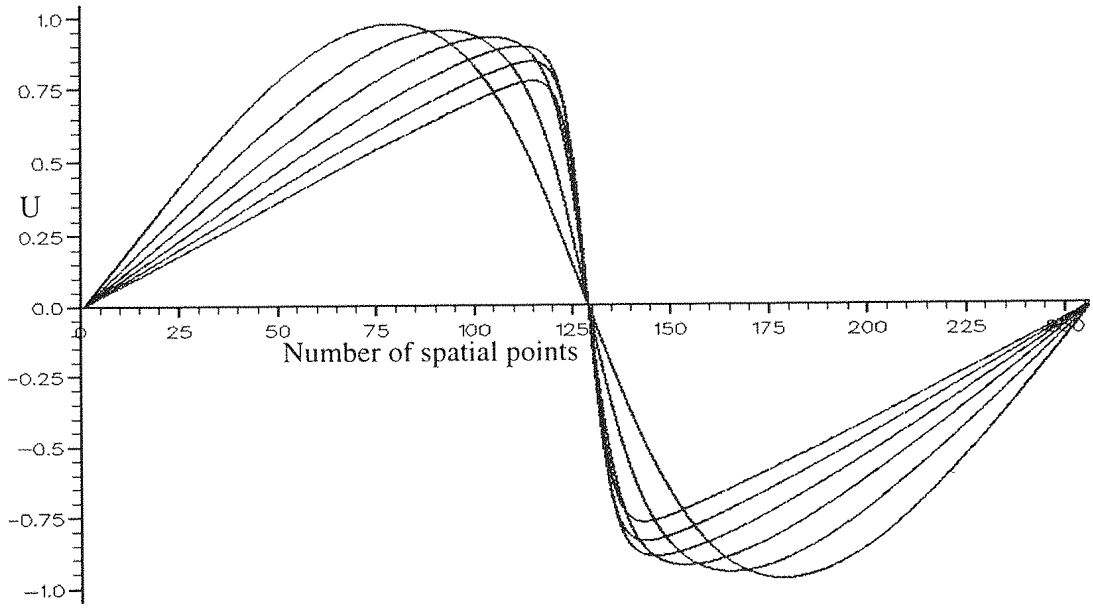

Figure 3.1: Nonlinear distortion for the periodic sine wave using Spectral method for $\bar{t} = 0, .375, .75, 1.12, 1.5$. Number of points is N = 256 and $R_L = 100$.

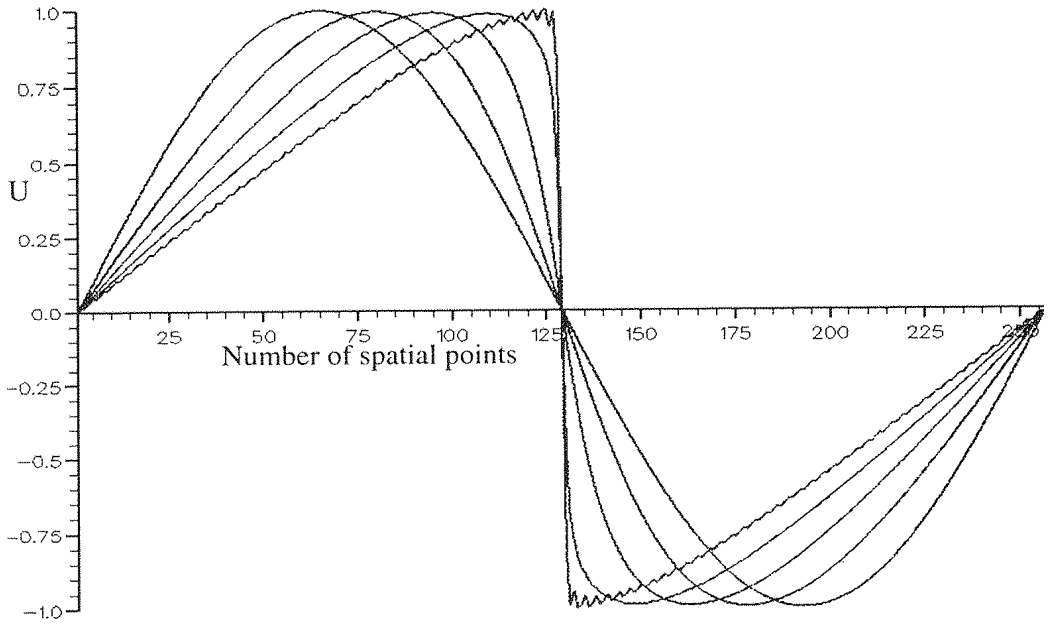

Figure 3.2: Nonlinear distortion of initial periodic sine wave using the Spectral method. $\bar{t} = 0, .375, .75, 1.12, 1.5$ $R_L = 200$.

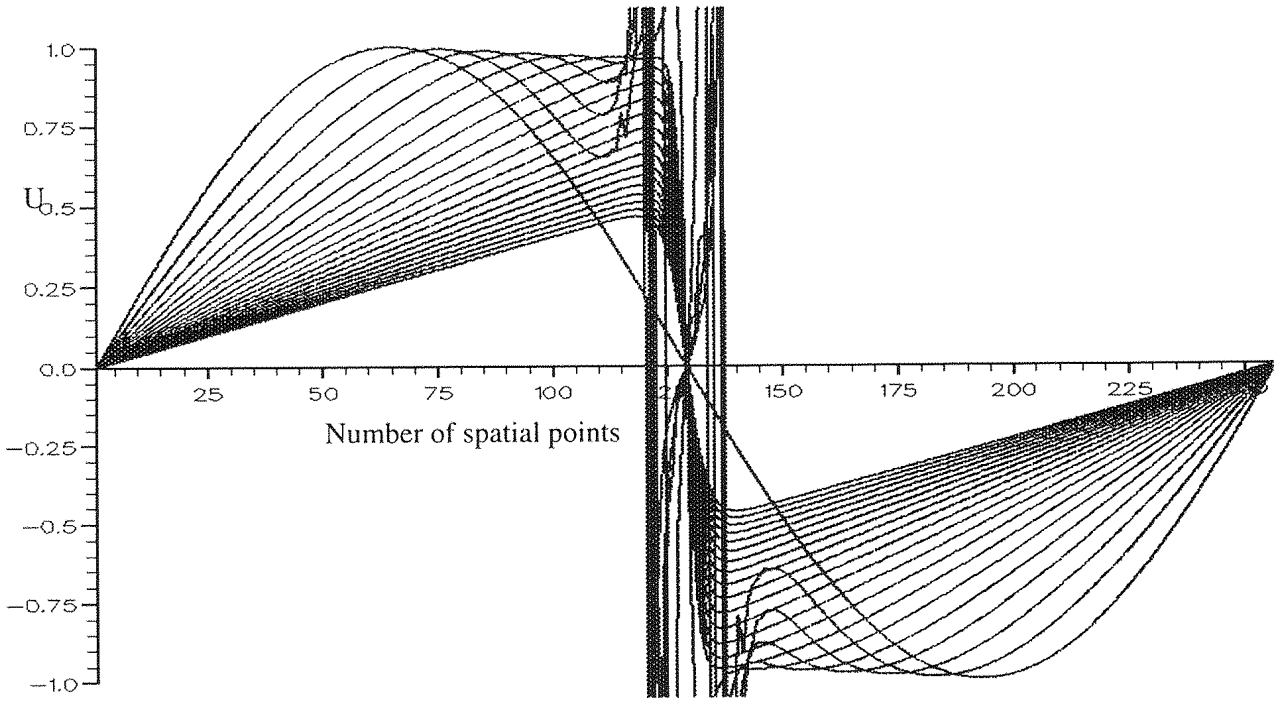

Figure 3.3: Nonlinear distortion of initial periodic sine wave using the Spectral method Curves are for $\bar{t} = 0, 0.2, 0.4, 0.6, 0.8, 1.0$. Number of spatial points is N= 512. $R_L = 220$.

3.2 Results

Results were obtained for 3 different Reynolds numbers of 100, 200 and 220 shown in figures 3.1, 3.2 and 3.3 respectively. It is seen in figures 3.2 and 3.3 that the method gives spurious oscillations at the time when the distortion in U approaches a discontinuity. It is seen there are spurious oscillations in the solution which are the result of Gibbs phenomenon. These oscillations arise due to the nonlinear term of the Burgers equation when solved in the spectral domain. This produces a characteristic oscillatory behaviour of a truncated Fourier series in the neighbourhood of a discontinuity as shown by Canuto(1987). The distortion of the velocity profile at the time when the discontinuity occurs cannot be resolved by the spectral method. The Spectral method does not possess an exponential convergence which is due to errors created by replacing u with a truncated Fourier series. The rate of convergence depends upon how fast the Fourier coefficients of U decay to zero shown by Canuto(1987). The exponential convergence is lost when u is not smooth and when its derivatives are not correctly evaluated in any region where new discontinuities in u exist. The difficulties experienced in the case of $R_L = 200$ and $R_L = 220$ are removed for a low Reynolds number of $R_L = 100$.

Hence for a low value of the Reynolds number of $R_L = 100$, the spectral method is shown to give smooth results. It is seen that the sine wave steepens and forms a near sawtooth wave. The finite thickness of the shock wave observed around the shock formation time is due to viscous broadening. At large times than shown in figure 3.1 viscous effects take over asymptotically reducing the near sawtooth to a sine wave of small amplitude.

The energy wavenumber spectrum at different times for the sine wave with $R_L = 100$ are shown in figure 3.4. k is the integer wavenumber and k_0 is the fundamental integer wavenumber equal to unity. It is seen that after the shock formation time the decay at sufficiently high wavenumbers is $1/t^2$. This is the result obtained from Cole's solution at moderately high Reynolds number. It is seen that the spectrum which initially was discrete rapidly extends to higher wavenumbers. It is difficult to study the processes of viscous dissipation and the energy transfer between modes, because the number of Fourier modes is limited. Analytically, as shown by Cole (1951), the amplitude of the Fourier coefficients are shown to decay exponentially as t increases.

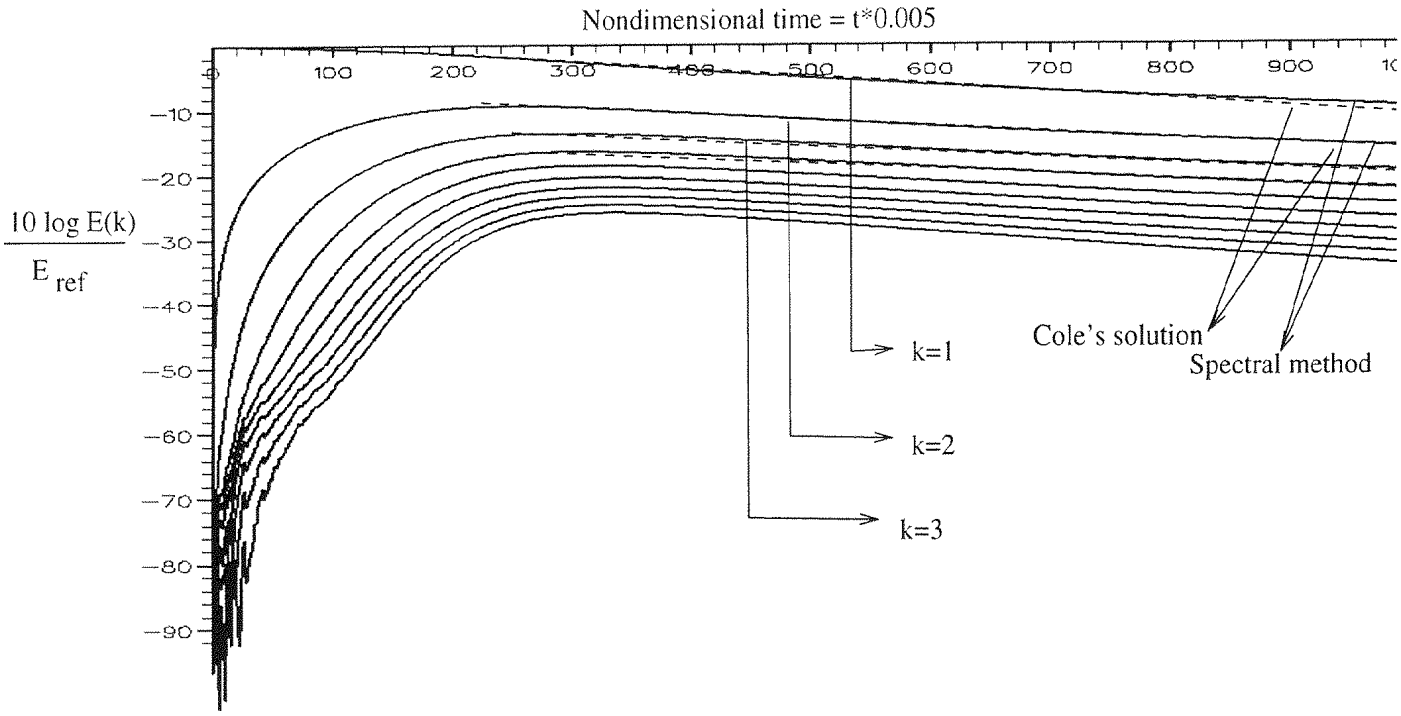

Figure 3.4: Change in spectral energy coefficients (k) with time for initial periodic sine wave. $k = 1, 2, 3....$ and $R_L = 100$. E_{ref} is the energy in the fundamental at $t = 0$. Dashed line's are Cole's(1951) asymptotic solutions for various k's for $t > T_s$, T_s is the shock formation time.

3.3 Conclusions

The spectral method solves the nonlinear Burgers equation in the spectral domain in which a discontinuity arises. The method cannot deal with the discontinuity and results in the Gibbs phenomena in the spectral domain which is a characteristic oscillatory behaviour in the neighbourhood of a discontinuity. From this numerical study it is shown that spectral methods are unable to compute near discontinuities in the field as required for large Reynolds numbers. Such difficulties are not present for low Reynolds numbers where the wave approaches a near sawtooth, which is rounded off due to the low value of R_L. It was found that the spectral method gives an acceptable accuracy upto the discontinuity for both inviscid and viscous solutions. When the velocity profile contains sharp variations the spectral method fails due to the spurious oscillations resulting from Gibbs phenomena. It was concluded that the spectral method is unsatisfactory for calculating the nonlinear distortion of a simple wave for large Reynolds numbers and hence could not be used for a more complex wave containing a broad band spectrum. Even though satisfactory results were obtained in the viscous case when the Reynolds number was moderate ($R_L = 100$) further exploratory tests showed the spectral method could not be used for large R_L beyond the shock formation time.

3.4 Fast Fourier Transform Method

It was shown above that the Spectral method could not resolve discontinuities for the periodic sine waveforms since the method solves for u which is the solution of the nonlinear Burgers equation in which a discontinuity arises. This discontinuity cannot be dealt with by the spectral method in the spectral domain. The method fails when a singularity occurs, ie when $|\partial u/\partial x| \rightarrow \infty$ which is a condition when $R_L \rightarrow \infty$. Once it had been established that the 'Spectral Method ', even when R is moderately high, could not give satisfactory results for the wave distortion beyond the 'shock' formation time, attention was turned to the solution of Burgers equation using the Cole-Hopf transformation and solving for the linear diffusion equation in the spectral domain. Hence there is no discontunuity arising in the spectral domain since the solution of the diffusion equation is smoothly varying and decays with time. In this case the initial conditions for $u(x) = u_0$ at $t = 0$ were transformed to $\theta(x) = \theta_0$ where θ satisfied the parabolic diffusion equation

$$\frac{\partial \theta}{\partial t} = \nu \frac{\partial^2 \theta}{\partial x^2} \tag{3.6}$$

The accuracy of this method depended on finding an accurate numerical solution for the linear diffusion equation. The method is thus spectral in $\theta(x,t)$ for all times. This method was also used by Mellen(1986) to solve initial wave distributions of simple geometry. However in the results presented below it is shown that they were restricted to low Reynolds numbers and for higher Reynolds numbers the use of the Fast Fourier transform caused spurious oscillations.

The method was shown to give improved results for the initial sine wave as compared with those obtained using spectral methods. The method was developed for periodic initial distributions only.

3.4.1 Numerical method

The discretised equations for the FFT method are given in Appendix C. Following the evaluation of $\theta(x,t)$ at a particular time step, $d\theta(x,t)/dx$ can be evaluated in the spectral domain described in section 3.4.3. The Cole-Hopf transformation is then used to find $u(x,t)$, the solution to Burgers equation, for the given initial distribution $u_0(x)$. The FFT method is spectral in θ, which is the solution of the diffusion equation.

3.4.2 Initial conditions

In the work on the spectral method as described above Burgers equation was used in its non-dimensional form given in equation 3.2. Again U is the maximum amplitude of the wave, L is the domain length and R_L is the Reynolds number.

The initial conditions were chosen as follows: The domain is $0 \leq \bar{x} \leq 1$, (periodic). The initial wave distribution $\bar{u}(0, \bar{x}) = \sin(2\pi\bar{x})$, was specified. The initial distribution of θ was given by [see equation 2.53 in chapter 2],

$$\theta(\bar{x}, 0) = \theta_0(\bar{x}) = \exp\left(-\frac{R}{2}\int_0^{\bar{x}} u_0(\xi)d\xi\right) \tag{3.7}$$

The evaluation of $d\theta/d\bar{x}$ is described below.

3.4.3 Evaluation of $d\theta/d\bar{x}$ and $d^2\theta/d\bar{x}^2$

In the FFT method both the initial values θ_0 and $d\theta_0/d\bar{x}$ are necessary to compute the solution of the diffusion equation at any time $\bar{t}$. The problem then arises in evaluating $d\theta_0(\bar{x})/d\bar{x}$. The two ways of calculating $d\theta_0(\bar{x})/d\bar{x}$ are

(i) In the spectral domain as

$$\left(\frac{\partial\tilde{\theta}_0}{\partial\bar{x}}\right)_k = -ik\tilde{\theta}_0(k) \tag{3.8}$$

$$\left(\frac{\partial^2\tilde{\theta}_0}{\partial\bar{x}^2}\right)_k = -k^2\tilde{\theta}_0(k) \tag{3.9}$$

where $\tilde{\theta}_0(k)$ is the Fourier transform of θ_0. It is this value of $\tilde{\theta}_0(k)$ that is used in time marching Crank Nicholson method to solve the diffusion equation. The method used is described in Appendix C.

(ii) The second way is to calculate it analytically by differentiating equation 3.7 so that

$$\frac{d\theta_0(\bar{x})}{d\bar{x}} = -\exp\left(-\frac{R}{2}\int_0^{\bar{x}} u_0(\xi)d\xi\right)\left(\frac{R}{2}\right)\frac{d}{d\bar{x}}\left(\int_0^{\bar{x}} u_0(\xi')d\xi'\right) \tag{3.10}$$

Once $d\theta_0(\bar{x})/d\bar{x}$ is known a forward transform is made and $(\frac{\partial^2\tilde{\theta}_0(k)}{\partial x^2})_k$ is found as given in equation 3.9 to solve the diffusion equation.

The first method, where $d\theta_0(\bar{x})/d\bar{x}$ is evaluated in the spectral domain causes aliasing errors. It is similar to evaluating the value of du/dx in the spectral domain used in spectral methods and fails for the same reason given above.

The second method is an improvement over the the first and has been used by Mellen. It

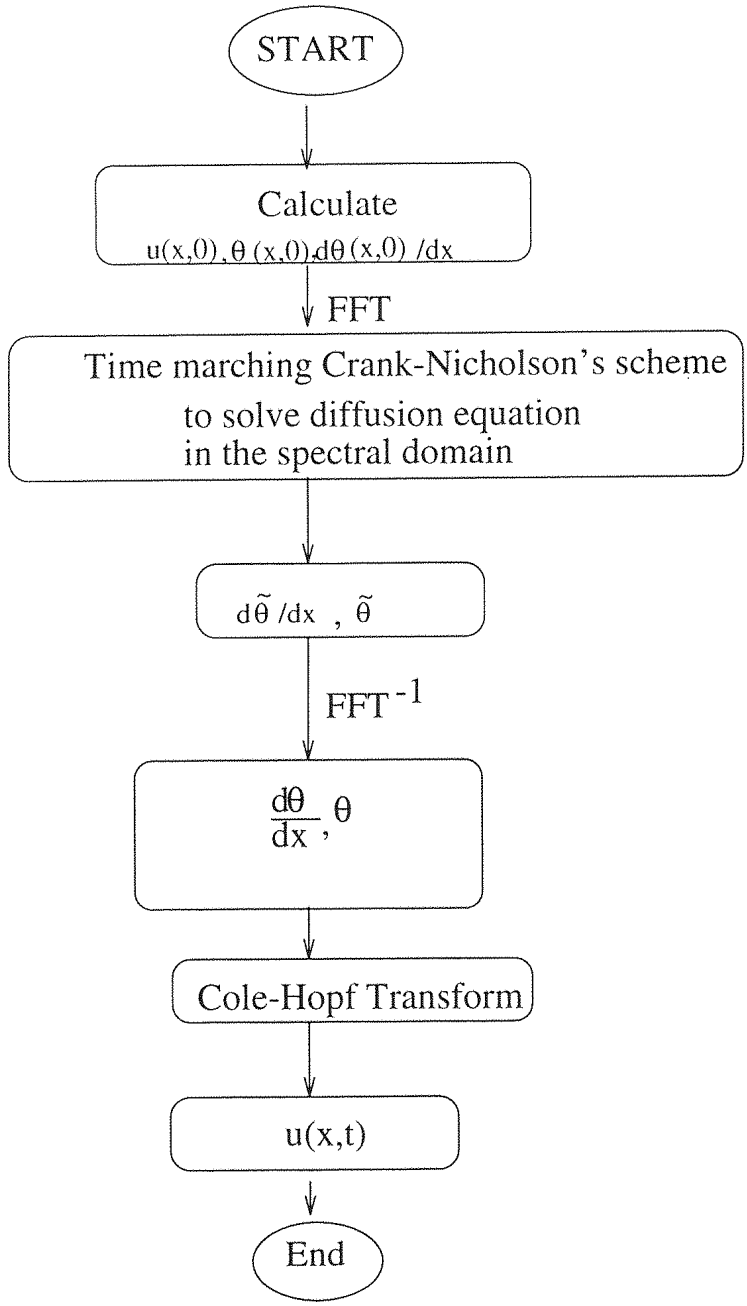

Figure 3.5: Algorithm for the FFT method

does not involve an FFT, but involves calculating the exponentials for large values of the argument and so imposing restrictions on the computer. Thus when the Reynolds number is increased, the exponential terms get very large and the computer cannot resolve the large exponentials involved.

However this problem was easily overcome by expressing $d\theta_0(\bar{x})/d\bar{x}$ as follows

$$\frac{d\theta_0(\bar{x})}{d\bar{x}} = -\frac{R}{2}u_0(\bar{x})\theta_0(\bar{x}) \tag{3.11}$$

This does not involve any exponential terms since it is a straight forward multiplication of $u_0(\bar{x})$ and $\theta_0(\bar{x})$.

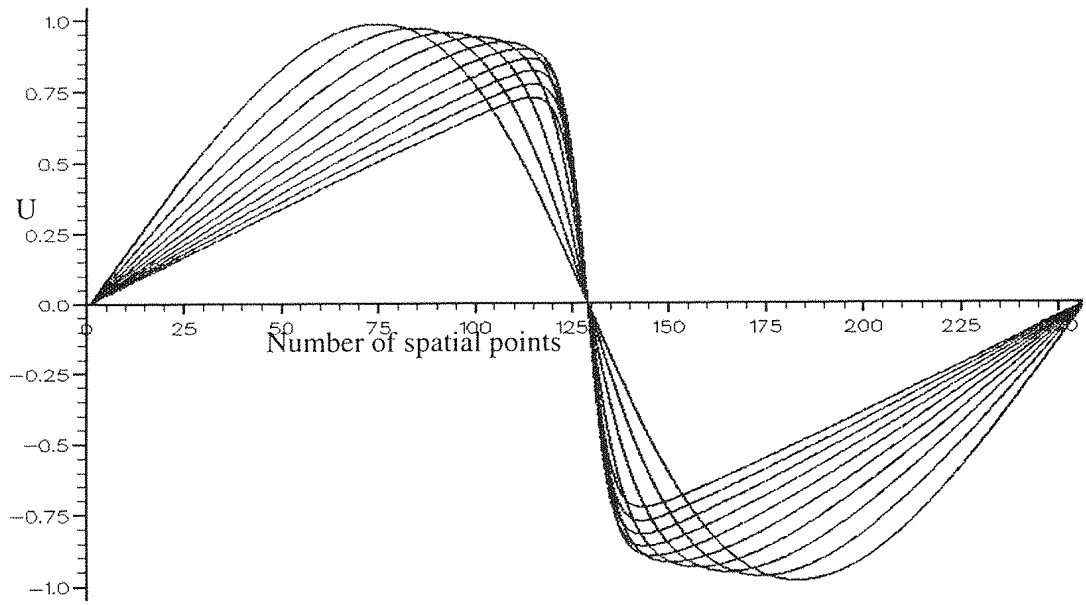

Figure 3.6: Evolution of the periodic sine wave using FFT method. $R_L = 100$.
$\bar{t} = 0, 0.25, 0.5, 0.75, 1.0, 1.25, ...$

The numerical procedure for the Fast Fourier Transform method to obtain the solution of Burgers equation is described in Appendix C. Solutions for this equation can be obtained numerically by the second order Crank Nicholson's semi implicit scheme for the diffusion equation. The solution for the diffusion equation θ_0 at time $t = 0$ is

$$\theta(\bar{x}, 0) = \theta_0(\bar{x}) = \exp(-\frac{R}{2}\int_0^x u_0(\xi)d\xi)$$

The Fourier coefficients for $\theta(x, t)$ are obtained by the Fast Fourier Transform and then calculated for a time step $\Delta\bar{t}$ using the implicit Crank-Nicholson method in the wavenumber space. N is chosen, such that the number of spatial points is 2^N. The method is

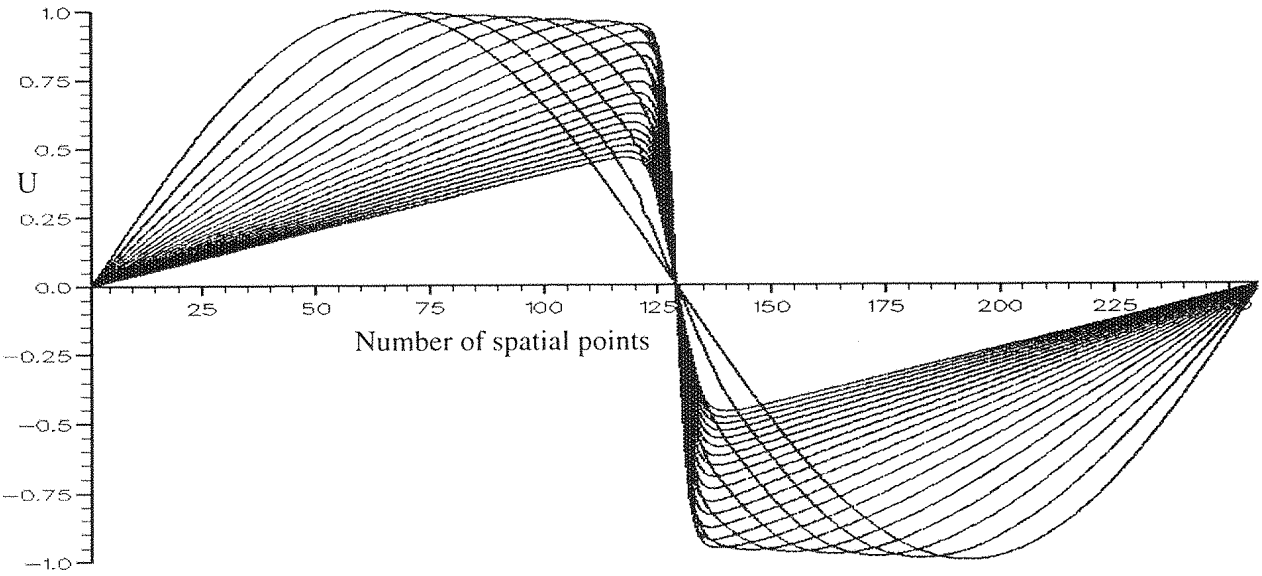

Figure 3.7: Evolution of the periodic sine wave using FFT method. $R_L = 200$.
$\bar{t} = 0, 0.2, 0.4, 0.6, 0.8, 1.0, 1.2, 1.4, 1.6.....$

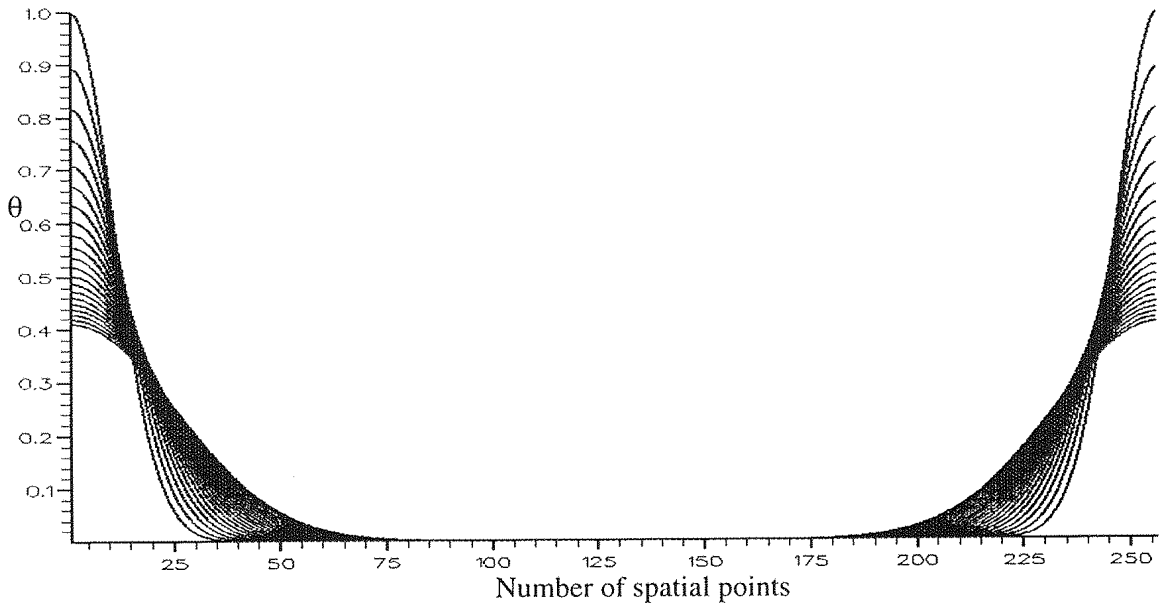

Figure 3.8: Evolution of θ for the periodic sine wave using FFT method. $R_L = 200$.
$\bar{t} = 0, 0.2, 0.4, 0.6, 0.8, 1.0, 1.2, 1.4, 1.6.....$

unconditionally stable and does not impose any restriction on the time step. Typical values of the non-dimensional time step used in this method was $\Delta\bar{t} = 0.005$. The function $\theta(\bar{x}, \bar{t})$ and its derivative with respect to $\bar{x}$ is found for any time $\bar{t}$ and the waveform $\bar{u}(\bar{x}, \bar{t})$, is then obtained from the Cole-Hopf transformation. A few examples with different wave geometries such as the sine wave, sawtooth waves, using FFT method are discussed below. These examples were computed using the FFT method to study the behaviour of these cases for their intrinsic interest.

3.4.4 Sine Wave:

The results presented are those computed by the FFT method for 3 different Reynolds numbers. Figures 3.6 shows the evolution of the sine wave for $R_L = 100$ and figure 3.7 shows the evolution for $R_L = 200$ and the corresponding $\theta(\bar{x}, \bar{t})$ when $R_L = 200$ is shown in figure 3.8 at times $\bar{t} = 0, 0.2, 0.4, 0.6, 0.8, 1.0, 1.2, 1.4, 1.6.....$ The number of spatial points is 2^N, where N=8. The shock formation time is $\bar{t} = 1.0$ for the inviscid case and is also approximately the shock formation time for the case $R_L = 200$. Also shown in figures 3.9 and 3.10 are the derivatives for $\theta(\bar{x}, \bar{t})$ and $\bar{u}(\bar{x}, \bar{t})$ respectively. θ_0 for the sine wave is

$$\theta_0(\bar{x}) = \theta(\bar{x}, 0) = \exp\left(-\frac{R}{2}\int_0^{\bar{x}} \sin\xi d\xi\right) = \exp\left(\frac{R}{2}(1 - \cos\bar{x})\right) \tag{3.12}$$

Differentiating equation 3.12

$$\frac{\partial\theta_0}{\partial\bar{x}} = -\frac{R}{2}\sin(\bar{x})\theta_0(\bar{x}) \tag{3.13}$$

θ_0 is always positive as is $\theta(\bar{x}, \bar{t})$, in $0 \leq \bar{x} \leq 1$. Equation 3.13 shows that $\frac{\partial\theta_0}{\partial\bar{x}}$ is antisymmetric in $\bar{x}$ as seen in figure 3.9.

Figure 3.10 shows the evolution of $\partial\bar{u}/\partial\bar{x}$ with time also showing when $\partial\bar{u}/\partial\bar{x}$ becomes minimum, that is the time of maximum distortion when the shock is formed. After this $\partial\bar{u}/\partial\bar{x}$ slowly increases. The periodic boundary conditions with $\bar{u} = 0$ at $\bar{x} = 0$ and $\bar{x} = l$ restrict the wave to remain within the boundary and the distortion is inwards. The initial waveform will finally reduces to a sine wave of small amplitude.

As the Reynolds number was increased the FFT method resulted in the same problem as the spectral method. Figure 3.11 shows the Gibbs phenomena caused by the FFT at a higher value of the Reynolds number equal to 220 when a near discontinuity is being formed. However, it was an improvement over the spectral method since it allowed a larger

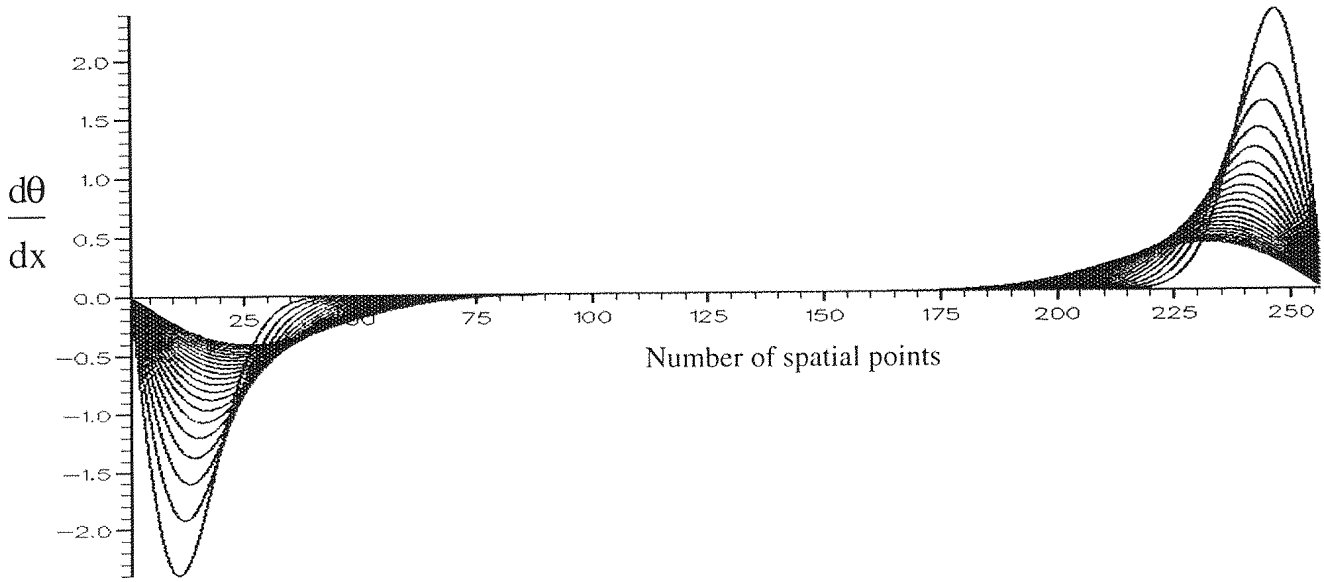

Figure 3.9: Evolution of $\partial\theta/\partial\bar{x}$ for the periodic sine wave using FFT method. $R_L = 200$. $\bar{t} = 0, 0.2, 0.4, 0.6, 0.8, 1.0, 1.2, 1.4, 1.6....$

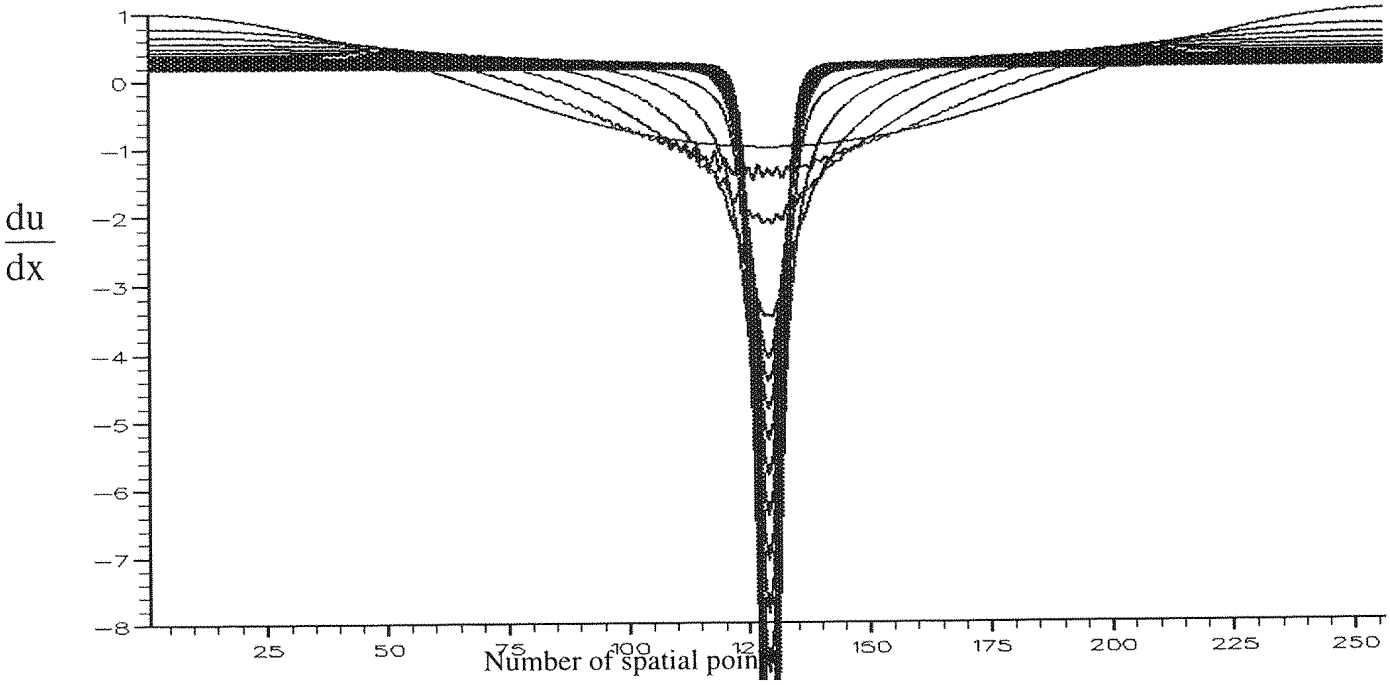

Figure 3.10: Evolution of $\partial\bar{u}/\partial\bar{x}$ for the periodic sine wave using FFT method. $R_L = 200$. $\bar{t} = 0, 0.2, 0.4, 0.6, 0.8, 1.0, 1.2, 1.4, 1.6....$

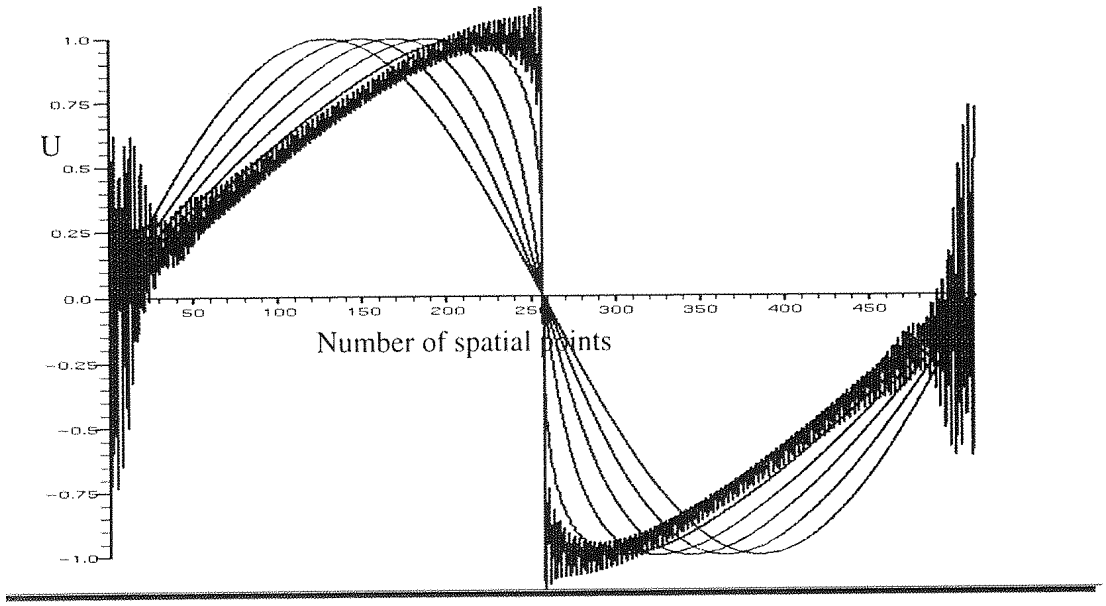

Figure 3.11: Evolution of the periodic sine wave using the FFT method. $R_L = 220$. $\bar{t} = 0, 0.2, 0.4, 0.6, 0.8, 1.0, 1.2, 1.4....$

Reynolds number, and as a result of the Cole-Hopf transform it gave a smooth solutions beyond the shock formation time. But the FFT method is restricted to low Reynolds number only and cannot be used at higher Reynolds (> 220) number.

3.4.5 Sawtooth waves

The next step to consider the distortion of an already formed sawtooth wave as the initial condition and study its distortion with time. Much research is already been done on this wave since it is the ultimate waveform attained by many transient disturbances. Periodicity conditions imply that the sawtooth waves can be produced initially by the generating series

$$u(x,0) = u_0(x) = \sum_{n=1}^{\infty} \exp(-an^2)\sin(\pi nx)/n. \tag{3.14}$$

where a is the Gaussian factor. The Cole-Hopf transformation gives

$$\theta(x,0) = \theta_0(x) = \exp\left(-\frac{R}{2}\int_0^{\bar{x}} u_0(\xi)d\xi\right) = \exp\frac{R}{2}\sum_{n=1}^{\infty}\frac{\exp(-an^2)}{n^2}(\cos(1-2\pi nx)) \tag{3.15}$$

where $n = 1, 2, 3, 4...$ Since it is impossible to evaluate an infinite series, the Fourier series is truncated to a finite value N. Thus equation 3.14 as given by Mellen(1986) after truncation is a trivial extension of equation 3.14

$$u(x,0) = u_0(x) = \sum_{n=1}^{N} \exp(-an^2)\sin(\pi nx)/n.$$

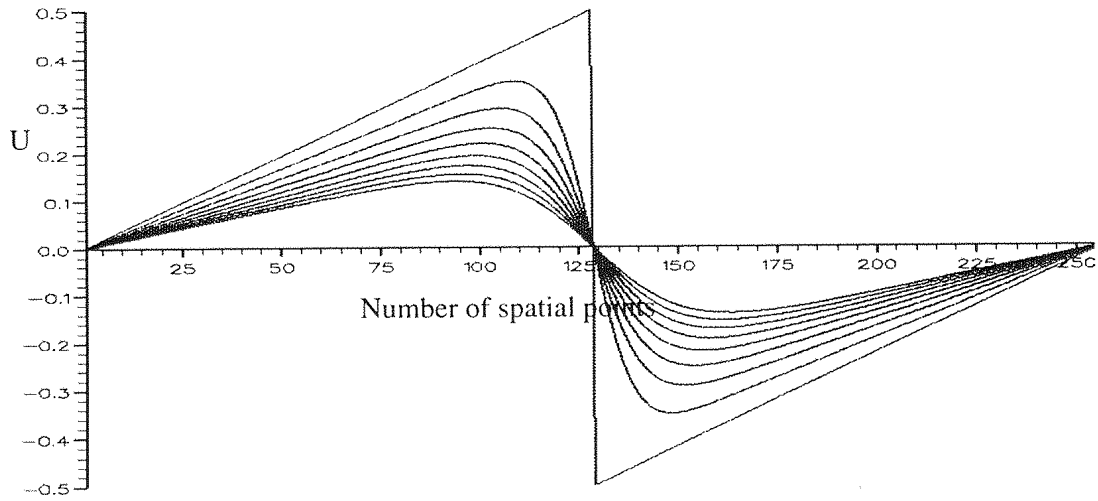

Figure 3.12: Nonlinear distortion of sawtooth wave. $R_L = 100$.
$\bar{t} = 0, 0.6, 1.2, 1.8, 2.4, 3.0, 3.6, 4.2, 4.8$.

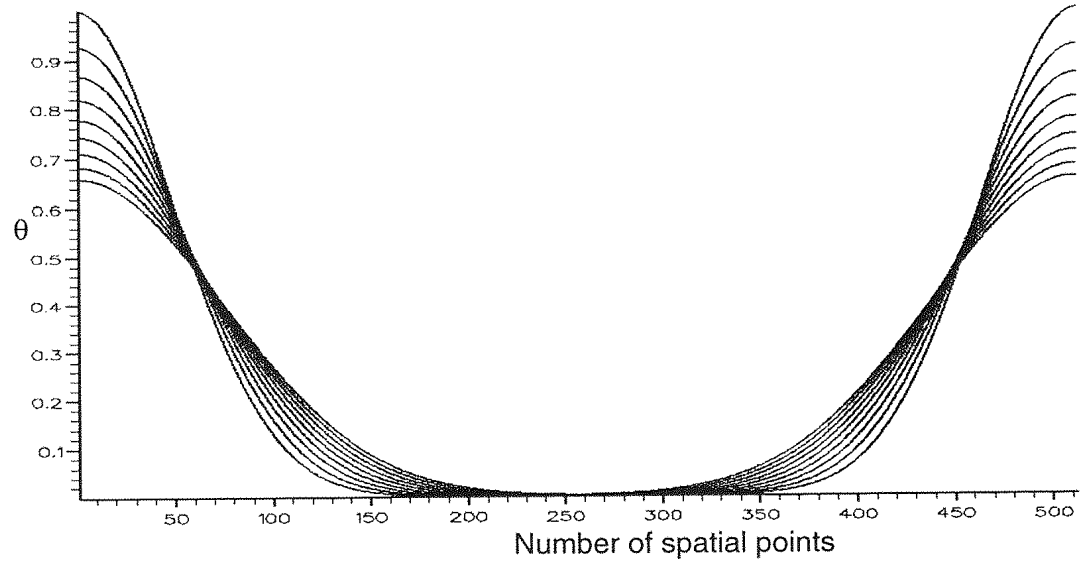

Figure 3.13: $\theta(\bar{x}, \bar{t})$ for the periodic sawtooth wave. $R_L = 100$
$\bar{t} = 0, 0.6, 1.2, 1.8, 2.4, 3.0, 3.6, 4.2, 4.8$.

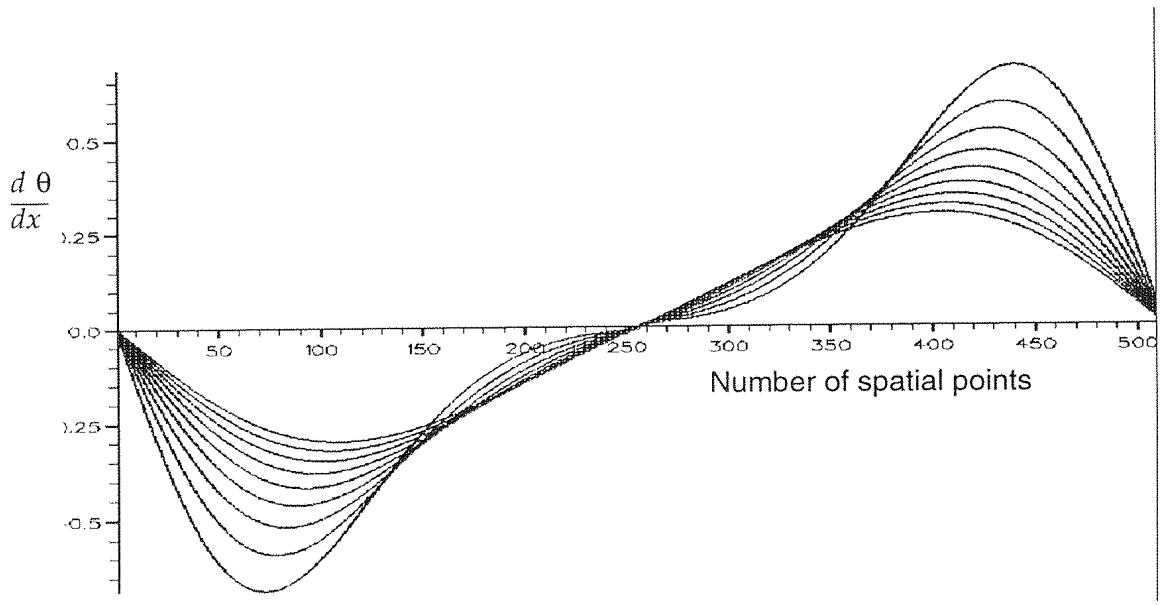

Figure 3.14: $\partial\theta/\partial x$ for periodic sawtooth wave. $R_L = 100$.
$\bar{t} = 0, 0.6, 1.2, 1.8, 2.4, 3.0, 3.6, 4.2, 4.8$.

Figure 3.13 shows $\theta(x,t)$ for a sawtooth wave and the corresponding waveform for u is shown in figure 3.12 for times $\bar{t} = 0, 0.6, 1.2, 1.8, 2.4, 3.0, 3.6, 4.2, 4.8$. Similar to the sine wave it is seen that $\theta(x,t)$ is always positive. The Reynolds number was 100. Comparing θ for the sine wave and for the sawtooth wave in figures 3.8 and 3.13 it is observed that although they are similar in shape, θ for the sawtooth wave at $\bar{t} = 0$ goes to zero much slowly than that for the sine wave. This arises from the Gaussian factor in the exponential term for the sawtooth wave. In figure 3.14 is shown the derivative of θ. It is seen that $\frac{\partial\theta}{\partial x}$ is symmetric which is obvious from equation 3.15 after differentiation. Again comparing $d\theta/dx$ for the sine wave and the sawtooth wave, $d\theta/dx$ for the sawtooth wave meets the x axis at only one point when compared to $d\theta/dx$ for the sine wave where $d\theta/dx$ meets the x domain at many points. It is seen that the sawtooth wave decays towards a sine wave monotonically for large times and viscous effects dominate over nonlinear effects. Thus all the high frequency components in the initial sawtooth wave are gradually lost and the wave attains a sine wave of small amplitude. If the nonperiodic boundaries were to be imposed on the sawtooth, the wave would spread in either direction and would attain the sine wave even faster than the periodic sawtooth. This is because as the wave diffuses it prevents it from steepening, unless the Reynolds number is very high.

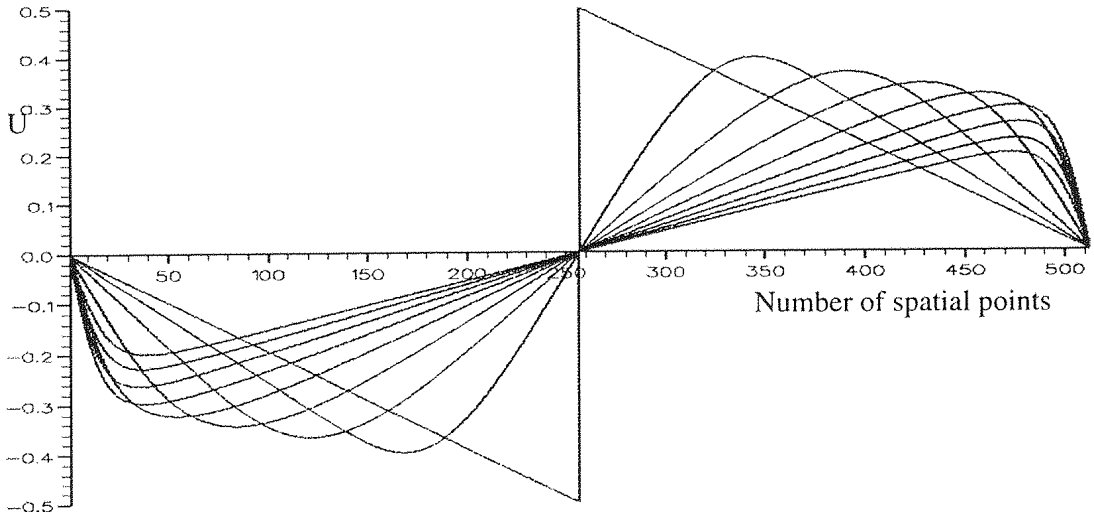

Figure 3.15: Nonlinear distortion of inverted sawtooth. $R_L = 100$

$\bar{t} = 0, 0.6, 1.2, 1.8, 2.4, 3.0, 3.6, 4.2, 4.8.$

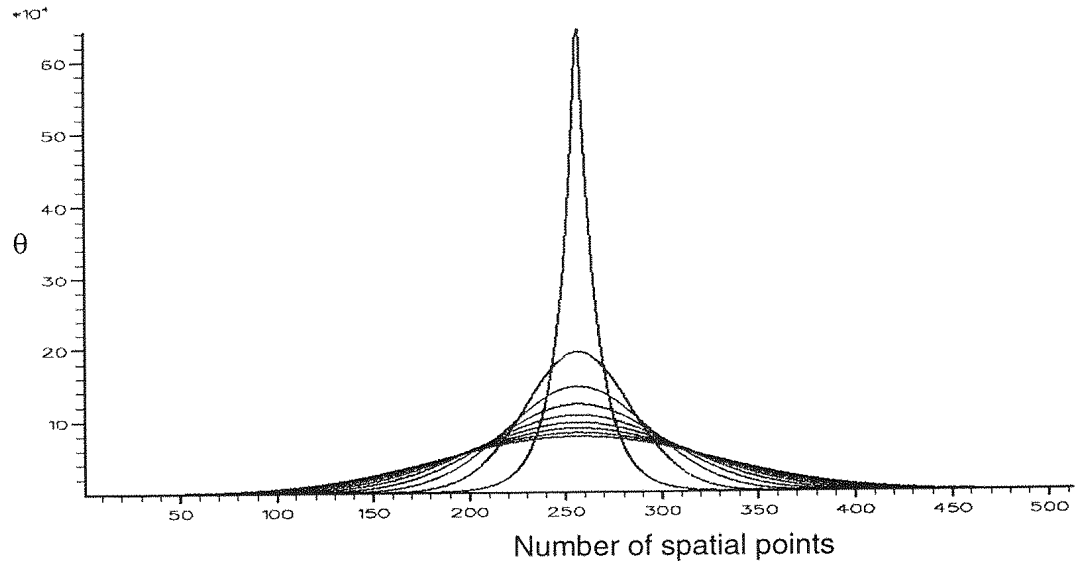

Figure 3.16: $\theta(x,t)$ for an inverted sawtooth wave. $R_L = 100$.

$\bar{t} = 0, 0.6, 1.2, 1.8, 2.4, 3.0, 3.6, 4.2, 4.8.$

3.4.6 Inverted Sawtooth

Figure 3.15 shows the inverted sawtooth which is generated by changing the sign of the sawtooth series. The corresponding θ distribution are shown in figure 3.16 for times $\bar{t} = 0, 0.6, 1.2, 1.8, 2.4, 3.0, 3.6, 4.2, 4.8$. The Reynolds number was 100. Polarity reversal causes θ to increase instead of decreasing as in the θ for the sawtooth wave. This initial sawtooth can also be visualised as inverting the curves around the endpoints of figure 3.13. Polarity reversal causes the waveform to first become sinusoidal and then proceed to steepen again before the final decay is reached. In other words the wave distorts on either sides just like a sine wave once all the energy is transferred towards the fundamental. This means the initial effect of the polarity reversal is clearly to feed energy back into the fundamental increasing the amplitude before the trend reverses. After this effect, the energy is again lost to higher harmonics and a shock begins to develop similar to the sine wave propagation. Eventually the wave reduces to the small amplitude sine wave at large times.

3.4.7 N wave

Figure 3.17 shows evolution of a periodic N wave. The time intervals are the same as for the inverted sawtooth. The N wave can also be considered as either starting from the N wave or rescaling the calculation after it has developed under different conditions of the sine wave propagating outwards. The case is similar to the sawtooth wave of figure 3.12, in which the viscous effects for a fully developed initial N wave will only feed energy towards low frequency region reducing it monotonically to a sine wave.

3.4.8 Isolated single cycle sine wave

It is known that a nonperiodic wave will form an N wave and will remain an N wave with reduced amplitude indefinitely when $R_L \to \infty$. Although it is convenient to think of u_0 as a periodic function, it was necessary to investigate the propagation of u_0 as a pulse. That is, one period of a sound wave train and u_0 is described in $0 < x < l$, and is zero outside this domain. But since the method uses periodic conditions only, it was not possible to compute this isolated pulse where u_0 is zero outside $0 < x < l$. To overcome this difficulty, u_0 was defined as occupying one third of the whole period $0 < x < l$, the rest being equal to zero.

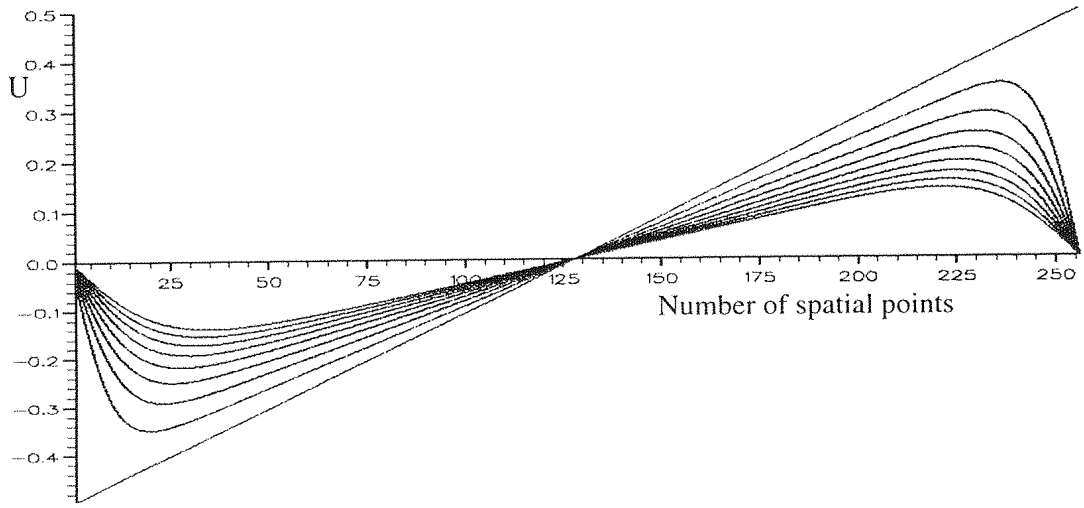

Figure 3.17: Evolution of the N-wave. $R_L = 100.\bar{t} = 0, 0.6, 1.2, 1.8, 2.4, 3.0, 3.6, 4.2, 4.8.$

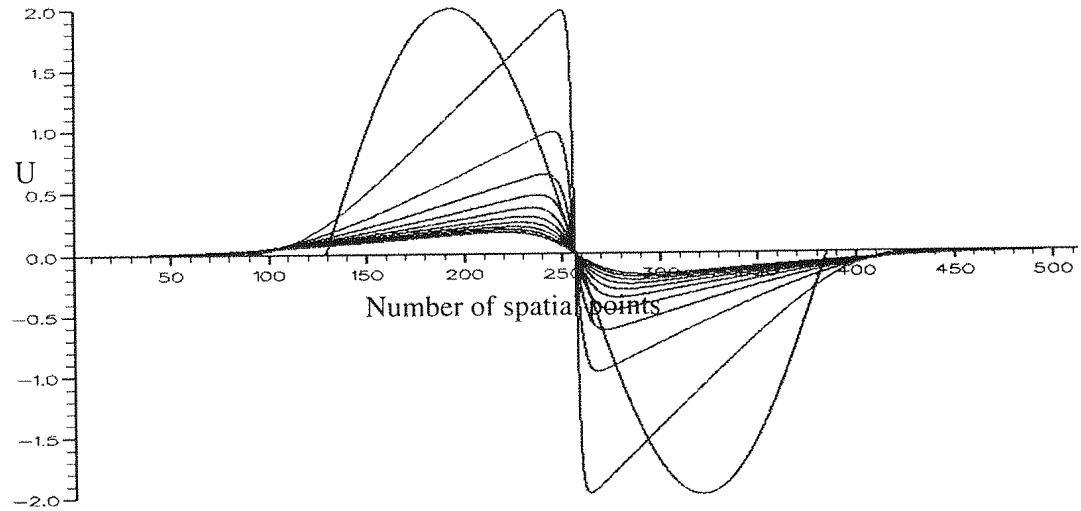

Figure 3.18: Evolution of the truncated sine wave. $R_L = 50$

$\bar{t} = 0, 0.6, 1.2, 1.8, 2.4, 3.0, 3.6, 4.2, 4.8.$

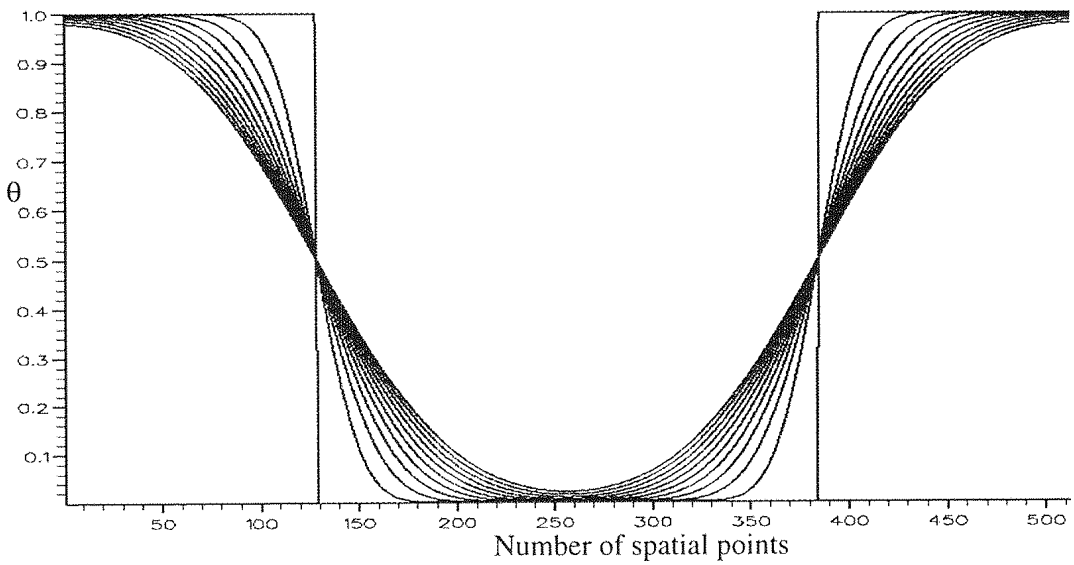

Figure 3.19: $\theta(\bar{x}, \bar{t})$ for the truncated sine wave. $R_L = 50$.
$\bar{t} = 0, 0.6, 1.2, 1.8, 2.4, 3.0, 3.6, 4.2, 4.8$.

In this section the nonlinear distortion of an isolated single cycle sine wave at moderate Reynolds number is considered. Although this initial wave can be considered as a nonperiodic wave allowed to diffuse out, a time comes when the wave hits the boundaries and the periodicity becomes important. An example of such a situation is described below. Figure 3.17 shows the evolution for an initial isolated single cycle sine wave contained in a domain $0 < \bar{x} < l$ for Reynolds number of 50. The initial sine wave occupies one third of the whole period the rest being equal to zero. With increase in time the waveforms show the development towards sawtooth wave which continues to expand as the fronts diffuse outward with increased pulse length. The wave diffuses along either sides and once the wave touches the boundaries the periodicity conditions become important. Due to the periodicity conditions all the properties of Cole's(1951) solution for wave become applicable. The wave no more behaves like a nonperiodic wave but can now be considered as an initial condition with periodic conditions obeying Cole's solution and reducing to a sine wave of small amplitude. Whatever happens in the domain $0 < \bar{x} < l$ is repeated in the neighbouring domains with $u(0, \bar{t}) = u(l, \bar{t}) = 0$. Figure 3.19 shows the corresponding $\theta(\bar{x}, \bar{t})$ with increasing time being always positive. Time values are $\bar{t} = 0, 0.6, 1.2, 1.8....$ Comparing the initial $\theta(\bar{x}, \bar{t})$ to the initial $\theta(\bar{x}, \bar{t})$ for the sine wave (see figures 3.19 and 3.8) it is observed that there is a sudden jump in the $\theta(x, t)$ for truncated sine wave due to the boundary conditions imposed. Thus $\theta(x, 0)$ is generated by filling the FFT array with

the appropriate constant value at each end [see figure 3.19]. A fully developed sawtooth is formed at a slightly later time than that for the periodic sine wave ($t = 1$) described in figure 3.7. This is because the wave is allowed to diffuse outside its boundaries upto $\bar{x} = 0$ and $\bar{x} = l$. It was seen that θ was always positive and within the domain of $\bar{u}$. As $\bar{t}$ increases the viscous broadening takes over and the wave will reduce to the sine wave of small amplitude. The period of the sine wave will now be between $\bar{x} = 0$ and $\bar{x} = l$ and will decay linearly with time as described by Cole.

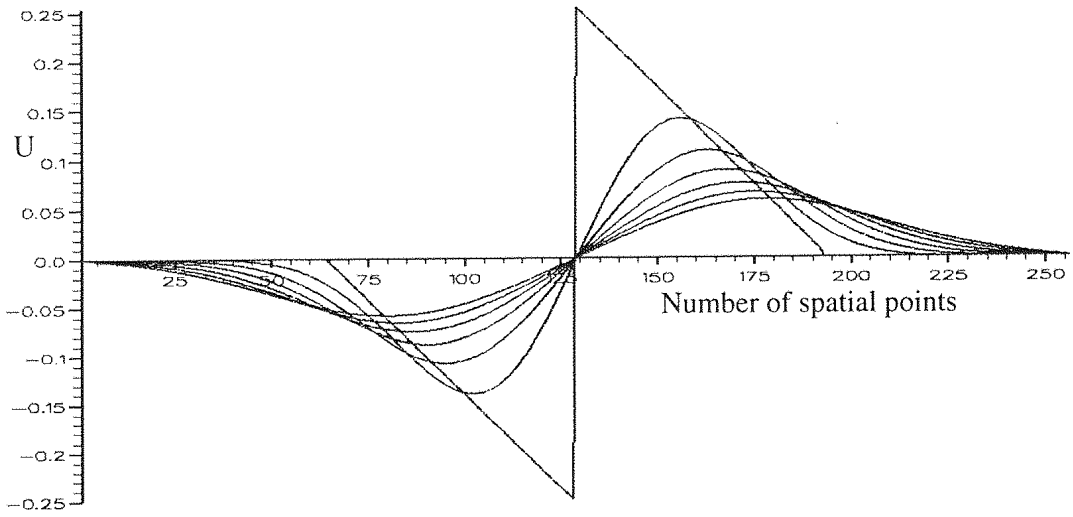

Figure 3.20: Nonlinear distortion of an truncated sawtooth wave. $R_L = 50$
$\bar{t} = 0, 1.2, 1.8, 2.4, 3.0, 3.6, 4.2, 4.8.$

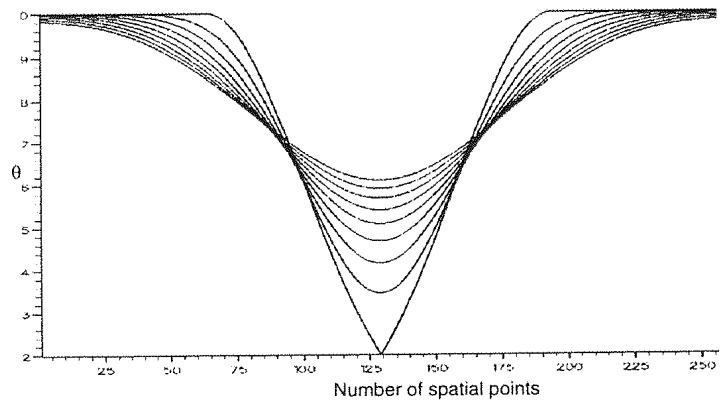

Figure 3.21: $\theta(\bar{x}, \bar{t})$ for truncated sawtooth wave. $R_L = 50$.
$\bar{t} = 0, 1.2, 1.8, 2.4, 3.0, 3.6, 4.2, 4.8.$

3.4.9 Isolated single cycle Sawtooth

The purpose of computing the nonlinear distortion of an isolated single cycle sawtooth is that it describes the nonperiodic behaviour of a sawtooth wave upto a certain time as described above when the periodicity conditions become important. Figure 3.20 shows the evolution of an initial sawtooth wave at $R_L = 50$. The wave occupies one third of the periodic domain, the rest being equal to zero. Time values are the same as that of the isolated single cycle sine wave as shown in figure 3.18. Its corresponding $\theta(\bar{x}, \bar{t})$ are shown in figure 3.21. Comparing it with θ for the sawtooth wave in figure 3.13, it is observed that the initial isolated single cycle sawtooth wave touches the $\bar{x}$ domain at only one spatial point. This is because the sawtooth is a small section occupying one third of the whole domain. The Gaussian factor in the exponential for the θ equation produces a rapid fall in the θ. The wave expands as the leading and the trailing edge diffuse outward. Nonlinear distortion does not give rise to steep fronts because the leading edges allow the wave to diffuse outwards and also due to moderate Reynolds number. Whereas in the case of a periodic inverted sawtooth [see figure 3.15] the nonlinear distortion gave rise to steep fronts. In other words waveform steepening is greatly reduced because there is no boundary to stop the expansion. Thus shocks are not formed and the wave progresses downstream finally will reduce into a sine wave of small amplitude. The periodicity conditions become important when the wave meets the boundaries and the wave no more behaves like an isolated wave but obeys Cole's(1951) solution reducing it to a sine wave of reduced amplitude. The extra harmonic content is rapidly dissipated and it is expected to decay towards a sinusoidal form of vanishingly small amplitude at large time. At large time due to periodicity condition the ultimate sine wave would lie in this period. But for a true nonperiodic sawtooth if the outer boundaries were not to imposed the wave would progress outside the outer boundaries having the same initial wave form but of greatly reduced amplitude. But if the Reynolds number is very high then the wave will continue to remain an N wave as described earlier.

3.5 Conclusions

Two different numerical methods have been evaluated to compute the propagation of finite amplitude waves. These are the spectral method and the FFT method. Simple examples have been solved like the initial sine wave using spectral method which shows

good accuracy upto the discontinuity for low and high Reynolds numbers solutions. For low Reynolds number of $R_L = 100$ both methods give smooth profile even after the near discontinuity. The spectral method fails to resolve the near discontinuity for large Reynolds numbers such as $R_L = 200$ and above due to the aliasing errors caused by the Fast Fourier transform. It is shown that the FFT method is also restricted to low Reynolds number due to the aliasing errors caused by the FFT. For $R_L = 200$ the spectral method fails near the discontinuity whereas the FFT method gives a smooth profile even after the discontinuity but for $R_L = 220$ both methods failed. It is seen clearly that the FFT method is an improvement over the earlier spectral method since it allowed a slightly larger Reynolds number (220) and more signals with various geometries to be computed. The method enables to evaluate the waveforms beyond the shock formation time which was not possible by the spectral method. However much the method uses Cole-Hopf transformation giving exact numerical solution to the Burgers equation, the method still uses the Fast Fourier Transform. The time marching in the spectral domain can give rise to numerical errors. The Fast Fourier transform causes aliasing errors and Gibbs phenomena, also occurring in the spectral methods, thus restricting the method to simple waveforms and low Reynolds numbers. This suggests that the spectral method or the FFT method would not be able to deal with a high intensity random noise signal. In the FFT method the solution θ of the diffusion equation is obtained in the spectral domain, whereas in the Spectral method the solution $\bar{u}$ of the nonlinear Burgers equation which gives rise to a discontinuity is obtained in the spectral domain. Thus no discontinuity can occur in the FFT method in the spectral domain since it solves the linear diffusion equation. In the Spectral method, the computation of the nonlinear term in the spectral domain will result in a near discontinuity, but the method cannot handle a discontinuity due to the Gibbs phenomenon. Thus the FFT method allows a higher Reynolds number than the spectral method since is is used to solve the linear diffusion equation in the spectral where no discontinuity arises. In fact as seen from above these methods cannot deal with initial conditions having simple geometries at moderately high Reynolds number. The Finite difference method could have been used, but the time marching technique could again cause accumulation of numerical errors and is hence not suitable [see Basevdant etal(1986)].

A variety of waveforms having periodic distributions have been studied using the FFT method. The temporary nonperiodic behaviour is shown for the isolated single cycle sine

wave and the isolated single cycle sawtooth when after some time the wave diffuses into the boundaries. This is when the periodicity conditions become important and the wave would behave as an initial condition for Cole's solution. The wave is no more isolated but with fixed boundaries and the wave at large times decays towards sine wave of reduced amplitude as given by Cole.

From the results for the sawtooth wave, isolated sine wave or the isolated sawtooth wave it is seen that if the nonperiodic boundaries were to be imposed, the wave would spread in either direction and would attain the sine wave even faster than the periodic sawtooth since the Reynolds number used in the computation is moderate. But if the Reynolds number is high the wave continues to remain an N wave indefinitely. It is also seen that at large times the decay towards the sine wave is monotonic. The study of these waveforms which are simple give an idea of complex wave consisting of all such simple waves randomly located. The random noise signal is more complex since it consists of many more varieties and combinations of such simple waves which have been studied.

Chapter 4

The Convolution Method (CM)

In chapter 3 it is shown that both the Spectral and the Fast Fourier Transform Methods are not suitable to compute the non-linear distortion of an initial high intensity sound wave distribution and its ultimate decay due to thermo-viscous dissipation at high Reynolds numbers. It was shown that both the Spectral and the FFT methods could not be used for large Reynolds number due to the aliasing errors caused by the Fast Fourier transform. Thus a numerical method was required which avoided the use of Fourier transforms. A requirement was to find a method which solved Burgers equation in the physical domain at any time for any given initial wave distribution. The Fast Fourier transform could be used only to obtain the power spectrum of the signal evolved and had nothing to do with the numerical computation. Once the numerical method had been developed, it was necessary to calibrate it by comparing solutions obtained at high Reynolds number with exact inviscid solutions for simple waveforms of different geometries in order to assess the accuracy of the numerical algorithm when used for any arbitrary initial waveform. It was clear that at sufficiently high Reynolds number the differences in the solution from the inviscid solution were small and confined to the neighbourhood of any discontinuity. It was assumed that once this had been established the method could then be confidently used for any arbitrary initial waveform. The method so developed enabled an investigation of the physical process of propagation at any time. Once the signal at any desired time is obtained, a forward transform of the signal using an FFT should then be able to describe the complete spectra of the evolved signal. Thus the method should be able to analyse the various processes involved in the propagation of this random signal at all times in both the physical and spectral domains as well as to compute the statistical evolution of the signal properties with time. In other words the goal of the present research was to develop a

numerical method which can give a complete description of the wave characteristics, and their statistics at any time.

After considering a number of standard numerical procedures for solving the Burgers equation the only available methods which do not use of Fourier transforms, are the Finite Difference and Convolution Methods. All other methods involved the use of Fourier transform (FFT) involved errors at high Reynolds number due to Gibbs phenomenon. The Finite Difference method used by Basevdant(1986) have proved to be less accurate when compared to the FFT method and is discussed by Basevdant et al(1986). The Convolution Method for solving the nonlinear Burgers equation as used in the present research, involves transforming Burgers equation using the Cole-Hopf transformation and finding the solution to the resulting standard diffusion equation for the prescribed initial and boundary conditions. At the commencement of this research it was not known whether this method would give accurate solutions to an initial random noise signal, and there was no existing literature supporting it. It was accordingly decided to use the Convolution Method (CM) for this problem and the method and results are described in detail later in this chapter. A necessary condition was to show that the method was space and time accurate and to be able to describe fully non-linear acoustic propagation including nonlinear distortion, the shock formation, the viscous dissipation and finally its degeneration into a damped acoustic wave.

As stated above the Convolution Method involved in obtaining the solution of the Burgers equation, which is a quasilinear parabolic partial differential equation, by transforming it to the linear diffusion equation using the Cole-Hopf transformation. Thus the complex solution to Burgers equation is reduced to the simple problem of solving the diffusion equation. The initial value problem in Burgers equation is then transformed to a corresponding initial value problem of the diffusion equation and finally the solution to Burgers equation is found by invoking the Cole-Hopf transformation in reverse.

The advantage in using the CM is that it does not make use of the Fast Fourier transform as described in chapter 3 and can be used for very large Reynolds number. The method uses the initial distribution of $\theta = \theta_0$ is used to compute the propagation at any time. This procedure is quite different from other methods which use the standard marching techniques, such as the Finite Difference method or the Finite Element method

resulting in accumulated errors. The CM avoids accumulation of any numerical errors and it will be shown that it gives accurate results at any time and particularly at large times much larger than would be available from other methods. The accuracy of the method can be validated by comparing it for high Reynolds number with exact inviscid solution for the sine wave. In addition the CM is not limited to initial waveforms which are quasi sinusoidal but can be applied to arbitrary initial complex waveforms if other factors such as the limits of integration are properly chosen. It was found that the Convolution method allowed us to handle large Reynolds number and obtain the wave characteristics with sufficient resolution.

4.1 Numerical procedure for the Convolution Method

The quasi-linear parabolic equation known as the one-dimensional Burgers equation is

$$\frac{\partial u}{\partial t} + u\frac{\partial u}{\partial x} = \nu\frac{\partial^2 u}{\partial x^2} \tag{4.1}$$

where u is the velocity and ν the kinematic viscosity which is assumed constant over all distance x and time t. As described in the earlier chapter nondimensionalise these quantities the equation reduces to a form of equation 3.2:

Choosing U, l and R as the characteristic length, velocity and Reynolds number respectively, then

$$R = \frac{Ul}{\nu}, \quad \bar{x} = \frac{x}{l} \quad \bar{t} = \frac{tU}{l}$$

the characteristic time is $T_1 = l/U$, and the viscous characteristic time is $T_2 = l^2/\nu$, where $T_2 >> T_1$, at high values of Reynolds number R. Thus in general in Burgers equation viscous effects lag behind the major inertial changes in the distribution of $\bar{u}(\bar{x}, \bar{t})$ which act on the faster time scale of T_1.

Since

$$\frac{T_1}{T_2} = \frac{l}{U}\frac{\nu}{l^2} = \frac{1}{R}$$

it is seen how important it is at high Reynolds number to be able to adequately resolve events forming in the fast time T_1. One such event is the shock formation time.

Due to the effects of non-linear steepening, the initial smooth waveform soon approaches a discontinuity or shock like structure. The resulting shock formation time has been given by Lighthill (1978) and described in chapter 2. It is

$$T_s = \left| -\frac{1}{min(\frac{du}{dx})_{t=0}} \right|$$

gives the time when the first shock is formed. It can be calculated for any initial distribution if the minimum value of du/dx is known

If $\bar{T}_s = T_s U/l$ is the non-dimensional shock formation time then

$$\bar{T}_s = \left| -\frac{1}{min(\frac{d\bar{u}}{d\bar{x}})_{\bar{t}=0}} \right|$$

Hence $T_s = \bar{T}_s T_1$ and $T_2 = T_1 R$

Thus T_1 is a characteristic of the short time effects such as the shock formation time, while T_2 is the characteristic of the long time effects such as viscous broadening.

Following section 2.6.1 in chapter 2, the Cole-Hopf transformation (1951) in its non-dimensional form is given as

$$\bar{u}(\bar{x},\bar{t}) = \frac{-2}{R}\frac{\partial}{\partial \bar{x}} \ln \theta \tag{4.2}$$

and relates $\bar{u}(\bar{x},\bar{t})$ to $\theta(\bar{x},\bar{t})$ where θ is the solution of the linear diffusion equation.

$$\frac{\partial \theta}{\partial \bar{t}} = \frac{1}{R}\frac{\partial^2 \theta}{\partial \bar{x}^2} \tag{4.3}$$

the initial conditions for $\theta(\bar{x},0)$ relate to the given initial distribution $\bar{u}(\bar{x},0)$.

Putting

$$\bar{u}(\bar{x},0) = \bar{u}_0(\bar{x}) = \bar{u}_0,$$

its initial distribution at time $\bar{t} = 0$, then the initial value for θ is

$$\theta(\bar{x},0) = \theta_0(\bar{x}) = \exp\left(-\frac{R}{2}\int_0^{\bar{x}} \bar{u}_0(\xi)d\xi\right) \tag{4.4}$$

It should be noted that $\bar{u}_0(\bar{x})$ may be positive or negative but $\theta_0(\bar{x})$ is a positive function only and similarly $\theta(\bar{x},\bar{t})$ is a positive function. The solution found by Cole(1951) is suitable for a domain $-\infty < \bar{x} < \infty$ and satisfies uniqueness conditions for the given initial conditions. In the examples given here, it is assumed an arbitrary infinitely periodic initial disturbance $\bar{u}_0(\bar{x})$ have period l and with periodic boundary conditions at $\bar{x} = 0$ and $\bar{x} = l$ for $\bar{t} > 0$.

Thus defining an initial wave having a distribution of particle velocity such that in the domain $0 \leq \bar{x} \leq l$

$\bar{u}(\bar{x},0) = \bar{u}_0(\bar{x})$

with periodic boundary conditions.

$\bar{u}(0,\bar{t}) = \bar{u}(\bar{l},\bar{t})$

4.1.1 The Convolution method (CM) for the determination of $\theta(\bar{x},\bar{t})$ and $\frac{\partial\theta(\bar{x},\bar{t})}{\partial\bar{x}}$

The Gaussian Convolution, which gives the solution of the diffusion equation has been derived by Cole(1951). The Convolution method which involves in obtaining the solution of Burgers equation via the solution of the diffusion equation by the Cole-Hopf transformation, is derived by Cole(1951) has been used by Mitome (1989) for the sine wave only. It gives values of $\theta(\bar{x},\bar{t})$ for the given $\theta_0(\bar{x})$ distribution. The general solution to the diffusion equation is [Carslaw (1941)]

$$\theta(\bar{x},\bar{t}) = \frac{1}{\sqrt{4\pi\bar{t}/R}}\int_{-\infty}^{\infty}\theta_0(\xi)exp(-(\bar{x}-\xi)^2R/4\bar{t})d\xi \tag{4.5}$$

with

$$\frac{\partial\theta(\bar{x},\bar{t})}{\partial\bar{x}} = \frac{1}{\sqrt{2\pi\bar{t}/R}}\int_{-\infty}^{\infty}\theta_0(\xi)\frac{(\bar{x}-\xi)R}{4\bar{t}}\exp\left(\frac{-(\bar{x}-\xi)^2R}{4\bar{t}}\right)d\xi \tag{4.6}$$

Equation 4.6 gives $\partial\theta(\bar{x},\bar{t})/\partial\bar{x}$ and hence $\bar{u}(\bar{x},\bar{t})$ can be recovered using the Cole-Hopf transformation as described in equation 4.2. When the present work was commenced there was little evidence from the existing literature that this method had received much attention. At first sight its advantages were not obvious, but only later, when difficulties with arbitrary initial conditions were found with other methods, the CM was considered superior to the others. A few papers (Mitome 1989) have used this method for simple waveforms, such as the sine wave, but none published so far have developed the method to handle complex wave propagation as presented in this work. The importance of this solution is that the solution to the nonlinear Burgers equation is obtained from the solution to the linear diffusion equation. The solution to the diffusion equation is similar to the initial temperature distribution in a solid. With time the distribution changes so that finally it is uniform everywhere. The nonlinear behaviour is recovered from the Cole-Hopf transformation. Thus accurate solutions to the Burgers equation can be found by numerically computing the diffusion equation which involves an exponential term to be integrated. This solution of Burgers equation is exact for any arbitrary initial distribution of $\bar{u}_0(\bar{x})$ and Reynolds number based on ν. The procedure, details of the limits of numerical integration to integrate $\theta(\bar{x},\bar{t})$ and the advantages in using this method are all described below.

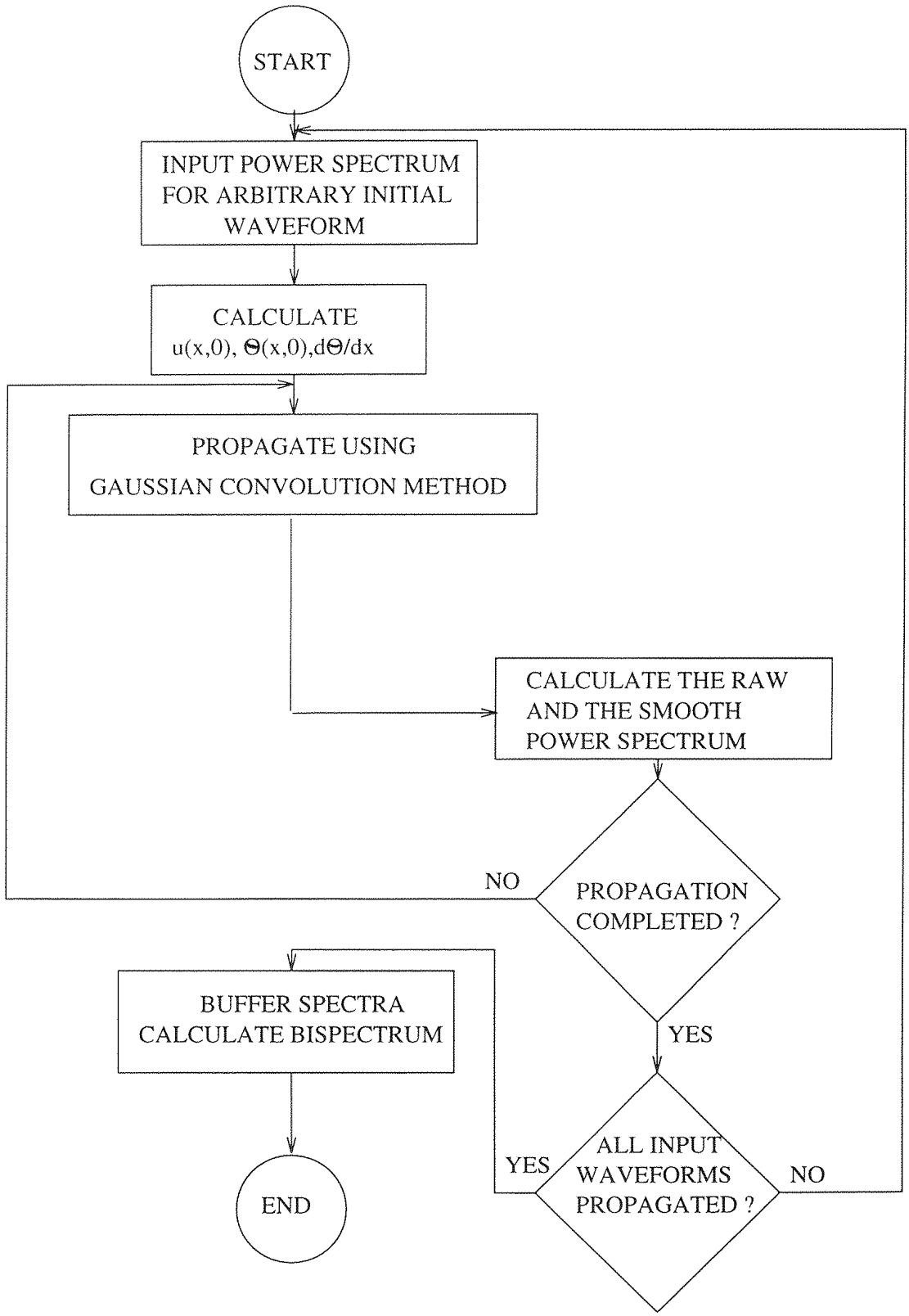

Figure 4.1: Algorithm of the numerical procedure

4.1.2 Algorithm for the CM

A simplified form of the computer algorithm for the Convolution Method is shown in figure 4.1. The initial values for simple waves such as a sine wave or a sawtooth wave is generated by defining the initial $\bar{u}_0$ and finding analytically $\theta_0(\bar{x})$ by integration. Having obtained $\theta_0(\bar{x})$, $d\theta_0/d\bar{x}$ can be evaluated by using equation 3.11 described in chapter 3. For any arbitrary waveform its corresponding spectrum is generated using the Fast Fourier Transform.

For a random signal with a large number of zero crossings, a different procedure is followed to evaluate the initial values, u_0 and θ_0 and is described in detail in chapter 6. The wave distortion due to finite amplitude effects is then computed at any required time when $\theta(\bar{x},\bar{t})$ and $d\theta(\bar{x},\bar{t})/d\bar{x}$ are obtained, and finally $\bar{u}(\bar{x},\bar{t})$ is recovered using the Cole-Hopf transformation. The Fast Fourier transform, used here, is only required to compute the power spectrum at the required observation time.

The integration of equation 4.5 gives the solution to the diffusion equation. Equation 4.5 involves the initial value θ_0 which has to be accurately evaluated as given in equation 4.4. For simple wave geometries such as the sine wave and sine wave with superimposed harmonics θ_0 is evaluated from equation 4.4, but for the initial random signal θ_0 is evaluated in the spectral domain and the method is described in chapter 6. The main problems in the integration of equation 4.5 were in setting the limits of integration and evaluating the exponential terms in equation 4.5. The infinite limits of integration were replaced by finite integration limits. The integration was carried out by trapezoidal rule and the method is described in Appendix E. The large values of the exponential terms required to be handled by the computer needed special treatment.

4.1.3 Numerical integration and its limits

The initial waveform is required to have a period l in the physical domain. Thus the problem is reduced to finding the solution $\bar{u}(\bar{x},\bar{t})$ in $0 < \bar{x} < l$ for the given initial periodic distribution $\bar{u_0}(\bar{x})$. From the latter can be obtained the value of $\theta_0(\bar{x})$ by the use of Cole-Hopf transformation. Finally the corresponding periodic solution $\theta(\bar{x},\bar{t})$, of the diffusion equation which is also of period l, in the domain $-\infty < \bar{x} < \infty$ is obtained using the CM.

The procedure to integrate equations 4.5 and 4.6 consists of multiplying the exponential

term by the given initial periodic distribution in $\theta_0(x)$ corresponding to $u_0(x)$. The product is then integrated over the domain described below using the standard Trapezoidal rule described in Appendix E. The main difficulty is with the infinite integration range, which is not convenient for numerical computation and truncation at large values of ξ is necessary. Figure 4.2 shows the 'Gaussian bell' which when multiplied by $\theta_0(\xi)$ has to be integrated over the whole domain. It is noted that $\theta_0(\xi)$ is periodic in ξ and the finite range of integration has to be extended until the 'Gaussian bell' is indefinitely small to a prescribed limit. The expression for the 'Gaussian bell' is

$$\phi(s) = \frac{1}{\sqrt{(4\pi\bar{t}/R)}} \exp\left(\frac{-s^2}{4\bar{t}/R}\right)$$

where $s = \bar{x} - \xi$ has the property that the area under the curve is equal to unity, or

$$\int_{-\infty}^{\infty} \phi(s)ds = 1.$$

Using this definition of the 'Gaussian bell' equation 4.5 can be written as

$$\theta(\bar{x}, t) = \int_{-\infty}^{\infty} \theta_0(\bar{x} - s)\phi(s)ds \tag{4.7}$$

The characteristic width of the Gaussian function $\phi(s)$ is very narrow for small t, resembling a delta function for $t = 0$. As t increases the range of s over which the function $\phi(s)$ is significant widens and the required practical range of integration covers a larger part of the s axis and includes many periods of $\theta_0(\bar{x} - s)$. For the numerical integration, the limits of integration were selected using statistical tables (see Murdoch and Barnes 1970) so that the discarded tails of $\phi(s)$ contained 0.001% of the total, ie.

$$\int_{-s_{lim}}^{s_{lim}} \phi(s)ds = 0.99999 \tag{4.8}$$

where

$$s_{lim} = 4.4172\sigma$$

and

$$\sigma = \sqrt{\frac{2\bar{t}}{R}}.$$

Numerical tests were then performed to establish the minimum number of spatial points per σ required to integrate equation 4.8 to an accuracy of 0.001% using the Trapezoidal rule. This number was found to be approximately 43 per σ. In most cases the number of spatial points used in the integration was far greater than 43. Newland(1984) discusses about the accuracy of the integrand when replaced by a discrete points and summed over

all points. He shows that the convergence to an accurate solution is possible when more number of points are used while summing.

The numerical integration needed for the solution of equation 4.7 was found to be increasingly complex as $\sigma = \sqrt{\frac{2\bar{t}}{R}}$ approached zero. The exponential became vanishingly small and was then multiplied by $1/\sigma$. The result for small σ was needed for small $\bar{t}$ for any R. It is shown in Appendix F by the use of the method of stationary phase that equation 4.7 approaches $\theta_0(\bar{x})$ uniformly as $\bar{t} \to 0$. For the other limit of small t when R is large for any $\bar{t}$ it was necessary to carefully evaluate the exponential function for large negative arguments.

Equation 4.7 is examined and for convenience is written here as

$$\theta(\bar{x},\bar{t}) = \frac{1}{\sqrt{4\pi\bar{t}/R}} \int_{-s_{lim}}^{s_{lim}} \theta_0(\xi) \exp\left(\frac{-(\bar{x}-\xi)^2}{4\bar{t}/R}\right) d\xi \tag{4.9}$$

As seen in equation 4.9 the argument of the exponential is

$$\frac{(\bar{x}-\xi)^2}{4\bar{t}/R} = X \tag{4.10}$$

For particular values of $\bar{x}$, ξ, $\bar{t}$ and R the values of X was very large and exceeded 256. A special method was used to evaluate exponentials of such large values, since the Sun-Sparc workstation could not calculate the exponential of such large argument accurately. This problem was overcome by setting up a counter in the numerical algorithm such that when the argument of the exponential exceeded 256 was then numerically obtained using the method described by Abramowitz and Stegun(1965) as follows: Let e^X be written as

$e^X = \exp\left(\frac{X}{\ln 10} \ln 10\right)$, and put

$\frac{X}{\ln 10} = n + d$

where n is the integer and d is the decimal part.

Therefore $e^X = 10^n \exp(d \ln 10)$

Since the exponential terms in both integrals for θ and $\partial\theta/\partial x$ are same it is seen that the multiplier 10^n is common to both numerator and denominator and hence may be cancelled. The numerical method is easy to use and provides values of both integrals to the necessary accuracy.

4.1.4 The determination of $\bar{u}(\bar{x},\bar{t})$

In section 4.1.1 the value of $\theta(\bar{x},\bar{t})$ and $\frac{\partial\theta(\bar{x},\bar{t})}{\partial\bar{x}}$ are determined using the Convolution method. In this subsection the corresponding value of $\bar{u}(\bar{x},\bar{t})$ is obtained.

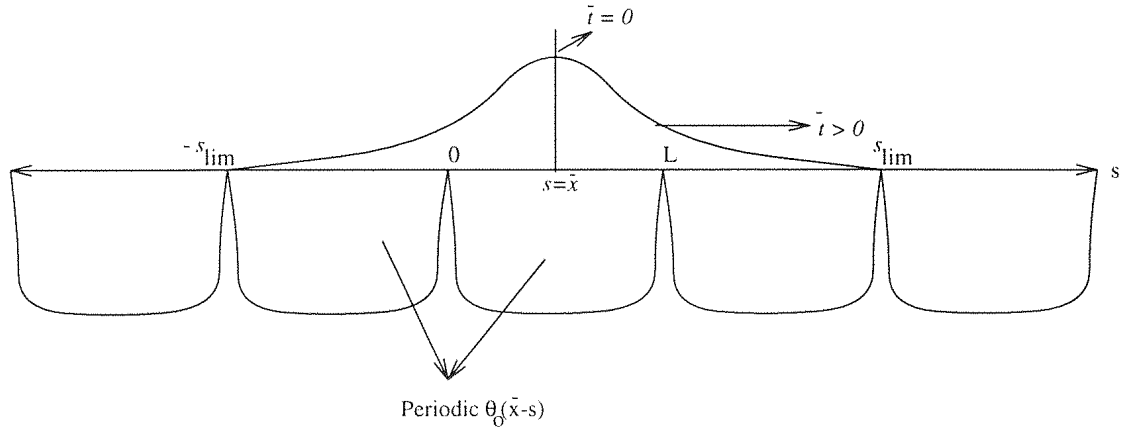

Figure 4.2: Diagram showing how the product of $\phi(s)$ and $\theta_0(\bar{x}-s)$ was obtained for the solution of equation 4.7.

The relation between $\bar{u}(\bar{x},\bar{t})$ and $\theta(\bar{x},\bar{t})$ is found from the Cole-Hopf transformation as given in equation 4.2. Thus with the use of the Convolution method the Burgers equation can be solved for any initial distribution and any Reynolds number and for very small propagation times. This is unlike the finite difference method where time marching schemes involve accumulated numerical errors.

4.2 Comparison of the CM for a high Reynolds number with the exact inviscid solution

The CM was generalised to include any arbitrary periodic initial distribution for u_0. These were the sine, sine wave with superimposed harmonic, and the most important one being the random noise signal. All these are discussed in detail below.

For the evolution of the sine wave with time for a finite Reynolds number, it was found that the solution to the Burgers equation at small times was dominated by nonlinear steepening (Cole 1951), especially when the diffusion coefficient $\nu \to 0$ or $R \to \infty$. Thus a comparison can be made for the results obtained from the Convolution Method with those obtained from the exact inviscid solution for the same simple wave geometry for small times. Strictly the solution of the inviscid hyperbolic equation cannot be compared with the parabolic viscous Burgers equation, but in the limit of $\nu \to 0$ when the equation switches from hyperbolic at $\nu = 0$ to parabolic at $\nu \to 0$ it is found their solutions converge.

4.3 The numerical solution of the inviscid Burgers equation

In chapter 1 the inviscid form of Burgers equation is discussed which is the limiting form of the equation as the Reynolds number tends to infinity. The numerical solution using the Convolution method for the Burgers equation presented in this chapter is concerned with solutions at high Reynolds numbers. Hence to validate these high Reynolds number solution it was felt essential to compare them with numerical solutions to the inviscid BE.

The exact inviscid solution is computed numerically for an initial sine wave and an inverted sine wave using the Newton Raphson iterative method. Appendix D gives the derivation of the Newton Raphson method. In the periodic case the position of the shocks are easily determined for they form by symmetry at the centre of the period. The exact inviscid solution is of the triple valued type for times beyond the shock formation time. The physically correct solution is easily obtained by using the equal area method of Lighthill and Whitham (1956). Thus the triple valued solution is replaced by a shock discontinuity whose position is also determined by symmetry. The equation is a transcendental equation and the solution at any time is obtained iteratively.

4.4 Results of comparison of CM with exact solution for the sine wave

The results using the CM are compared with the exact solution of the Burgers equation for $R = 100 - 2000$ for times $\bar{t} = 0.1, 0.2, 0.3.....$ in figures 4.3- 4.6 respectively. It is seen the shock formation time $t_s \approx 0.3$, as derived in Appendix D. The Reynolds number for this comparison is based on the domain length and the maximum amplitude of the sine wave U is equal to 1 for convenience. It is seen from the plots that as Reynolds number increases the solution from the CM gradually converges with the exact inviscid solution. The solution for $R = 2000$ can almost be regarded as inviscid where the two solutions are almost indistinguishable.

The inviscid solution develops triple valued solutions which are not physically possible. The physically realisable solutions contain shock waves which are shown in figures 4.5 or 4.6. From these results it can be seen that the shock formation time is slightly beyond $\bar{t} = 0.3$ as expected from the characteristic equation as shown in Appendix D.

Tables 4.2 and 4.1 give the comparisons of the Convolution method with the exact inviscid solution for $\bar{u}(\bar{x}, \bar{t})$ at times less than the shock formation time. After the shock

formation time the solution from the CM gradually departs from the exact inviscid solution. This is when the viscous broadening takes over due to the finite viscosity and the solution begins to converge to a sine wave at very large time. In the inviscid solution the amplitude of the shock decreases with increase in time. In the numerical solution at finite Reynolds number, the shock is of finite thickness and its structure is continuous. The exact inviscid solution for time $\bar{t} = 0.1, 0.2, 0.3$ is compared with the solution of the CM for a Reynolds number of 2000 in the tables 4.2 and 4.1 at $n = 250, 254$, where $N = 512$ is the number of spatial points over the whole domain and n is the spatial point. The results are in good agreement. The spatial point $n = 250, 254$ were chosen since they clearly demonstrate the region of the shock wave. Comparing the results of CM and exact inviscid solution it is seen that $\bar{u}(\bar{x}, \bar{t})$ for CM is slightly less than $\bar{u}(\bar{x}, \bar{t})$ for exact solution. This is expected since the diffusive broadening in the CM takes place at the steep front preventing the wave becoming discontinuous. It is seen in figure 4.4 that the effects due to diffusion are to round the discontinuity at the edges where the inviscid solution displays no rounding off. It is seen that the two results are almost indistinguishable at all other spatial points except at the edges at the time of discontinuity. It can be deduced therefore that the solution of the viscous Burgers equation for high Reynolds can be regarded as a satisfactory solution to the inviscid problem. The CM, at high Reynolds number, with the computational limits chosen for the numerical integration described earlier in this chapter can therefore be used as a standard solution for any arbitrary initial waveform.

$\bar{t}$	Convolution Mtd	Exact
0.1	2.02349899E-01	2.024599855951E-01
0.2	7.27589431E-01	7.2788917830E-01
0.3	9.9743597241E-01	9.9994569761E-01

Table 4.1: Comparison of the exact inviscid solution with the solution of the CM for $\bar{u}(\bar{x}, \bar{t})$ and $R = 2000$ for a inverted sine wave. $n = 250$.

Comparison of the Convolution method with other methods described earlier for an initial sine are given in table 4.3. Comparison is made for $|(\partial u/\partial x)_{max}|$ at the non-dimensional time $t = 0.3$ and $\nu = 0.006$ [taken from Basevdant et al(1986)].

From figures 4.3- 4.6 it can be seen that once the solution approaches the exact solution, increasing the Reynolds number has no effect on the solution. Figures display first half

$\bar{t}$	Convolution Mtd	Exact
0.1	1.02613272857E-01	1.026947073E-01
0.2	5.1363528682E-01	5.13810066E-01
0.3	9.97175171278E-01	9.98345373392E-01

Table 4.2: Comparison of the exact inviscid solution with the solution of the CM for $\bar{u}(\bar{x}, \bar{t})$ and $R = 2000$ for a sine wave. $n = 254$.

Method	$\lvert(\partial\bar{u}/\partial\bar{x})_{max}\rvert$
Spectral	151.82
Finite difference	150.08
FFT Method	152.00150
Convolution method	152.00154
Analytic Solution	152.00156

Table 4.3: Comparison of the Spectral, Finite difference, FFT, Convolution and exact solution for $\lvert(\partial\bar{u}/\partial\bar{x})_{max}\rvert$ [taken from Basevdant et al(1986)]

cycle of the sine wave. In other words increasing the Reynolds number after a certain value of 1000 as shown in figure 4.5 there is hardly any change in the waveform and the solution almost equals the inviscid solution. Hence the solution at $R = 1000$ can almost be regarded as equal to the inviscid solution. It is assumed that for practical purposes the solution remains invariant for any $R > 1000$.

4.5 Conclusion

A program has been written for the Convolution Method which uses the Cole-Hopf transformation to give solution to the Burgers equation by transforming it to the linear diffusion equation. A program has also been written for the exact solution of the inviscid Burgers equation using Newton Raphson's iterative method. The numerical integration in computing the exponential curve for the solution of the diffusion equation has all been described in detail. A comparison has been made between the Convolution method for high Reynolds number and the exact inviscid solution both before and after the shock formation time

for the sine wave. It is shown that the agreement is almost exact between the two results, showing the solution at high R converge to the inviscid solution. Thus the changes in the waveform profile at high Reynolds number beyond $R = 1000$ are infinitesimal and that the high Reynolds number solution of the Convolution Method asymptotes to the inviscid solution. From the figures 4.5 it is seen that the shock formation time is approximately $T_s = 0.3$, and is in agreement with the exact solution. It is shown that further increasing the Reynolds number after it has converged with the exact inviscid solution in the CM has no effect on the solution and the solution remains invariant. Thus it is possible to use a large Reynolds number to compute the propagation of any arbitrary distribution, accurately, which any other methods would not have allowed.

The advantages in using the CM over other numerical methods has been discussed. The main is that there is no time marching as in other methods and hence the CM avoids accumulation of any numerical errors. It also avoids the use of the Fast Fourier transform and hence is not subjected to any aliasing errors or the Gibbs phenomena as observed in the earlier methods. The Fast Fourier transform is used only to compute the Power spectrum using the solution of $\bar{u}(\bar{x}, \bar{t})$ and has nothing to do with the actual computation of the waveform at any time. The method also gives the solution at any desired time with one single time step, whereas other methods use a time marching scheme either in the space domain or in the spectral domain. Hence the CM method has least accumulated errors and maximum accuracy.

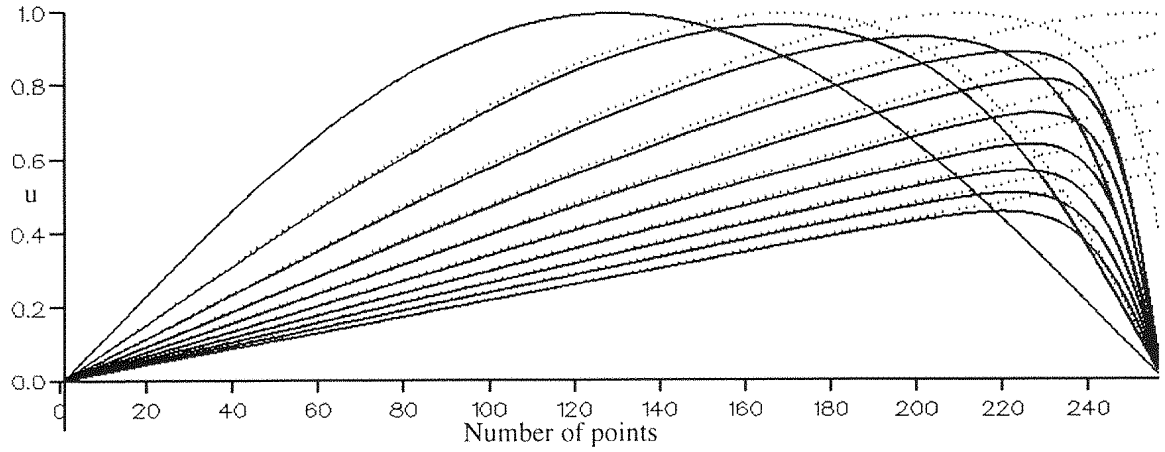

Figure 4.3: Comparison of the exact inviscid solution shown by the dotted line with the solution of the CM for $\bar{u}(\bar{x},\bar{t})$ and $R = 100$ for a sine wave with N= 512. $\bar{t} = 0, 0.1, 0.2, 0.3, 0.4....$

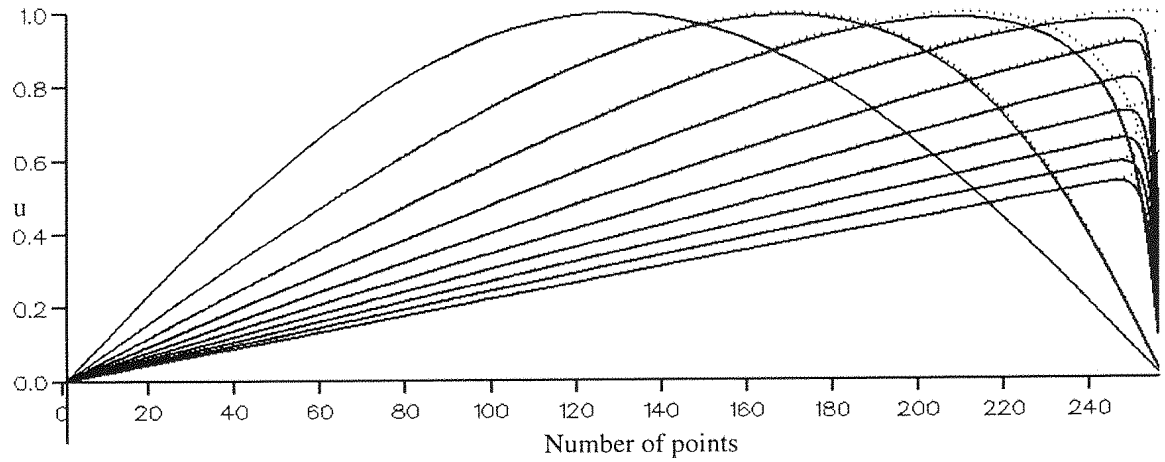

Figure 4.4: Comparison of the exact inviscid solution shown by the dotted line with the solution of the CM for $\bar{u}(\bar{x},\bar{t})$ and $R = 500$ for a sine wave with N= 512. $\bar{t} = 0, 0.1, 0.2, 0.3, 0.4....$

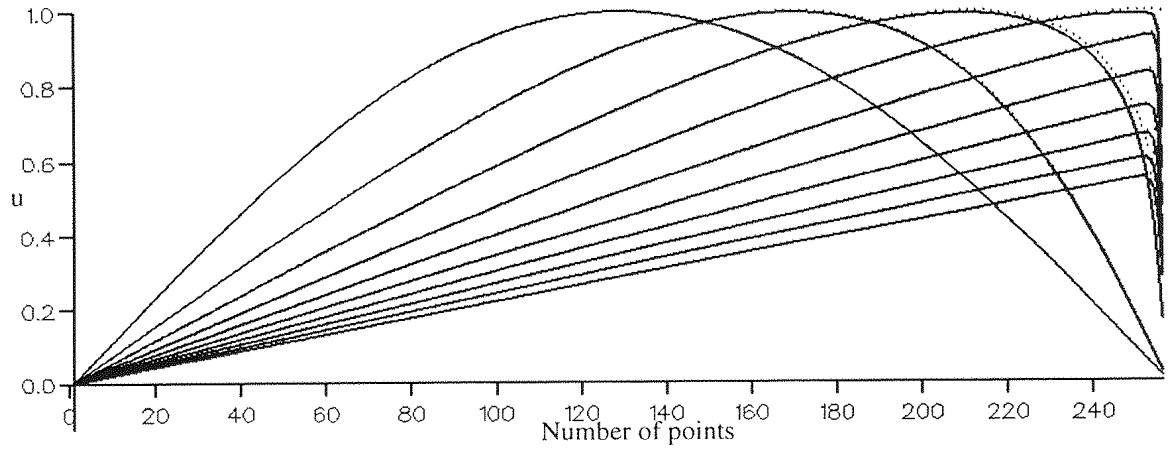

Figure 4.5: Comparison of the exact inviscid solution shown by the dotted line with the solution of the CM for $\bar{u}(\bar{x},\bar{t})$ and $R = 1000$ for a sine wave with N= 512. $\bar{t} = 0, 0.1, 0.2, 0.3, 0.4....$

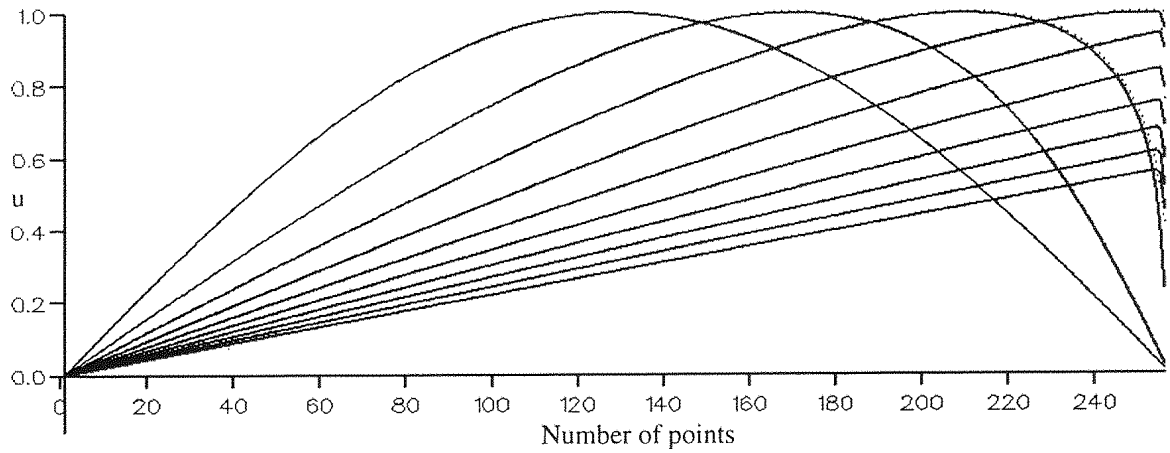

Figure 4.6: Comparison of the exact inviscid solution shown by the dotted line with the solution of the CM for $\bar{u}(\bar{x},\bar{t})$ and $R = 2000$ for a sine wave with N= 512. $\bar{t} = 0, 0.1, 0.2, 0.3, 0.4....$

Chapter 5

Evolution of the sine wave with harmonics

As stated earlier the goal of this research was to investigate the non-linear distortion during propagation of an initial distribution of complex random waves. The study of the nonlinear propagation of acoustic waves is primarily concerned with their distortion due to nonlinear steepening and thermo-viscous broadening. This includes the formation of shock waves and in the case of complex waves, the interaction of shocks of different strengths in a lossless medium and their ultimate 'bunching' introduced by Lighthill(1992). Although the structure of isolated shock waves of finite thickness has been known since the work of Taylor(1910) and Lighthill(1956), in terms of the competing processes of non-linear steepening and thermo-viscous broadening, there were many gaps to be explored of the formation of shock waves arising from the non-linear distortion of complex waveform or distributions. Fundamental work in this field was pioneered by Lighthill(1956) and Whitham(1956) with one of its major applications to the theory of the sonic boom generated by aircraft travelling at supersonic speeds. The study would not be complete without investigating the changes that occur in the energy spectrum of the wave during its propagation. In linear acoustics a sound wave propagating into a nondispersive medium retains its frequency throughout. In nonlinear acoustic propagation the distortion of the wave due to nonlinear

steepening results in the production of a broadband spectrum with the higher and lower frequencies being populated by the sum and difference mechanism. The harmonics add up to form the high wavenumbers and subtract to form the low wavenumbers. This is readily seen in the exact solution to the Burgers equation by Cole(1951) for the initial sine wave profile where it is shown at time $t > 0$ the initial single discretized frequency is broadened to include all frequencies.

In this chapter corresponding changes in the energy spectrum due the non-linear distortion and ultimately to its shock formation that arise in the propagation of initial waveforms of simple geometries such as the sine wave with superimposed harmonics is studied. A similar problem is considered here relating to a simpler wave distribution which comprises an initial large amplitude sine wave on which is superimposed a harmonic of various amplitudes and phases. The distortion of such a simple wave was examined over a range of Reynolds numbers and the temporal changes in its energy spectrum arising due to the two main wave modifying mechanisms namely, the nonlinear distortion and viscous dissipation. Comparisons are made with the results in chapter 3 above for the sine wave alone. The present research covers the case of an initial sine wave superimposed with a harmonic of various amplitudes which eventually degenerates into a sawtooth-like shock wave, as well as the interaction and merging of a sine wave of large amplitude with one of smaller amplitude and different phase, and the consequent temporal changes in the energy spectrum. The study extends to the case of the initial superposition of a harmonic of different amplitudes onto a periodic sine wave distribution and its subsequent development including the non-linear distortion, shock formation and viscous broadening over a range of Reynolds numbers. The main aim was to elucidate the effects of non-linear distortion and viscous broadening at moderate to high Reynolds numbers. It studies the non-linear processes arising from wave interactions and changes in the energy spectrum resulting from sum and difference frequencies and the progressive changes in the wave structure where its distortion ultimately leads to shock formation. The research also investigates the effects of different initial wave distributions on the shock formation time. In this initial phase of the distortion it shows how the changes in wave signature are dominated by mainly inviscid flow effects leading to the development of ramp-function or sawtooth-like waves, and the evolution of a very wide broad-band spectrum having a high frequency character largely independent of the initial waveform. After shock formation it was examined that the thermo-viscous dissipation and its potential for the destruction of the higher frequen-

cies and investigate how diffusive and dissipative effects are confined predominantly to the vicinity of the shocks preventing them from being discontinuous. An important aspect of this numerical study was also to determine how the thermo-viscous broadening processes continue with time.

Wu et al(1990) has investigated the dependence on finite-amplitude loss suffered by a signal with a view to the determination of the waveform for minimum loss. For the case of parametric arrays Wu studied periodic signals of given amplitude which travelled long distances without forming shock waves. Wu showed that superimposing harmonics produced significant changes in the structure of the propagating wave from that of the fundamental alone. Wu considered the analytic solution in a case when the 3rd and higher harmonics were neglected and showed in particular when the harmonic is in phase with the fundamental, a zero crossing occurs in the second harmonic B_2, but when there is a 180^0 shift in the phase of B_2 no zero crossing occurs. These are a result of the nonlinear effects which give rise to a redistribution in the energy of the wavenumber components.

Wu considers the Fourier series representation of a wave expressed as

$$u(x,t) = \sum_{n=1}^{\infty} [A_n(t) \cos n(kt) + B_n(t) \sin n(kt)] \tag{5.1}$$

Wu shows that substituting $u(x,t)$ in the Burgers equation with $A_n(t) = 0$ and neglecting third and higher harmonics, the rate of change of amplitude for any wavenumber can be written determined. Wu considers the boundary value problem of the Burgers equation and hence is signs for the Fourier coefficients B_n are different from the B_n in the present work. Thus Wu shows that when $B_2 > 0$, a zero crossing occurs at a certain t which causes a sharp change in $\log B_2^2$, which in this work is referred to as a "cusp". Thus the formation of the cusp or the phase reversal B_n was explained by Wu et al who showed how the A_n's and B_n's changed at a particular time according to the nonlinear equations for A_n's and B_n's summing the effect of the product terms of A_n and B_n for all other harmonics other than A_n.

The work to be presented in this chapter on periodic waves with superimposed harmonics was performed independently of the work of Wu(1990) and completed before the work became available. Although the work presented here is based on numerical solutions to the Burgers equation(BE) for a range of Reynolds numbers, it was possible to compare the present results with Wu's analytic model for the superimposed harmonics. In this work numerical solutions were obtained to Burgers equation using the so called

Convolution Method, based on the Cole-Hopf transformation and solutions to the linear diffusion equation. The wavenumber energy spectra were computed using Fast Fourier Transforms discretised in wavenumber space, (definition of the Fast Fourier transform is given in chapter 6), of the space-time velocity function found from solutions to the BE equation. The cases presented below emphasise the time history of the energy spectrum.

The study of the wavenumber spectrum with time was commenced by first considering the sine wave alone, and later comparing it with that obtained by superimposing a harmonic of small, equal and large amplitudes. It was found the wave number spectrum changed from its initial spectrum in two distinct phases. The first occurred up to the effective shock formation time and the second following the shock formation time. The effect of the harmonics on the effective 'shock formation time' was investigated, and especially the changes in the geometry of the wave which can change the shock formation time.

An extensive study of the various spectra for various superimposed harmonics obtained at different times is given below. The waveform plots and the energy spectrum for various wavenumber components have been plotted against time. The cases studied below are simple, emphasising mainly the energy spectrum time histories.

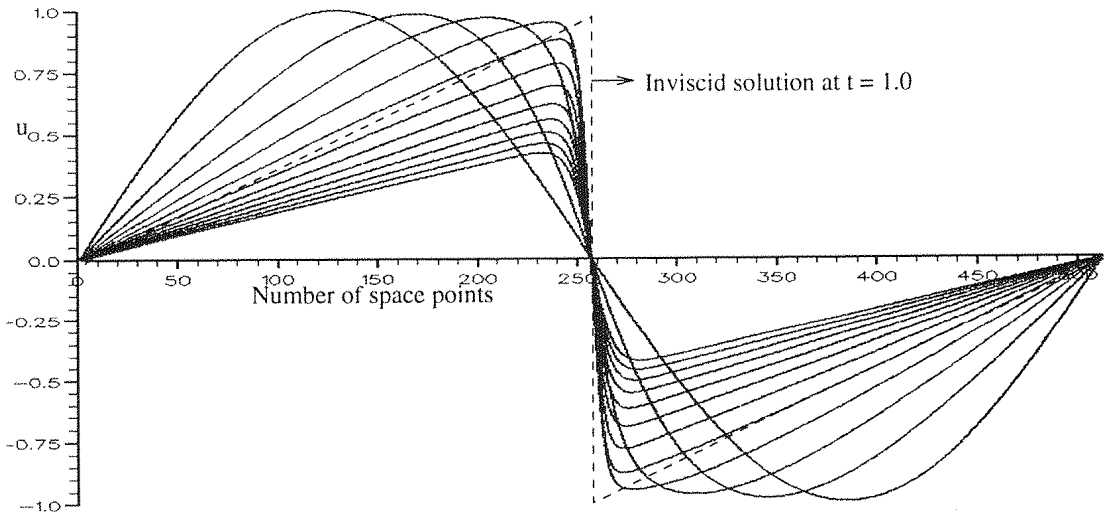

Figure 5.1: Evolution in time of the initial periodic sine wave. $R = 200$.
$T = 0, 0.5, 0.75, 1.0, 1.25, 1.75.....$

Figure 5.2: Change in spectral energy coefficients (k) with time for initial periodic sine wave at $k = 1, 2, 3.....$ and $R = 200$. E_{ref} is the energy in the fundamental at $T = 0$. Dashed line's are Cole's asymptotic solution for large times as functions of k.

5.1 The initial periodic sine wave

Fig. 5.1 shows the numerical results for the distortion of an initial periodic sine wave propagating with time and undergoing non-linear interactions. It is seen the wave tends progressively to a triangular or sawtooth waveform. The idealised sawtooth waveform is only obtained when the flow is inviscid. The results are presented for an initial Reynolds number $R = 200$, based on a wavelength of unity and an initial amplitude of unity. In Figure 5.1 the wave signature is given for $T = 0, 0.5, 0.75, 1.0, 1.25, 1.75.....$ In the inviscid case the shock formation time is $T_s = 1$. When viscous effects are included the effective 'shock formation time' is the same but the shock wave has finite thickness. The corresponding development of the spectral coefficients, $E(k)$, with time is shown in figure 5.2. The energy in the fundamental wavenumber ($k = 1$) at time $T = 0$ is transferred, through nonlinear distortion for $T > 0$, to the higher wavenumbers thus generating a broad spectrum while the waveform in the physical plane rapidly changes from a sine wave to a ramp function. The rapid growth in the population of energy in the high wavenumbers, while the $k = 1$ mode slowly loses energy at $T > 0$, arises from nonlinear interactions, which is the distinguishing feature between linear and nonlinear acoustics.

In this simple case of the initial periodic sine wave the present numerical results are compared with the complete analytic solution of Cole (1951), where the wavelength is l and the amplitude, $u = 1$ at $T = 0$. The periodic solution for $u(x, t)$ given by Cole is

$$u/u_0 = \frac{4\nu\pi \sum_{n=1}^{\infty} n \exp(-\nu n^2\pi^2 t/l^2) n I_n(u_0 l/2\pi\nu) \sin(n\pi x/l)}{I_0(u_0 l/2\pi\nu) + 2\sum_{n=1}^{\infty} \exp(-\nu n^2\pi^2 t/l^2) I_n(u_0 l/2\pi\nu) \cos(n\pi x/l)} \tag{5.2}$$

The solution simplifies for high Reynolds number, $R = u_0 l/\nu$, since the Bessel function, of imaginary argument, I_n, become very large and asymptotically has similar values $I_n \sim \exp z/\sqrt{2\pi z}$ for all n. Thus corresponding terms cancel in numerator and denominator. The infinite series solution due to Cole in equation 5.2 in terms of the integer n is equivalent in the present numerical work to the spectrum in wavenumber k. Cole's solution shows

that there is a rapid growth in the spectrum at all wavenumbers $n > 1$ when $t > 0$. As the energy in the fundamental $n = 1$ decreases so the values of $E(n)$ rapidly increase and the spectral energy for $n \geq 2$ approaches that in the fundamental $n = 1$, before decaying as $1/n^2t$ as discussed below.

The phase of the Fourier coefficients for all wave numbers alternate according to Cole's solution and the spectral energy increases smoothly up to a time when the gradient of u becomes a maximum, corresponding to the shock formation time.

Fig. 5.2 shows that the spectral energy as a function of time. Now Cole found the approximate solution for $t > t_1$ at high Reynolds number, where $t_1 \approx O(1)$ is of the order of the shock formation time given by

$$u(x,t) = \frac{2\nu\pi}{l} \sum_{n=1}^{\infty} \frac{(-)^n \sin(n\pi x/l)}{\sinh \nu(n^2\pi^2 t/l^2)} \tag{5.3}$$

Beyond $t = t_1$, $t_1 \approx O(1)$, the energy spectrum decays like $1/n^2$, and the numerical results agree with Cole's solution. Writing

$$B_n = -\frac{2\pi(-1)^n \nu}{\sinh(\nu n\pi^2 t/l^2)}$$

then equation 5.3 can be written as

$$u(x,t) = \sum_{n=1}^{\infty} B_n \sin(n\pi x) \tag{5.4}$$

Thus since ν is very small Cole showed for $t > t_1$ that approximately

$$B_n \sim -\frac{2(-1)^n}{n\pi t} \tag{5.5}$$

Thus the coefficients $B_n \sim 1/n$. From figure 5.2 it is seen that the decay for $k > 1$, where k is the integer wavenumber in this numerical work is $\propto 1/k^2$ and hence in agreement with Cole. For large times

$$B_n = \frac{-4\pi}{R}(-1)^n \exp -(n\pi^2 t/R) \tag{5.6}$$

and B_n falls exponentially with increase in n. Thus Cole's solution shows that there is a growth in energy in all wavenumbers $n > 1$ at $t > 0$ but with increase in time the high wavenumbers fall in amplitude as $1/nt$, although ultimately they fall as $\exp(n\pi^2 t/R)$ as shown in equation 5.6. At any time and when the Reynolds number is high, the spectral energy in the high wavenumbers becomes increasingly small and effectively there

is a high wavenumber cutoff, which can be related to viscous dissipation. Clearly the amplitude decay of $1/n$ cannot continue to very large wavenumbers for it produces spectral energy$\sim 1/n^2$ which in turn generates an infinite dissipation unless $\nu = 0$.

For the sine wave, the first term in equation 5.1 is zero and only B_1 exists. At $t > 0$ it can be seen by reference to Cole's solution the amplitudes of all the harmonics can be determined and the wavenumbers beyond $k = 1$ are all populated. Thus at all times the Fourier coefficients of the sine series are generated.

The reason for the population of the higher harmonics can also be explained in the physical domain arising from nonlinear distortion governed by the nonlinear term $(u\partial u/\partial x)$ in the Burgers equation. The fundamental decreases in amplitude thereby increasing the amplitude of the second and higher harmonics it produces due to 'sum and difference' mechanism. The phases of these harmonics alternate and obey Cole's solution. Thus when $u = \sin nx$, then $\partial u/\partial x = n\cos nx$ then the nonlinear term in the Burgers equation is

$$u\frac{\partial u}{\partial x} = \frac{n}{2}\sin(2nx) \tag{5.7}$$

so there is now a fundamental and its second harmonic which gives a sine component as seen in equation 5.7 which then generate higher wavenumbers. ie the interaction between an n^{th} harmonic of u with an m^{th} harmonic of $\partial u/\partial x$ generates contribution to wavenumbers such as $(n + m)$ and $(n - m)$ respectively. This is normally known as the population of high wavenumbers by the 'sum and difference' mechanism. Accordingly it is seen from figure 5.2 the fundamental decreases in amplitude, the second harmonic, the 3rd harmonic and so on increase and smoothly decay at large times.

5.2 Harmonic $(k = 2)$ of small amplitude added to the fundamental $(k = 1)$ of unit amplitude

Figure 5.3 shows the results for the interaction between a harmonic of small amplitude (0.1) superimposed in phase on the fundamental of unit amplitude for Reynolds number of $R = 200$. The corresponding development of spectral coefficients, $E(k)$, with time is shown in figure 5.4. It is seen that the fundamental loses energy slowly and transfers energy to its higher harmonics rapidly for $T > 0$. A remarkable feature of the plots of

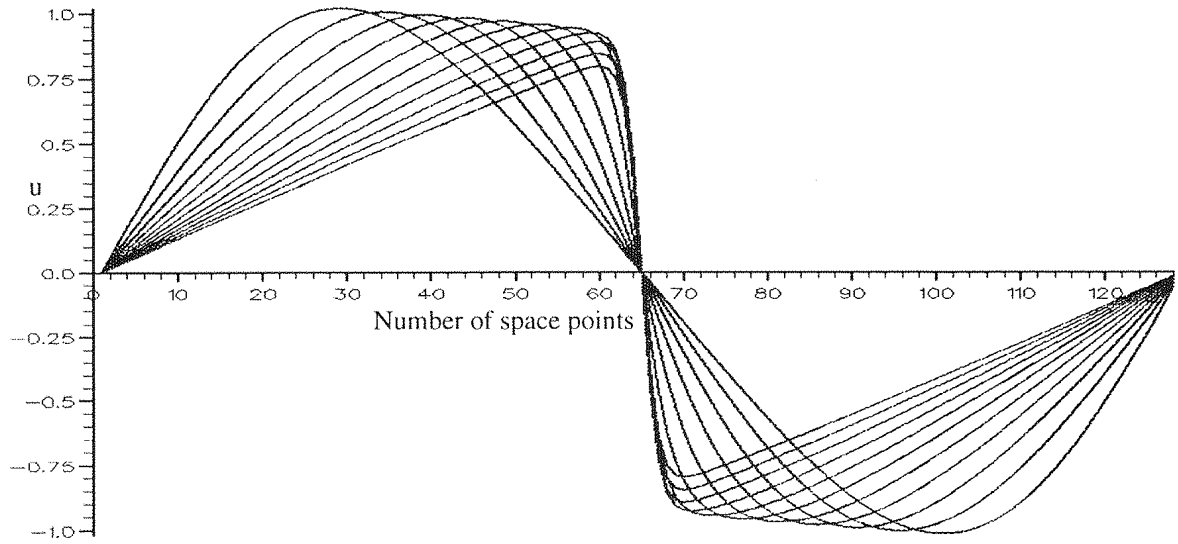

Figure 5.3: Velocity distribution. Initial condition: Sine wave of amplitude 1 + 2nd. harmonic of amplitude 0.1 in phase with the fundamental and $R = 200$. $T = 0, 0.5, 0.75, 1.0, 1.25, 1.75....$.

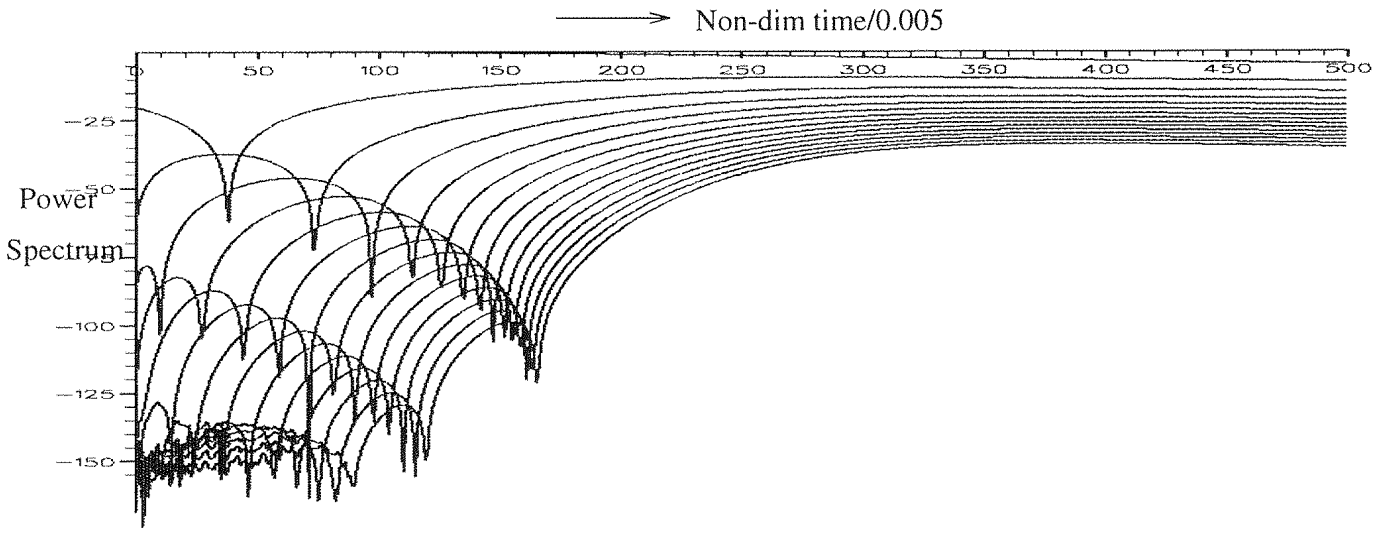

Figure 5.4: Change in spectral energy with time. Initial condition: Sine wave of amplitude 1 + 2nd harmonic of amplitude 0.1 in phase with the fundamental at $k = 1, 2, 3...$ and $R = 200$

$E(k)$ against time for each value of k shown in figure 5.4 for $R = 200$, is the rapid growth of each spectral component followed by a rapid fall represented by a succession of cusps. These are confined to the initial wave distortion before the time when the wave approaches its ramp-like waveform near the shock formation time. After the shock formation time the spectral energy coefficients all decay smoothly in amplitude as was found for the case

of the sine wave alone.

The sine harmonic superimposed on the sine wave can be written in Fourier series represented in equation 5.1 where all $A_n = 0$. B_1 denotes the fundamental sine wave and B_2 is the added harmonic. Wu's(1990) analytic work describes the superimposed harmonic in phase with the fundamental which he refers to as 'pre-biased'. Such a superimposition which is investigated here, delays the shock formation time since the initial wave is distorted away from the mid position[see figure 5.3]. In Wu et al's analytic model for the superimposed harmonic, a cusp was obtained in the wavenumber spectrum arising from the energy redistribution phenomenon where there is interaction between the fundamental and the second harmonic. It is seen from the figure 5.4 that as the energy in the fundamental decreases, the energy in the second harmonic increases. The results are in agreement with Wu's results when cusp was formed when the harmonic was superimposed on the fundamental sine wave. In addition more cusps were formed for higher wavenumbers. The present numerical work goes even further and investigates the case of superimposed cosine harmonics with the fundamental. Wu's work does not predict the cusping phenomena at the shock formation time.

The present work shows that cusps are not formed in the wavenumber spectrum after the 'shock formation time' and hence the cusping phenomena is only due to the nonlinear interactions giving rise to redistribution of energy in the wavenumber spectra. It is known that the Cole's solution for the sine wave is an exact solution in which the Fourier coefficients alternate in phase. This is shown schematically in figure 5.5:(a) is the sine wave at $T = 0$ and (b) at $T >> 0$. At $T > 0$, the solution evolves dominated by the nonlinear effects undergoing sum and difference mechanism and the pattern 5.5b) in the Fourier coefficients is obtained when the sawtooth wave is formed.

As soon as a harmonic is superimposed on the initial sine wave the evolution of the Fourier coefficients becomes more complex. The fundamental on its own produces higher harmonics, the superimposed harmonic produces higher harmonics and the interaction between the fundamental and the superimposed harmonic also produces harmonics. The resulting spectrum does not initially display the alternating phase pattern characteristic of Cole's solution. The signal evolves so that, by the shock formation time, a series of sawtooth waves is formed with a spectrum similar to that of Cole's solution. ie. with wavenumber components of alternating phase. During the transition period, between $T = 0$ and the shock formation time, the structure shifts towards the stable alternating

pattern by means of a series of phase reversals in the various wavenumber components, which correspond to the cusping events. This process becomes very complicated, with the number of phase reversals increasing in the higher harmonics. This process continues until the appearance of the sawtooth wave, when the Fourier coefficients cease to undergo phase reversal. Thus once the sawtooth is formed the Fourier coefficients alternate in phase and converge to a pattern shown in figure 5.5(b) which is the Cole's solution. Thus Cole's solution is a stable solution and any superimposed harmonic will eventually obey when the sawtooth wave evolves.

For wave numbers other than the fundamental the energy falls rapidly towards zero as shown in figure 5.4 at certain times, and appears in the plots of logE(k) as a cusp followed by an increase as the coefficients again become populated in the spectral energy.

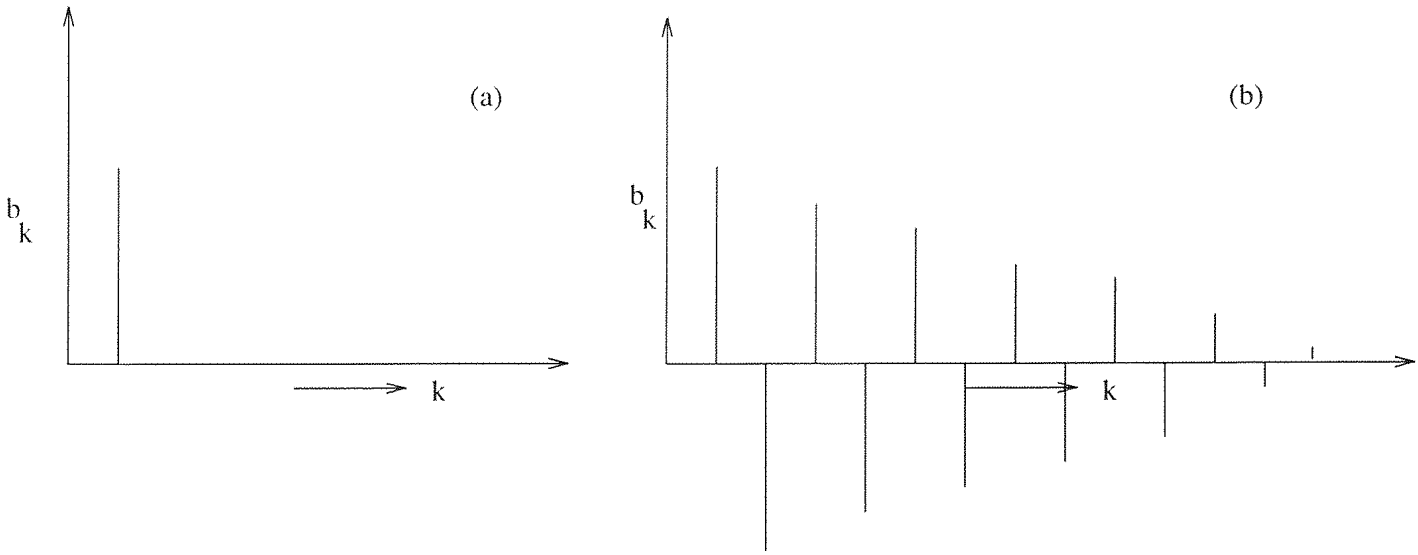

Figure 5.5: (a) Discrete Fourier coefficient b_k for the sine wave at $T = 0$,
(b) Fourier coefficients b_k's for sine wave at $T >> 0$.

Thus cusps arise when the Fourier coefficients are zero due to the 'sum and difference ' mechanism of the nonlinear term. Cole's solution for the sine wave is a steady solution where the phases of the harmonics alternate. When the superimposed harmonic is introduced, the nonlinear effects disrupt this alternating phase behaviour, which is Cole's steady state solution. They eventually after the shock formation time converge themselves to the steady state solution of Cole's with phases alternating. The results presented here are similar to Wu's analytic work where cusps are formed when the added harmonic is in phase with the fundamental. The present investigation is more complex than Wu's since

in this investigation cases are considered where there is a phase difference from $0 - 180^0$ and also third and higher higher harmonics are present. Hence Wu's analytic solution cannot be used in such cases. Wu used the boundary value form of the Burgers equation, with time replaced by distance, where as the present work is based on the initial value problem of the Burgers equation. In the spectral evolution the fundamental in isolation, would obey Cole's solution with the Fourier coefficients B_n's alternating in phase. Thus for the sine wave, at $T > 0$ the 2nd harmonic would be in opposite phase with the fundamental, the 3rd harmonic in phase with the fundamental and so on as described above. But once the fundamental encounters a superimposed harmonic at $T > 0$ which is in phase with the fundamental, the fundamental on its own produces a 2nd harmonic of opposite phase which adds up with the already existing 2nd harmonic and the result is that amplitude is reduced, forming a cusp. The fundamental produces harmonics, the superimposed harmonics produce higher harmonics, there is interaction between the fundamental, the superimposed harmonic and the higher harmonics all governed by the 'sum and difference' mechanism. This process of addition and subtraction continues and clearly with increase in harmonics the process gets even more complicated and more cusps are formed, which is in agreement with the results shown in figure 5.4. Thus cusps are formed due to the sum and difference mechanism which arise from the nonlinear term in the Burgers equation.

It is seen from figure 5.4 that the cusps form envelopes which asymptote to a particular time. Thus the $m = 1^{\text{th}}$ corresponds to the envelope formed by the last cusp of each wavenumber. Thus the asymptotic time ($T_a = 1.4$) for sine wave superimposed with small amplitude as seen in figure 5.4 corresponds to the time of maximum gradient for the distorted sine wave. The time when the peak occurs is the shock formation time.

5.2.1 The variation of cusp formation with wavenumber

The variation of the cusp formation with time for a given wavenumber associated with a superimposed harmonic of equal amplitude is given in figure 5.4 and shows that the number of cusps formed increases with increase in wave number. It is seen there is almost a linear increase in the number of cusps with wavenumber. To detect a cusp, the wavenumber spectrum with time for each wavenumber was scanned. Whenever the energy between the wavenumbers suddenly fell, this implied a cusp was present. This is the three point approach. The three points are the 3 time coordinate interpolations. This was considered not very accurate since cusps can occur between any 2 time step and a cusp can be lost.

So the 7 point approach was made use when 7 time interpolation were performed to detect a cusp. Thus all the cusps were detected. Since more cusps are formed for large wave numbers it becomes more difficult to detect cusps as the wavenumber is increased.

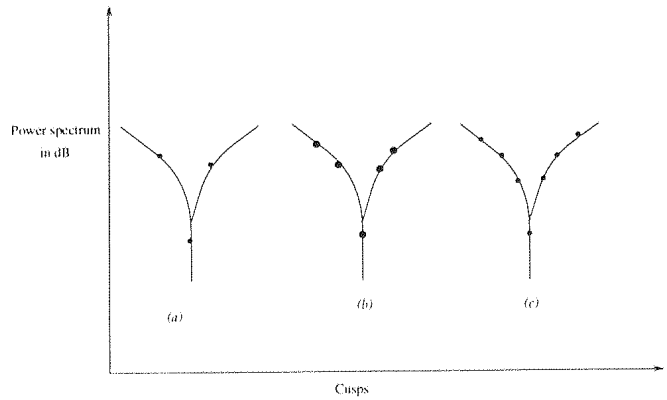

Figure 5.6: Three, five and seven point time interpolation to detect a cusp

It was observed that the amplitude of the harmonic is further decreased, cusps did occur and the asymptotic shock formation time approaches that of the sine wave.

Figure 5.7 shows the results for low Reynolds numbers ($R = 20$). Here the viscous broadening greatly exceeds the nonlinear steepening. Shock wave is formed but the shock thickness is large in this case. The wave quickly reduces to a sine wave of small amplitude.

newpage

5.2.2 Harmonic ($k = 2$) of equal amplitude added to the fundamental ($k = 1$) of unit amplitude

Figure 5.8 shows the results when a harmonic of equal amplitude is added to the initial periodic fundamental sine wave of unit amplitude, when the Reynolds number is 200. The temporal changes in the energy spectrum are shown in Fig 5.9 and the change in the amplitude with time are shown in figure 5.11. It is seen clearly in figure 5.11 that the Fourier coefficients undergo phase reversal and this trend increases with wavenumber. The energy in the fundamental initially increases but then decays at greater times. The formation of the cusps for all other wavenumbers for $k > 1$ increased with increase in the wavenumbers. A similar pattern of the formation of cusps observed in the earlier case is seen here. It is seen from Fig 5.9 that the cusps form envelopes which asymptote to a particular time. Thus the $m = 1^{\text{th}}$ which corresponds to the envelope formed by the last cusp of each wavenumber similar to the case described earlier for the superimposed

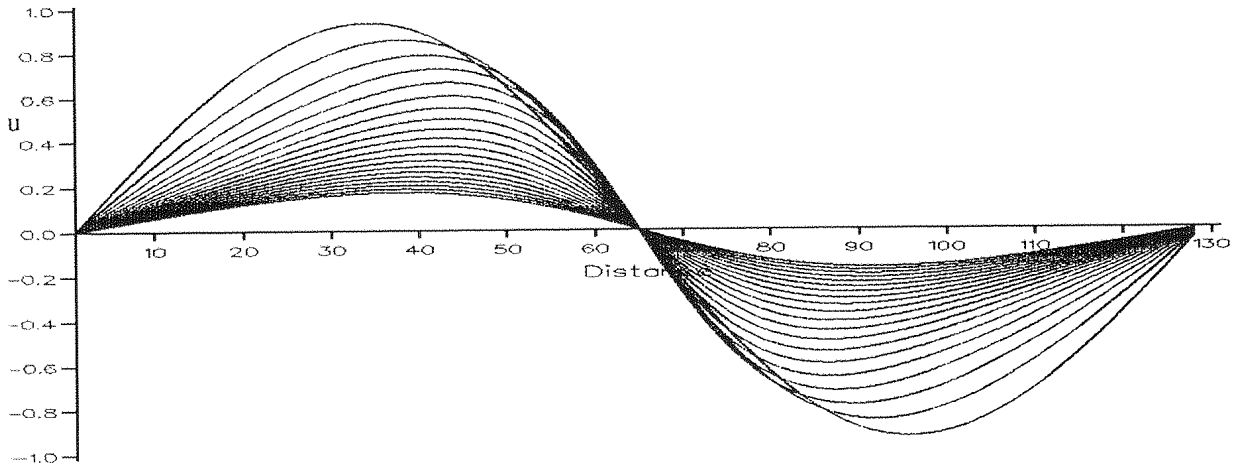

Figure 5.7: Effects of low Reynolds number $R = 20$. Initial condition: Sine wave of amplitude 1 + 1 harmonic of amplitude 0.1 in phase with the fundamental. $T = 0, 0.5, 0.75, 1.0, 1.25, 1.75.....$

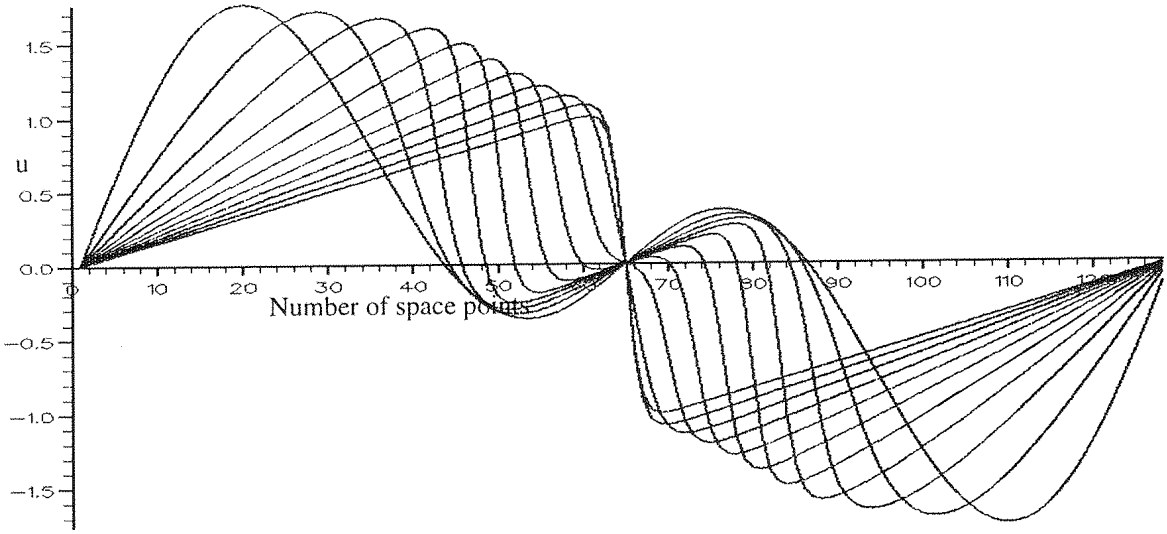

Figure 5.8: Velocity distribution. Initial condition: Sine wave of amplitude 1 + second harmonic of amplitude 1 in phase with the fundamental. $R = 200$.
$T = 0, 0.25, 0.5, 0.75, 1, 1.25, 1.5, 1.75...$

harmonic of small amplitude. This $m = 1^{\text{th}}$ envelope of cusps as shown in figure 5.9 occurs at a later time than for the case of small harmonic superimposed on the fundamental shown in figure 5.4. Comparing the present case with that of small amplitude, it is seen that the number of cusps formed increases with the initial amplitude of the harmonic.

A regular pattern of cusps with increased wave number is observed in figure 5.9. The first cusp for wavenumber $n = 2$, the second harmonic, is always at a greater time than the

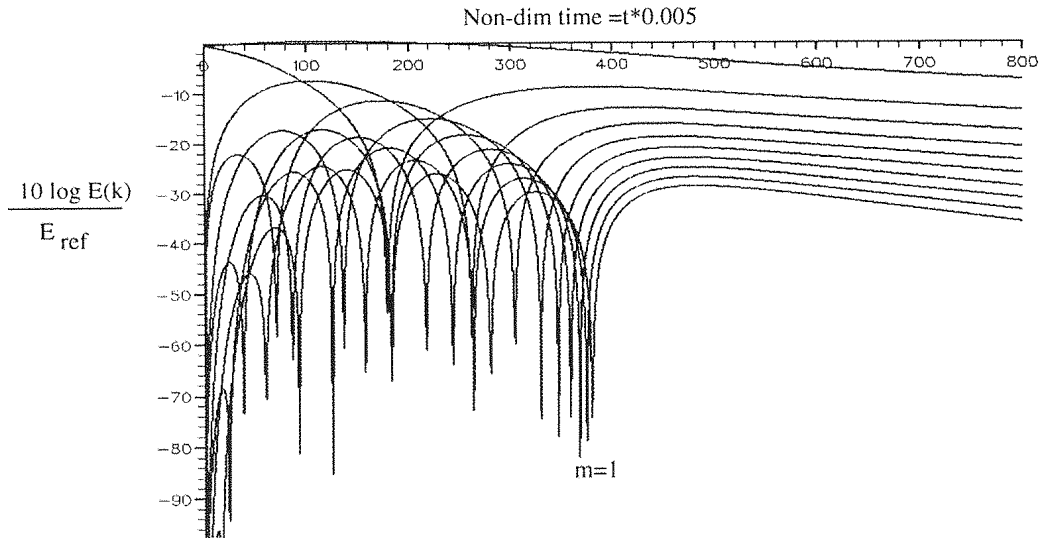

Figure 5.9: Change in spectral energy with time. Initial condition: Sine wave of amplitude 1 + second harmonic of amplitude 1 in phase with the fundamental at $k = 1, 2, 3...$ and $R = 200$

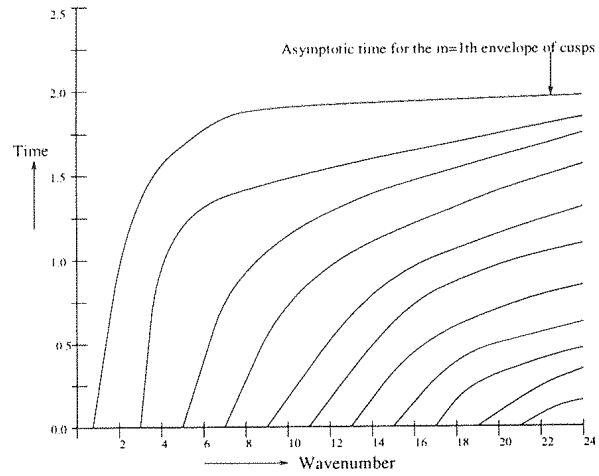

Figure 5.10: The time of cusp formation for $m = 1^{\text{th}}$ envelope ≈ 1.75 . Initial condition: Sine wave of amplitude 1 + second harmonic of amplitude 1 in phase with fundamental. $R = 200$

cusp for $n = 3$ and so on. For high wavenumbers, it is observed that cusps are embedded so closely that it is difficult to distinguish them. The number of cusps increases linearly with the wave number. The local peaks of all the spectral energy curves around the cusps form envelopes. These envelopes do not occur after a certain time and have an asymptotic behaviour with time for all wavenumbers. Various envelopes of cusps shown in figure 5.9 for Reynolds numbers 200 are plotted against time in figure 5.10. Each envelope of cusps

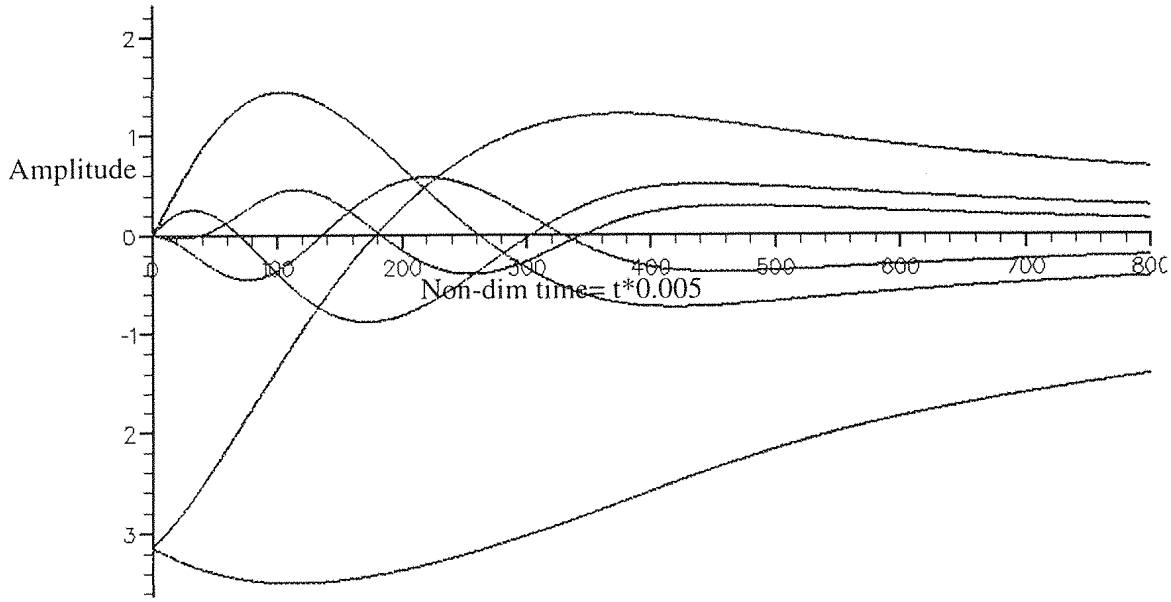

Figure 5.11: Change in amplitude verses time. Initial condition sine + second harmonic of amplitude 1 in phase with the fundamental at $k = 1, 2, 3, 4, 5$. $R = 200$.

asymptotes to a certain time called the asymptotic time. In the figure 5.9, the asymptotic time for the $m = 1^{\text{th}}$ envelope of cusps (which is also the envelope formed by last cusps of each wavenumber) corresponds to the 'shock formation time ' defined in equation 2.57 in chapter 4. This asymptotic 'shock formation time is shown in figure 5.4 and 5.9 for the two cases respectively.

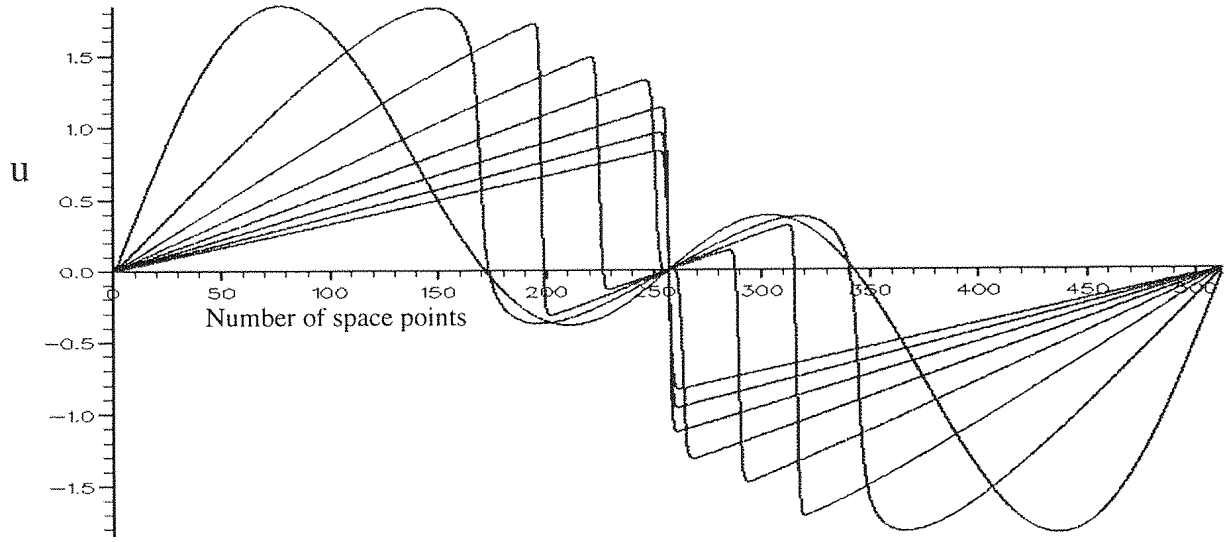

Figure 5.12: Velocity distribution. Initial condition: Sine wave of amplitude 1 + second harmonic of amplitude 1 in phase with the fundamental. $R = 500$.
$T = 0, 0.5, 1, 1.5, 2, 2.5, 3, 3.5$

Figure 5.10 clearly shows the asymptotic time for the superimposed harmonic of equal amplitude. This would accordingly corresponds with the shock formation time. This is the time when the middle N wave is formed and is seen more distinctly in figure 5.12.

Comparison of the asymptotic time with the shock formation time for harmonics with varying amplitude is given in table 5.1. Comparing them it is clear that the asymptotic time approaches the shock formation time. After this time no envelopes were observed but the nonlinear effects are dominant, which is indicated by the rise in the spectral energy.

The change in the velocity distribution with time shows the change in wave pattern has the form of two ramp functions separated by the middle N-wave as seen in figure 5.12. From then onwards the wave looks similar to that of the distorted sine wave. At large time, increased viscous dissipation causes the wave to progress downstream with reduced energy obeying Cole's solution until it finally reduces to a sine wave of vanishingly small amplitude.

The change in phase observed at the formation of the cusps is of particular interest. There is a change in phase of 180^0 of the Fourier coefficients at the formation of each cusp. From the above results it is concluded that energy transfers both in the low and high wavenumbers and is mainly dependent upon the initial conditions.

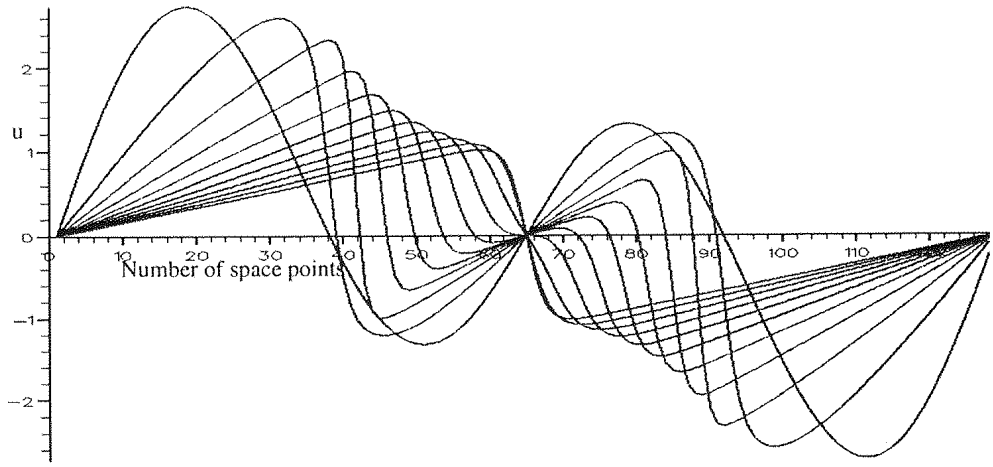

Figure 5.13: Velocity distribution at various times for sine wave of amplitude 1 + second harmonic of amplitude 2 in phase with the fundamental. $R = 200$.
$T = 0, 0.5, 0.75, 1.0, 1.25, 1.75....$

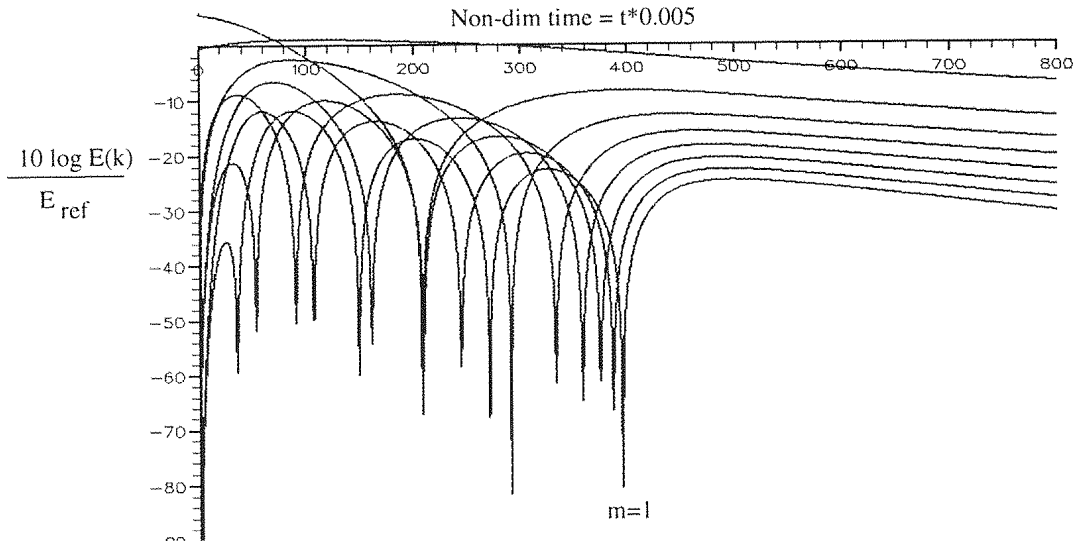

Figure 5.14: Change in spectral energy with time. Initial condition: sine wave + second harmonic of amplitude 2 in phase with the fundamental. $R = 200$.
$k = 1, 2, 3....$

5.2.3 Harmonic $(k = 2)$ of large amplitude superimposed on the fundamental $(k = 1)$ of unit amplitude

Figure 5.13 shows the waveform and figure 5.14 the wavenumber spectrum of a superimposed harmonic of large amplitude than the fundamental for Reynolds number of 150. A harmonic of larger amplitude on the fundamental behaves similarly to that of equal amplitudes except that the asymptotic time of the first envelope in this case is at a larger time then the superimposed harmonic of small and equal amplitude. Thus the shock formation time gets delayed by increasing the amplitude of the harmonic.

5.3 The distortion of the waveform in the $x - t$ space

The changes in the geometry of the wave with time are more complex when the initial periodic wave has superimposed harmonics as shown by comparison between figures 5.3, 5.8 and 5.13. It is shown the wave distortion due to nonlinear effects is produced according to the signs of the velocity in the adjacent domains. Thus domains in which u is negative move towards the left of a zero, and where u is positive the distortion is to the right. This results in a ' steepening ' of the wave in both the domains. After a while the steepening develops into two ramp functions but as time increases the nonlinear process becomes overshadowed by viscous dissipation and the wave finally reduces to the form of a sine

wave of small amplitude. The formation of shocks is more clearly seen when the Reynolds number is high as seen in figure 5.12. The steep wavefronts eventually form a ramp function which can be regarded as almost inviscid. The shock thickness is negligible compared with that found in the low Reynolds number case of figure 5.8. The asymptotic time when the wave develops into a near sawtooth is given in table 5.1 and described earlier for all the three cases discussed above. It is compared with the time of the last maximum gradient, which is the gradient for the sine wave, $(\partial u/\partial x)$ is maximum at the beginning of a shock wave in all cases studied in the present work. At large times the wave gradually decreases in amplitude and the wave approaches that of the sine wave of reduced amplitude. In this range of large times the high wavenumber components are destroyed due to viscous dissipation.

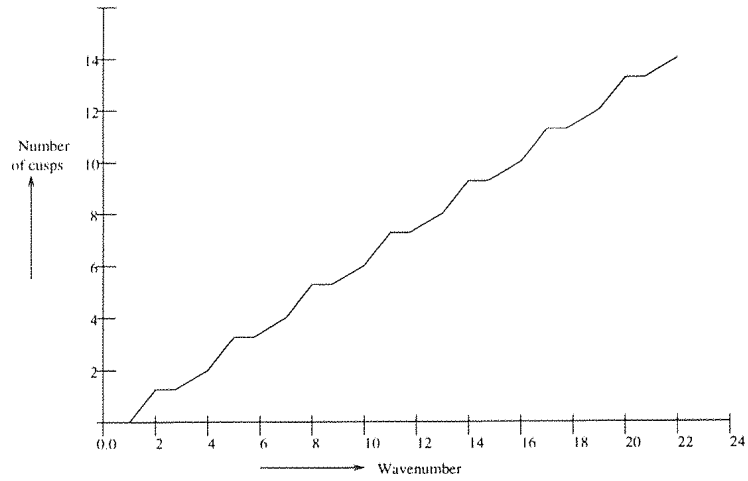

Figure 5.15: Number of cusps verses wavenumber. Initial condition: Sine + superimposed second harmonic of amplitude 1 in phase with the fundamental. $R = 200$

Amplitude of 2nd Harmonic	Asymptotic time T_a	time at which last $T_s = (\frac{\partial u}{\partial x})_{max}$ occurs
0.0		1
0.01	1.4	1.6
0.1	1.6	1.85
1.0	2.3	2.45
2.0	2.3	2.5
4.0	2.5	2.58

Table 5.1: Harmonics of different amplitudes superimposed on the initial sine wave of amplitude 1. $R = 150$. The asymptotic time and the time at which the last $(\frac{\partial u}{\partial x})_{max}$ occurs are also shown.

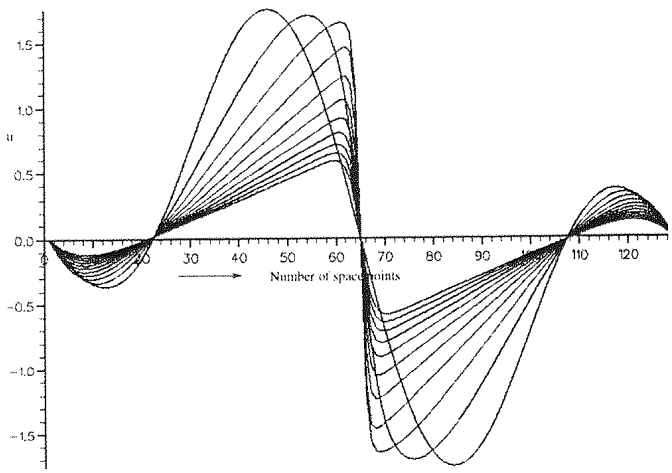

Figure 5.16: Velocity distribution for sine wave of amplitude 1 + second harmonic of amplitude 1 with opposite phase to the fundamental. $R = 200$.
$T = 0, 0.5, 0.75, 1.0, 1.25, 1.75.....$

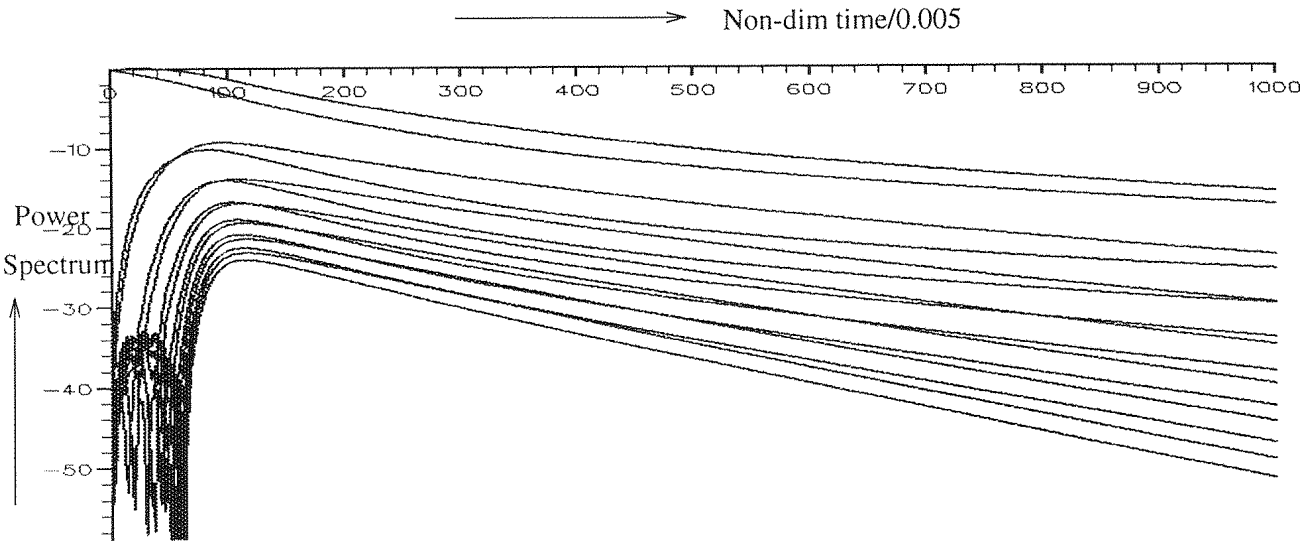

Figure 5.17: Change in spectral energy with time. Initial condition: Sine + second harmonic of amplitude 1 with opposite phase. $k = 1, 2, 3...$ and $R = 200$

5.4 Harmonic($k = 2$) of equal amplitude but opposite phase added to the initial periodic fundamental($k = 1$) sine wave

A change occurs in the wave pattern when a harmonic of equal amplitude but opposite phase is added to the fundamental is shown in figure 5.16 along with the corresponding changes in the spectra shown in figure 5.17. In such a case of the superimposed harmonic in opposite phase with the fundamental, the wave at $T = 0$ is distorted towards the mid-position as seen in figure 5.16. The Reynolds number was equal to 200. The sine wave superimposed with harmonic of opposite phase can be written in the form of the Fourier series expressed in equation 5.1. $A_n = 0$ at $T = 0$. But B_1 is the fundamental and and $B_2 < 0$. Hence the shock is formed earlier than the pure sine wave. The fundamental decays in amplitude and transfers energy to the higher harmonics. It is shown that a rapid growth in energy of other harmonics is found to occur at small times. No cusps were observed in these results implying that there were no zeroes in the Fourier coefficients at any time. Hence although sums and differences in the interactions occur, they did not result in switching of phases from $+180^0$ to -180^0 in the Fourier coefficients. These results are in agreement with Wu's results where no cusp was formed when $B_2 < 0$. The harmonics appear to grow in pairs with time and their spectrum at any time differs from

that of the evolving spectrum due to the pure sine wave. For the sine wave the phase for all wavenumbers was alternating according to Cole's approximate solution (see equation 5.3) at all times. The shock formation time in this case is $T_s = 0.8$ which is earlier to the shock formation time for the pure sine wave where ($T_s = 1$). Thus superimposing the sine wave with a harmonic of opposite phase causes the shock formation time to appear earlier than that of the pure sine wave. In the present numerical results for the superimposed harmonic of opposite phase with the fundamental, the spectral energy falls as a smooth function of time at large times and the phases of the Fourier coefficients alternate. In the space time domain there is a wave distortion due to the nonlinear effects but at large times this is overtaken by increased viscous dissipation causing the wave to propagate downstream with reduced energy until it finally dies away.

5.5 An initial periodic sine wave with a superimposed cosine harmonic

When a cosine harmonic is superimposed on an initially periodic sine wave it was found the distortion with time differed greatly from the results obtained in section 5.2. A notable feature was that cusps occurred in this case too.

The cosine harmonic superimposed on an initially periodic sine wave is expressed in the Fourier series described in equation 5.1. Wu has not dealt with this situation of the cosine harmonic. But the change in the amplitudes of the A_n's and B_n's was found to be different from the previous case of the added sine harmonic in phase with the fundamental. It was observed that cusps were formed in the wavenumber spectrum with time, though these were different from those observed for the superimposed sine harmonic described earlier.

Initial Wave with amplitude	Amplitude of the 2nd cosine Harmonic	Shock formation time (T_s)
Sine (1)	0.1	2.1
Sine (1)	1.0	2.6
Sine (1)	2.0	3.1

Table 5.2: 'Shock formation times' for the superimposed cosine harmonics. $R = 200$.

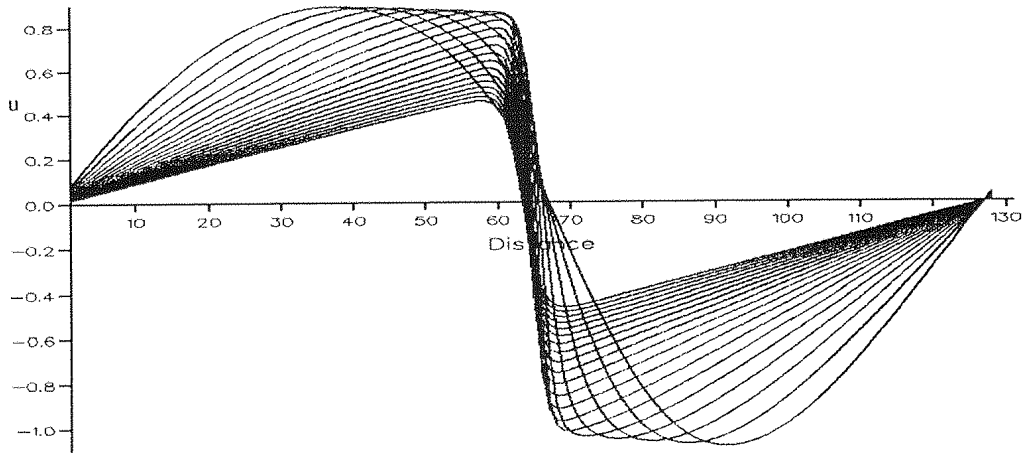

Figure 5.18: Velocity distribution. Initial condition: Sine (amplitude 1) + Cosine harmonic of amplitude 0.1. $R = 200$. $T = 0, 0.5, 0.75, 1.0, 1.25, 1.75...$

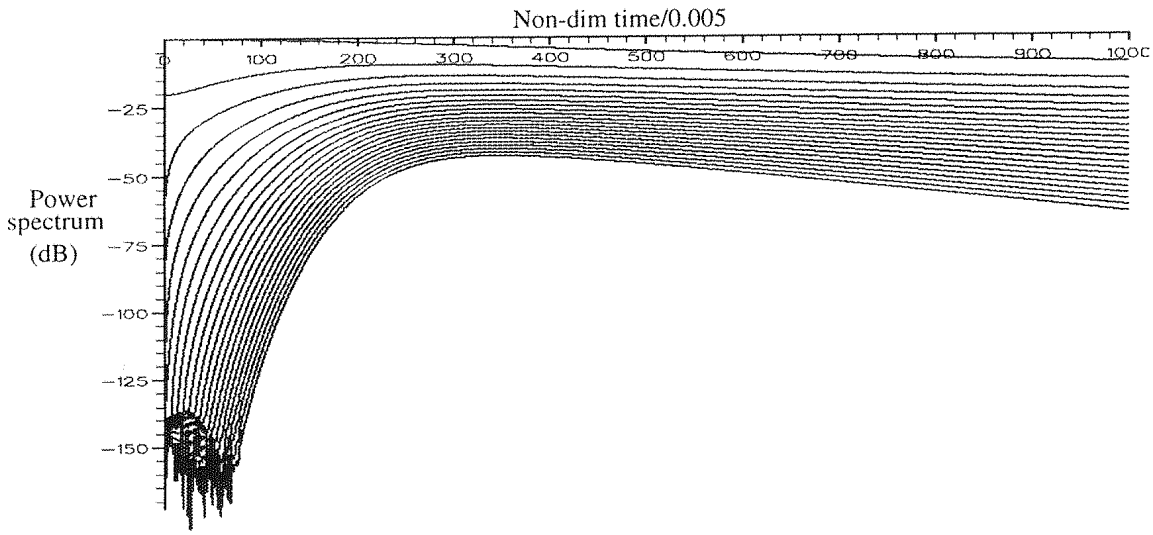

Figure 5.19: Change in spectral energy with time. Initial condition: Sine (amplitude 1) + Cosine harmonic of amplitude 0.1. $k = 1, 2, 3...$ and $R = 200$

Harmonic($k = 2$) of various amplitudes added to the fundamental($k = 1$)

A cosine harmonic of $k = 2$ of small(0.1), equal (1.0) and large (2.0) amplitudes were superimposed on the fundamental sine wave of amplitude (1.0) as shown in figures 5.18, 5.20 and 5.22 respectively for an initial Reynolds number of 200. The corresponding spectra are given in figures 5.19, 5.21 and 5.23 respectively. A study of the wavenumber spectrum with time for all these cases was made. The shock formation time in each case is greater than the sine wave superimposed with sine harmonic having the same amplitude. Thus $T_s = 2.6$ for the case of superimposed cosine harmonic of equal amplitude, whereas

the corresponding case of sine harmonic with equal amplitude has $T_s = 2.45$. Cusps are not formed for the added cosine harmonic of small amplitude but as the amplitude of the harmonic is increased beyond 0.1, cusps are formed, but is different from the spectrum of the superimposed sine harmonic. The spectrum looks undulated upto the shock formation time after which it becomes smooth, when the spectrum would obey Cole's solution for the sine wave. At very large times it is expected the wave to asymptote into a sine wave of small amplitude.

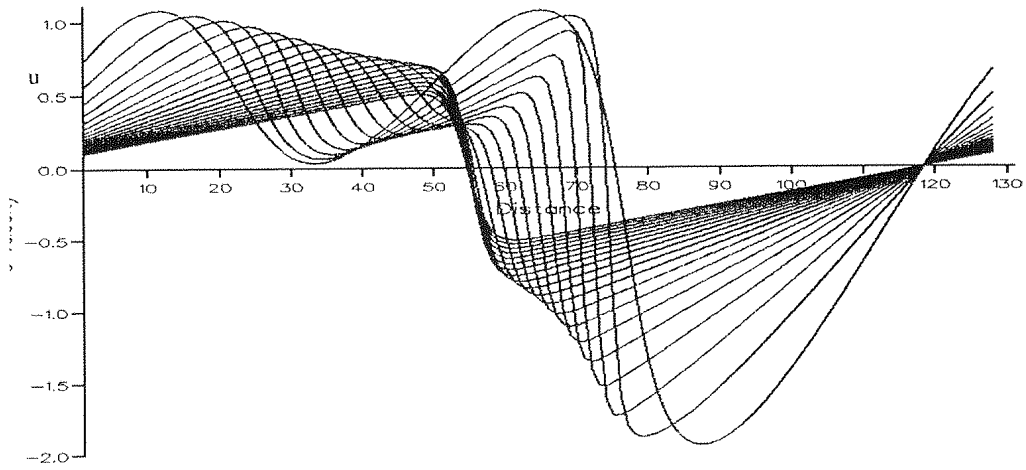

Figure 5.20: Velocity distribution. Initial condition: Sine (amplitude 1) + Cosine harmonic of amplitude 1. $R = 200$. $T = 0, 0.5, 0.75, 1.0, 1.25, 1.75...$

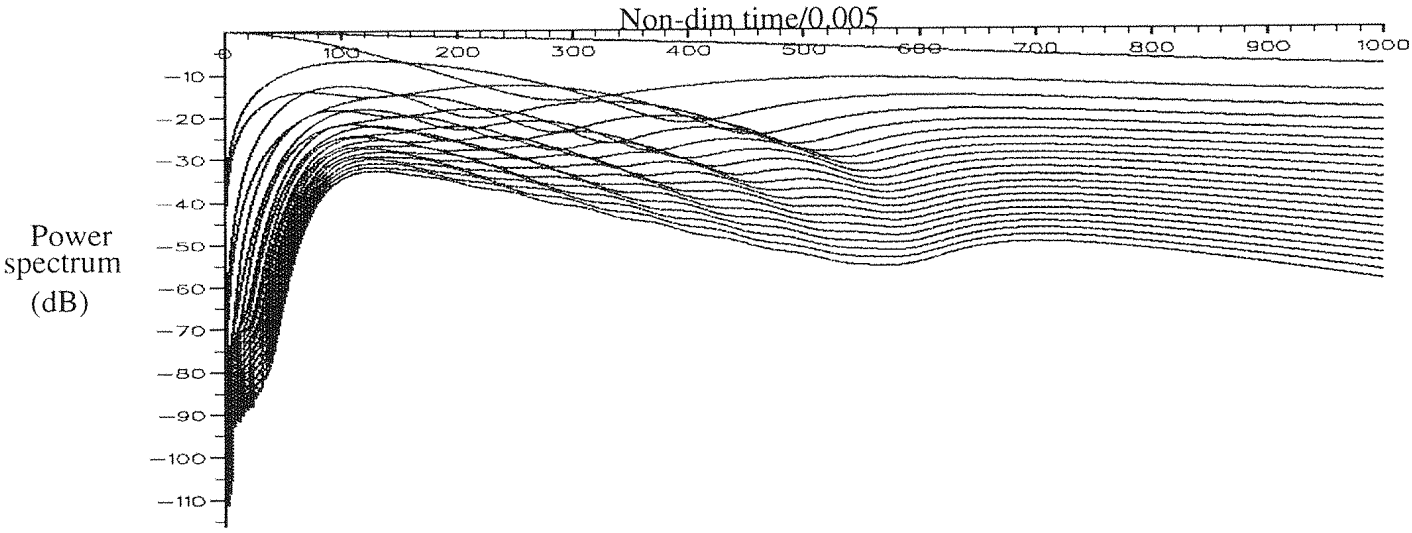

Figure 5.21: Change in spectral energy with time. Initial condition: Sine (amplitude 1) + 1 Cosine harmonic of amplitude 1. $R = 200$. $k = 1, 2, 3...$

It is seen in figure 5.18 that the superimposed cosine harmonic of small amplitude(0.1) is very different from the superimposed sine harmonic of small amplitude in phase with the fundamental described earlier. Adding cosine harmonic increases the amplitude of the wave at $x = 0$, where for the pure sine wave, $u = 0$ at $t \geq 0$. But the overall amplitude for the cosine harmonic in the positive half domain decreases. Though the energy spectrum resembles the sine wave spectrum, shock occurs much later than the sine wave. Table 5.2 gives the 'shock formation time' for the pure sine wave superimposed with cosine harmonic with varying amplitudes. Comparing figures 5.19 and figure 5.4, for the initial condition of small amplitude cosine and sine harmonic respectively, it is seen that the sine wave with

a cosine harmonic does not produce cusps and behaves similar to the sine wave spectrum, whereas the superimposed sine harmonic produces cusps. From the figures 5.18, 5.20 and 5.22 it is seen that as the amplitude of the harmonic is increased the shock formation time also increases.

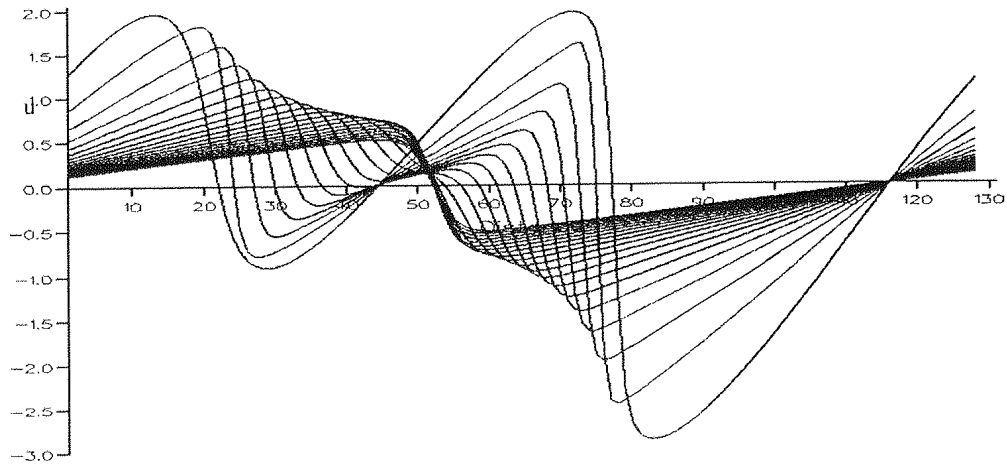

Figure 5.22: Velocity distribution. Initial condition: Sine (amplitude 1) + Cosine harmonic of amplitude 2. $R = 200$. $T = 0, 0.5, 0.75, 1.0, 1.25, 1.75...$ and

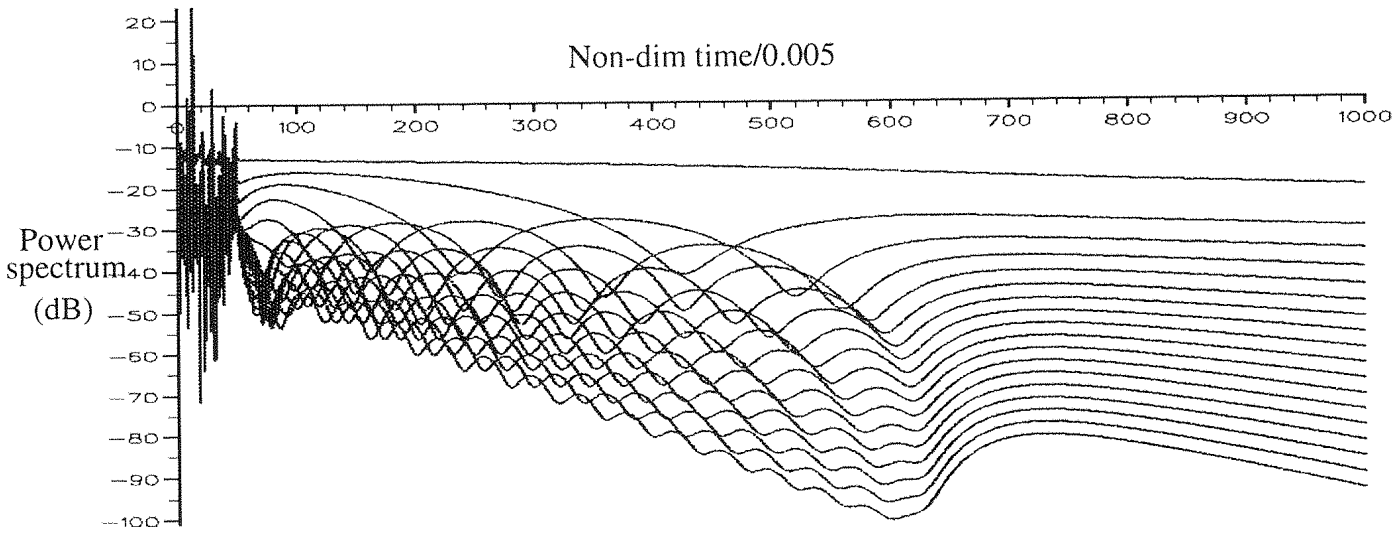

Figure 5.23: Change in spectral energy with time. Initial condition: Sine (amplitude 1) + second cosine harmonic of amplitude 2. $k = 1, 2, 3...$ and $R = 200$.

5.6 Conclusion

The change in the wave distribution structure with distance has been considered for the initial waveforms with simple geometries having periodic boundary conditions. It has been shown that at moderately high Reynolds numbers the wave distortion is dominated by nonlinear effects. The thermo-viscous effects are confined predominantly to the vicinity of the shock waves thus preventing the discontinuity and have a negligible effect on the shock formation time. The changes in the wavenumber spectrum obtained at various times of the propagation are studied in detail for harmonics of various amplitude superimposed on the sine wave. The development of cusps in the Fourier coefficients has been found in the spectrum of the developing wave for various amplitudes of the superimposed harmonics. They arise from the nonlinear term due to the 'sum and difference' mechanism of the harmonics, and occur only up until the shock formation time.

Once a harmonic is superimposed on the fundamental, the harmonics no more alternate because the harmonic add and subtract with the fundamental and the harmonics of the fundamental which at a particular time reduces the amplitude of the harmonic to zero, thus a zero crossing occurs in the Fourier coefficients which is a cusp. The cusping phenomena and hence the shifting of the phases of the Fourier coefficients rearrange themselves to obtain the Cole's solution at the shock formation time in which the phases of the Fourier coefficients alternate. Thus for any superimposed harmonic the nonlinear effects result in a complex sum and difference mechanism, in which phase reversal of the Fourier coefficients take place. But once the shock is formed for any superimposed harmonic, the Fourier coefficients obey Cole's solution which is a stable solution.

It is shown that the number of cusps increases with harmonics. The interaction between the fundamental and higher harmonics, the 2nd harmonic and higher harmonics is even more complicated.

The present results agree with Wu's results for the case of the superimposed sine harmonic on the fundamental. Wu shows that the cusp occurs for the second harmonic only when the phase of the superimposed harmonic(prebias) is in phase with the fundamental. The present work goes further to show the formation of cusps for higher harmonics arising due to the nonlinear effects. It also shows the formation of cusps for the superimposed cosine harmonic.

No cusps are formed when the phase of the harmonic is 180^0 to the fundamental. The

formation of cusps is due to the sum and difference of the energy in each wavenumber resulting in a transfer of the energy from the fundamental to higher wavenumbers. The formation of cusps determines the shock formation time and hence by adjusting the harmonic it is possible to distort a wave which could then travel a greater distance without forming shocks. Thus cusps are formed only upto the shock formation time and hence it is possible to predict the shock formation time by observing the spectra is an important investigation uncovered in the present work. This is an important conclusion arising from the nonlinear propagation of waves of special waveforms.

The numerical results confirmed Cole's conclusions that with increase in time the sine wave becomes distorted and approaches a near sawtooth profile, with the discontinuity being replaced by a shock wave of finite thickness. Its thickness is a function of Reynolds number. For very large Reynolds number the numerical results confirmed that the waveform with an almost discontinuous profile was almost identical with that predicted for inviscid flow in agreement with Cole's solution. Following the shock formation time the amplitude of the shock decreases and the thickness broadens due to viscous effects. Ultimately the wave becomes weak when it approaches a sine wave profile of small amplitude. This asymptotic state of the initial sine wave was an important conclusion of Cole's work and is confirmed in this numerical solution.

Numerical results obtained from CM for the initial periodic distorted sine wave with superposition of harmonics with various phases have shown that although the initial distortion with time can be very different from that of the simple sine wave, nevertheless when the shock wave has reached the mid position, the subsequent decay asymptotes to that of the initial sine wave. Thus in all cases considered here the wave distortion at large time resembles that of the simple sine wave.

Thus superposition of harmonics in and out of phase with the initial periodic fundamental changes the wavenumber spectrum with time and the energy transfer mechanism. A sine harmonic of equal amplitude in phase with the fundamental delays the shock formation time by almost one and half times that of the pure sine wave whereas a harmonic of equal amplitude but opposite in phase causes the shock to appear earlier than that for the pure sine wave. The case of a cosine harmonic superimposed on the fundamental sine

wave is different from the case of sine harmonic for small and large amplitudes. Once the amplitude of the added harmonic is increased, the spectrum for the cosine harmonic, produces cusps, which looks undulated upto the shock formation time. After this time the spectrum becomes smooth, when the spectrum is expected to obey Cole's solution for the sine wave. The shock formation time in each of the cases for the superimposed cosine harmonic is greater than the shock formation time for the corresponding superimposed sine harmonic. The trends observed in all cases show that interactions take place, resulting in the generation of sums and differences of the wavenumber components.

Numerical results for all these cases indicate that energy is transferred from the fundamental to the high wavenumbers and is very dependent upon the initial conditions (ie the harmonic superimposed on the sine wave and its phase with respect to the fundamental sine wave). At large times all these solutions obey Cole's asymptotic solution described earlier, where the phases in the Fourier coefficients of the developing wave alternate and the spectral energy fall as a smooth function of time. On increasing the amplitude of the harmonic it is shown how the shock formation time can be delayed for a periodic signal. The reason underlying the formation of cusps in plots of spectral energy verses time at small times and before the shock formation time for Cole's asymptotic solution for the sine wave to be valid, are the result of wavenumber interactions. However the prediction of the shock formation time for the sine wave with harmonics is dependent on the initial waveform and thus on the presence or absence of cusps in the energy spectrum.

The investigation has shown that dependent on the initial waveform cusps occur at a particular wavenumber at a particular time. It is thus possible from this work to find such a waveform having the necessary conditions of a cusp at a particular wavenumber and propagating it to a desired distance to form a shock.

Chapter 6

Nonlinear Propagation of Random Noise

6.1 Introduction

In chapter 5 the changes in plane wave structure with time have been considered for a simple wave geometry when the initial waveform is a periodic sine wave with a superimposed harmonic. The progressive wave structure at moderate Reynolds number is dominated by nonlinear effects and the thermoviscous effects are confined to the vicinity of the shock waves, preventing them from being discontinuous, which is the case when viscosity is zero. The evolution of the wavenumber spectrum for the superimposed harmonic with time has been studied and it has been shown that as the amplitude of the superimposed harmonic is increased there is a change in the shock formation time. It was also shown that for any simple periodic waveform the wave progresses with time to form a sawtooth like profile provided the Reynolds number is large enough. The subsequent changes in the waveform are then independent of the initial waveform.

In this chapter the aim is to extend the investigation to periodic wave distributions which comprise waves of arbitrary shape and which include sawtooth like structures and ramp functions as well as random noise signals in amplitude and phase at time $t = 0$. In any one period the general waveform chosen is typical of an acoustic random noise signal with a large number of zero crossings as measured in experiment. It was assumed that the initial waveform satisfies Gaussian statistics. This gave the opportunity to study the importance of the development of the waveform under statistics changing from Gaus-

sian initially to non-Gaussian during the propagation in a thermoviscous medium. It was known from previous studies on Burgers equation that the waveform statistics would become non-Gaussian but these latter studies gave little evidence of the extent the change in statistics would have on the changes to the waveform as displayed by the velocity and its derivative at small and large times. Recent work on this subject has been presented by Gurbatov(1991) .

One of the aims of this investigation was to understand the complete physical process of the propagation of an initial Gaussian noise signal comprising a large complex wavetrain for all times both in the physical and spectral domains using the Convolution Method(CM) at large Reynolds number. In particular it was shown that the numerical computation using the (CM) for a random noise signal of finite amplitude propagating in air at high Reynolds numbers showed little difference from inviscid results. This is consistent with the work of Cole and others who showed that the solution to Burgers equation for vanishing viscosity reduced to the limiting inviscid solution. Accurate simulations dealing with such finite amplitude random noise propagating in a thermoviscous medium do not appear to have been published in the open literature.

In this chapter numerical computations of the evolution of the statistical characteristics for a random noise signal are described using CM. It is shown that a high amplitude random noise signal as input develops nonlinearly with time, suffers gross distortion and its spectrum changes. The effects of nonlinearity at first are associated with the formation of shocks and later are accompanied by an increase in absorption due to dissipation resulting in a broadening of the wave. A detailed description of these flow processes together with the energy spectra, signal moments, and probability distributions for an initial Gaussian signal are given for various times. From the changes in the energy spectra the wavenumber interaction processes taking place in the spectral domain corresponding to the wave distortion process in the physical domain were studied. From this it was possible to predict the shock formation time as well as the shock thickness in the physical domain. It was also shown that when the statistics become non-Gaussian they remain non-Gaussian for all time. In the present work two test cases covering different type of initial spectra have been investigated. It is shown that the initial wave distribution of given sample length can be described in terms of its mean kinetic energy, $< u^2/2 >$ and the Taylor microscale,

λ, which together form the Taylor microscale Reynolds number,

$$R_T = \frac{< u^2 >^{1/2} \lambda}{\nu_e}.$$

λ is a length parameter for the initial spectrum and critically depends on the choice of the upper truncation wavenumber and/or the Nyquist wavenumber. Since λ is a parameter determined by the high frequency content in the spectrum, it is convenient to define two further Reynolds numbers but based on the low frequency content of the spectrum. The first is

$$R_p = \frac{< u^2 >^{\frac{1}{2}} l_p}{\nu_e},$$

where l_p is the wavelength corresponding to the integer wavenumber, k_p, at the peak in the spectrum. The second is

$$R_L = \frac{< u^2 >^{\frac{1}{2}} L}{\nu_e},$$

where L is the sample or the periodic length and represents the overall initial Reynolds number of the wave. It is clear that for a given k_p, R_L is proportional to R_p. However $R_T \propto \sqrt{R_p}$ as described in Appendix O.

Following the presentation of results obtained from CM at moderate Reynolds numbers the method is extended to provide results for arbitrary wave distributions, at high Reynolds numbers which are then compared with Lighthill's(1994) inviscid results. Lighthill(1994) has previously shown that for an initial overall periodic waveform of similar type to that used in this work, but comprising a series of sawtooth waves of random amplitude and phase, the time development of the shock waves can be predicted by inviscid theory.

As stated earlier in chapter 1, the nonlinear distortion of an isolated wave leads to the development of a multiple shock wave distribution which can be determined from the Lighthill-Witham theory similar to the solution of the inviscid Burgers equation. The progressive development of the shock wave pattern is also derived by a geometrical description based on the 'equal area rule'. The change in shock wave strength with time is found, which for the plane wave case shows a variation $\sim 1/\sqrt{t}$. As time $t \to \infty$ the multiple shock wave pattern approaches a single N-wave, thus retaining its nonlinear properties for all time, although its strength is ultimately reduced to zero. The wavenumber power spectrum for the N-wave both with or without a finite rise time, or shock thickness, can easily be obtained. The major properties of the spectrum are that the increase at low wavenumbers follows k^2 and at wavenumbers beyond the peak it falls first as $1/k^2$ and at

high wavenumbers, when the rise time is finite, it falls as $1/k^4$. As discussed earlier the numerical solution using the Convolution Method was adapted to determine the progressive distortion of an arbitrary periodic complex waveform at time $t = 0$. The initial wave is assumed to be everywhere continuous and to possess no discontinuities. It was assumed that within the periodic length L, which is equal to the sampling length, a complex wave distribution exists having in particular a very large number of zero crossings. The assumption is made that the periodic wave is one sample of an ensemble of such waves, and that initially it possesses Gaussian statistics. Thus for any given member of the ensemble at $t = 0$, the progressive properties of this wave at all subsequent times could in principle be determined exactly from the solution of Burgers equation using the Convolution Method. However this process is simplified on the assumption of the ergodic hypothesis in which the statistics of the ensemble are approximated by the statistics of any single realization. This approximation was adopted in this investigation.

In chapter 5 it was shown for a wide range of initial waveforms that the energy wavenumber spectra at times greater than the shock formation time decayed as $1/k^2$ over a large range of wavenumbers and the extent of the $1/k^2$ decay increased as the Reynolds number increased. The total energy which can be derived from the integral of the energy spectrum with respect to k, is hence finite for all values of ν including the inviscid case of $\nu = 0$. This was also consistent with Cole's results for the sine wave. The description of the formation for isolated shock wave applies equally to the case of an initial random wave forming multiple shocks, beyond some average shock formation time. The multiple shocks eventually 'bunch' together or 'bunching' as described by Lighthill. However the rate of dissipation, $\epsilon = \nu \int_0^\infty k^2 E(k) dk$, corresponding to an increase in entropy, is finite for all values of ν different from zero, since the $1/k^2$ energy spectrum does not persist to $k \to \infty$. As $\nu \to 0$ a limiting value for ϵ can be found corresponding to the formation of shock waves of small but finite thickness. (The rate of dissipation, ϵ, is only large when $(\partial u/\partial x)^2$ is large and hence most of the viscous dissipation beyond the shock formation time is confined to the shock waves).

In solving Burgers equation the viscosity, ν, must remain finite even when it is vanishingly small. The so called inviscid limit, or $\nu = 0$, cannot produce a real solution beyond the shock formation time. However when ν is vanishingly small the finite solution to Burgers equation differ only slightly, as discussed above, from the inviscid solution with

shock waves of almost zero thickness replacing the triple valued solutions to the Riemann equations which replace Burgers equation in this limit. Thus the so called inviscid solution is one in which a finite rate of dissipation exists and the shock waves are almost discontinuous. Their structure is discussed below. The asymptotic state as $t \to \infty$ of the periodic assemblage of shock waves of random amplitude and phase is of particular interest. Numerical results presented below show agreement with Lighthill's conclusions that the average shock strength decreases as $1/\sqrt{t}$, as the number of shocks in the period decreases due to 'bunching', even though the sawtooth waveform is maintained ultimately approaching that of an N-wave. At large times viscous broadening engulfs the complete wave and the wave loses its non-linear characteristics reducing it to a damped acoustic wave in agreement with Cole's(1951) solution. The case of the propagation of a single plane shock or an assemblage of sawtooth waves in a lossless medium is different. As stated previously in inviscid flow the N-wave retains its shape for all time.

The conservation equations of mass and momentum for the shocks lead to the Rankine-Hugoniot(1870, 1889) relations which predict finite pressure and density differences across them. It is found there is a rise in entropy across the shock wave which is proportional to the cube of shock strength and hence for weak shocks is very small. To a 'good' approximation it can be assumed that the flow is isentropic except at the shock waves itself. Since this increase in entropy can only exist through a dissipation of mechanical energy into heat, it is found that shock waves cannot exist in a lossless medium even though it is a useful approximation to assume at sufficiently high Reynolds numbers that a shock wave exists of near zero thickness. Thus in the interior of the shock wave there exists thermoviscous dissipation processes which provide the necessary entropy increase across the shock as required by the Rankine-Hugoniot relations. The thermoviscous effects prevent a discontinuity from occurring at the shock wave and all fluid processes are continuous across it including the changes from the upstream to the downstream faces. Thus for a given shock strength and viscosity there is an effective finite thickness for the shock wave. For strong shocks this is in general extremely small being a few mean free paths in thickness and for many practical purposes shock thickness can therefore be neglected. However for weak shock waves the thickness is inversely proportional to shock strength and a finite thickness or rise time exists which in some practical circumstances may be greatly amplified when shocks propagate through relaxing media and turbulence.

An important aspect of this rise in entropy and the resultant rate of dissipation of energy is its effect on the progressive changes in the energy spectrum in the high wavenumber domain coupled with changes in shock thickness. The derivation of the energy equation showing the rate of fall of kinetic energy balanced by the rate of energy dissipation is given in Appendix J. At times exceeding the shock formation time it is found a wave of sawtooth form is generated having shock waves at its extremities separated by a region of uniform expansion. The resulting energy wavenumber spectrum increases as k^2 in the low wavenumber and falls as $1/k^2$ in the high wavenumbers with its peak wavenumber near the lower wavenumbers. Thus the total kinetic energy, which is the integral of $E(k)$ over all wavenumbers, is finite. However, the rate of dissipation of mechanical energy into heat, $\epsilon \to \infty$ unless $\nu_e = 0$. As soon as a finite value of viscosity is introduced and bearing in mind that shock wave development involve nonlinear processes, the viscous action is to cause a change in the high wavenumber part of the spectrum and automatically there is a cutoff at some high wavenumber. This can be expressed in terms of the inverse of the Taylor microscale, and results in a finite ϵ. All these mechanisms are built into the Burgers equation and its corresponding energy equation. The dissipative mechanism becomes active following the shock formation time. Thus for any medium the right hand side of Burgers equation is finite.

6.2 The Taylor microscale(λ)

An analysis of the mechanisms controlling the nonlinear development of the wave distribution is crucial in understanding the characteristics of the wave structure at any time. It is essential therefore to determine the scaling laws appropriate in each time domain which describe the detailed physical processes which dominate at a particular length scale. In isotropic turbulence it is well known fact that the large and small scale structures are represented respectively by their integral and Taylor microscales. In isotropic turbulence, as discussed by Batchelor(1956), the Taylor microscale is defined as

$$\lambda = \sqrt{5 \frac{\int_0^\infty E(\tilde{k}) d\tilde{k}}{\int_0^\infty k^2 E(\tilde{k}) d\tilde{k}}}$$

where $\tilde{k}$ is the radian wavenumber and the kinetic energy is

$$KE = \frac{1}{2}\overline{u_i u_i} = \int_0^\infty E(\tilde{k}) d\tilde{k},$$

involving the sum of the squares of the velocity components in three mutually orthogonal directions. In the present work, the constant 5 is reduced to unity in defining the Taylor microscale since the present numerical work deals with one dimensional wave propagation only. Thus in this work

$$\lambda = \sqrt{\frac{\int_0^\infty E(\tilde{k})d\tilde{k}}{\int_0^\infty k^2 E(\tilde{k})d\tilde{k}}}. \tag{6.1}$$

Equation 6.1 shows that the Taylor microscale in finite amplitude wave propagation is the result of the ratio of the total energy to the rate of dissipation. It therefore describes the relative effects of thermoviscous diffusivity to nonlinearity in the propagation of an initial complex wave in a dispersive medium and should be compared with the typical wavelength corresponding to the wavenumber containing maximum energy. Thus λ defines the lower wavenumber in the high frequency end of the spectrum responsible for viscous dissipation. In the corresponding velocity correlation function it describes the radius of curvature of the correlation function at the origin. When a wavenumber spectrum is truncated it is found that λ is related to this truncation wavenumber. When the wavenumber spectrum is truncated at $k = k_T$, the Taylor microscale, λ, is then equal to the ratio of the total energy to k_T. Thus when the energy spectrum is truncated at $t = 0$ but no such truncation is present at $t > 0$, the Taylor microscale decreases from its value at $t = 0$. Appendix N describes the two moments, I_0, I_2 of the energy spectrum function from which the Taylor microscale is defined.

The propagation of one dimensional nonlinear acoustic plane waves and Burgers turbulence, which is also one dimensional, have much in common. There are also some similarities with the theory of isotropic turbulence. From the energy equation it is found that when $< u^2 > \sim 1/t$ so the Taylor microscale $\lambda \propto \sqrt{t}$ [see Appendix N]. In this case the Taylor microscale Reynolds number,

$$R_T = \frac{\sqrt{< u^2 >}\lambda}{\nu_e}$$

is a constant independent of time. A similar result is obtained in both isotropic turbulence and Burgers turbulence. The wave integer k_λ corresponding to λ relates to the end of the inertial subrange in $E(k)$ and the commencement of the dissipation range. Normally the peak of the dissipation occurs at wavenumbers well beyond k_λ with the peak contribution to the dissipation occurring in the Kolmogoroff range of wavenumbers[1]. However when

[1] In isotropic turbulence [Hinze (1959)], the Taylor microscale, λ, is a measure of the average dimension of the eddies that are mainly responsible for dissipation.

$E(k)$ is truncated at a wavenumber, k_T, it is seen that k_λ is closely related to k_T implying that all dissipation then occurs at k_T and hence close to k_λ.

6.3 Statistical Characteristics of a random signal

In signal analysis, the goal is to extract information about a random process by estimating the moments and characteristics of its probability description. However, it is much more difficult to develop a large ensemble of sample functions. It is hence desirable to describe properties and parameters of a random process from a single sample function by using discrete averages as estimators for ensemble averages. For example to estimate the mean of the signal, the average

$$\bar{u} = \frac{1}{N}\sum_{1}^{N} u.$$

A random process is said to satisfy an ergodic theorem if the ensemble averages may be found from a single realisation.

An important aspect of this investigation is the evolution of the statistical characteristics of the random signal with time starting from a given initial signal. In the past 10 years a great deal of research [Gurbatov(1986)] has been done on the change in the statistical properties with time of an initial random signal. The aim has been to derive the probability of the waveform u and its derivatives at any particular time. This requires a complete knowledge of the signal moments and the changes to its probability density function at various times. Hence starting from an initial signal having Gaussian statistics it is necessary to explore how the statistics change with time as a result of nonlinear effects and at still larger times those due to viscous effects.

The definitions of the probability distribution function and the signal moments are given in Appendix H. A complete survey of the statistical properties and higher order moments for Burgers equation is given by Gurbatov (1991). The changes in the statistical properties of the signal with time depend critically on the energy transfer mechanism associated with the nonlinear wave distribution. In Gurbatov(1986) an analytic treatment has shown that this energy transfer process is dominated by nonlinear effects resulting in the growth of higher wavenumbers following a sum and difference mechanism. Naugol'nykh et al(1963) have described the bispectrum as one of the important tools in understanding

wave interaction especially when tones are present. Gurbatov et al(1991) have also discussed the statistical properties of discontinuous waves such as sawtoothed waves and in particular shows that solutions to the linear diffusion equation having Gaussian statistics give rise, on application of the Cole-Hopf transform, to the solution of the Burgers equation in which the statistics become non-Gaussian.

Although the present research is devoted to nonlinear sound propagation it has similarities to the spatial-temporal changes in the properties of Burgers turbulence as discussed by Kraichnan (1990). The changes with time in the PDF's of u and $\partial u/\partial x$ for the acoustic case are described in detail below and are compared with Kraichnan's results. It is shown that an initial Gaussian field u becomes highly non-Gaussian in its derivative $\partial u/\partial x$.

The signal moments, mainly the third moment and fourth moments are important since they provide information on the extent the probability distribution has deviated with time from its initial Gaussian distribution. From the zeroth and second moments at $t = 0$, the Taylor microscale, λ can be derived and from it the shock formation time as well as the rate of dissipation.

6.3.1 Properties for Gaussian statistics

For a process to be Gaussian the following statistical properties need to be satisfied.
(i) The average amplitude of the spatial waveform over the whole domain is zero.
(ii) The skewness or the third order moment is zero.
(iii) The flatness or the fourth order moment is 3.
These moments above may not be sufficient to prove that a signal is Gaussian [2]. It can be shown that if the bispectrum, described later in this report, for a signal is zero then the signal is Gaussian. It should be noted that even when the initial distribution $U(X, 0)$, is Gaussian, it does not mean that the corresponding θ_0, $\partial\theta_0/dX$, where θ_0 is the Cole-Hopf transformed function satisfying the standard linear diffusion equation, should also be Gaussian. However, the initial $\partial U_0/\partial X$ has to be Gaussian if $U(X, 0)$ is Gaussian. It has been shown by Gurbatov(1991) when an initial signal satisfying the diffusion equation is Gaussian, it continues to remain Gaussian for all times. In the present case it was observed that the initial distribution of θ_0 was almost Gaussian.

[2]Definitions of these moments are given in Appendix H

The Convolution Method provides a numerical programme for the evaluation of the propagation characteristics of any arbitrary initial signal provided the initial signal is of a sufficiently long sample length to realise the given statistical properties. Many processes occurring in nature are Gaussian and the Central Limit Theorem, as described by Mayer (1965) helps to explain why the probability distributions of many naturally occurring processes should be Gaussian. Thus a random process resulting from the summation of infinitely many random elementary events will tend to have a Gaussian distributions. Most noise signals are represented as Gaussian processes and as such are easy to describe. However the assumed Gaussian probability distributions may give a poor approximation to the tails of the distribution function and hence such an assumed distribution must be treated with caution. In the present work an initial distribution satisfying Gaussian statistics is chosen by describing its moments. For this initial signal, which is Gaussian, all odd moments are zero (see Lin (1967)).

6.4 Non-dimensional Burgers equation

The non-dimensional form of the Burgers equation is given in equation 2.49 in chapter 2. In this chapter U, X, T and R are the nondimensional parameters and the non-dimensional Burgers equation is

$$\frac{\partial U}{\partial T} + U\frac{\partial U}{\partial X} = \frac{1}{R}\frac{\partial^2 U}{\partial X^2} \tag{6.2}$$

R is the computational Reynolds number, significant viscous effects are generally limited to $R < 1000$. No restrictions are placed on the numerical value of the non-dimensional velocity $U(X,T)$ which is obtained directly from the inverse transform of the initial amplitude spectrum [see section 6.5.2]. Hence in the non-dimensional form of the Burgers equation, the Reynolds number R is large, X varies between 0 to 1, T is small and U fluctuates about large positive and negative values with the average of zero. These conditions were chosen for convenience in performing the computation and do not affect the accuracy of the solution. The Cole-Hopf transformation

$$\theta(X,T) = \exp\left(-\frac{R}{2}\int_0^X U(\xi,T)d\xi\right)$$

reduces equation 6.2 to the standard diffusion equation

$$\frac{\partial \theta}{\partial T} = \frac{1}{R}\frac{\partial^2 \theta}{\partial X^2}$$

and the initial distribution

$$\theta(X,0) = \theta_0(X) = \exp\left(-\frac{R}{2}\int_0^X U_0(\xi)d\xi\right). \tag{6.3}$$

The corresponding value for $\theta_0(X)$ was obtained by an inverse transform of the logarithmic derivative of $\theta_0(X)$ which can also be written in the transformed domain as

$$\theta_0(X_j) = \exp\frac{-iR}{4\pi}\sum_{k=1}^{M}\frac{\tilde{U}_k}{k}\left(e^{i2\pi kj/N} - 1\right)$$

From the initial values of θ_0, U_0, $d\theta_0/dX = (-\frac{R}{2}\theta_0 U)$ can be obtained as given above.

6.4.1 Boundary conditions

The Convolution Method uses periodic boundary conditions for $U(X,T)$ and similarly for $\theta(X,T)$. Thus for the Burgers equation

$$U(0,T) = U(1,T), \qquad \frac{\partial U(0,T)}{\partial X} = \frac{\partial U(1,T)}{\partial X}$$

and for the diffusion equation

$$\theta(0,T) = \theta(1,T), \qquad \frac{\partial \theta(0,T)}{\partial X} = \frac{\partial \theta(1,T)}{\partial X}.$$

6.5 Scaling of digitally generated initial random signals

A detailed description of the scaling laws used to generate the initial power spectrum starting from the Fourier transform of the random noise signal is given here.

6.5.1 Discrete Fourier transform

It is known that the initial waveform of a random signal can be generated by randomising the phases of the Fourier coefficients. A suitable expression for U at time $t = 0$ is

$$U(X,0) = \sum_{n=1}^{\infty} b_n \sin nX + c_n \cos nX \tag{6.4}$$

where b_n and c_n are suitably chosen. From equation 6.4 a corresponding expression can be found for $\tilde{U}(k,0)$ in the spectral domain. This corresponds to the method used in this

investigation. The factors b_n and c_n are Fourier coefficients in the range 0 to 1. Hence it is possible to develop an initial signal by randomising the phases of the Fourier coefficients in the spectral domain.

In order to generate the random signal in the spectral domain a discretised 'time' series in the non-dimensional coordinate X [see Morfey(1994)] is considered. The spacing in X is given by ΔX and noting $0 < X < 1$, since the sample nondimensional length is unity, then for N samples, $N\Delta X = 1$. Thus any value of X_j is given by $X_j = j\Delta X$, and the integer j is such that $(0 \leq j \leq N)$. The discrete Fourier transform has been used in this numerical work. The non-dimensional DFT pairs of the random signal used in the computation with U_j, $(j = 1, N)$ and $\tilde{W}_k$ with $(k = 1, M)$, noting both j and k are integers, are given by

$$U_j = \sum_{k=1}^{M} \tilde{W}_k \exp\left(i2\pi kj/N\right), \qquad \tilde{W}_k = \frac{1}{N} \sum_{k=1}^{N-1} U_j \exp\left(-i2\pi kj/N\right). \tag{6.5}$$

The wavenumbers k in the Discrete Fourier transforms are integers and $\tilde{W}_k$ is complex. The corresponding integral Fourier transforms are defined as

$$U(X) = \int_{-\infty}^{\infty} \tilde{U}(\tilde{k}) \exp\left(i\tilde{k}X\right) d\tilde{k}, \qquad \tilde{U}(\tilde{k}) = \frac{1}{2\pi} \int_{-\infty}^{\infty} U \exp\left(-i\tilde{k}X\right) dX \tag{6.6}$$

Where $\tilde{k}$ is the radian wavenumber and is given by

$$\tilde{k} = \frac{2\pi k}{N\Delta X} = 2\pi k \tag{6.7}$$

k on the right hand side of equation 6.7 is an integer such that $0 \leq k \leq M$. The factors 2π arises from specifying a periodic length of unity. The relation between $\tilde{U}(\tilde{k})$ and $\tilde{W}_k$ appearing in the integral Fourier transforms and in the DFT is

$$\tilde{U}(\tilde{k}) = \frac{\tilde{W}_k}{2\pi}$$

Similarly the discrete power spectrum $E(k)$

$$\sum_{k=1}^{M} E(k) = 2\tilde{U}\tilde{U}^* = \frac{2}{4\pi^2} \sum_{k=1}^{M} \tilde{W}_k \tilde{W}_k^* \tag{6.8}$$

where $\tilde{U}^*$ is the complex conjugate of $\tilde{U}$ and like wise for $\tilde{W}_k^*$. $E(\tilde{k})$ is a real quantity and all phase information is lost. The Nyquist or the folding integer wavenumber is $k = M = N/2$. The $\tilde{W}_k$'s are therefore completely specified by 2 real numbers and (N/2 -1) complex numbers, ie. a total of $[2 + 2(N/2 - 1)] = N$ real numbers as expected.

6.5.2 Discrete Power spectrum for the initial random signal

In defining the initial signal two approaches were considered. The first involved an ensemble average of a large number of randomly different initial waveforms such that they satisfied the above statistical properties for a Gaussian probability distribution. The drawback was that the computational time for this approach was felt to be prohibitive. The second, and favoured method, consisted of choosing for the test cases a single initial waveform covering a large number of waves with the amplitudes for each wavenumber (k) having a prescribed energy law and a random phase. Thus random phase at each wavenumber was alloted using the random number generator described by Press(1986). These are drawn from uniform deviate which lie within the specified range (0 to 1) with any one number in the range just as likely as any other. These numbers were multiplied by 2π in order to obtain a Gaussian distribution of the initial random signal of specified mean and standard deviation. A sufficiently long sample length was chosen so as to reflect the above statistical properties for the noise. This approach was considered satisfactory and time saving. Thus it was assumed that the initial signal was spatially homogeneous and U was a stationary function of X.

For a discretely sampled random signal U_j which is periodic satisfies the condition as discussed earlier

$$U(X_{j=1}) = U(X_{j=N})$$

for all times. The power spectrum is given by equation 6.8 above. The total energy is proportional to

$$\frac{1}{N}\sum_{1}^{N-1} U_j^2 - \overline{U}^2 = \frac{1}{N}\sum_{1}^{N-1} U_j^2 =< U^2 > \tag{6.9}$$

since $\overline{U} = 0$. Thus from equation 6.8 and 6.9 it is found

$$< U^2 >= \int_0^\infty E(\tilde{k})d\tilde{k} = 2\pi\sum_{1}^{M} E(k) = \frac{1}{\pi}\sum_{k=1}^{M} \tilde{W}_k\tilde{W}_k^*. \tag{6.10}$$

The validity of the Fourier transform was satisfied from equation 6.10. It is to be noted that the number of sample points N is even, and the Nyquist integer wavenumber $M = N/2$. Appendix N shows the derivations for the nondimensional quantities derived from the energy equation.

The initial signal shown in figure 6.1 is synthesised from a set of $\tilde{W}_k$ values where integer wavenumbers from $k = 1$ to k_T, with $k_T \approx M/2$ are energised. k_T is the truncation wavenumber and this truncation is only applied at $t = 0$. For all other times the range of

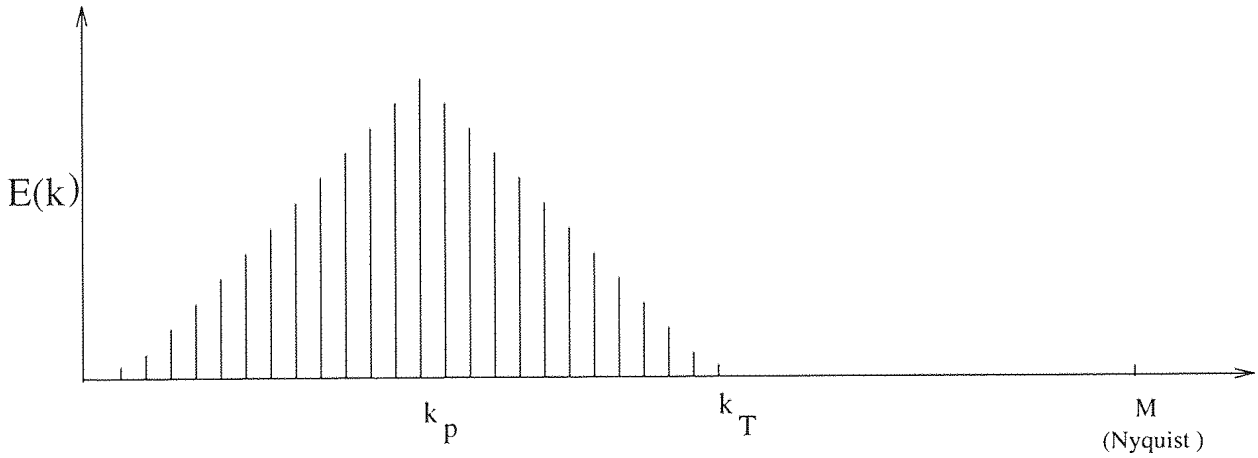

Figure 6.1: Discrete power spectrum representing random noise at $t = 0$.

k is from $1 \leq k \leq M$. The wavenumbers for which $k_T < k \leq M$ have zero energy at $t = 0$. It is known from experience that only data below M will remain unaliased, and thus it is a good rule to keep the spectrum well below M at time $t = 0$. But for the progression of the wave with time it is allowed to populate the spectrum upto the Nyquist wavenumber, M. Fourier components $\tilde{W}_k(k = 1 \text{ to } M)$ are synthesized numerically, by following the rules described for the Discrete Fourier transforms above with random phases assigned to each $\tilde{W}_k$. The square of the amplitudes of the Fourier coefficients determine the power spectrum. The result is a signal having Gaussian statistics.

As stated above an initial random wave distribution was defined which in the physical domain had a large number of zero crossings. In the non-dimensionalised space the periodic length was taken as unity. A high value of R was chosen but as defined R is just a convenient parameter in the numerical solution of Burgers equation and is not a Reynolds number for a physical problem. Three Reynolds numbers have accordingly been defined in section 6.1 for the physical problem and here it is discussed how they are evaluated from the choice of the initial profile, $U_0(X)$, and the solution $U(X,T)$. From a series of preliminary numerical tests it was found that when R exceeded about 500 only small changes in $U(X,T)$ occurred and even for $R = 500$ the waveform for all times had the appearance of an inviscid profile, with shock waves being of small thickness compared with the sample length. Thus a value of $R = 500$ was chosen as a suitable initial value for the present numerical calculations. The truncation integer wavenumber, k_T, in the initial distribution for test case 1 and 2(i) described later was taken as $k_T = 1000$ and $k_T = 1400$ respectively. Now when $\tilde{U}(\tilde{k}, 0)$ at times $T = 0$ is described the corresponding

$U_0 = U(X, 0)$ is defined also.

The root mean square velocity and length scale (U_0, λ) are defined via the zeroth and second moments of the wavenumber spectrum of the initial waveform and are defined in Appendix N.

For a given shape of initial spectrum different realizations are possible arising from

(a) Different choices of random phases;

(b) Different values of Nyquist wavenumber M (note $M > k_T$);

(c) Different values of peak wavenumber k_p.

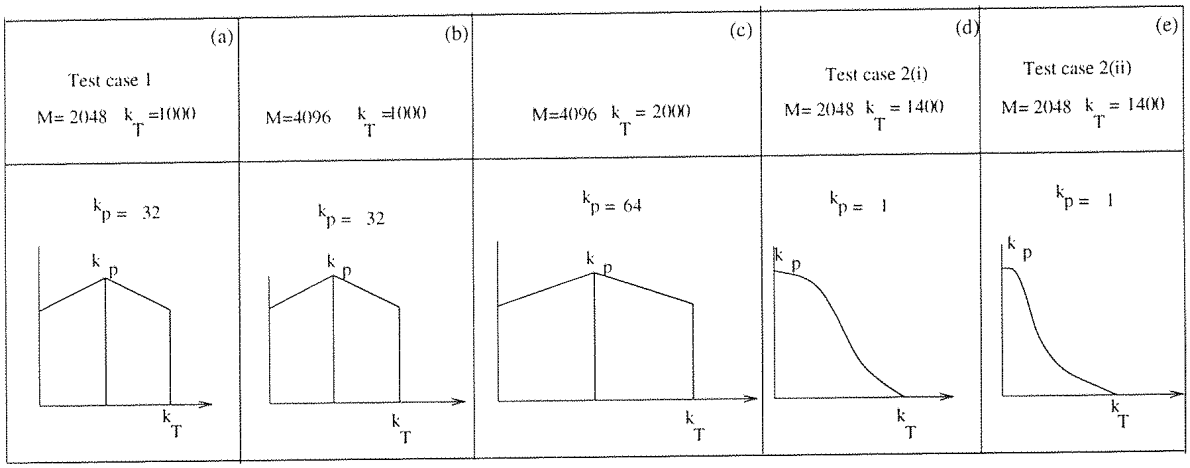

Figure 6.2: Initial spectra to be propagated

6.6 Test cases to be propagated

The aim was to investigate the effects of non-Gaussian statistics on the evolution of the energy spectrum. Since the major effect of nonlinear distortion is to generate shock waves from a random signal at $t = 0$ and since a random array of sawtoothed waves has a spectrum $1/k^2$ at high wavenumbers, which eventually change to $1/k^4$ as a result of finite shock thickness due to viscous dissipation [see N-wave structure by Robinson and Johnson(1967)] it was decided to investigate 2 cases. These are test case 1 and test case 2 and the power spectrum are described in figure 6.2. Test case 2 (ii) is an extension of test case 2(i).

6.6.1 Defining the Power spectrum

Test case 1 involves the input signal shown in figure 6.2(a). It is also called the reference signal since all the comparisons in this numerical calculations are based on this signal.

Figure 6.3 shows the actual initial spectrum for test case 1 and figure 6.4 shows the waveform as a function of X. The abscissa in figure 6.4 gives the sample number which is the number of points the signal is sampled between $X = 0$ and 1 at a constant distance ΔX. The ordinate gives the non-dimensional signal velocity U. The Fourier coefficients at $T = 0$ are complex with random phase but the power spectrum is real increasing like k^2 in the low wave numbers and falling like k^{-2} in the high wavenumbers. The inverse transform gives the signal shown in figure 6.4. The number of harmonics energised at $T = 0$ was 1000 and the characteristic wavenumber corresponding to the peak in the spectrum was chosen at $k_p = 32$. The truncation integer wavenumber $k_T = 1000$ and was approximately equal to $M/2$ where $M = N/2 = 2048$ is the Nyquist integer wavenumber.

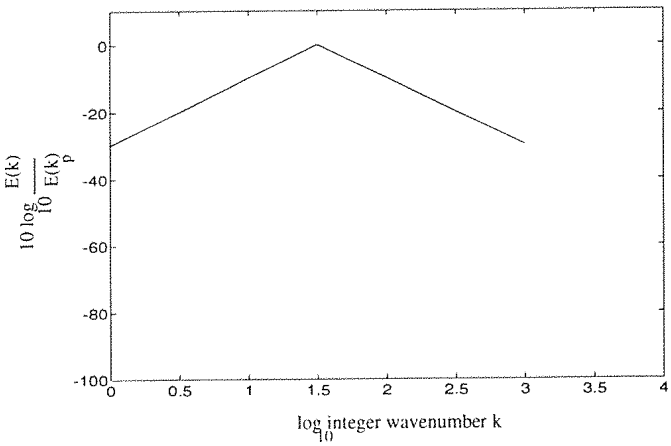

Figure 6.3: Initial spectrum for test case 1. $E(k) = k^2$, $1 < k < k_p$, $E(k) = 1/k^2$, $k_p < k < k_T$

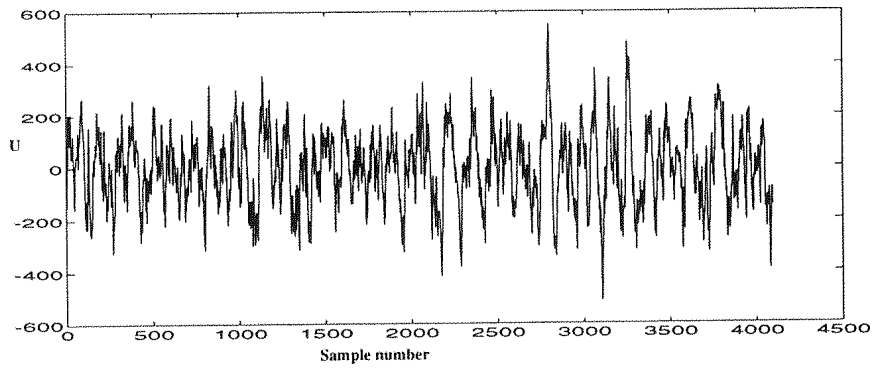

Figure 6.4: Initial waveform for test case 1.

In both the test cases 1 and 2 the input signals have a Gaussian probability distribution

and the moments, namely the variance, skewness and the flatness, were computed. The average velocity at time $t = 0$ satisfied the condition $< U >= 0$, where U is the particle velocity of the waveform. Over the whole domain at $t = 0$ for test case 2 the wavenumber followed an energy law $\exp(-2a^2k^2)$. The highest wave-number k_T, is well below the Nyquist value so as to avoid aliasing. Plots are presented using a decibel scale given by $10\log\left(\frac{E(k)}{E_{ref}(k_p)}\right)$ verses logarithm of the wavenumber. $E_{ref}(k_p)$ is the energy in the characteristic (peak) wavenumber k_p, having the maximum energy. The k^2 increasing and $1/k^2$ decreasing spectrum of test case 1 and $\exp(-2a^2k^2)$ decay spectrum of test case 2 for the initial spectra were chosen to cover the extremes of possible acoustic spectra.

6.7 Computational parameters for test case 1

Table 6.1 gives the computational values at an initial Reynolds number of 500 at time $T = 0$ for test case 1. I_0 is proportional to the non-dimensional total energy and I_2 is proportional to the non-dimensional rate of dissipation. As shown in Appendix N the Taylor microscale can be determined from the ratio of I_0 and I_2. The values of I_0 and I_2 are independent of R and were obtained from the initial setting of the spectrum and are derived in Appendix N. Table 6.2 are the parameters obtained for test case 1.

I_0	$\sqrt{I_0}$	I_2	$T_s = \frac{1}{(2\pi)^{3/2}\sqrt{I_2}}$
4.16E+04	202.87	9.75E+08	2.03E-06

Table 6.1: Parameters for test case 1 obtained computationally.

T_s in the table gives the average value of the nondimensional shock formation time and is derived in Appendix N. In the case of the initial random signal which is Gaussian $\partial U/\partial X$ (positive) is equal to $\partial U/\partial X$ (negative) on average. These numerical values of I_0 and I_2 have been checked at $t = 0$ against analytic evaluation of the integral.

The nondimensional velocity $U_0 = 2\pi\sqrt{I_0} = 508.51$. Following section 6.1, the Reynolds number R_T based on the Taylor microscale can be obtained as

$$R_T = R < U_0^2 >^{1/2} \frac{1}{2\pi}\sqrt{I_0/I_2} = 261.88$$

$$\frac{1}{\lambda} = \frac{2\pi}{L}\sqrt{\frac{\sum_{k=1}^{M} k^2 E(k)}{\sum_{k=1}^{M} E(k)}}$$

From the mathematical analysis of random noise, Rice(1945) finds that the average number of zero crossings in the period for positive (or negative) slopes, n_z is given by

$$n_z = \sqrt{\frac{\sum_{k=1}^{M} k^2 E(k)}{\sum_{k=1}^{M} E(k)}} \tag{6.11}$$

here the non-dimensional periodic length is unity.

Equation 6.11 is valid for an initial Gaussian signal. Beyond shock formation time $t > t_s$, Rice's formula needs to be modified to allow for the PDF being non-Gaussian. The correction to Rice's formula has been given by Kac(1944). The numerical calculations showed also that $n_z \propto 1/\sqrt{t}$ after the shock formation time by counting the number of zero crossings in figure 6.11 at each time. Thus at $t = -$ from Rice's formula, $n_z = 154$, is the number of zero crossings in the initial signal described in figure 6.4 is 149 and hence is in approximate agreement with that predicted by Rice. Thus it can be inferred that in the spatial distribution the inverse of the number of crossings per unit length is λ.

U_0	$\lambda/L = \frac{1}{2\pi}\sqrt{I_0/I_2}$	R_T	n_z
508.51	0.00103	261.8	154

Table 6.2: Parameters for test case 1 at $T = 0$

The thickness of a shock wave evolving from the nonlinear distortion of a random wave is different from that of a steady shock wave. The thickness for a single isolated wave is

$$\delta_s = \frac{6\delta\rho_0 c_0}{\Delta p(\gamma + 1)/2}$$

but this formula only applies in the steady state. The shock thickness is inversely proportional to shock strength but for strong shocks it is of the order of a few mean free paths and hence for weak shocks the thickness is much greater. The shock thickness is controlled by the entropy rise across the shock and the corresponding rate of energy dissipation. It is determined by the energy in the small scale motion. In the steady state shock this small scale motion is molecular and accounts for the thickness of the shock being related to the molecular mean free path. The isolated shock wave is formed in the case of steady motion when a supersonic flow changes discontinuously to a subsonic flow as a result of the changes in the downstream pressure. Since the fluid is viscous no discontinuities can occur and the gradients are very steep and the resulting shock thickness is small being a few mean free paths as given in the formula above. The isolated steady shock wave possesses

different properties from that of an initial random signal which form shock waves under nonlinear distortion even in the case when at large times the periodic signal reduces to a single wave. This single wave is an N wave having a bow and stern wave and its structure is therefore different from that of an isolated wave in the steady case. In the case of random periodic waves the energetic wavenumbers are considerably lower than that of the molecular motion and consequently when shocks occur the shock thickness is greater than for the isolated shock wave discussed above. In the random periodic case the mean square value of $\partial u/\partial x$ is dominated by its values at the shock waves and the shock thickness is of order $\frac{<u>^2}{<\dot{u}>^2}$. But this ratio is also given by definition, the Taylor microscale, λ. Thus beyond the near shock formation time the shock thickness is of order λ. This thickness is many orders of magnitude greater than the isolated shock thickness. A shock wave crossing turbulence is a related problem and the small scale turbulence can provide the necessary unsteady motion in the interior of the shocks to increase their thickness above that of the Taylor thickness. Relaxation effects can also add to the thickness of the wave and may well be a dominant factor in the determination of its thickness.

The non-dimensional time T as used in the computations and the value of λ/L for various times is given below in table 6.3 for test case 1.

Thus the Reynolds number R_T is determined from the initial waveform and its spectrum. However beyond the shock formation time for test case 1 it was found that λ/L increases as $\sqrt{t}$ while the shock strength falls as $1/\sqrt{t}$. Hence R_T at any time remains constant and approximately equal to that at $t = 0$. Thus R_T is a suitable parameter on which to base the effect of Reynolds number on the nonlinear characteristics of the wave distribution and including its viscous broadening. Now from equation 6.11, $\lambda \propto 1/n_z$, where n_z is the number of zero crossings in the initial sample and λ/L decreases with increase in k_T and/or M. Hence it is possible to optimise the initial conditions in order to obtain large value of R_T using the present Convolution Method. The present work suggests it is unnecessary to perform numerical calculations at values of $R > 500$ for test case 1 which becomes increasingly computationally expensive, since the present results show little change with increase in R beyond 500.

Non-dim T	λ/L
0	0.289
8E-07	0.272
8E-06	0.255
8E-05	0.765
8E-04	2.24
8E-03	
8E-02	
8E-01	

Table 6.3: Nondimensional times for which test case 1 was propagated and λ/L for Test case 1.

6.8 Effects of aliasing in the spectral domain for test case 1

In order to fully validate the reference signal of test case 1 it was necessary to investigate any spurious effects such as aliasing. However much the sample length was sufficiently long to describe Gaussian statistics nevertheless it was important to understand whether this signal with 4096 sample points was sufficient to discard any other spurious effects evolving at later times.

This test was carried out in order to show that the test case 1 defined in figure 6.2(a), (also shown in figure 6.3) is unaffected by aliasing at any advanced time. To validate the signal was constructed whose power spectrum is shown in figure 6.2(b). The power spectrum was the same as the initial test case 1 (or case (a) in figure 6.2) but more zeros were added in the wavenumber space. Thus the truncation wavenumber $k_T = 1000$ was the same. The peak wavenumber was $k_p = 32$ but the Nyquist wavenumber M was chosen as 4096 instead of 2048. The sample length is hence double that of the reference signal. The spectrum had the same energy law as the reference signal with $E(k) = k^2$, $1 < k < k_p$, $E(k) = 1/k^2$, $k_p < k < k_T$.

Table 6.4 gives the values of I_0 and I_2 for test case 6.2(b). This signal was then propagated for various times for the same initial Reynolds number of 500. Figure 6.5 shows comparison of this signal with the reference signal at time $T = 8.E-03$. It is seen

	I_0	$\sqrt{I_0}$	I_2
case b	4.16E+04	202.87	9.75E+08

Table 6.4: Parameters obtained computational for the case (b)

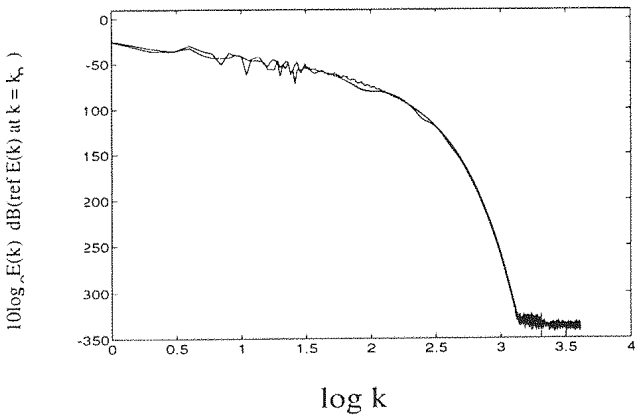

Figure 6.5: Test case 1 at $T = 8.E-03$ with superimposed case b

clearly that the solutions are indistinguishable. It is hence concluded that test case 1 has adequate spatial resolution for the numerical investigation.

6.9 Spectral Smoothing

When the spectra at various times were first obtained they appeared to show some scatter about the expected levels as shown in figure 6.6. The type of scatter was similar to that frequently found in time series analysis, which require a smoothing routine which retains the real information while only removing the random scatter. This routine is equivalent to averaging over a large number of samples. The smoothing routine was accordingly applied proposed by Newland(1984). Nevertheless the reason for the scatter remained unexplained. The Convolution Method used for solving Burgers equation was carefully checked both for a single sine wave and multiple waves and in each case no scatter of the kind shown in figure 6.6 was found. An analysis of a single sawtooth wave both with and without a shock wave of finite thickness is given by Robinson and Johnson(1967). The spectrum for this N wave is shown in figure 6.7 and is described in detail by Lilley(1970) for an isolated N wave with finite rise time. The spectrum involves sine and cosine components which rapidly change with wavenumber even though the envelope is smooth falling as $1/k^2$ in the

case of a discontinuous shock followed by $1/k^4$ for a shock of finite thickness as shown in figure 6.7. The breakpoint occurs at a wavenumber related to the shock thickness. Thus $E(k)$ already varies in the high wavenumber region for a single sawtooth wave and hence a variation of $E(k)$ is also expected for an assemblage of random sawtooth waves. Hence the application of the smoothing routine of Newland(1984) was found not to be necessary since the results shown in figure 6.6 were finally judged to be accurate and not the result of numerical errors in the Convolution method. However the smoothing routine assisted in the determining the average results.

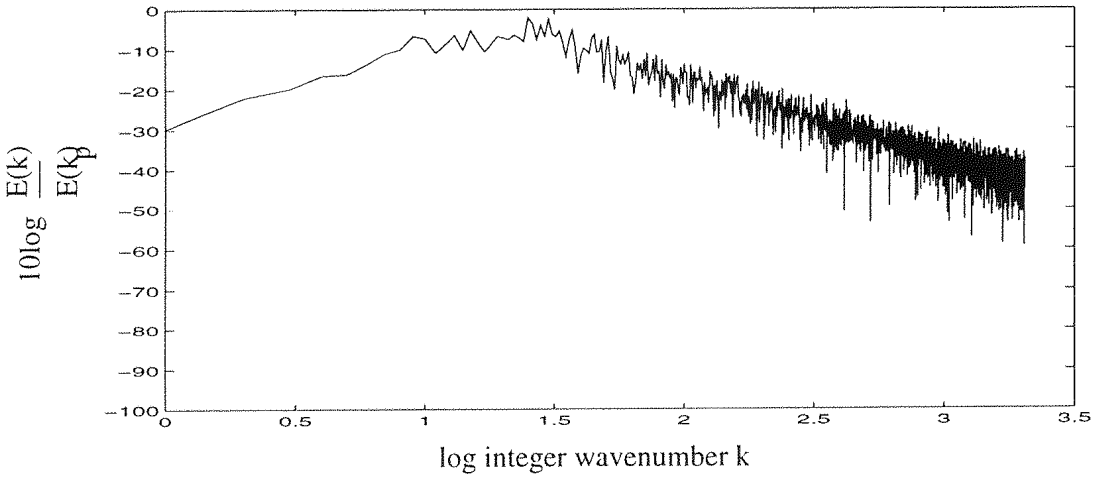

Figure 6.6: Unsmoothed Power spectrum at time $T = 8E-07$ and $R = 500$.

First the arithmetic average over every three adjacent wavenumbers of the raw spectrum was taken and the smoothed spectrum plotted. This gave very poor results without removing much of the scatter and the spectrum looked very much the same as the original unsmoothed one. Next an average over five adjacent wavenumbers showed improvement without any loss of the real effects as described by Newland. Figures[6.8 b,c,d] show the results due to spectral smoothing for advanced times. Smoothing the spectra did not alter the total energy of the signal.

6.10 Description of the propagation of Gaussian noise

This section gives a complete description of the changes in the waveform with time, for the given initial noise of Test case 1, from time $T = 0$ upto shock formation time, and then at much larger times when viscous effects are dominant. As time advanced the high wavenumbers population increased due to non-linear interactions. Figures 6.8 (a, b,c,d)

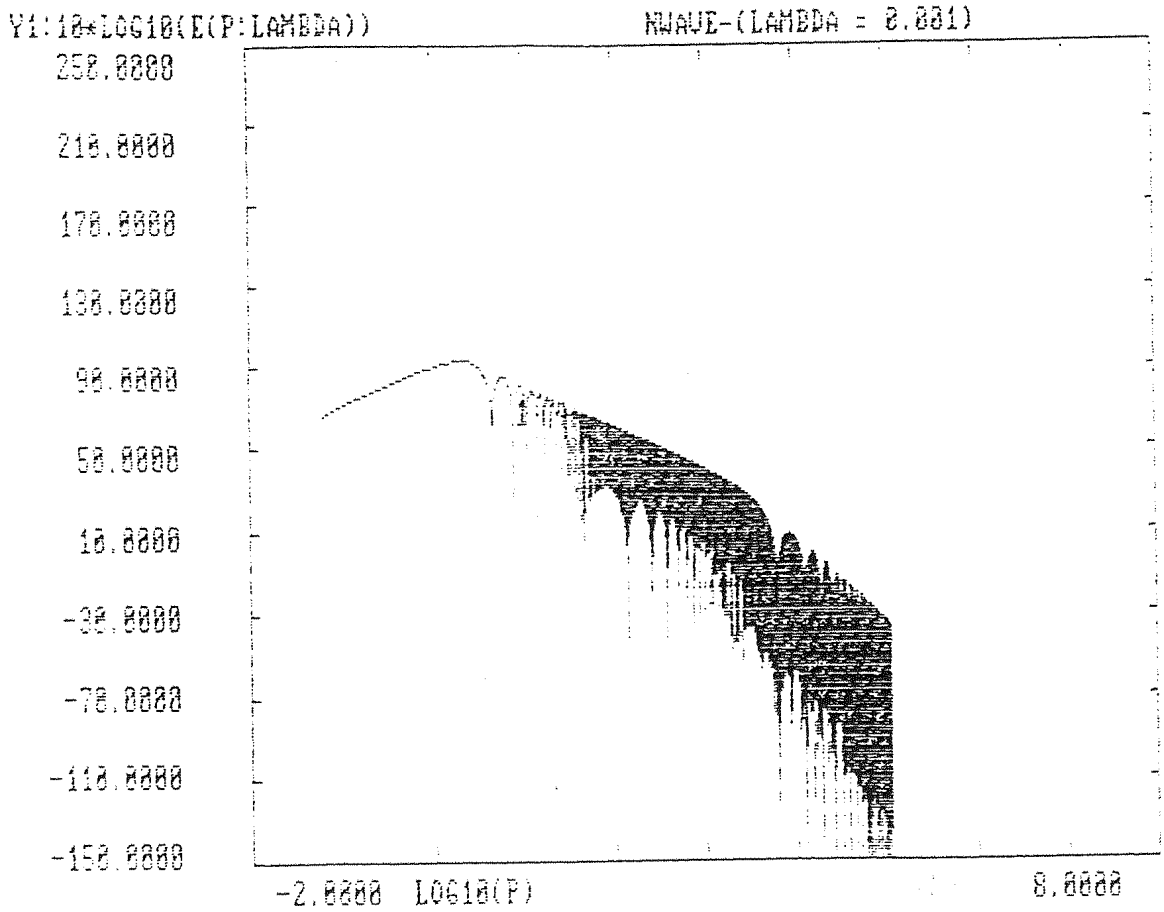

Figure 6.7: Spectrum for an isolated N wave with a finite rise time. See Lilley(1970)

show the spectra at various times. Figures 6.9 (a,b,c,d) shows the power spectrum at various times.

6.10.1 Description in the space domain coupled with the description in the spectral domain

The time advanced solutions of the waveform for $R = 500$ are shown sequentially in figures 6.11 (a,b,c,d) . It is shown that the propagation of an initial random waveform takes on different types of spectra with increase in time. As a result of nonlinear processes waves of near symmetrical form become distorted with upstream and downstream faces having a small positive $\partial u/\partial x$, and a large negative $\partial u/\partial x$ respectively. As time progresses the slope of the upstream face decreases as $1/t$, while the downstream face retains its large negative $\partial u/\partial x$ even though the shock thickness, increasing with time, produces a slight reduction in negative $\partial u/\partial x$. The distribution having positive u moves to the right and that having negative u moves to the left thus forming a series of sawtooth like structures. These sawtooths eventually 'bunch' and ultimately form a single N wave. With further increase in time the N-wave gradually decreases in amplitude and asymptotically viscous

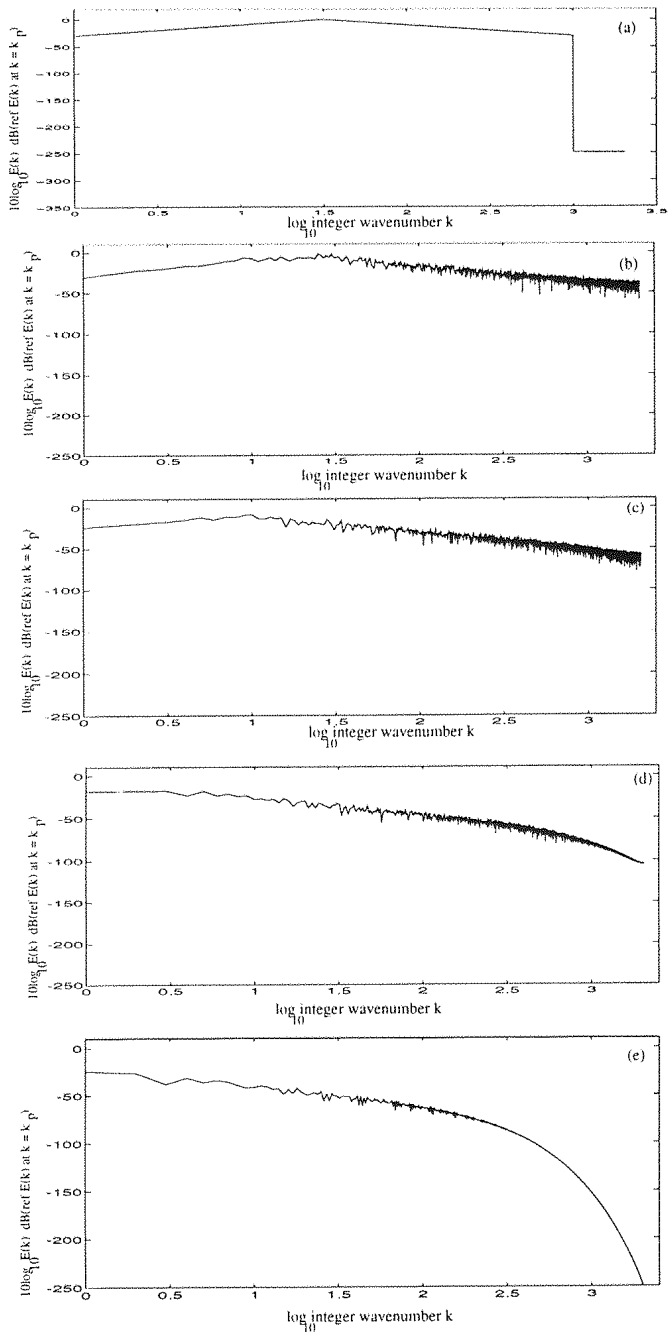

Figure 6.8: Smoothed power spectrum in decibels at $T = 0$, $8E-07$, $8E-06$, $8E-05$, $8E-04$ for Test case 1 $R = 500$ shown in a, b, c, d, e respectively.

effects broaden the wave reducing it to a sine wave as in Coles(1951) solution.

At relatively small times in $0 < T < T_S$ nonlinear steepening of the compression phases of the wave distribution occurs and the wave rapidly becomes distorted from its pattern at $T = 0$. Unless the smoothing due to the viscous effects is stronger than the steepening effects, shocks eventually form in the waveform. Shocks can occur only from zero cross-

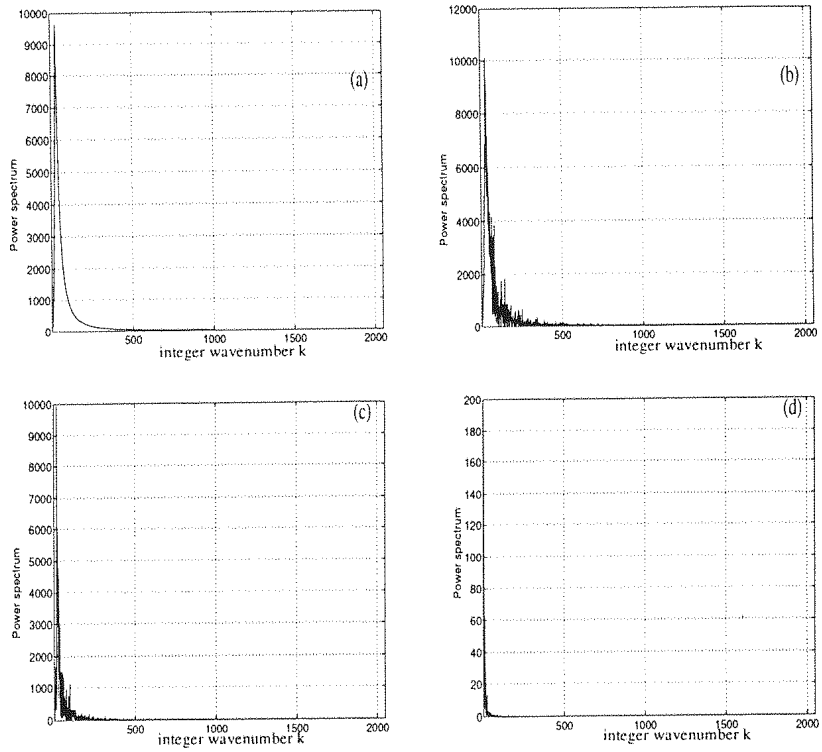

Figure 6.9: Power spectrum at $T = 0{,}8E-07,\ 8E-06,\ 8E-05$ for Test case 1 $R = 500$ shown in $a,\ b,\ c,\ d$ respectively.

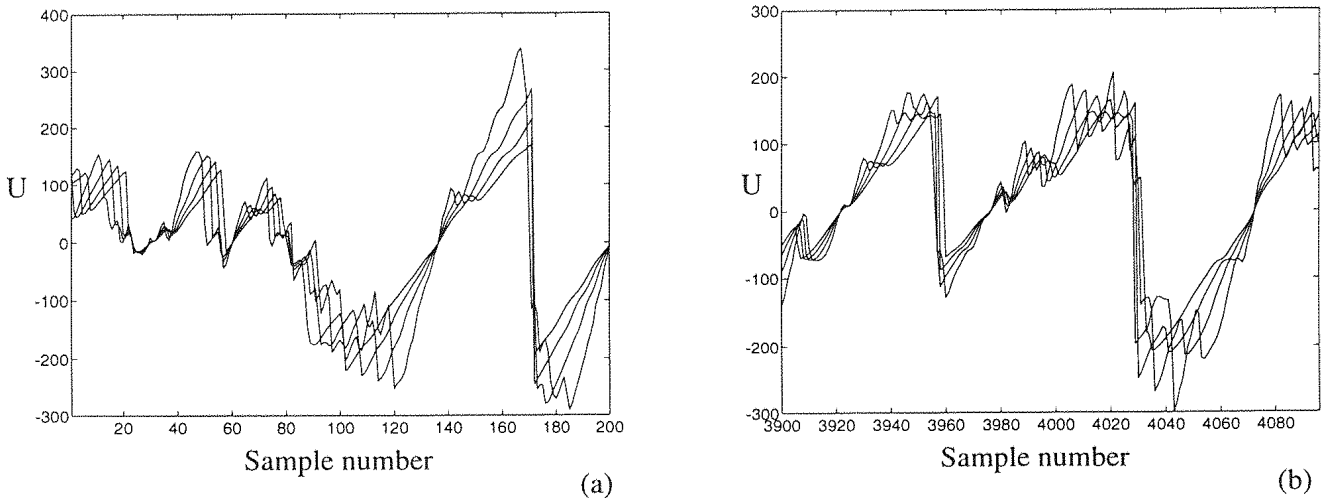

Figure 6.10: Propagation of waveform distortion at small times before the average shock formation time $T_s = 2.03E-06$ for Test case 1 shown at the extreme regions of the signal in $(a,\ b)$ for $R = 500$.

ings and it has been shown by Lighthill (1994) that the minimum number of zero crossings required for a shock to occur are 2. Thus the wave steepening starting from one of these

zero crossings and eventually forms a shock wave whose slope is proportional to $1/t$.

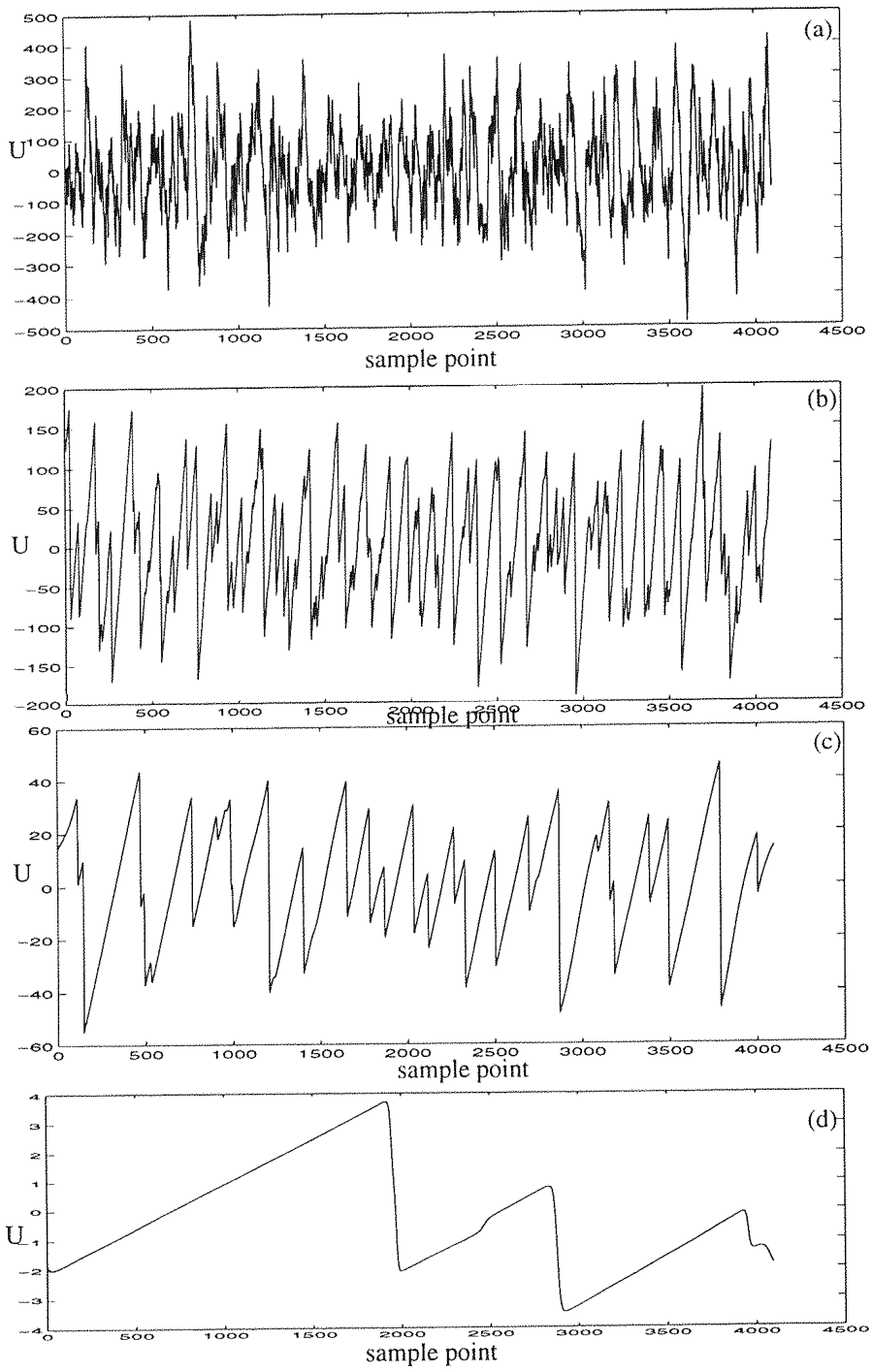

Figure 6.11: Propagation of the complex wave for Test case 1. Distortion at $T = 0$, $T = 8E-07$,$8E-06$, $8E-04$ shown in a, b, c, d for $R = 500$.

In the first stage of the distortion process, many shocks form as a result of the overtaking of troughs by peaks. In this process of the distortion, the most noticeable effects

due to the nonlinear interaction terms is the formation of shock waves [see figure(6.11b)]. A series of randomly located shocks with random strengths are observed, noting a shock wave with larger amplitude moves faster than a shock wave of smaller amplitude. It is seen that a certain 'bunching' in space occurs as described by Lighthill for inviscid calculations tend to arise because a union of two adjacent shocks is found to increase the likelihood of further union with other neighbouring shocks.

Figure 6.10 a, b shows propagation for small times before the shock formation time $T_s = 2.03E-06$, at two extreme regions of the signal where the gradual bunching of the waves is seen. Because each shock has its own particular propagation speed, the shock positions in the waveform slowly change as the wave propagates. Thus the speed of a shock is equal to the smaller and greater values of the velocity u which appear ahead of and behind it. In other words the shock absorbs characteristics ahead of it by running into them, while absorbing characteristics from behind as they run into it. The wave with larger amplitude merges with the wave having smaller amplitude which further merges with the neighbouring one and the process continues. The amount of distortion, which is the distance travelled by the wave during propagation, varies as $1/t$ for plane periodic waves. It can be seen from figures 6.11(b,c,d) that the slope of the sawtooth waves at any time are constant and is in agreement with Lighthill's theory for periodic sawtooth waves with slope of each shock wave proportional to $1/t$.

From the figures 6.8a,b,c it is seen clearly that there is a sudden cutoff of the high wavenumbers at the Nyquist wavenumber ($M = 2048$). However, the contribution to the total energy from wavenumbers beyond the Nyquist wavenumber ($E(k) \sim 1/k^2$) is so small that this contribution is neglected.

In the spectral domain starting from time $T = 0$ the appearance of shock waves in the waveform heralds a shifting of energy towards the high wavenumber end of the spectrum as shown in fig 6.8 (a,b). Distortion in the early stage of shock formation is manifested primarily by high wavenumber development with hardly any dissipation. The spectrum falls as $1/k^2$ in the wavenumber beyond $k = 100$ and would continue to have $1/k^2$ decay if an infinite range of wavenumbers were considered.

The merging of shocks causes the high wavenumber part of the noise spectrum to become more intense than would otherwise be the case by the 'bunching' tendency and most of the changes are found to occur in the high wavenumber region as seen in figure

6.8 (b), at wavenumbers greater than the peak wavenumber.

Once shock waves are formed, a new effect becomes apparent. The wave shape becomes drastically changed and simplifies as the propagation time increases as shown in figure 6.11(b,c,d). The simplification derives from the action of the shock waves, which do not maintain a constant position in the wave form but move, sweeping the minor irregularities in the signal and merging with other shocks in the process. This results in a marked decrease in the number of zero crossings as seen in figures 6.11(b,c,d).

A conflict between the nonlinear steepening effect which tries to distort the wave and the viscous broadening effects which try to broaden the wave is observed. The sum and difference of the wavenumber components results in additional population of the high wavenumber.

From the figures 6.11(b,c) it is seen that the gradients are sharp and viscous effects only provide the necessary broadening of the wave preventing shock discontinuities. The latter appear similar to that in the inviscid case since the viscous effects of broadening still results in a shock wave of small thickness. The reduction in the number of zero crossing continues to large times until only two zero crossing exists in the entire space time domain. In figure 6.11(e) there is strong distortion with a reduced number of zero crossings, but the amplitude of the high intensity noise is reduced. From here onwards, after the initial period of wave steepening and intensification, the wave subsides under linear laws where the dominant effect is a broadening due to viscous effects. This phase of the decay referred to as 'old age' is discussed by Sparrow (1991). For lower Reynolds number the 'steepening ' type of distortion develops relatively slowly. Absorption then has ample time to exercise its smoothing effects on the waveform. When this happens the distortion process slowly disappears and eventually stops at relatively small times. In all cases the critical parameter is $\lambda(t)/L$ since it represents the balance between viscous broadening and inertial steepening.

The waveform at large times reduces to a near sawtooth wave. This would then be the initial condition for the sine wave and obey Cole's solution when at very large times it is expected that the spectrum would become independent of its initial spectrum and would decay to a sine wave of reduced amplitude.

6.10.2 Propagation of the initial Gaussian signal with different phases

Different initial phase (different realisations) were used to propagate the initial Gaussian signal described in test case 1 and compare the spectra at various times. When the phase structure of the initial signal is changed, but retaining Gaussian statistics, it was observed that the resulting energy spectra remain almost the same at any time. Hence for a Gaussian signal, phase is not an important parameter. Figures 6.12 shows the spectra for 3 arbitrary different initial phase values satisfying Gaussian statistics without smoothing at $T = 8E-07$. Similarly 6.13, 6.14 show the spectra for 3 arbitrary different initial phase values without smoothing for times $T = 8E-05$ and $T = 8E-02$ respectively. Figure 6.15 (a,b,c) give the spectra at times $T = 8E-07$, $T = 8E-05$ and $T = 8E-02$ respectively having been smoothed with 5 arbitrary initial phase values satisfying Gaussian statistics. It is seen from the figures that at any time the decay of the spectrum is almost the same irrespective of the initial phase structure and therefore is independent of the initial signal. For small times of $T = 8E-07$ as seen in figure 6.15(a) the spectra for any different arbitrary realization was the same in both the low and high wavenumber components.

With increase in time, the spectra differed slightly in the high wavenumber components. This was probably mainly due to the method used in choosing the initial phase value satisfying Gaussian statistics. Since in any numerical method it is not possible to obtain an exact Gaussian signal with skewness equal to zero and flatness equal to 3, an approximation of these values of skewness and flatness was accepted in this numerical work. The tolerence for the skewness was 10^{-2} and skewness which was larger than this value was unacceptable. The tolerence for the flatness was within the range $2.89 and 3.19$. Any value below 2.89 and above 3.19 was unacceptable. This results to a small difference in the high wavenumber components for moderate and large times which is seen in the figure 6.15(b) and (c) respectively. It is seen that figure 6.14(c) is less smooth than (a) or (b) which is again due to the choice of the initial phase. Figure 6.16 gives the solution at large time $T = 8E-02$ with 2 different initial phases which gave an approximation of skewness and flatness almost exact Gaussian statistics showing that at large times the high wavenumber spectrum decays smoothly and therefore is independent of the initial signal, though dependent on the initial spectrum. The exactness of this result was also confirmed with more initial phase values by increasing the number of sample values N in a period for the same test case.

It can be concluded that if the initial signal is Gaussian, with a prescribed spectrum, the spectra at any time would decay similarly for any initial phase value.

In the case of a sawtooth wave the energy spectrum $E(k_p)$ has a peak wavenumber k_p and it is shown by Johnson and and Robinson(1967) that the spectrum for a sawtooth is given by

$$E(k) \sim k^2 \qquad 0 < k < k_p$$

$$E(k) \sim \frac{1}{k^2} \qquad k_p < k < \infty.$$

Ideally the energy spectrum for the sawtooth falls like $1/k^2$ in the inviscid Burgers equation. Thus when $E(k) \sim 1/k^2$ at high wavenumbers it is found the rate of dissipation $\epsilon \to \infty$ for finite ν and hence $\lambda = 0$ and the shock thickness is therefore zero. In case of finite Reynolds number the shock has finite thickness and hence a finite rise time. For a shock thickness of $O(\lambda)$ there is a change in the spectrum from $1/k^2$ to $1/k^4$ and is described in detail by Johnson and Robinson(1967). The cutoff between $1/k^2$ and $1/k^4$ occurs when $\lambda = 1/k_T$. Thus the truncation at $k = k_T$ is nearly equivalent to a change in the spectrum from $1/k^2$ to $1/k^4$ at $k = k_T$. λ/L is a measure of the scale of the dissipation range, with all dissipation occurring at the shock and its slope at any time gives the rise time (which is similar to the shock thickness) as described by Johnson and Robinson(1967) for the case when time spectra are used. The spectrum in their case falls as $1/k^2$ between the peak wavenumber k_p upto a wavenumber of k_T, after which the spectrum falls as $1/k^4$ and the spectrum rings at the harmonics of k_T. It is seen from figures 6.8*b,c,d* that the energy falls as $1/k^2$ and later for high wavenumbers the fall is almost exponential. The total kinetic energy and the rate of dissipation (ϵ) are both finite. Nonlinear effects are still present though viscous effects are taken over and due to dissipation the amplitude is reduced considerably.

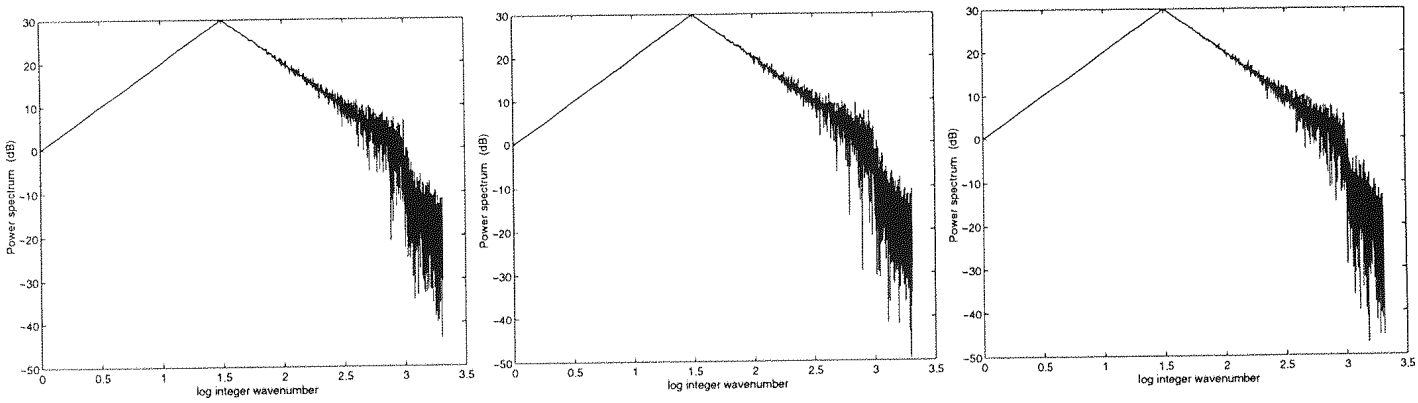

Figure 6.12: Spectra at $T = 8E-08$ for 3 different initial realizations.

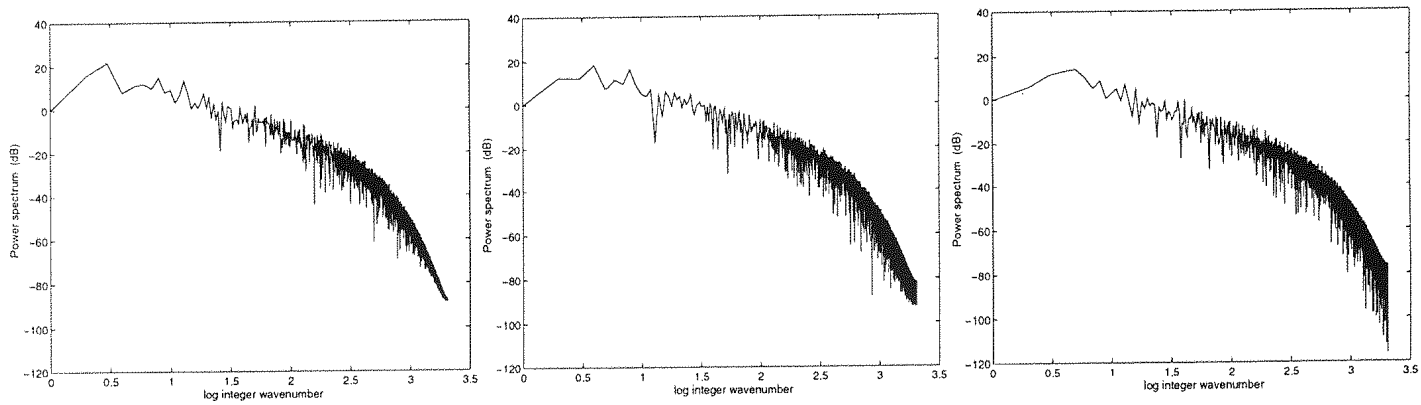

Figure 6.13: Spectra at $T = 8E-05$ for 3 different initial realizations.

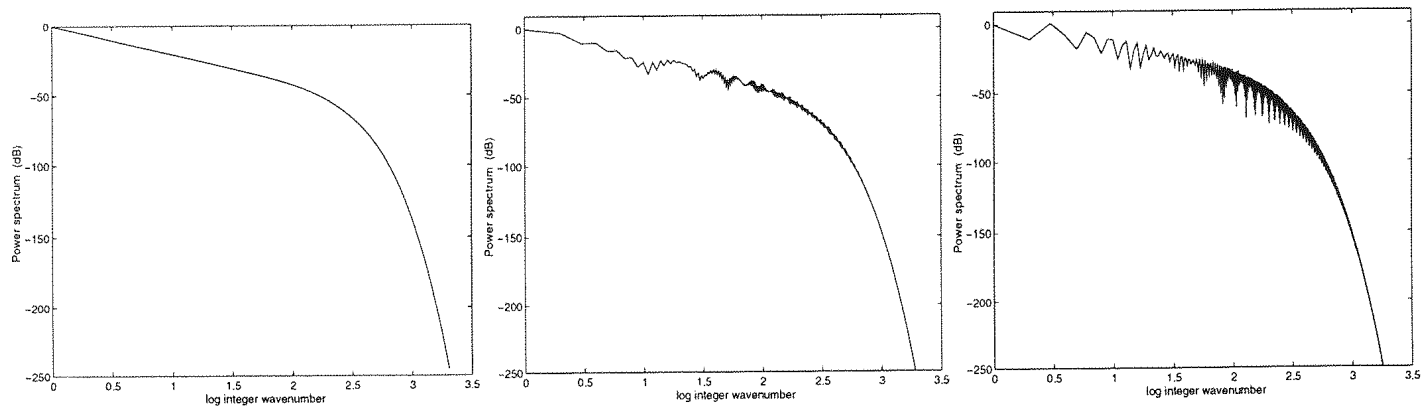

Figure 6.14: Spectra at $T = 8E-02$ for 3 different initial realizations.

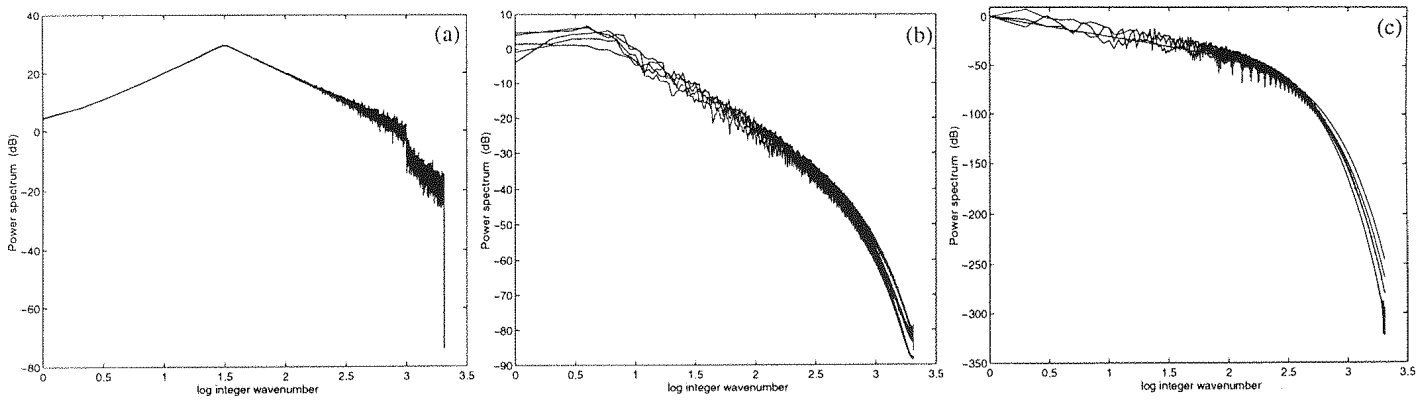

Figure 6.15: Smoothed Spectra at 5 different realizations.
a corresponds to $T = 8E-08$, b corresponds to $T = 8E-05$,
c corresponds to $T = 8E-03$ respectively.

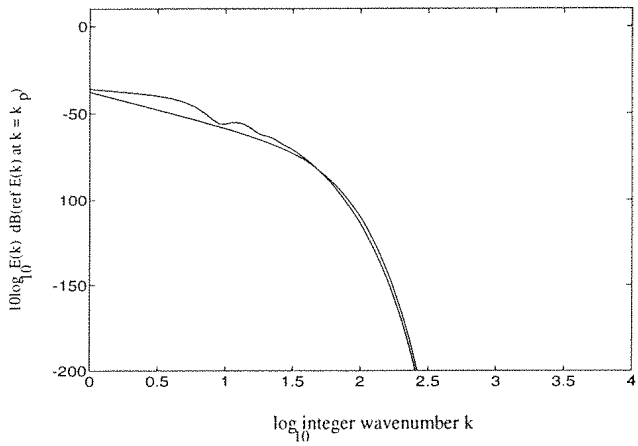

Figure 6.16: Spectrum for two different initial realizations at large times $T = 8E-03$.

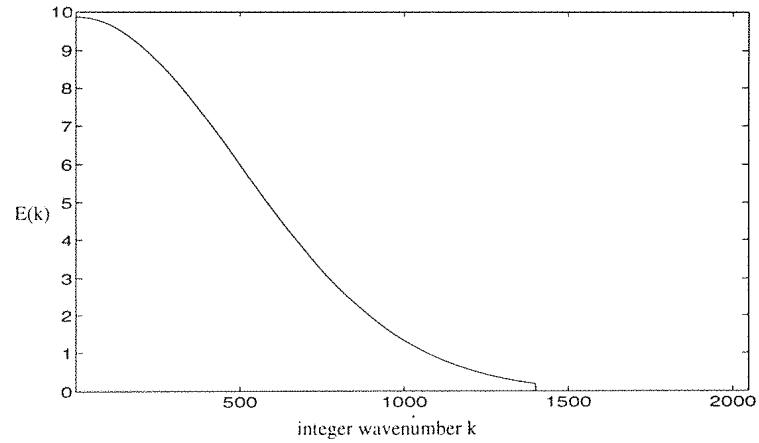

Figure 6.17: Initial spectrum for test case 2 *(i)*. $E(k) = e^{-2a^2k^2} \quad 1 < k < k_T$, $a = 0.001$.

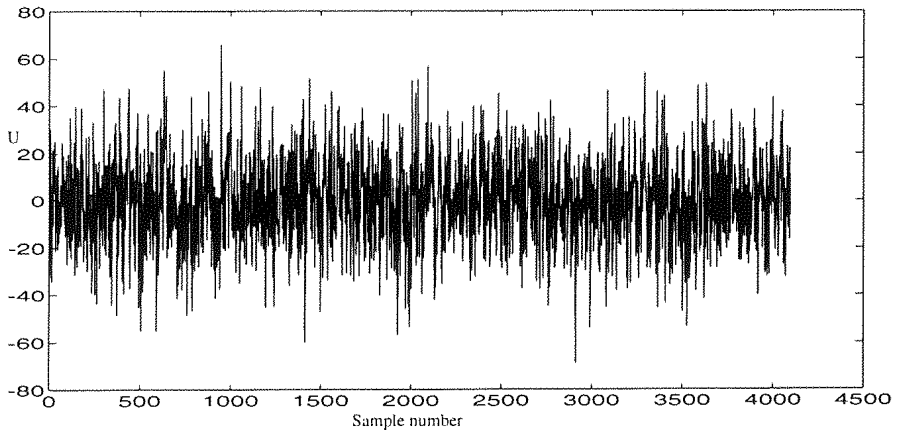

Figure 6.18: Initial waveform for test case 2 *(i)*

6.11 Computational parameters for test case 2(i)

The second test case is an initial waveform which is random but has a power spectrum, found by taking an ensemble average of waves, having amplitudes for each wavenumber decreasing like $\exp(-a^2k^2)$, where a is a weighting factor equal to 0.001, and random phases. This gave an exponentially decaying spectrum, which is shown in figure 6.17 when plotted on a linear wavenumber scale. The number of harmonics energised initially were 1400. The corresponding signal waveform is shown in figure 6.18. The introduction of such a spectrum at time $T = 0$ with its peak energy at wavenumber $k = 1$, was only introduced to provide as a large difference from the spectrum used initially in Test case 1. With such a large number of waves in the space domain ($N = 4096$) it was possible to

obtain a Gaussian distribution initially.

Table 6.5 gives the computational values at an initial Reynolds number of 1000 for test case 2(i). The values of I_0 and I_2 are independent of R and were obtained from the initial setting of the spectrum.

I_0	$\sqrt{I_0}$	I_2	$T_s = \frac{1}{(2\pi)^{3/2}\sqrt{I_2}}$
623	24.9	$1.48E+08$	5.3E-06

Table 6.5: Parameters for Test case 2(i) obtained computationally.

T_s in the table gives the average value of the shock formation time. These numerical values of I_0 and I_2 have been checked at $t = 0$ against analytic evaluation of the integral.

The exponential spectrum with $E(k) = \exp(-2a^2k^2)$ was propagated for an initial Reynolds number $R = 1000$. The number of zero crossings in the initial signal at $T = 0$ from equation 6.11 is $n_z = 487$, compared with the number of zero crossings in the initial signal of 480 as measured from figure 6.4. Hence there is fair agreement between the calculated value and that predicted by Rice's(1945) formula. Table 6.6 are the parameters for test case 2 at $T = 0$.

U_0	$\lambda/L = \frac{1}{2\pi}\sqrt{I_0/I_2}$	R_T	n_z
62.41	0.000332	20.5	474

Table 6.6: Parameters for test case 2 at $T = 0$

Figures 6.19 b,c,d show the spectral evolution with time for $R = 1000$ when the numerical results have not been smoothed. In figure 6.20 similar results are presented when plotted in decibels. From the figures it is seen that the high wavenumber spectral components become random in amplitude and phase as a result of nonlinear effects. Since the energy spectrum at $t = 0$ is falling like $\exp(-2a^2k^2)$, the dissipation spectrum for this would increase like $k^2\exp(-2a^2k^2)$ and peak beyond the Nyquist wavenumber. It is therefore not surprising that at $t > 0$, as shocks develop and bunching occurs, the typical $1/k^2$ spectrum for the sawtoothed waves develops for a small range of wavenumbers as seen in figure 6.20 and soon the fall becomes exponential. Thus as seen in figure 6.20, that at $T > 0$ the energy spectrum falls at high wavenumbers and the kinetic energy quickly

falls. The result is that with increase in time, ϵ falls as $t^{-1.5}$ as shown in figure 6.25 and the energy varies as $t^{-3/4}$ shown in figure 6.26. These differ considerably from test case 1 where the kinetic energy decays as $1/t$ and ϵ decays as $1/t^2$. At later times the spectral components show a rapid decay in the high wavenumbers. This is because the peak wavenumber, which contains the maximum energy, is chosen in the low wavenumber region. Thus although the nonlinear effects populate the high wavenumbers, due to the dissipation mechanism the spectrum at high wavenumbers falls faster than $1/k^4$. This result is entirely due to the extreme low value of the peak wavenumber. The rates of dissipation for the two test cases is described below. The reason for the differences in the results for both the Test cases 1 and 2 are also given below.

The interdependence of λ, k_p and k_T is given in Appendix M. Thus as k_T is increased so λ decreases. For a given ratio of k_p/k_T, λ is inversely proportional to the peak wavenumber k_p. For the same shape of the initial spectrum, the dissipation rate, ϵ, increases with increase in k_T, and is reflected in a decrease in λ.

In case 2 the initial spectrum decays smoothly since there is no sudden cutoff wavenumber as in case 1. In the high wavenumbers it therefore represents a more physical spectrum than in case 1. However choosing the peak, at $k_p = 1$, is aphysical since it is unlikely, in a practical situation that the peak wavenumber occurs in such a low wavenumber region. The exponential type of spectrum represents a case where viscous broadening is seen to dominate and the effects of nonlinear distortion in populating the higher wavenumbers is much reduced as compared with test case 1. Figure 6.21(*f*) shows the waveform after a long propagation time and which will asymptotically approach a sinusoidal waveform as predicted in Cole's(1951) analysis.

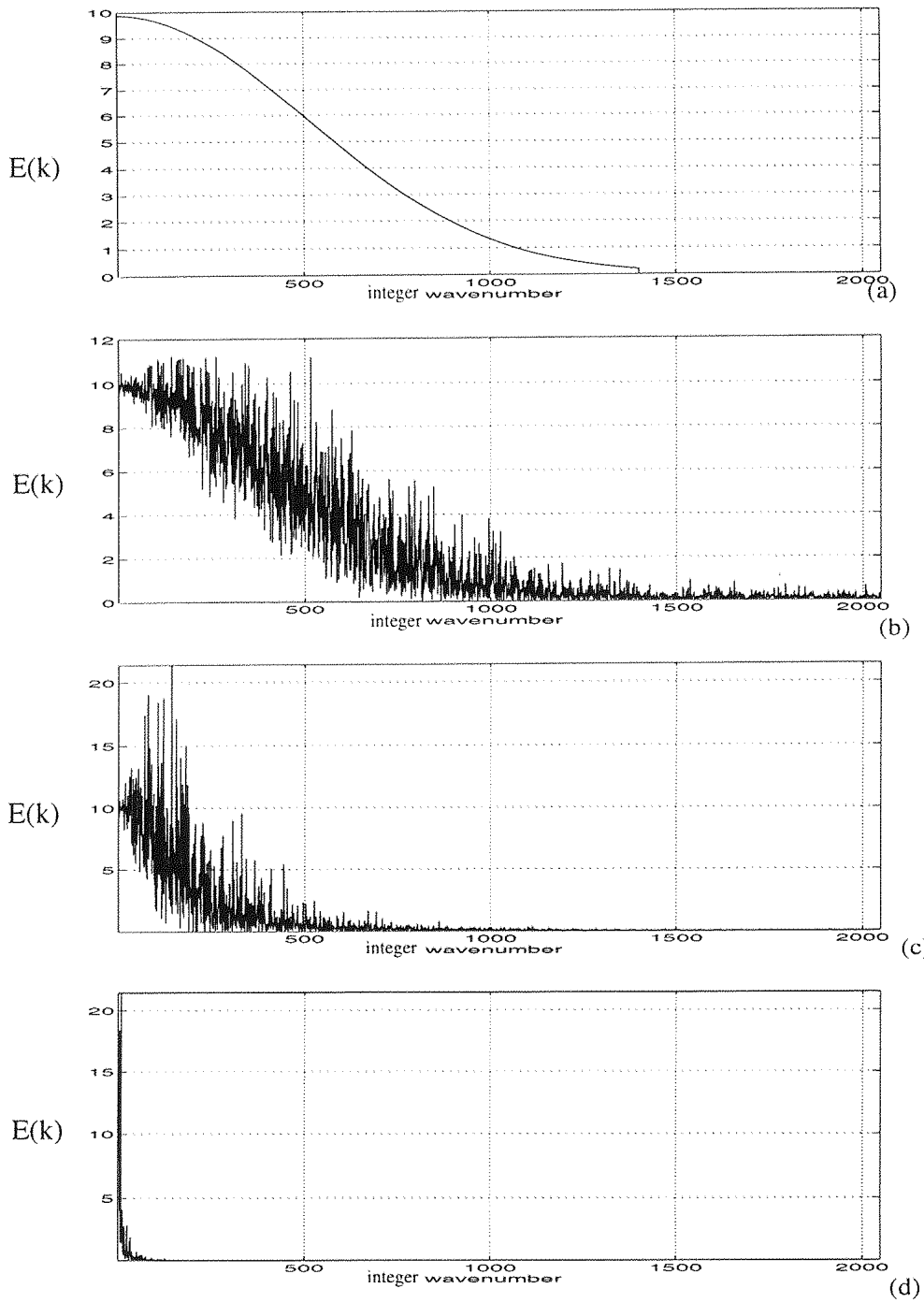

Figure 6.19: Power spectrum. $T = 0.0,\ 8.0E-05,\ 8.0E-04,\ T = 8.0E-03$, shown in a, b, c, d respectively for test case 2. $R = 1000$. $E(k) = e^{-2a^2k^2} \quad 1 < k < k_T$, $a = 0.001$.

6.11.1 Propagation of Test case 2 (ii)

Test case 2(ii) was set up to demonstrate the effect on the nonlinear distortion and viscous broadening of a small change in the low frequency compared with a very large change (amounting to 60dB) in the high frequency end of the initial spectrum. Figure 6.22 *(ii)*

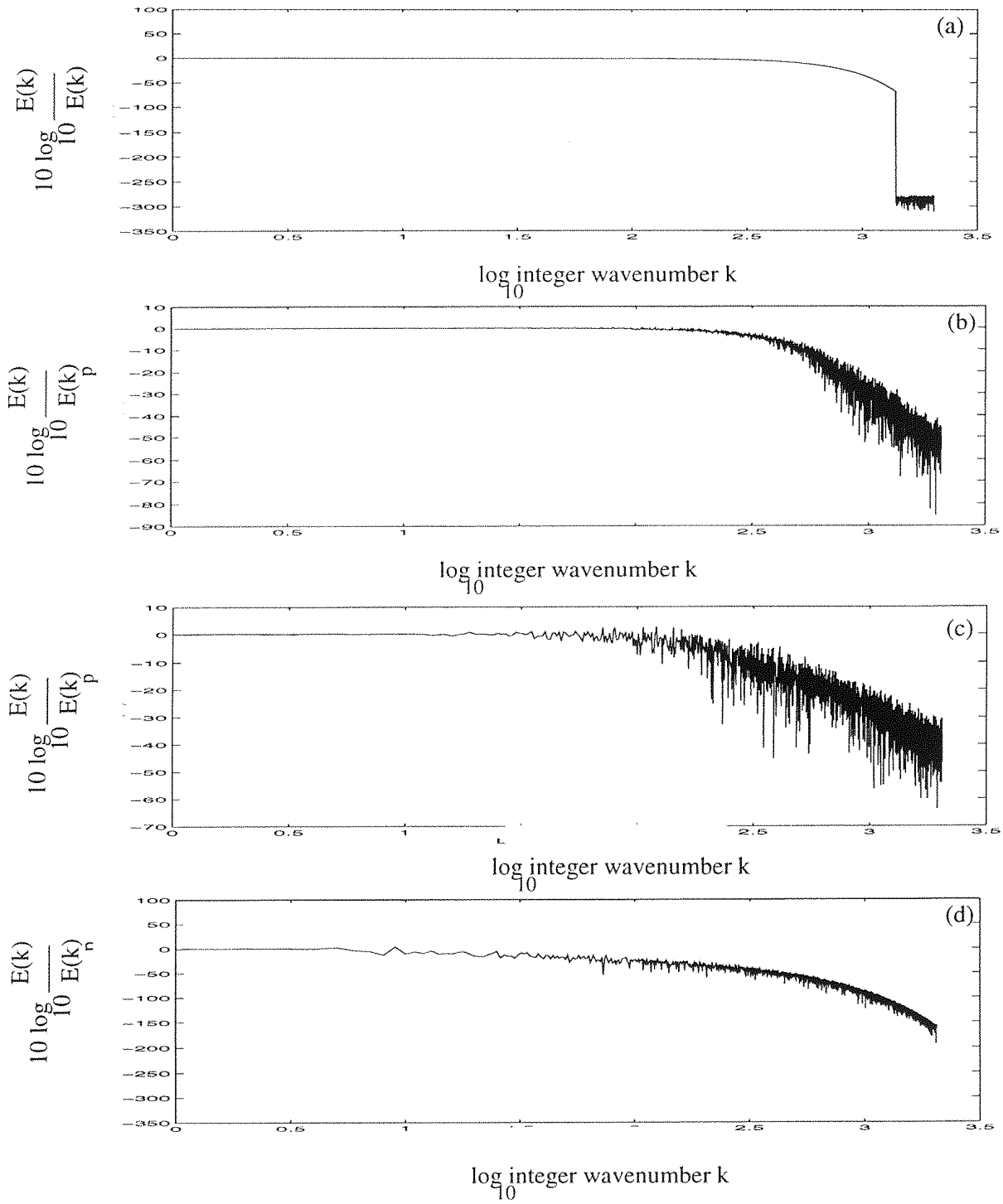

Figure 6.20: Power spectrum in decibels at various times for test case 2*(i)*. $R = 1000$. $E(k) = e^{-2a^2k^2}$, where a is 0.001. $T = 0.0,\ 8.0E-05,\ 8.0E-04,\ 8.0E-03$ shown in a, b, c, d respectively.

shows the initial spectra in comparison with that of the earlier case 2*(i)*. Test case 2 (ii), with $a = 0.002$ was propagated for the same $R = 1000$ and time T defined in table ?? as that of test case 2 (i).

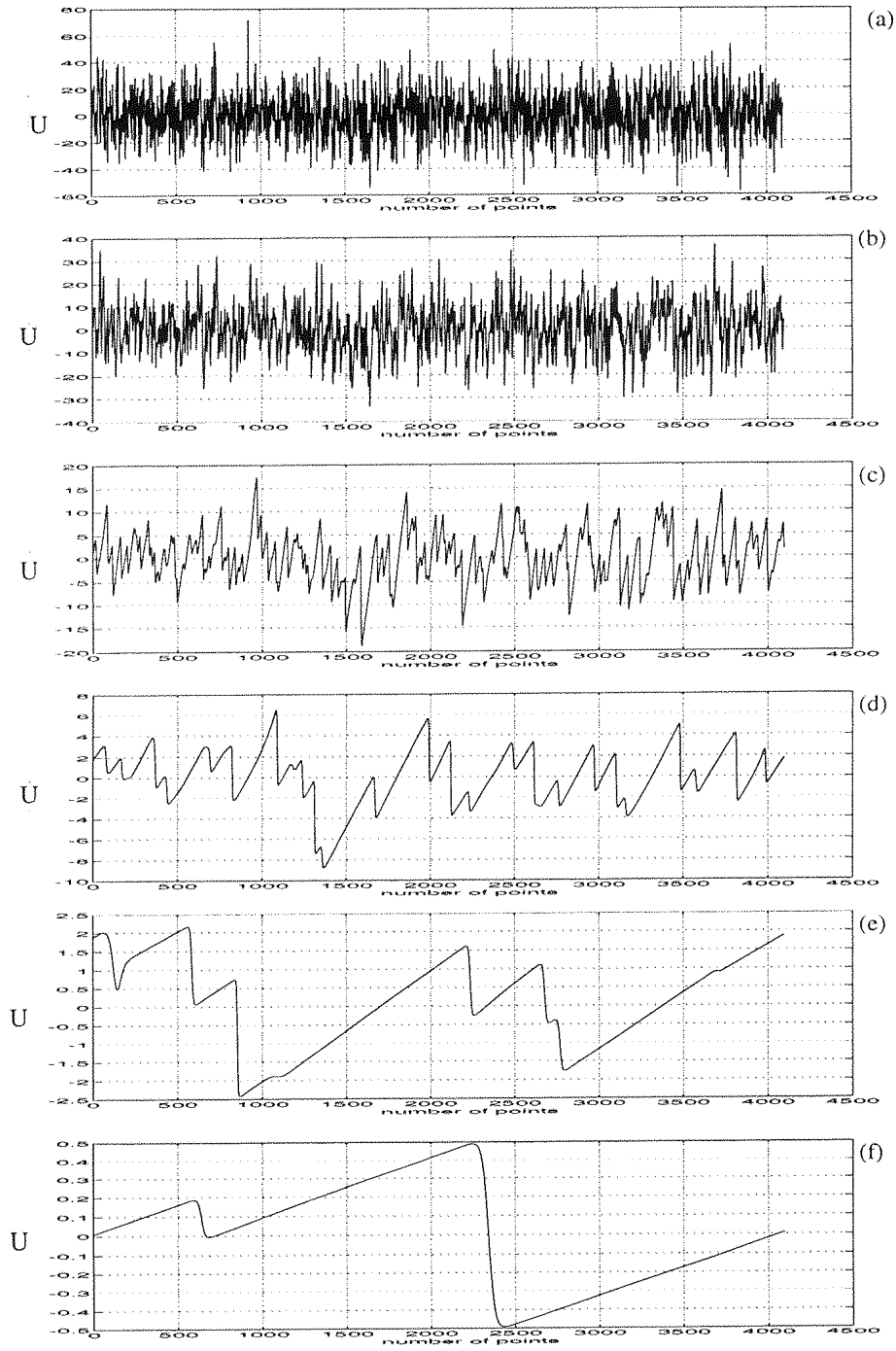

Figure 6.21: Propagation of the complex wave for Test case 2(i). Distortion at $T = 0$, $T = 8.0E-06$, $8.0E-05$, $8.0E-04$, $8.0E-03$, $8.0E-02$shown in *a*, *b*, *c*, *d*, *e*, *f* respectively. $R = 1000$.

Figure 6.23 show the power spectral density at various times for the same initial Reynolds number of 1000, when the exponential factors a is given the values 0.001 and 0.002 in *(i)* and *(ii)* respectively. These spectra have not been smoothed. From the figure

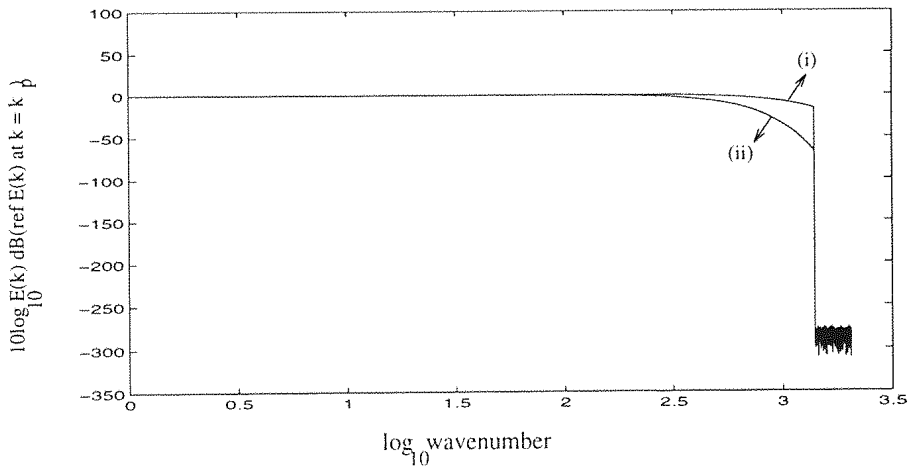

Figure 6.22: Initial spectrum for test case 2 *(i), (ii).* $E(k) = e^{-2a^2k^2} \quad 1 < k < k_T$, where $a = 0.001$ for *(i)* and $a = 0.002$ for *(ii)* respectively.

it is seen that the two spectra diverge with increase in time. But at large times the divergence increases to more than 100 dB as compared with their 60dB difference initially. This represents a case where the rate of dissipation is more in test case 2(i) than in case 2 (ii).

6.12 Rates of dissipation for test cases 1 and 2(i)

As shown in Appendix J, $dK/dt = -\epsilon$ where K is the kinetic energy and ϵ is the rate of dissipation where $\epsilon = 2\nu_e \int_0^\infty \tilde{k}^2 E(\tilde{k}) d\tilde{k}$. It is therefore seen that spectrum function, $E(k)$, which falls as $1/k^2$ in the high wavenumber at $t = 0$, as described in test case 1, generates an infinite rate of dissipation at $t = 0$, and represents the case of the entropy catastrophe. However for finite viscosity and a truncation in $E(k)$ at $k = k_T$ the result is a finite rate of dissipation and hence at small times though the total kinetic energy K remains almost constant. Beyond a certain time and greater than the shock formation time the effects of viscous dissipation spread into the lower wavenumbers and the high wavenumber spectrum no longer falls as $1/k^2$, but more exponentially. For all times the total kinetic energy K and ϵ can be calculated [3]. At small times the truncation for the initial spectrum (for test case 1) causes the high wavenumber growth to be sharply truncated at the Nyquist wavenumber (see figure 6.8 at time $T = 8.E-07$), though ideally the spectrum would develop at wavenumbers greater than the Nyquist wavenumber. Hence at small times as

[3]Test case 1 has been checked and validated both against aliasing and by doubling the sample length. The result was that there were no aliasing errors.

discussed above this sudden cutoff at the high wavenumber does not affect the total kinetic energy, but affects the rate of dissipation. When at large times the spectrum becomes sufficiently depopulated below the Nyquist wavenumber and recovers the properties of an infinite range spectrum provided the peak wavenumber of the dissipation is also below the Nyquist wavenumber. Figure 6.24 and 6.25 gives ϵ for test case 1 and 2 respectively.

The influence of the value of the truncation wavenumber, k_T, on the rate of dissipation and total energy is a function of $E(k)$. In general it is expected that an increase in k_T for the same spectrum shape and for the same total kinetic energy, increases ϵ and λ decreases. In test case 1 the truncation of the spectrum at $k_T = 1000$, shown in figure 6.3 results in ϵ at $T = 0$ being dominated by the spectrum at this cutoff wavenumber. It is seen that viscous dissipation at all higher wavenumbers is thereby excluded. Thus in any theoretical analysis the choice of truncation wavenumber can prove critical in comparison with an experiment where no cutoff in wavenumber exists. This is particularly important in experiments at high Reynolds number, where λ is likely to be very small, noting $\epsilon = \frac{\nu_\epsilon < u^2 >}{\lambda^2}$. As stated previously when $E(k) \sim 1/k^2$ at high wavenumbers upto a cutoff at $k = k_T$, λ is inversely proportional to k_T.

Clearly the choice of the initial spectrum has a major effect on the rate of dissipation. In test case 1 $k_p = 32$ corresponding to the maximum spectral energy in the initial spectrum. In the exponential decay spectrum $k_p = 1$. In test case 1, the rate of dissipation increases a little initially and then falls rapidly as seen in figure 6.24. Figure 6.25 shows that for test case 2 (i) the dissipation rate starts decreasing from $t = 0$ as $1/t^{1.5}$ instead of $1/t^2$.

6.13 Comparison of spectra with equal kinetic energy

The initial kinetic energy of Test case 1 was changed so that it was approximately equal to the initial kinetic energy of test case 2. However the statistics remained Gaussian at $T = 0$. The statistical properties of Test case 1 were then computed from $T = 0$ for various evolution times as shown in table 6.7 for $R = 1000$. It is observed that the kinetic energy of test case 1 falls off less rapidly for small times than test case 2. But at large times there is only a very small difference in the kinetic energy for the two cases. The numerical calculation was not proceeded further, but it is possible that still larger times

T	K.E	RMS Velocity
0.0	1.0	1.0
$8.0E-07$	1.00000	1.0
$8.0E-06$	0.986098	0.993
$8.0E-05$	0.885123	0.94
$8.0E-04$	0.27543	0.52
$8.0E-03$	0.019890	0.14
$8.0E-02$	0.0017643	0.0417

Table 6.7: Kinetic energy of test case 1 with initial kinetic energy decreased to that of the initial energy of the Test case 2. $R = 1000$.

the energy in the two cases would not be the same. More numerical experiment need to be performed using a greater variety of initial spectra having equal initial energy to conclude on this result.

T	K.E	RMS Velocity	Skewness for u	Flatness for u	Skewness for $\partial u/\partial x$	Flatness for $\partial u/\partial x$
0.0	1.0	1.0	-7.1E-02	2.973	-1.05E-15	3.14
$8.0E-07$	0.9972	0.9986	-7.08E-01	2.99	-4.12	4.19
$8.0E-06$	0.942	0.9707	-6.03E-01	2.97	-7.01	5.150
$8.0E-05$	0.328	0.5763	-5.07E-01	2.84	-9.67	5.96
$8.0E-04$	0.0225	0.15				
$8.0E-03$	0.0032	0.057				
$8.0E-02$	0.00028	0.017				

Table 6.8: The statistical evolution for Test case 1 at $R = 500$.

6.14 Statistical evolution of the PDF's

The variation of the statistical parameters skewness and flatness with time for test cases 1 and 2 (i) are shown in table 6.8 and 6.9 respectively. Up to the shock formation time ($T_s = 2.0E-06$ for test case 1 and $T_s = 3.E-06$ for test case 2) it is seen that the skewness

T	K.E	RMS Velocity	Skewness u	Flatness u
0.0	1.0	1.0	-4.13E-03	2.9443
$8.0E-06$	1.0000	1.0	-4.65E-02	2.943
$8.0E-05$	0.866456	0.9308	-3.63E-02	2.942
$8.0E-04$	0.360987	0.603	-1.19E-01	2.92
$8.0E-03$	0.088903	0.29		
$8.0E-02$	0.001709	0.133		
$8.0E-01$	0.000186	0.042		

Table 6.9: The statistical evolution for Test case 2(i) at $R = 1000$.

and flatness of the velocity change only slightly from their initial Gaussian values of 0 and 3 respectively. It is seen that for $T > 0$ nonlinear distortion of the wave distribution occurs and results in the asymmetry between positive and negative counterpart. This is reflected by the change in skewness of u from 0 to about (-0.5) as seen in table 6.8. Hence the deduction is that the statistics of the initial random wave distribution are slowly changing from Gaussian to non-Gaussian. The changes in skewness and flatness for the velocity are small but in the same time domain, $0 < T < T_s$, it is expected that the skewness and flatness of the velocity derivatives to change more dramatically and this is confirmed as shown in table 6.8. There is therefore no doubt that the statistics change from Gaussian for all $T > 0$. In Appendix I is shown the differential equations giving the changes in skewness and flatness with time. These equations show that skewness and flatness change from their Gaussian values for $T > 0$ and that the critical parameter is the value of the Taylor microscale, λ, and its variation with time. The variation of λ/L in the time domain, $0 < T < T_s$, is complex since it suffers a decrease owing to the increasing population of the higher wavenumbers due to nonlinear distortion and is shown in table 6.3 for test case 1. Beyond T_s, λ/L increases approximately as $\sqrt{t}$. These changes in λ/L reflect in the solution of the equations for skewness and flatness and the consequent changes in the changes in kinetic energy and the rate of dissipation with time.

The key role played by the Taylor microscale, λ, at all times in the propagation of the complex finite amplitude acoustic wave can be deduced from these results. Its role in the wave distribution process is far more important than the relatively small changes in the

peak wavenumber with time. λ is related in particular to the shock wave thickness and is proportional to the average spacing between shocks at any time. It relates directly to the number of shocks present at any time within the periodic length, L.

6.15 Comparison of the PDF's with Kraichnan's analytic work

In Kraichnan's (1990) model for the evolution of the probability distribution function obtained from Burgers turbulence, it is shown that the non-Gaussian statistics develop from nonlinearity of the negative velocity gradients $(\partial u/\partial x)_-$ into viscosity limited shocks. The model consists in finding the joint probability distribution of u and $\frac{\partial u}{\partial x}$ which are statistically independent. Kraichnan's(1990) model is based on an equation of the PDF of $\partial u/\partial x$ which is similar to the Fokker-Planck equation. The analysis shows an asymmetry in the PDF of $\frac{\partial u}{\partial x}$. Thus from an initial Gaussian field u becomes highly non-Gaussian in its derivative $\frac{\partial u}{\partial x}$. The departure from the Gaussian shape can be predicted from the analytic form of the closure PDF. Figure 6.28 shows the departure of $\partial u/\partial x$ from its initial Gaussian statistics and remains non-Gaussian for all times, which confirms with Gurbatov's work for a random signal (1991). In the case of u, the statistics remain Gaussian until the shock formation time and then gradually tends towards non-Gaussian behaviour for all times. Kraichnan's treatment for Burgers equation is directly applicable to the present study of the propagation of finite amplitude acoustic waves.

Kraichnan(1990), in the work described above, shows that the PDF for $\partial u/\partial x$ after nonlinear distortion rises steeply near the origin in the positive half domain, reaches a maximum close to the origin and then falls nearly exponentially. The numerical results are in agreement with Kraichnan's solution and show that the flatness for $\partial u/\partial x$ increases from its value 3.14 at $t = 0$. The corresponding skewness changes from zero at $t = 0$ to -4 in the same time range. The corresponding values of flatness for velocity remain approximately constant, vary around 3.0. As a simple approximation to the PDF, near the shock formation time it is assumed that the PDF is one sided and occupies only the negative half of plane for $\partial u/\partial x$ and that it is exponential in the half domain. The values of flatness and skewness are 4.20 and -4.12 respectively. This result indicates that the PDF is changing from the 2 sided symmetric Gaussian distribution at $t = 0$ when the positive

and negative slopes are equally probable to the asymmetric PDF near and beyond the shock formation time. Here the most probable value of $\partial u/\partial x$ is dominated by its large negative values. Thus it is clearly seen there is a progressive change of the flatness of $\partial u/\partial x$ from 3 to 5.19 and the skewness changing from 0 to -4.12.

In the present work for test case 1 the values of the PDF of u for various times is shown in figure 6.27 and for $\partial u/\partial x$ in figure 6.28 when $R = 500$. These results show that for u the changes from an initial Gaussian distribution towards a quasi-sawtooth wave generate only small changes from Gaussian and the result is the flatness and skewness do not change much. However, for $\partial u/\partial x$ it was found the corresponding changes were more dramatic and the flatness and skewness respectively change from (3.14, 0) to (5.98, -4.12). The PDF's were obtained using the above numerical results for the propagating signal, and a statistical package, 'S-Plus' provided by Kuha(1995).

The above results refer to the changes in the PDF's upto the shock formation time. Beyond the shock formation time the results for the skewness and flatness of both u and $\partial u/\partial x$ suggest the non-Gaussian statistics continue to evolve with time. However, for the positive gradient $\partial u/\partial x$ becomes very small ie ($\sim 1/t$) whereas the negative gradients become very large and PDF is dominated by the negative values of $\partial u/\partial x$.

Hence in finding any change in the statistics from an ensemble of random processes from the initial statistics such as Gaussian, this change from the inviscid equations neglecting ϵ cannot be derived. The terms in ϵ become more and more important the higher the order of the moments. If ϵ were neglected , it will wrongly be concluded that the average moments were independent of time and hence an initial Gaussian distribution would remain Gaussian. When the dissipation such as the complete Burgers equation is included it is seen that the nonlinear terms cause a redistribution of energy along with change in the dissipation and hence all moments are time dependent and an initial Gaussian distribution becomes non-Gaussian.

6.16 Bispectrum

In a recent paper Gurbatov(1986) has shown the importance of the bispectrum for an initial signal which is Gaussian. In his paper, Gurbatov has shown that the transfer of spectral energy due to non-linear interactions for a particular wavenumber occurs due

to the sum and difference in the wavenumbers. It is shown in chapter 5 that the sum and difference mechanism is governed by the nonlinear term where the harmonics add up to form the sum components and subtract to form the difference components. In particular, Gurbatov has shown that the spectral energy at a particular wavenumber can be transferred to the sum and difference wavenumbers. Since Gurbatov explains this via the use of the bispectrum in his analytic work, the present work on the numerical evaluation of the bispectrum was undertaken for more general waveforms. A recent paper by Novikov(1994) describes the use of bispectrum especially in investigating the tones observed in a spectrum. The bispectrum, which is an ensemble average of the product of three spectral components, is a very useful diagnostic tool in experimental studies of nonlinear wave random interactions and is given by Kim (1978). If the bispectrum for a signal is zero then the signal is Gaussian. It is defined as

$B(k,l) = E[X_k X_l X^*_{k+l}]$

where X_k, X_l and X^*_{k+l} are the signal Fourier transforms for 3 different wavenumbers, E[ ] is the expectation operator and * denotes the complex conjugate. E[ ] is complex, and has two wavenumber indices k and l. The bispectral measurement in this report deals only with the magnitude of the bispectrum. It is plotted in 3-dimensions, with two orthogonal wavenumber axes defining the k,l plane, and the bispectral content is normal to that plane. The power spectrum treats each wavenumber component as independent from all others, and measures the signal's energy distribution at each wavenumber. The bispectrum, on the other hand, measures the amount of coupling between the three wavenumber components at wavenumbers k, l and $k+l$.

The first order moment of a signal is the mean, the second order moment is the variance, and higher order moments can be found by Taylor expansion of the Moment Generating Function[see Newland(1984)]. The useful property of these moments is that all odd moments of orders three and higher for a Gaussian process are zero because of the symmetry of the signal PDF. The even moments of order four and higher are all linear combinations of the lower moments. In a similar way for all Gaussian processes, all the cumulants of order three and higher are zero (see Piersol 1966). From these statements it is deduced that for such normal process the bispectrum of such a signal is zero. The zero lag component of the second cumulant is the signal variance which is found by integrating the power spectrum. In a similar way, the zero lag component of the third cumulant is the skewness which can be found by integrating the bispectrum over all wavenumber

pairs. Thus the average height of the bispectrum can be used as an indication of the signal skewness. Following on from the fact that the cumulants of order three and higher are zero for a Gaussian process, the bispectrum of such a signal is zero. The computational procedures for the bispectrum are given by Nikias et al(1993) and are given below. The cumulants are related to the higher order spectra via the Fourier transform: the power spectrum is the Fourier transform of the second order cumulant, the bispectrum is the double Fourier transform of the third order cumulant. The procedure is as follows:

(i) Thus M sets of data recorded over a length N having an average zero were formed, and an appropriate window was applied to it to reduce leakage.

(ii) Compute the Fast Fourier Transform so that its complex spectrum can be obtained.

(iii) Estimate the bispectrum by

$$\hat{B}(k,l) = \frac{1}{M}\sum_{i=1}^{M} X_k^{(i)} X_l^{(i)} X_{k+l}^{*(i)} \tag{6.12}$$

where $\hat{}$ denotes an estimator.

From the results obtained from the bispectrum the following deductions are made:

(i) Figure $6.29a,b,c,d,e$ show the evolution of the bispectra for Test case 2 at various times respectively.

(ii) It is seen that with advance in time an initial Gaussian distribution becomes non-Gaussian. This is demonstrated from figures $6.29a,b,c,d,e$ where the initial bispectrum which is flat(Gaussian) (a) increases in height(nonGaussian)(b,c,d,e) and remains non-Gaussian for all later times.

(iii) The area under the bispectrum gives the skewness, showing the distribution becomes more and more skew with time.

(iv) It was found difficult to compute the bispectrum at large times since the waveform gets simplified with lesser numbers of zero crossings. To do so, a large number of waves are required to obtain the necessary numerical accuracy and this is not possible at large times. In the present study the bispectrum was used to display the non-Gaussian development of the statistics from the initial random Gaussian wave distribution.

6.17 Conclusion and summary

The following conclusions can be drawn from the present chapter

From the numerical solution to the Burgers equation using the Cole-Hopf transformation, has been developed the necessary computer programme to enable the developing characteristics with time of an arbitrary random initial high amplitude noise signal, having a Gaussian probability distribution function, to be computed. The development of the initial wave into an assemblage of sawtooth like structures has been investigated. The wave distribution is assumed to be periodic having a periodic length L containing a very large number of zero crossings and hence eventually a large number of shock waves. All the statistics are performed on this single realization of an ensemble of such waves.

The initial spectrum for test case 1 which had a k^2 increasing in the low wavenumbers and $1/k^2$ decreasing in the high wavenumbers was chosen similar to the spectrum for an N-wave. Thus as the initial random wave distorts to form sawtooth like structures the high wavenumber spectrum extends upto the Nyquist wavenumber as $1/k^2$ spectrum with a random spread. Test case 2 is different from test case 1 since however much nonlinear distortion tries to produce a $1/k^2$ spectrum, $< U >^2$ falls immediately beyond $t = 0$ and hence the the spectrum falls more exponentially than $1/k^2$ in the high wavenumbers. The kinetic energy for test case 2(i) thus falls as $t^{-3/4}$ compared with $1/t$ for test case 1. The rate of dissipation falls as $1/t^{-1.5}$ compared with $1/t^2$ for test case 1.

The nonlinear distortion at $T > 0$ resulting in the sudden population of energy into higher wavenumber thus giving a $1/k^2$ spectrum is clearly shown. This is when the waveform distortion is a maximum when it is shown that sawtooth like structures are formed. These sawtooths merge according to Lighthill's 'bunching' phenomenon when the waves with large amplitude overtake the waves with smaller amplitude in time and this process reduces the number of shocks in a given sample length. The number of sawtooth waves reduce to a small number. It follows that the waves at large time have a structure independent of the initial random wave. At still larger times far greater than was possible in the present numerical work, it is expected that the wave will reduce to a single periodic sawtooth wave. This then becomes the initial condition for Cole's analytic solution where it is shown that ultimately all initial waves reduce to a single sine wave of vanishingly small amplitude.

It is shown that at small times the periodic boundary conditions imposed on the signal

possesses different temporal features from that of the isolated signal. Nevertheless the periodic case was simpler to compute and presented results similar to the nonperiodic case provided a large number of shocks (zero crossings) were retained over the given overall time of propagation. With a large number of shocks the statistics of the random process involved in the nonlinear distortion could be examined. The present study comprises two interconnecting features covering the nonlinear distortion of a complex random wave and its progressive development in time. The first feature considers its spatial development of the particle velocity distribution with distance over the periodic length, L. The second considers its change in spectrum with time. The first feature relates to the distortion of the complex random wave into an assemblage of sawtoothed waves and their reduction in number with time due to 'bunching'. The second feature concerns the nonlinear development of the spectrum whereby the main interaction process involves the population of the high wavenumber end of the spectrum by the 'sums and difference ' mechanism which populates the high wavenumber components arising from the nonlinear term. This is followed at later times by depopulation of the higher wavenumbers owing to viscous broadening.

At very large times than possible in the present calculation the random signal is expected to asymptote to a waveform independent of its initial waveform. Thus when viscous broadening dominates at large times and engulfs the complete wave it loses its non-linear characteristics and it is reduced it to a damped acoustic wave. However in the inviscid case it reduces to the universal waveform of an N-wave, indeed an infinite periodic array of N-waves. In the viscous periodic case any initial waveform distribution comprising a large number of individual waves will ultimately reduce to a single symmetric wave. From Cole(1951) it is expected that this wave to be a damped sine wave.

It is shown that the non-dimensional value of the Taylor microscale, λ/L, at all times in the propagation of the complex finite amplitude acoustic wave is an important parameter. It is shown that λ and n_z are dependent on the skewness and flatness of U and $\dot{U}$ and that a knowledge of the skewness and flatness alone cannot determine the joint pdf and the values of λ and n_z. $< U > 2$, $< \dot{U} >$ and λ can be determined from the 2-point velocity correlation function. It is shown that for an initial distribution u at $T = 0$, corresponding to a given spectrum, λ/L can be determined. Its role in the wave distribution process is far more important than the relatively small changes in the peak wavenumber with time. It is shown that λ is related to the shock wave thickness and is proportional to

the average spacing between shocks at any time. It also relates directly to the number of shocks present at any time within the periodic length, L.

The non-dimensional value of the Taylor microscale λ/L for both test cases 1 and 2 has been computed from the predictions of I_0 and I_2, where λ/L for test case 2 is smaller than λ/L for test case 1. For test case 1 it is shown the value of λ/L first decreases upto the shock formation time and then increases approximately as $\sqrt{t}$. The rate of dissipation for both test cases is described and shown that the rate of dissipation depends on the initial spectrum. It is shown that however much the rate of dissipation is expected to depend on the truncation wavenumber, it also depends on the initial shape of the spectrum and is different for the two test cases.

Another version of test case 2(i) with a very large change in the high frequency end of the initial spectrum was compared with test case 2(i) for all times. It is shown that at large times the divergence increases to more than its initial spectrum because rate of dissipation takes over and is more in the case of test case 2 (ii).

The effects of Reynolds number is discussed. It is shown from this numerical calculation that beyond an initial $R = 500$ the results for test case 1, do not change much and compare favourable with Lighthill's inviscid results for random sawtoothed waves.

In the investigation of the propagation of two initial waveforms having completely different initial spectrums but same initial kinetic energy is yet to be investigated for more realisations. But for a single realisation, it was found that the total energy at large times was found to be equal. It was also found that the initial rate of dissipation for test case 1 was larger than test case 2 though the truncation wavenumber k_T for test case 2 was larger than test case 1. Thus the rate of dissipation depends on the shape of the spectrum.

The effects of the initial phase is discussed in detail. It is shown that the initial phase is not important as long as the signal is Gaussian. This is an important result uncovered in the present investigation. It is shown that for any initial phase value having Gaussian statistics, the spectra at any time has the same decay. The choice of the initial phase is important in determining how much the initial signal is Gaussian. If the initial phase is selected to have an approximate Gaussian statistics, the spectra at large times will approximately converge with other spectra in the high wavenumber region whose initial signal was Gaussian.

The statistical characteristics, such as the average, variance, skewness and flatness for

test cases 1 and 2. With values of average or U_0, the skewness (≈ 0) and the flatness (≈ 3) at $t = 0$ confirmed the signals were Gaussian. It is shown that with a single sample function which is sufficiently long it is possible to describe properties and parameters of a random process. This represents an ensemble having a Gaussian statistics. The average, skewness and flatness for thus ensemble were computed giving an initial Gaussian PDF. These parameters have been computed for all times for both the test cases, each representing an ensemble. In other words for any given member of the ensemble the progressive properties at all subsequent times have been computed. It is seen that that both these initial Gaussian signals became non-Gaussian with advance in time. In terms of the probability distribution function the probability follows the sub Gaussian (eg flatness increases) statistics (see Bayesian inference in statistical analysis 1973) for Test case 1. The bispectrum of the signal is numerically computed with time. Thus an initial Gaussian distribution, which is seen in the bispectrum plot to be flat, becomes non-Gaussian (the height of the bispectrum) and remains non-Gaussian for all later times.

The changes in the PDF with time for nonlinear propagating waves are similar to the distortions in Burgers turbulence as described by Kraichnan(1990), where the the PDF for negative $\partial u/\partial x$ becomes approximately exponential instead of the initial Gaussian form. The numerical results as discussed above are in broad agreement with Kraichnan's results and conclusions.

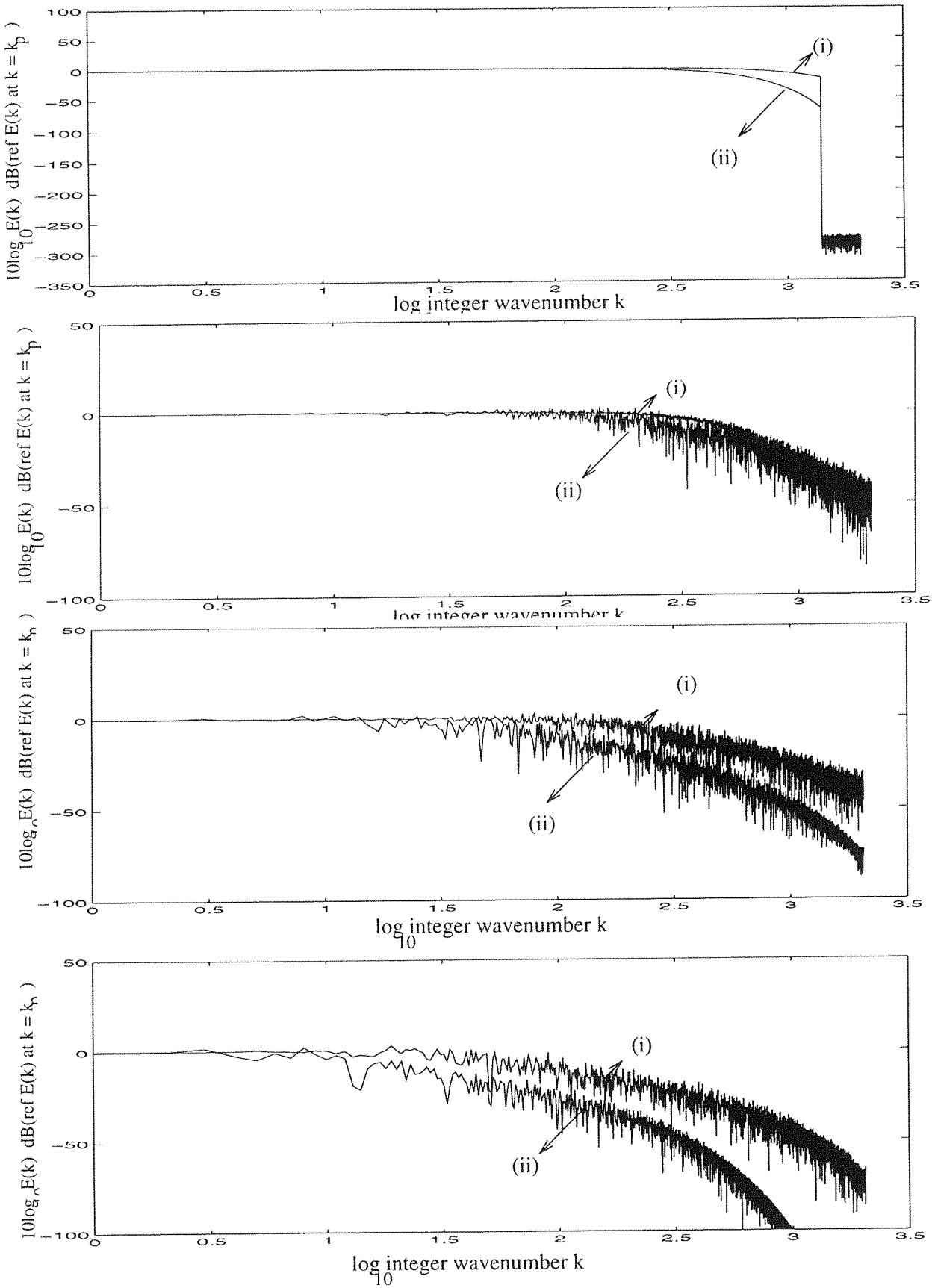

Figure 6.23: Comparisons for test case 2 *(i),(ii)*. $E(k) = e^{-2a^2k^2}$ $1 < k < k_T$, where $a = 0.001$ for *(i)* $a = 0.002$ for *(ii)* respectively. $T = 0, T = 8.0E{-}06, 8.0E{-}05, 8.0E{-}04$. $R = 1000$

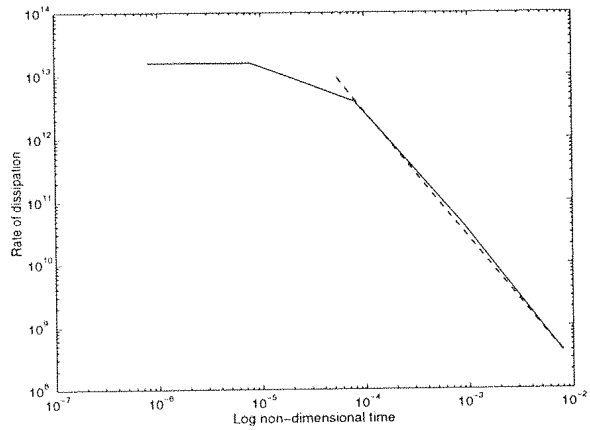

Figure 6.24: Rate of dissipation (ϵ) with time for Test case 1. $R = 500$.

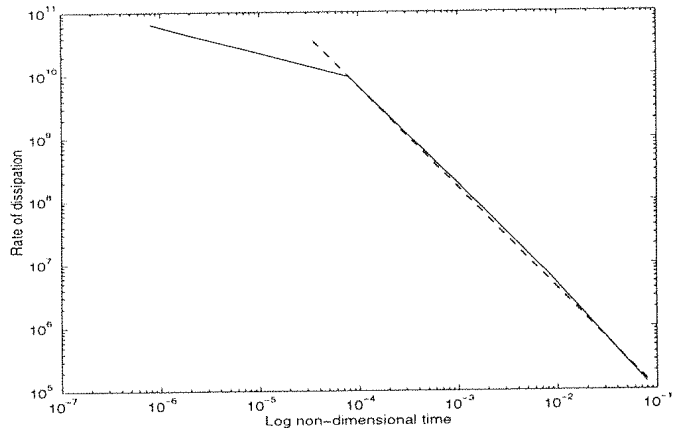

Figure 6.25: Rate of dissipation for test case 2(i). $R = 1000$.

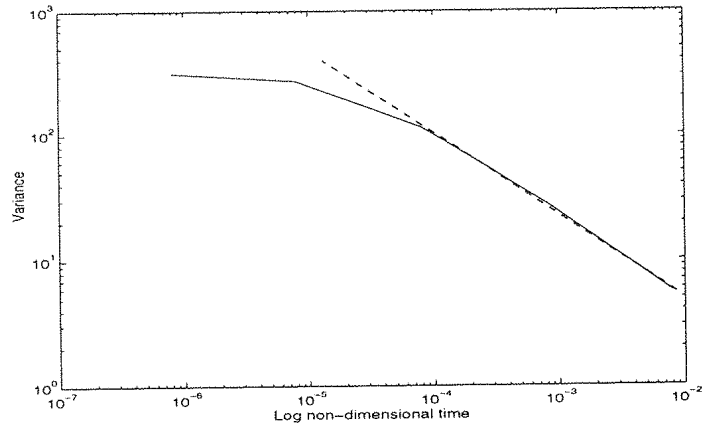

Figure 6.26: Kinetic energy with time for test case 2(i). $R = 1000$.

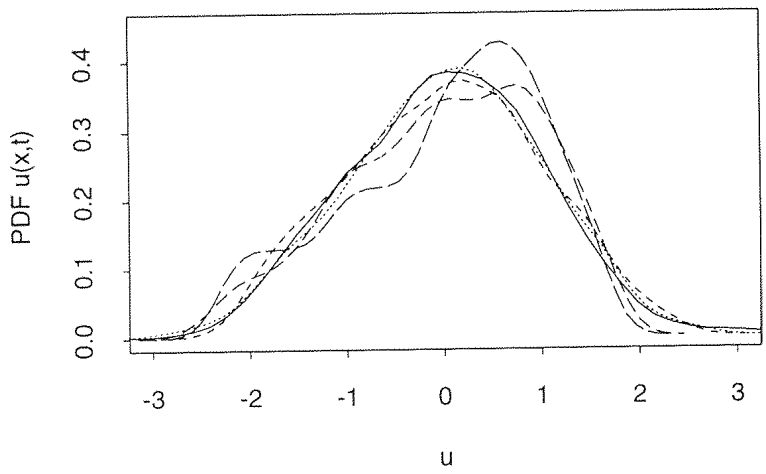

Figure 6.27: PDF of U with times for $R = 500$. Key; ——$T^* = 0$, ... $= 8.0E-07$, - - - - $= 8.0E-06$, - - - $= 8.0E-05$ respectively.

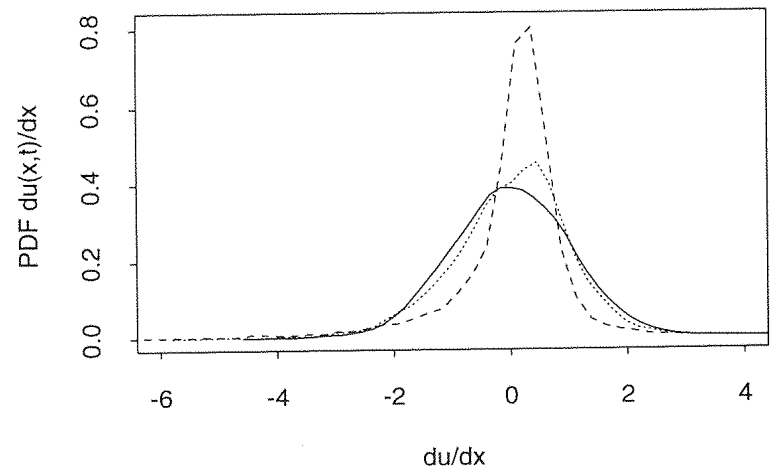

Figure 6.28: PDF of $\partial U/\partial X$ with time for $R = 500$. Key; ——$T = 0$, ... $= 8.0E-07$, - - - - $= 8.0E-06$ respectively.

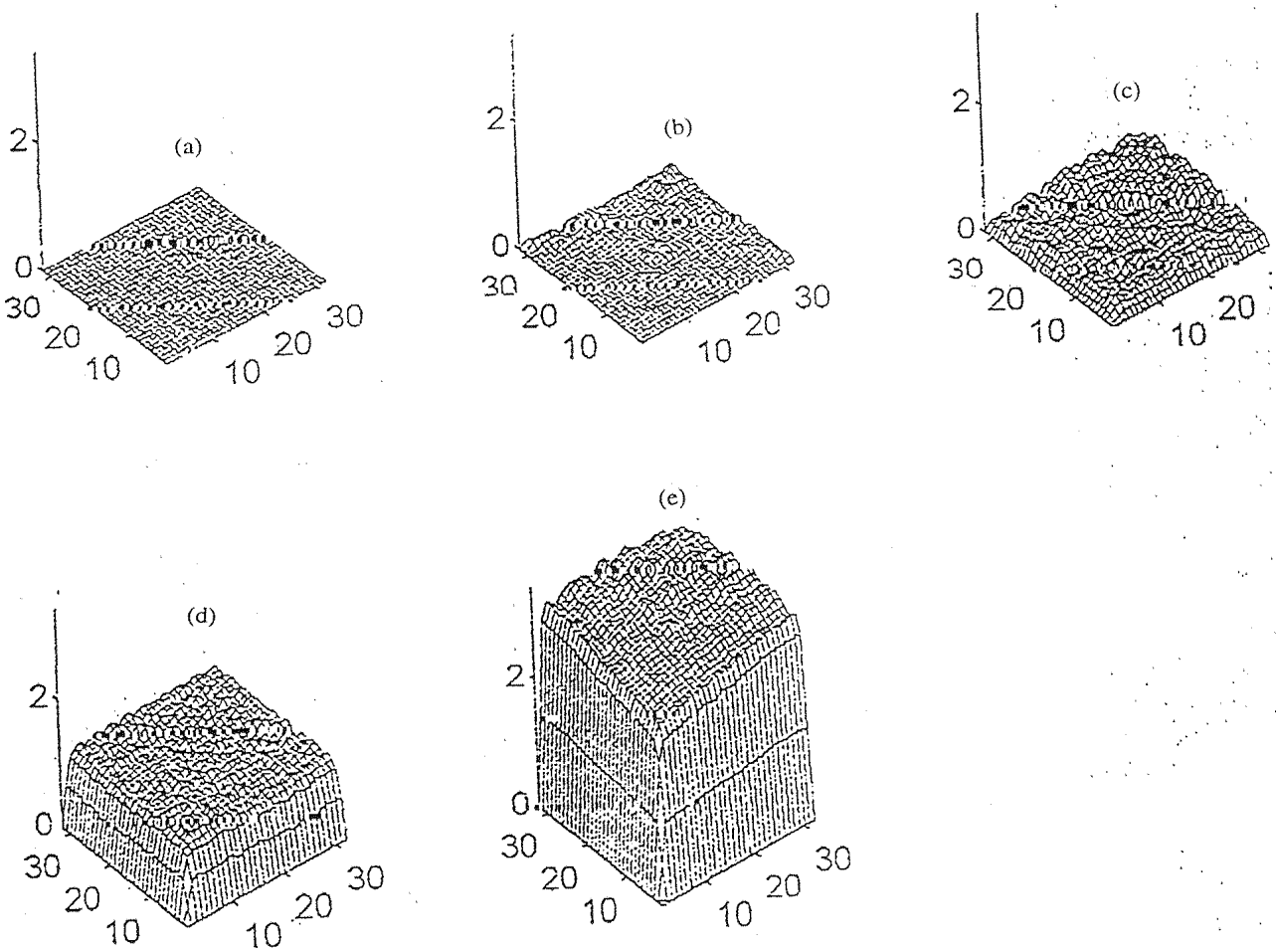

Figure 6.29: Evolution of bispectrum for test case 1. $R = 500$.

$T = 0, 8.0E-07, 8.0E-06, 8.0E-05, 8.0E-04$ shown in *a, b, c, d, e* respectively.

Chapter 7

Difference between the propagation of Gaussian and Non-Gaussian initial signals

7.1 Introduction

Chapter 6 describes the changes in the statistical properties of an initial random noise signal during nonlinear propagation. It is shown that a high amplitude initial random noise signal suffers gross distortion with time through nonlinear steepening and viscous broadening. As a result there are gross changes in its energy spectrum. These numerical results were concerned with an initial random signal obeying Gaussian statistics. In this chapter the difference in the nonlinear propagation between an initial signal having either Gaussian or non-Gaussian statistics is considered. In other words the case is investigated where at different times during the propagation the signal is re-randomised to restore Gaussian statistics before its propagation is recommenced. This result is compared with the propagation of the same initial random noise signal which suffers no such interruption.

This problem relating to the differences in the propagation of Gaussian or non-Gaussian initial waveforms has arisen in the work of Webster and Blackstock(1978) when comparing their experimental results with computed results using the numerical method of Pestorious(1973). Although the experiments were concerned with the nonlinear spreading of partially spherical waves the corresponding case of plane wave propagation has been studied and the results are presented below. It is found that they explain qualitatively many

of the features reported by Webster and Blackstock.

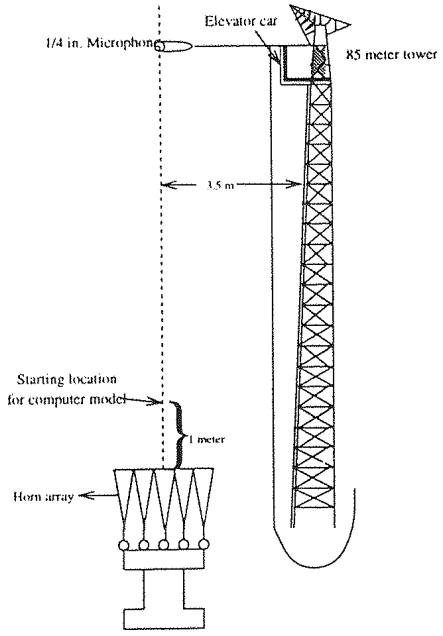

Figure 7.1: Blackstock and Webster's experiment on outdoor noise propagation

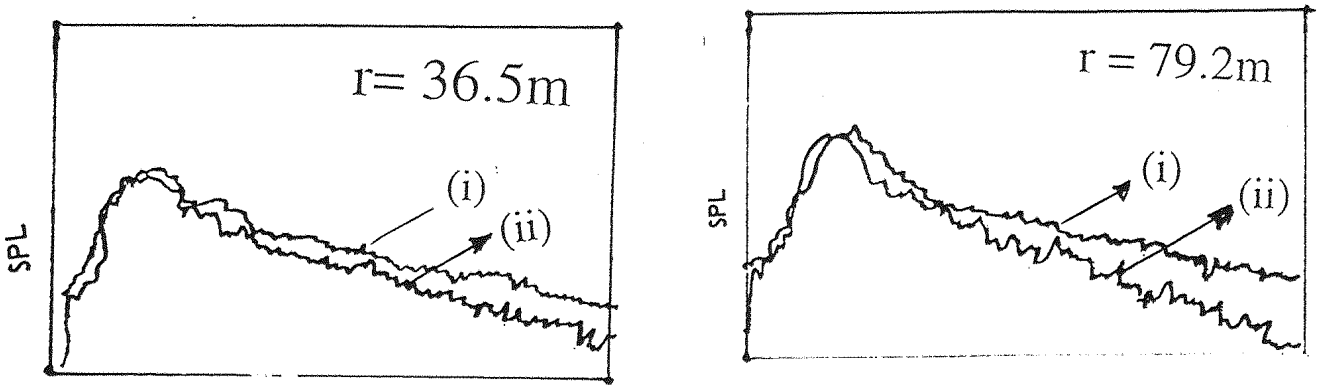

Figure 7.2: Comparison of the Blackstock and Webster's experimental(i) and computed (ii) spectra.

7.2 The Webster-Blackstock's experiment on nonlinear noise propagation

Outdoor measurements were performed by Blackstock and Webster (1978) on the near spherical spreading of broadband noise of high intensity. The experimental setup is de-

scribed in figure 7.1. For comparison with a theoretical model of nonlinear sound propagation to obtain their initial signal, Blackstock and Webster reconstructed the waveform at the start of the propagation path by assuming this initial signal to have Gaussian statistics. The start of the propagation path could not be taken at the source itself because of the finite source dimensions (see figure 7.1), so Blackstock and Webster chose a distance of 1m from their source for their initial station in their computational model. They then assumed the initial signal at 1m was part of a spherical wave. They matched the initial signal in the computation with that measured experimentally at 1m. In their computational model random phases were assigned to the Fourier components of the reconstructed waveform sample, while the amplitudes were chosen to fit the experimentally measured power spectrum obtained using a microphone. Their computational model was based on weak shock theory. The numerical algorithm is due to Pestorious(1973) which consists in propagating the signal step by step with a step length Δx. A Fourier transform at each step length is made when corrections due to absorption for the appropriate distance Δx are applied. The signal is then propagated for a further step distance Δx until the desired total distance is reached. At each step the results are corrected for absorption. The numerical code includes the effects of spherical spreading and diffraction. They found the actual spectral decay with distance was much less rapid at high wavenumbers than the model predicted. Figure 7.2 shows the comparison between Webster and Blackstock's(1978) measured and their computed spectra.

7.2.1 Description of Webster and Blackstock's numerical experiment

The main aim of the present numerical study was to show the changes in nonlinear distortion and viscous broadening arising in an 'equivalent' plane wave propagation case as a means to explain the major differences that arose between the experimental data obtained in the Webster and Blackstock(1978) experiment and their computational results based on the use of the Pestorious algorithm(1973). The present results are based on the Convolution Method described in chapter 4. It is therefore necessary to first explain the major differences between their experiment method and those incorporated in their numerical method using Pestorious algorithm.

The Pestorious algorithm is based on nonlinear geometrical acoustics and, for comparison with the Webster and Blackstock experiment, includes the effects of spherical spreading. It also includes diffraction effects and the changes in the effective diffusion

coefficient allowing for both thermoviscous and lag effects arising from molecular absorption along a ray. As discussed above Webster and Blackstock(1978) were concerned with the definition of the properties of the wave at the initial station. They decided, following earlier work by Pestorious et al(1974) that the initial model signal should have the same spectrum as in the experiment but that the phases would be random and subject to Gaussian statistics. In their experiment Webster and Blackstock used a Gaussian random signal generator to drive the horn array. Their initial signal generated by 20 horns in a close array, is a random high intensity signal and is probably initially planar with diffraction at the edges. Clearly in the experiment nonlinear distortion sets in close to the horn faces and at distances less than 1m from the source. Thus at 1m the signal is already non-Gaussian and shocks soon dominate the waveform and the amplitude decays, for plane waves, as $1/\sqrt{t}$. Due to nonlinear distortion the energy spectrum at high wavenumbers will be populated way beyond the upper frequency of the sound generated by the horn array. In their computational model Webster and Blackstock re-randomised the signal at 1m having random phases following Gaussian statistics with the same spectrum and variance. The assumption of a Gaussian signal however had the effect of cancelling the nonlinear distortion and particularly the asymmetry in the $(\partial u/\partial x)_+$ and $(\partial u/\partial x)_-$ which had taken place between the source and 1m distance and is clearly the reason why the signal at 1m is non-Gaussian. They therefore assumed the statistics of the noise at the face of the horns was Gaussian and remained Gaussian to an 'initial' station 1m from the horns. The assumption was that over a short distance of 1m the initial Gaussian signal would not suffer sufficient distortion to change the statistics to non-Gaussian. This assumption may be found to be adequate for the statistics of u but clearly it is likely to prove a poor assumption for $\partial u/\partial x$ and higher derivatives.

In their numerical calculations they investigated many different initial waveforms each having the same energy spectrum but different random phase distributions. Although they noted resultant changes in the spectra with time they concluded that the 'initial phase distribution was not of major significance in nonlinear propagation provided it was random'.

In the present work the changes in the wave statistics were similarly studied and in particular the difference in the energy spectrum at various times arising from waves having initially Gaussian statistics to those having initially non-Gaussian statistics. A further comparison was made by re-randomising the phase of the signal to restore Gaussian

statistics after a later time interval than that re-randomised at an earlier time.

A major difference between the Pestorious algorithm and the Convolution method is that the latter is concerned with complex yet overall periodic wave trains at all times, whereas the former deals with a time marching procedure for the wave described as a spatially nonperiodic distribution. In the Convolution Method calculations are made at selected values of time and do not involve the usual finite difference techniques involving spatial grids and time marching procedures as used in the method of Pestorious(1973).

At first sight it appeared that the results using the Convolution Method for the propagation of nonlinear periodic plane waves could not be compared with the results of the Webster and Blackstock experiments and the corresponding numerical results based on the Pestorious algorithm. This was because they propagated spherical waves with different boundary conditions and included the effects due to diffraction, whereas the CM dealt with plane wave propagation having periodic boundary conditions and did not include any effects due to diffraction. Nevertheless once it was realised that the major differences between the Webster and Blackstock experiments and their numerical results was in the assumptions connected with the statistics of the initial wave at 1m. it seemed appropriate to perform an independent calculation based on plane waves and to note the changes in waveform and spectra at various distances using different statistical assumptions for the initial waveform. Thus a qualitative comparison was possible between the present work and those of Blackstock's experimental and computational work. The results based on the Convolution method over the propagation distance of 80 m, are expected to be different in overall amplitude from those found in the Webster and Blackstock experiment but it is expected this is not to be of major importance since it only involves a correction to allow for spherical spreading and diffraction just as used in the Pestorious algorithm. Their initial signals (both experimental and computational) was almost of similar shape to the spectrum of test case 1 described in detail in chapter 6 which was propagated in the present work. Hence it was more easier to compare their results with the present calculation. It is conjectured that of greater importance is the difference between the results at various times obtained with different statistical assumptions for the initial spectrum and this difference is not affected by spherical spreading as opposed to linear propagation.

The long time behaviour of periodic and nonperiodic wave trains are very different and arise from the different boundary conditions involved. An isolated wave packet propagating in undisturbed air is referred to as non-periodic. A periodic sawtooth wave is

more influenced by the periodicity boundary condition than randomly placed sawtooths within a periodic domain. When a random periodic wavetrain propagates over a small time, its random shocks distort and 'bunch' with neighbouring shocks within the periodic length. When a nonperiodic distribution of random sawtooth waves propagates the overall wavelength increases with time. But since at least 3 zero crossings are required to form a shock, a maximum of 2 shocks could be lost at both ends for a wave consisting initially of more than 100 zero crossings. The difference in waveform between the periodic and non-periodic case is small for small propagation times and can be neglected although at sufficiently large times the two cases are different. For the propagation over short distances it is possible to compare the present results for the periodic case with Webster and Blackstock's experimental results, provided at least 40 zero crossings remain in the signal. It should be noted that in Blackstock's experiment the maximum propagation distance in the atmosphere was 80m. This distance is such that only a small increase in the length of the distribution occurred. This is confirmed in Webster and Blackstock's(1978) numerical results, and from their measured waveform distribution with distance it is seen that not a single zero crossing has propagated outside the initial sample length in the distance of 80m. The number of zero crossings is however reduced due to the 'bunching' phenomenon, and this nonlinear process as well as the effects of spherical spreading reduces the amplitude of the wave train with time.

If then a suitable method can be found to allow for the amplitude changes due to spherical spreading and diffraction there appears to be some justification in making a comparison between the experimental results of Webster and Blackstock and the numerical results using the present Convolution Method for the propagation of nonlinear periodic plane waves. The effective absorption is thermoviscous. In Webster and Blackstock's experiment the effects of molecular absorption and lag effects were in fact small over 80m. As shown in figure 7.2 the differences between the results obtained for the sound pressure level at 80 m of the numerical model and in the experiment are large and of order 20dB in the high frequencies. It is argued here that this difference must arise from statistics of the initial waveforms being changed from non-Gaussian to Gaussian.

7.3 Signals to be propagated using CM

In the Convolution method a similar initial broadband noise signal was used where the initial plane wave statistics were Gaussian. A number of different cases were evaluated as detailed below. These include the case where an initial signal is Gaussian $T = 0$ and is then allowed to propagate a small distance. This signal is then re-randomised to have Gaussian statistics and then recommences propagation to times equivalent to a distance of 80m and more. The waveform and spectra are then compared with that of the uninterrupted signal. The third case was investigated when the signal was interrupted at a later time and then re-randomised to have Gaussian statistics before recommencing propagation to 80m. The results for the 3 different cases are shown in figure 7.5 where:

(i) The signal is non-Gaussian at $T = 8E-07$ and is propagated over a time $T = 8E-03$

(ii) The signal is re-randomised and made Gaussian at $T = 8E-07$ and is then propagated over a time $T = 8E-03$.

(iii) The signal is re-randomised and made Gaussian at $T = 8E-06$ and is then propagated over a time $T = 8E-03$.

7.4 Comparison of Gaussian and non-Gaussian initial signals

Tables 6.1 and 6.2 in chapter 6 gives the values of the various parameters used for the reference signal. Webster and Blackstock's propagation distance was 80 meters which lies between the propagation times $8E-07$ and $8E-06$. The initial waveform containing a large number of Fourier components was numerically generated with random phase and with the amplitudes for each wavenumber (k) increasing like k^2 in the low wavenumbers and $1/k^2$ in the high wavenumbers. It also had a certain variance and a cutoff wavenumber, $k_T = 1000$, and obeying Gaussian statistics as described earlier in chapter 6. The spectrum for this reference signal is shown in figure 6.3. The procedure for solving BE using the Convolution method with periodic boundary conditions is the same as described in chapter 4. The initial Reynolds number was chosen as $R = 500$ which was found to be large enough and the results using this Reynolds number compare favourable with Lighthill's inviscid results for random sawtoothed waves. This waveform was allowed to propagate and the subsequent evolution of the spectra and waveforms were calculated for various times.

Under nonlinear propagation resulting in nonlinear distortion an increase in the spectrum at high wavenumbers occurs than were present at $T = 0$. The spectrum is therefore allowed to extend beyond the original cutoff wavenumber $k_T = 1000$ upto the Nyquist wavenumber $k_M = 2096$. The numerical results show that the spectrum falls as $1/k^2$ as at time $T = 0$ and also in the range between k_T and the Nyquist wavenumber. However due to nonlinear distortion the signal is now non-Gaussian since the signal becomes skew[see 6.8 in chapter 6]. From the energy spectrum at $T = 0$ the number of positive (or negative) slope zero crossings can be obtained from Rice's formula described in chapter 6 when the signal is Gaussian. In addition $\lambda(T = 0)$ can be determined. Thus as the signal propagates from time $T = 0$ to $T = T_1 = 8E - 07$, say, the spectrum falls as $1/k^2$ in the high wavenumber region. As time increases, the spectrum in the high wavenumbers become progressively more depopulated due to dissipation. In addition due to the bunching phenomenon the number of zero crossings is reduced, but Rice's formula can no longer be used since the signal is non-Gaussian. It is found however that the correction for the number of zero crossings for a non-Gaussian signal depends on the joint pdf between u and $\dot{u}$ which differ considerable from those for a Gaussian signal and is described in Appendix H. Kac(1964) has presented the correction to Rice's formula but this correction depends on knowing the joint pdf.

If the case is now considered where the signal has been re-randomised [case (ii) described in section 7.3] at $T = T_1 = 8E - 07$, where the re-randomised signal has the same spectrum and variance, it is immediately noted that changing the statistics from non-Gaussian to Gaussian imposes important changes to the waveform. The re-randomised signal (ii) at $T = 8E - 07$ and the uninterrupted signal (i) are shown in figure 7.4 (a,b) respectively, from which it is clear that re-randomising the signal results in more zero crossings. The uninterrupted signal 7.4a at $T = 8E - 07$ shows that the number of zero crossings are reduced from that at $T = 0$[the signal at $T = 0$ is shown in figure 6.4 in chapter 6], implying that at $T > 0$ the strong shocks overtake the weaker ones even before the average shock formation time, and ' bunching' has taken place. Thus the shock formation time for each wave is different. Thus the signal at $T = 0$ truncated at k_T, produces high wavenumbers due to nonlinear distortion and the number of zero crossings at $T = 8E - 07$ are reduced. This signal [which is now case (ii) of section 7.3] at $T = 8E - 07$ has more zero crossings when re-randomised and made Gaussian. The reason for this is that k_T has now been changed from k_T at $T = 0$ to k_M at $T = 8E - 07$, the Nyquist wavenumber.

When $\frac{k_M}{k_T} = 2$, the number of zero crossings is increased by 40% for a spectrum falling as $1/k^2$ at high wavenumbers. When this re-randomised signal is allowed to propagate, the larger number of zero crossings produces more shock waves, resulting in more 'bunching' which leads to a greater population in the high wavenumber spectrum as discussed by Lighthill(1993). However this leads to greater dissipation and as time progresses the combined result is a depopulation of the high wavenumber components in the spectrum than in the uninterrupted signal. This is clearly shown in figure 7.3 by comparing the upper and middle rows at values of $T = 8E-04$ and $T = 8E-03$.

If next the initial signal (i) is interrupted at time $T_2 = 8E-06$ where $T_2 > T_1$ and re-randomised [case (iii)] with Gaussian statistics, then it is found that the number of zero crossings will of course be greater than the number of zero crossings in the uninterrupted signal at the same time. Thus it is found that the high wavenumber part of the spectrum decays faster than that of the uninterrupted signal and also the signal interrupted at $T = T_1$. These changes in the high wavenumber part of the spectrum do not greatly change the total energy, which according to the 'bunching ' theory is found to decay as $1/t$ for the plane wave propagation.

From figure 7.5 the energy spectrum for (ii) falls faster over all wavelengths than (i). The energy spectrum for (iii) falls faster than both (i) and (ii). This is consistent with the energy decay falling faster for a Gaussian signal than for a non-Gaussian signal. The spectra in each of the cases (i), (ii) and (iii) have been averaged over 3 realization involving different random phases. In order to obtain a smooth spectrum it would be necessary to average over many more realizations. Though the numerical method is accurate since the method has been validated (see chapter 4] it is clear that at any time the energy spectrum cannot not be smooth because of the sines and cosines arising due to nonlinear distortion described in chapter 6.

Thus it is conjectured that the differences in the high wavenumber spectrum in the Webster Blackstock(1978) experiment, is a result of re-randomisation from the source to the artificial origin at 1m. These differences are very large and were shown in the high frequency region around 20kHz to be of the order of 18dB as seen in figure 7.2.

It is concluded that in any numerical simulation of an experiment concerning nonlinear propagation, the statistics of the initial signal must be known with great accuracy. The present work explaining the discrepancy of the results of Webster and Blackstock(1978) experiment and their numerical method show that it is a very poor assumption to assume

the initial signal is Gaussian at 1m. from the source in the nonlinear propagation.

In an earlier paper by Pestorious et al(1974) it was argued that the statistics of the phase of the initial signal was unimportant but this was later to be found inconsistant with the numerical results of Webster and Blackstock(1978). It is also inconsistant with the present numerical results.

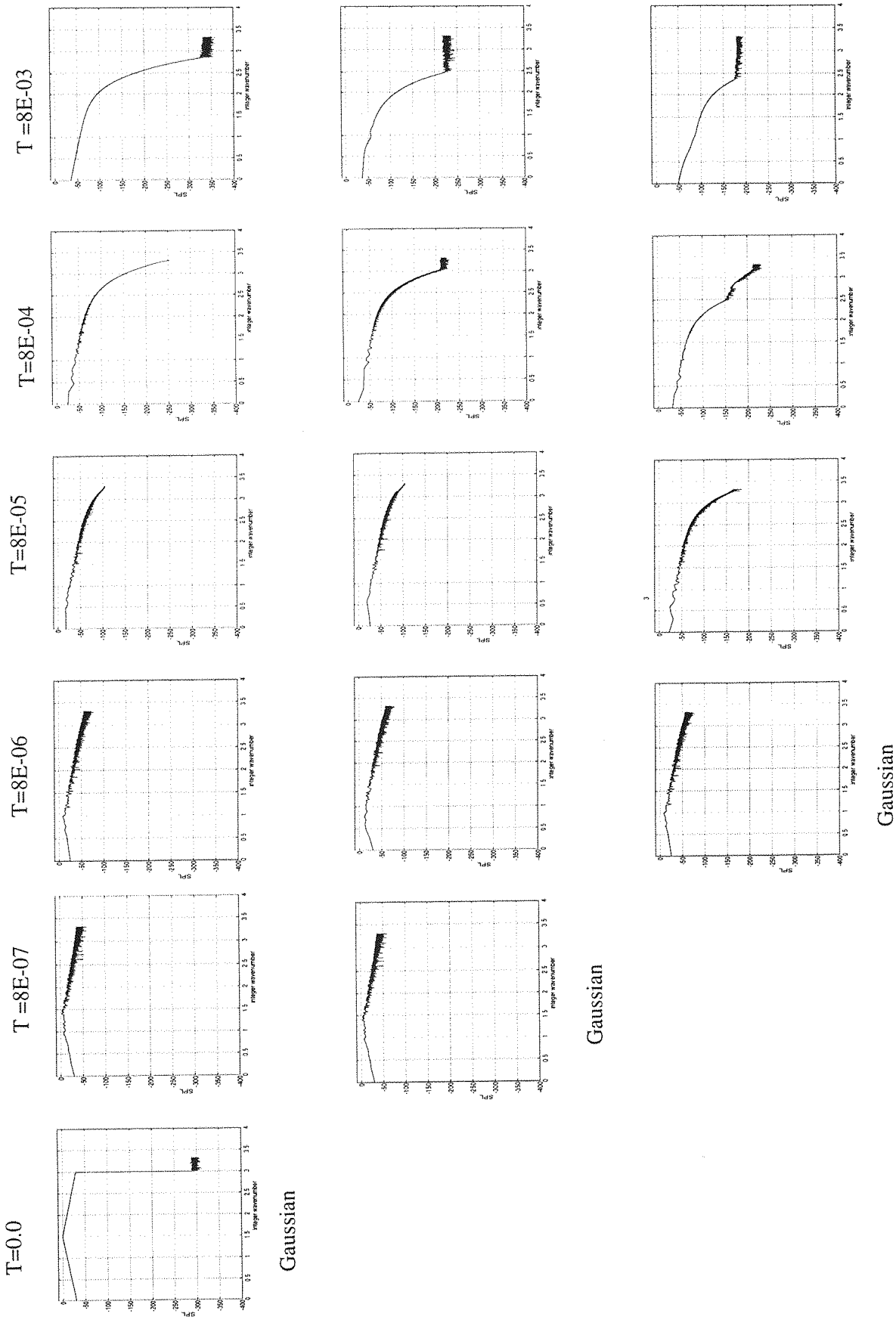

Figure 7.3: Schematic processes of re-randomisation the reference signal at 2 different times.

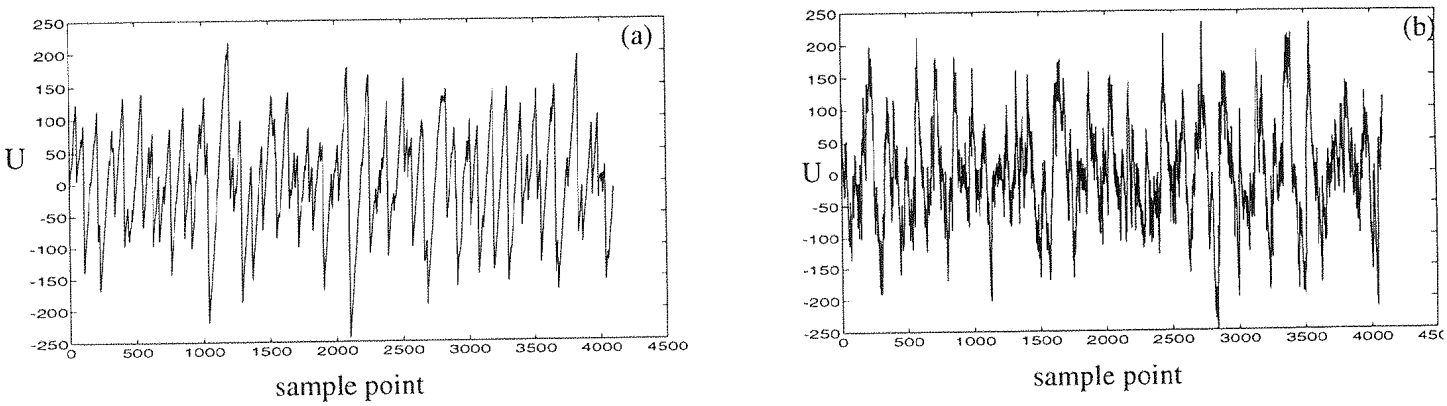

Figure 7.4: Signal at $T = 8E-07$ *(a)* before and *(b)* after re-randomisation

7.5 Conclusion and summary

The present numerical algorithm has been applied to the propagation of initial random plane waveforms having a broadband spectrum, showing that the statistics of the signal change rapidly as a result of nonlinear distortion. It is shown that the phases in the initial random signal are important in the propagation of the signal at $T > 0$. Due to nonlinear distortion, the statistics of the signal rapidly changes from Gaussian at $T = 0$ to strongly non-Gaussian at $T > 0$. The reference signal was propagated and the spectrum due to nonlinear distortion at time $T > 0$ retained its $1/k^2$ decay but is extended up to the Nyquist wavenumber, (k_M). The 'bunching' phenomenon, whereby strong shocks overtake weaker shocks ones takes place at $T > 0$, even before the average shock formation time. The result is the number of zero crossings is reduced.

The difference of propagating a Gaussian and a non-Gaussian signal found in the present numerical calculations amounts to a significant change at the higher wavenumbers. When the propagating signal is interrupted at a given time and the signal is re-randomising with Gaussian statistics, it is found that with increase in time the spectrum at high wavenumber become rapidly depopulated. It is established that the reason for these change in the spectrum due to re-randomising arises from an increase in the number of zero crossings than present for the uninterrupted signal at the same time. Finally it is shown that the numerical calculation display clearly the effect of re-randomising the signal after interruption and the results are qualitatively consistent with Blackstock and Webster's experiment and their calculations based on an interrupted re-randomised Gaussian signal. Thus re-randomising the signal at $T > 0$ does not greatly effect the total energy, but does affect the dissipation and hence shortly afterwards the high wavenumber components are

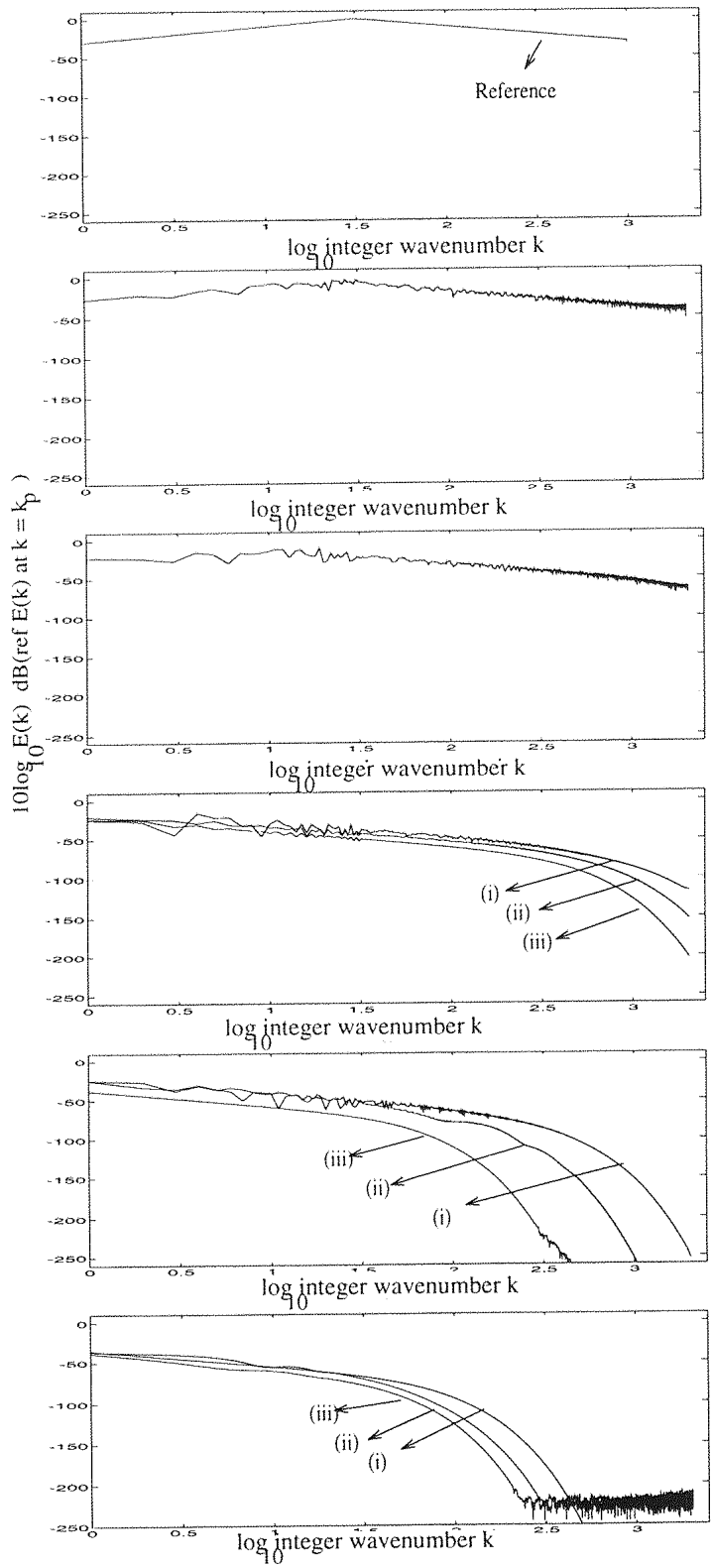

Figure 7.5: Comparison of the evolution of the spectra. Cases (i), (ii), (iii) correspond respectively to the reference signal, interrupted at $T_i = 8.0E-07$ and $T_i = 8.0E-06$. Propagation times are $T = 0$, $T = 8E-07$,$8E-06$, $8E-05$, $8E-04$ and $8E-03$.

rapidly depopulated. The differences in level in the high wavenumbers found here were similar in magnitude to those obtained in the Blackstock and Webster's computation and experiment at a given distance from the horn array. The difference in $< u >^2$ over the distance of 80 m results mainly from spherical spreading. In the present case of plane wave calculations, the decay in $< u >^2$ is smaller. However in the corresponding spectra the changes are large between the uninterrupted signal and re-randomised signal.

In conclusion, it was found that at a high Reynolds number, the power spectrum of the evolving waveform depends critically on the phase statistics of the initial waveform, once the time exceeds that of the shock formation time.

Chapter 8

Comparison of the propagation of random noise with Lighthill's inviscid theory

8.1 Introduction

In chapter 7 the difference between the propagation of an initial Gaussian signal and an initial non-Gaussian signals has been considered. It is shown that nonlinearity affects the phase and hence phase is an important quantity in a random signal. This results in a gross change in the energy spectrum showing that a Gaussian signal decays faster than a non-Gaussian signal.

This chapter studies the formation of shocks during the propagation of different initial random signals at high values of the Reynolds number. The results are compared with the 'bunching' theory introduced by Lighthill(1994) for the propagation of an assemblage of periodic sawtoothed plane shock waves in the limit of inviscid flow. Lighthill's theory, which became available after this work on random waves was completed, also served as a validation on the numerical accuracy of the Convolution method.

In Lighthill(1978) there is a detailed discussion of the Witham-Lighthill theory of nonlinear wave distortion. The geometric construction of the distorted wave at any time is shown using the 'equal area rule' where multivalued solutions are replaced by shocks. The results show the position of shock waves at any time, and these results are in agreement with the solution to the inviscid Burgers equation. Lighthill discusses results for the

propagation of an arbitrary simple wave and shows that beyond a time T_s, which is the shock formation time, shock waves develop with the expansion wave having a slope proportional to $1/t$ and the shock wave strength falls like $1/\sqrt{t}$ for the plane wave case. This result differs from the propagation of linear small amplitude plane waves whose amplitude remains independent of time. Results for cylindrical and spherical waves follow different laws and these are discussed by Lighthill and Witham.

In 1994 Lighthill returned to this problem and argued that the distortion of the arbitrary simple wave which asymptotically degenerates into an N wave differs from the nonlinear distortion of a periodic assemblage of random sawtooth waves. Such a set of random sawtooth waves could have evolved from a train of random waves of large amplitude after a time T_s. In the latter case the periodic length of the waves is fixed at all times where as in the isolated wave case the distance between the bow and the stern wave increases with time. In both the isolated and periodic cases, Lighthill shows that the variation of $u(x,t)$ in a frame moving at the local speed of sound is found from solutions to the inviscid Burgers equation with different boundary conditions in each case. Lighthill further discusses the kinematics of the propagation and distortion of the assemblage of random sawtooth waves. The periodic case treated by Lighthill is a particular case of the present numerical work in the limit of $R \to \infty$. The conclusions reached by Lighthill are described here and are of importance in comparison with the numerical results discussed below.

Lighthill considers the case when the initial complex random wave train is overall periodic and comprises a series of sawtooth waves of random amplitude with a large number of wavelets in a period. As time progresses such a shock system is shown to distort and the stronger shocks overtake weaker shocks and engulf them. However the sawtooth profiles of the individual waves are retained; the main changes are that the amplitudes decrease and the number of individual sawtoothed waves is reduced. Lighthill shows that the expansion waves of ramp like form have a slope of $1/t$ in the $x-t$ plane and all waves irrespective of their amplitude maintain this 'slope' at any given time. Thus Lighthill shows that the mean square of the amplitude of the shocks decreases as $1/t$. This is compared with the attenuation of plane shocks, which follow the amplitude decay law $1/\sqrt{t}$ in the non-periodic case. A further observation of Lighthill for the random periodic waves is that the mean energy does not follow a $1/t^2$ law. Due to the 'bunching' of shocks

with time each shock addition provides an increase in energy in the high wavenumber range and thus the mean energy instead of falling like $1/t^2$, decreases approximately as $1/t$ was found by Lighthill from a numerical example.

The total shock strength, which is the pressure difference in either side of the shock, in a period, z_n, where z_n is the strength of the n^{th} shock, is found by summing the strengths given by $\sum_1^N z_n = L/t$, where L is the overall periodic length. This suggests that on an average the amplitude of each shock wave decays as $1/t$ due to the effects of nonlinear distortion. But for the isolated wave case Lighthill and Witham showed as discussed above that shock waves decay as $1/\sqrt{t}$. Thus it appears that a difference exists between the decay rate of an isolated sawtooth wave and the corresponding decay of the sawtooth wave in a periodic assemblage of such waves. Lighthill refers to this difference in decay rates and argues that the paradox arises from neglect of the 'bunching' phenomenon. He shows that when account is taken of the weaker shock waves being absorbed into shock waves of greater amplitude the result is that shocks decay at a rate less than $1/t$. This is confirmed from a simple numerical analysis based on an initial assemblage of 25 shock waves where it is shown that the decay in shock strength is approximately proportional to $1/\sqrt{t}$ which is exactly that in the isolated sawtooth wave case. In fact it follows from the result given above that although at any one time the sum of the shock strength is proportional to L/t, account must be taken of the decrease with time of the total number of shocks in the period arising from 'bunching'. It is easily shown that the number of shocks at any time decreases as $1/\sqrt{t}$ and hence Lighthill's formula is in complete agreement with his simple numerical result and, as shown later, the results of this work based on the Convolution method.

Hence on average the shocks decay like $1/\sqrt{t}$ exactly as for the isolated case. The existence of a high frequency content of the noise spectrum is essential to satisfy the increase in dissipation that must occur due to 'bunching'. It is not surprising that the decay of the assemblage of sawtooths in the periodic case had a different rate of decay from that in the isolated case.

The reason for the apparent paradox between the $1/t$ and the $1/\sqrt{t}$ amplitude decay laws for shock strength is easily explained. As stated above Lighthill finds $\sum_1^N z_n = L/t$ for the sum of the shock strengths covering a periodic length L at any time t. But it is

argued here that the average shock strength is

$$\frac{1}{N}\sum_{1}^{N} z_n = \frac{L/N}{t}$$

where L/N is the average distance between shocks. However the number of shocks in the assemblage decreases on average as $1/\sqrt{t}$ so the average shock strength decreases not as $1/t$ but as $1/\sqrt{t}$ in agreement with Lighthill's findings from his numerical example. The results from this study, reported below are shown to be in good agreement with those of Lighthill.

The Fourier transform of the N wave was considered. This was because the Fourier transform of the N wave is similar to each individual wave present in an assemblage of sawtooths was first considered. The energy spectrum for the N wave has been discussed earlier by Johnson and Robinson(1967) and by many authors such as Pierce(1981) and Blackstock(1970). The above authors have considered the energy spectrum for both pure N-wave and an N-wave having a specified shock thickness or rise time. It is found that the low wavenumber spectrum increases as k^2 and the high wavenumbers decrease as $1/k^2$. The expansion wave is of length $L - 2\Delta$ where Δ is the shock thickness which is proportional to λ, where λ is the Taylor microscale. The k^2 spectrum reaches its peak at a wavenumber, k_p, corresponding to the half width of the N-wave and beyond k_p the spectrum oscillates between $1/k^2$ and $1/k^4$ and is discussed in chapter 6 [see figure 6.7]. This continues until a wavenumber corresponding to the shock thickness is reached where the envelope of the spectrum falls as $1/k^4$ even though the spectrum continues to oscillate. The complete spectrum involves the incomplete gamma function which provides all the details of the rapidly changing energy levels from one wavenumber to the next. In the case of the pure N-wave the envelope of the energy levels follows the law $1/k^2$ to $k \to \infty$. As expected, such a wave suffers the entropy catastrophe in which there is a sudden increase in entropy and an infinite rate of dissipation. Thus all practical N-waves must have shocks of finite thickness and the above results show the break in the spectrum from $1/k^2$ to $1/k^4$ occurs at a wavenumber equivalent to the shock thickness of λ.

The results obtained from the present work using the Convolution method at high Reynolds number, where the shock wave are of small thickness, can then be compared with Lighthill's results for an assemblage of sawtoothed waves in the special case of inviscid flow.

The present numerical results for the propagation of an initial random noise signal for

large value of R were found to resemble an assemblage of sawtoothed waves having small thickness beyond the shock formation time.

It is important to mention the decay rate of series of sawtooths of equal amplitude in a period. In this situation, the number of waves in the period remains independent of time as can be proved by equal area rule of Lighthill and Witham. However nonlinear effects still remain and the amplitude of the shock waves decreases as $1/t$ instead of $1/\sqrt{t}$.

8.2 Amplitude decay laws

The present work concerns the nonlinear propagation of an assemblage of periodic plane waves. Unlike the propagation of acoustic (linear) waves, which in the non diffusive limit travel without loss in amplitude, periodic nonlinear acoustic waves decay in amplitude as the wave propagates with time. The amplitude decay laws for isolated N-waves, which are plane, cylindrical or spherical, are shown in the table 8.1 below. These results have been obtained by Lighthill(1978), Crighton et al(1992), and others. The results shown in table 8.1 however require some explanation since all of them have been derived using inviscid theory. The amplitude decay of shock waves in these cases arises from nonlinear interactions where the shock waves, in the inviscid limit, are pure discontinuities. However even in this limit a finite increase in entropy is generated as determined by the Rankine-Hugoniot relationship. There is thus a finite dissipation of energy and the result is an amplitude decay in time of the shock. It is the finite increase in entropy that results in the amplitude decay laws in the inviscid limit for each of the three different types of shock waves examined in table 8.1. The variable 'r' refers to the distance propagated by the wave. (The discussion here has concentrated on the entropy rise for a single N wave.) The physical explanation holds also for the assemblage of sawtoothed waves. Results for the periodic case are restricted to the case of plane waves and have been derived by Lighthill(1994).

8.2.1 Description of the random sawtooth waves

In investigating the nonlinear propagation of random noise of high amplitude an initial signal as a function of x was chosen having a zero mean and which had a periodic length $= L$. It contained a large number of zero crossings. The wave distribution was part of a

Plane	$1/\sqrt{r}$
Cylindrical	$1/r^{3/4}$
Spherical	$1/r\sqrt{\ln r}$

Table 8.1: Amplitude decay laws for the isolated N wave

large ensemble of such random waves but since each member of the ensemble contained a large number of random waves it was possible to use the ergodic hypothesis and consider the time development and the statistics of just one realisation over one period of length L. The initial wave had a prescribed power spectrum and the phase of its velocity components in X was randomised. The initial signal was comprised of individual waves of different amplitudes and different distances between adjacent zero crossings. The only difference between the present work and Lighthill's is that in the present work an initial signal is Gaussian, which due to nonlinear distortion at $T > 0$ becomes non-Gaussian. In Lighthill's case the initial distribution is an assemblage of randomly placed sawtooths which is non-Gaussian. The maximum positive and negative slopes $\partial u/\partial x$ throughout the distribution at $t = 0$ although not equal were unlikely to be subjected to large variations and it was assumed their root mean square values was representative of their peak values. Thus the initial signal could be characterised by its kinetic energy $< \frac{u^2}{2} >$, and $< \frac{\partial u}{\partial x}^2 >$. The $< ... >$ denotes an ensemble average but in this study $< u^2 >= \frac{1}{L}\int_0^\infty u^2(x)dx$, its mean square value. The energy equation in this work based on Burgers equation is

$$\frac{d}{dt}\frac{< u^2 >}{2} = -\epsilon$$

where the rate of dissipation of energy, ϵ, in its dimensional form is given by $\epsilon = \nu_e < \frac{\partial u}{\partial x} >^2$. Defining $\phi(\tilde{k}, t)$, is a complex scalar quantity, as the wave energy density such that

$$< u^2 >= \int_{-\infty}^{\infty} \phi(\tilde{k})d\tilde{k}$$

it is found from the Burgers equation that the flow energy in the wavenumber space is governed by the equation

$$\frac{\partial \phi}{\partial t} + ik\Gamma(\tilde{k}) = -2\nu_e \tilde{k}^2 \phi(\tilde{k}) \tag{8.1}$$

where $\Gamma(\tilde{k})$ is the transfer term corresponding to the nonlinear term $(u\partial u/\partial x)$ in Burgers equation. These values were sufficient to determine the number of zero crossings in the

initial signal over a period.

$$n_z = \sqrt{\frac{\sum_{k=1}^{M} k^2 E(k)}{\sum_{k=1}^{M} E(k)}}$$

Now the shock formation time

$$t_s = \left| -\frac{1}{\left(\frac{\partial u}{\partial x}\right)_{\min}} \right|$$

is governed by the maximum slope in the initial profile and as discussed above it is convenient to approximate this in the case of a random noise signal by

$$t_s = -\frac{1}{\left(< \frac{\partial u}{\partial x} >^{1/2}\right)_{t=0}}$$

$$= \frac{\lambda}{(\sqrt{< u^2 >})_{t=0}}$$

a result having a simple physical explanation. It is just the time for the average speed $\sqrt{< u^2 >}$ to travel the distance λ in the moving frame at the speed of sound resulting from nonlinear distortion.

For times $t > t_s$ the distorted wave pattern resembles an assemblage of sawtoothed waves of random amplitude all having the same slope of their expansions $\sim 1/t$ and near discontinuous shock waves. In the present study at finite but large Reynolds numbers the shock thickness was finite and was of order λ, showing that all dissipation processes were confined to the shock itself. As time advanced the number of shocks were shown to decrease [refer to chapter 6 in figure 6.11 (a,b,c,d)] as shocks of greater strength engulfed weaker shocks by the 'bunching' process described by Lighthill(1994). It is shown that the energy decayed as $1/t$. It is to be noted that R_T [see Appendix N] becomes independent of time for $t > t_s$ and although its value differs at $t = 0$ the differences are not great. Thus R_T is an important parameter for this study and represents the relative importance of nonlinear steepening to viscous broadening. All the results obtained in this study showed that when the computational Reynolds number R was of the order of 500 the results were approaching those of a very high Reynolds number with shocks of small but finite thickness.

8.2.2 Comparison with Lighthill's inviscid theory for test case 1

The results for test case 1 described in chapter 6 were obtained using the Convolution Method for finite, but large, $R = 500$ and showed a similar wave distortion with time to that obtained analytically by Lighthill(1994) for the case of infinite Reynolds number.

An important conclusion from Lighthill's theory, which is in agreement with the present numerical results, is that although the amplitude of individual shocks is attenuated as $1/t$, the mean energy does not vary as $1/t^2$ and is indeed close to $1/t$. As Lighthill(1994) explains ' ....the 'bunching' process, in short, significantly enhances the high wavenumber part of the noise spectrum'. Results from the numerical calculations are shown in figure 8.1 where the average kinetic energy falls approximately as $O(1/t)$, in agreement with Lighthill's results. Figure 8.2 shows results for a lower Reynolds numbers of $R = 100$ and $R = 200$ where the decay is $\sim 1/t$ after the shock formation time and continues approximately as $1/t$. At smaller times the kinetic energy remains almost constant and it is in this time interval $t < t_s$ that strong nonlinear distortion of the initial signal takes place resulting in the formation of an assemblage of sawtooth waves. The results shown here are accurate since a number of realizations with different initial phase have been propagated retaining Gaussian statistics. These results have been averaged over 2 realizations and plotted.

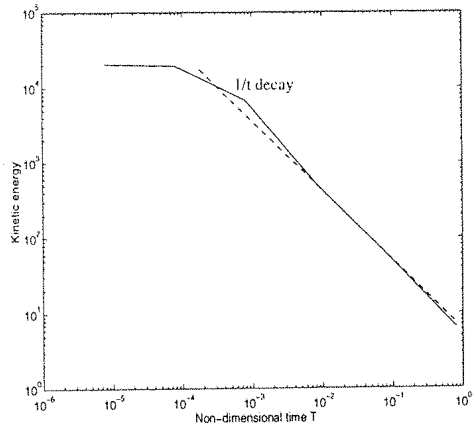

Figure 8.1: Evolution of average kinetic energy for Test case 1 at $R = 500$. Dashed line corresponds to 1/t decay.

8.3 Effects due to Reynolds number for test case 1

The effect of varying the Reynolds number on the shock formation time was investigated for test case 1. It was shown that with increase in Reynolds number the shock formation time was unchanged. The shock thickness was reduced with increase in Reynolds number but at all times the thickness of shock waves remained small compared with the distance

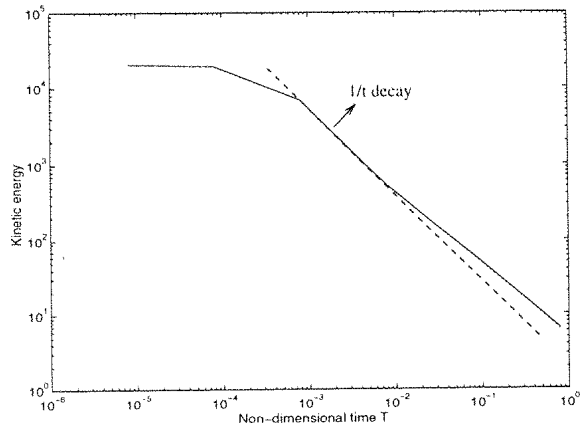

Figure 8.2: Evolution of average kinetic energy for Test case 1 at $R = 100$ shown by the dotted line and $R = 200$ shown by the solid line. Dashed line corresponds to 1/t decay.

between adjacent shocks. Reynolds number changes were observed especially in the high wavenumbers, being associated with viscous dissipation setting in and depopulating the the high wavenumbers.

Figure 8.3 shows the spectra of test case 1 for two different Reynolds numbers of 100 and 600 respectively. It is seen clearly that the Reynolds number effects are seen only in the high wavenumber part of the spectrum. The low wavenumber region is almost unaffected by Reynolds numbers and thus independent of it.

8.4 Conclusion and summary

The numerical results from Burgers equation using the Convolution Method for the non-linear propagation of an initial periodic random waveform showed how under nonlinear distortion the waveform soon reduced to a series of sawtooth waves of random amplitudes have shown the development of pseudo-sawtoothed waves beyond the effective shock formation time. For test case 1 it is seen that beyond the shock formation time, the amplitude falls as $1/t$. Upto this time the energy remains almost constant and the wave distorts to form sawtooths. Results agree for test case 1 at high Reynolds number of 500 with the recent work of Lighthill for the propagation of inviscid random sawtooth waves and the consequent 'bunching ' with energy decaying as $1/t$. The slopes are proportional to $1/t$. It has been shown that these slopes are constant at any particular time. It is seen that for the low Reynolds number case the energy is $\sim 1/t$ in some time range after the average

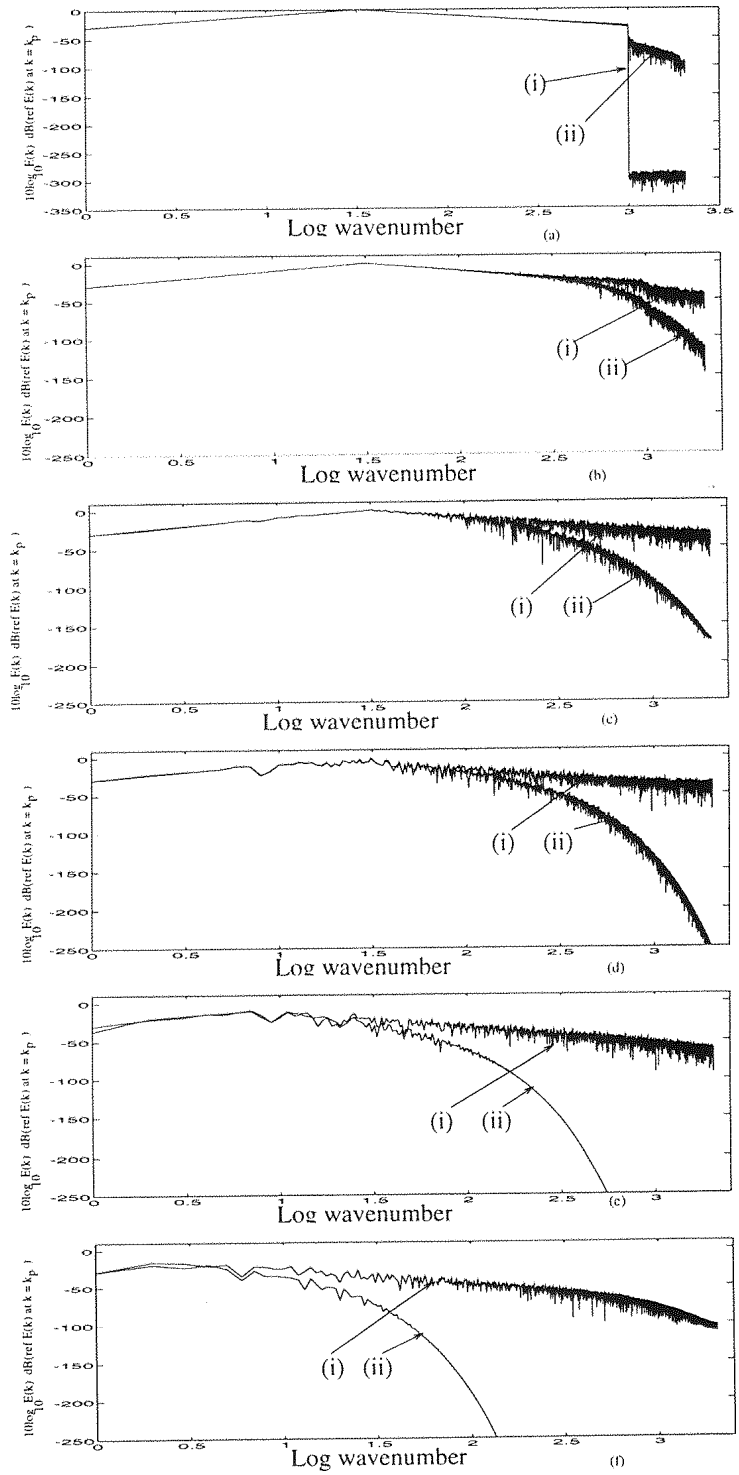

Figure 8.3: Effects of Reynolds number on test case 1 with time (i) $R = 600$, (ii) $R = 100$. $T = 0, 8.0E-07, 8.0E-06, 8.0E-05, 8.0E-04, 8.0E-03$ respectively

shock formation time after which it falls more like $1/t^{3/4}$. It is shown that the Convolution Method can give results over a wide range of Reynolds numbers, and in particular at very high Reynolds numbers where the solution approaches the inviscid limit. The viscous effects for this large Reynolds number are confined at the vicinity of the shocks and provide the necessary dissipation mechanism and thereby prevent discontinuities for the shocks.

Numerical results from the present work have shown that propagating a sawtooth wave in an isolated medium is similar to propagation of periodic sawtooths. This is an important result which had been raised by Lighthill in his work on random sawtoothed waves. Thus the $1/t$ decay of Lighthill for both the isolated wave and the random periodic waves has been confirmed.

The effects of Reynolds number is discussed and it is shown that Reynolds numbers effects are observed only after a certain wavenumber in the spectrum. It is shown that the low and high Reynolds number spectrum gradually diverge. The low wavenumber region is almost unaffected by Reynolds numbers and thus independent of it. Results at low wavenumber would produce different effects but only in those cases where the shock thickness becomes of the same order as the distance between adjacent shocks.

Chapter 9

Discussion and Conclusions

Introduction

Although there have been many studies on finite amplitude noise, there have been very few attempts at the prediction of the finite amplitude changes in a random initial signal with distance from the source. The present work has been undertaken with the main objective to investigate the complete physical processes which take place during the propagation of a complex wave.

This study has investigated the various aspects of the propagation of a finite amplitude noise signal with time for a class of waves which have initially a Gaussian probability distribution. The early history of nonlinear acoustics has been examined and a full derivation of the finite amplitude acoustic wave equation is described starting from the exact equations of motion. The ray or geometric acoustic approximation for nonplanar waves is discussed and it is shown that the propagation of nonplanar waves along a ray reduces by a simple transformation to the Burgers equation.

Use of different numerical methods

The fundamental processes governing the formation of shock waves, such as the populating higher wavenumbers in the spectrum due to nonlinear effects followed by depopulating the higher wavenumbers due to viscous dissipation have been investigated using different numerical methods. Initially Spectral methods and the FFT method were used to compute the propagation of simple waves but failed to resolve the wave structure near discontinuities. The spectral method is suitable for low Reynolds numbers only and particularly for single waves. However the method breaks down near discontinuities. Even the low Reynolds number cases dealt with did not give accurate resolution for the case of sawtooth waves. The FFT method could be used for simple initial conditions beyond the

shock formation time and hence it was an improvement over the spectral method. The method however could not be used for higher Reynolds numbers. The main difference between the 2 methods is that the spectral method solves the nonlinear Burgers equation in the spectral domain whereas the FFT method solves the linear diffusion equation in the spectral domain. Thus the spectral method breaks down very quickly when a discontinuity approaches, whereas the FFT method solves the linear diffusion equation where no discontinuity arise but fails when the Cole-Hopf transform is made at the shock formation time to get the nonlinear solution of the Burgers equation. Thus both methods are unsuitable to predict wave structure evolution as $R \to \infty$. Thus the attack on the high Reynolds number problem for all waveforms necessitated the development of a new numerical method which has been called the Convolution method(CM).

Calibration against Cole's exact solution

Preliminary studies on simple waves were first performed to isolate the effects of distortion due to nonlinear steepening and thermoviscous broadening. The simple waves used in these studies included the single cycle sine wave, and the single cycle sawtooth wave.

In all these studies periodic boundary conditions were used and hence the numerical methods for both these simple waves and the more complex wave which was studied later on could be calibrated against the exact Cole's solution. It is shown that nonlinear steepening, formation of the shock wave and the viscous broadening is different in each case. In these periodic waves it was shown in agreement with Cole's(1951) solution that the waveform reduced asymptotically to a sine wave of vanishingly small amplitude.

Nonlinear dependence on the initial waveform for simple waves

The investigation on different waveforms showed that the structure of the wave during its early evolution depended critically on the initial waveform. Thus whereas the single simple sine wave steepened into a mid position shock wave, a sine wave of opposite polarity formed shock waves at the boundaries. However in all cases at large times all waves reduced to a sine wave of vanishing small amplitude. It was found that for all the initial waves examined energy was transferred between the fundamental and the higher wavenumbers by the nonlinear mechanism. But it was seen that in the case of an initial sawtooth whose polarity is reversed, there is a feedback of energy into the fundamental after which the energy is transferred to the higher harmonics and a shock begins to develop. As time increased viscous effects depopulated the high wavenumber spectrum and the wave at very

large times reduces to a sine wave of small amplitude in agreement with those predicted analytically by Cole.

A class of more complex periodic waves have been studied which represents waves initially of finite amplitude only for a fraction of the overall period. These are referred to loosely as single cycle isolated waves. Initially such waves propagate outwards and only when their fronts reach the boundaries do they have the structure of periodic waves.

The Convolution method

The Convolution method is a numerical solution to the Burgers equation which involves the Cole-Hopf nonlinear transformation. It reduces Burgers equation to the linear diffusion equation in which the boundary conditions are related to those of Burgers equation in the physical domain. Hence the numerical procedure involves an infinite integration in which the integrand includes an infinite 'Gaussian bell'. High Reynolds number solutions using the CM have been compared with exact solution obtained numerically from the inviscid Burgers equation including the shock formation characteristics and the 'shock formation time'. From the comparisons it was found that there was little difference between the results from the Convolution method at $R \geq 1000$ and the exact inviscid solution. The conclusion from the preliminary studies is that Convolution method is a robust numerical tool to describe nonlinear finite amplitude complex wave propagation at high Reynolds number.

Evolution of superimposed harmonic

A number of previous studies have been concerned with waveforms containing a fundamental and its second harmonic. Thus before investigating the evolution of general complex waves the Convolution method was used to study the distortion of a sine wave with superimposed harmonics of varying amplitudes and phases. For the periodic case it was found, in the initial times before the shock formation time, that the nonlinear distortion resulted in the development of cusps in the wavenumber spectrum arising from the zero crossings in the Fourier coefficients of the developing wave. It is shown how they arise from the nonlinear term due to the 'sum and difference' mechanism of the harmonics and occur only up until the shock formation time.

It is shown that the interaction between an n^{th} harmonic of u with an m^{th} harmonic of $\partial u/\partial x$ generates contribution to wavenumbers such as $(n+m)$ and $(n-m)$ respectively. Once a harmonic is superimposed on the fundamental the harmonics no more alternate because the harmonic add and subtract with the fundamental and the harmonics of the

fundamental which at a particular time reduces the amplitude of the harmonic to zero, thus forming a 'cups'. It is shown that for the superimposed harmonic more cusps were formed with increase in the wavenumbers. The interaction between the fundamental and higher harmonics, the 2nd harmonic and higher harmonics is even more complicated. After the 'shock formation time ' when the viscous effects dominate the nonlinear effects, no cusps are formed and the spectrum behaves smoothly similar to that of the sine wave. Thus for any superimposed harmonic the nonlinear effects result in a complex sum and difference mechanism, in which phase reversal of the Fourier coefficients take place. But once the shock is formed for any superimposed harmonic, the Fourier coefficients obey Cole's solution with phases alternating.

The cosine wave of various amplitudes was superimposed on the initial sine wave and the spectral evolution was studied. It was found that once the amplitude of the harmonic increased a critical value, 'cusps' occurred, but the spectral characteristics was different from that of the superimposed sine harmonic.

Comparison of superimposed harmonic with analytic results

These results were compared with the results of Wu(1991) for a sine wave having harmonic in phase with the fundamental. It is shown that the 'cusps' only occur when the superimposed harmonic is in phase with the fundamental in agreement with Wu's analytic results. The present work includes the third and higher harmonics and shows that cusps occur for all higher harmonics, whereas Wu work is restricted to the cusping phenomena for the 2nd harmonic only. Wu also shows that no cusp arise when the harmonic is in opposite phase with the fundamental and these results are similar to that found in this investigation. The cusping phenomena has been explained in terms of the Fourier series and the Fourier coefficients which results in the 'sum and difference' mechanism arising due to the nonlinear effects. This results in a redistribution of energy in the wavenumbers due to the nonlinear distortion. Further results showed that when the phase difference varied between $0^0 - 180^0$, the cusps progressively reduced and were absent completely when the phase was 180^0. It was also shown that no cusps occured after the shock formation time in any superimposed waveforms considered in this work which is an important result uncovered in this investigation. Hence it is possible to predict the shock formation time by observing the wavenumber spectra with time. These results regarding nonlinear interactions led naturally to a deeper understanding of the nonlinear effects for more complex waveforms.

It was now clear that the numerical Convolution method could be used with confidence to the nonlinear evolution of an assemblage of shock waves. In all cases the spectrum of the initial random single was chosen and its corresponding waveform in the physical domain was obtained from its FFT. The chosen spectrum had random phase and the wavenumber amplitude followed a given arbitrary law. Two main cases were studied which are referred to as test case 1 and 2 respectively.

Scaling of the Reynolds number

In the case of single periodic complex wave studies the Reynolds number was based on the initial peak amplitude and wavelength. In the case of the multiple periodic random wave problems, no unique definition of the initial Reynolds number existed. A Reynolds number based on the mean amplitude and period was clearly unrepresentative for these test cases. It was therefore decided to include two different Reynolds number, the first one based on the mean amplitude and the wavelength corresponding to the peak wavenumber. The second one based on the mean amplitude and the Taylor microscale, λ/L, which was calculated from the initial prescribed spectrum. It is shown that the two are related for the given initial spectrum.

Validation of the random noise signal of test case 1

Test case 1 which is the k^2 increasing in the low wavenumber and $1/k^2$ in the high wavenumber has been validated. Errors arising due to aliasing effects were eliminated by propagating the signal with more zeros added and increasing the Nyquist wavenumber.

Description of the random noise signal

In the case of a set of random waves a sample length giving the digitised velocity containing a large number of samples at equal spacings of distance is first selected. The amplitude and phase of the initial signal are described at each point. The corresponding energy wavenumber spectrum is obtained at initial time. By means of the Cole-Hopf transformation the solution of the velocity distribution at $t = 0$ in the physical domain is transformed to the θ distribution, where θ satisfies the linear diffusion equation with the same Reynolds number, R, as in the nonlinear Burgers equation. The solution of θ is then obtained by evaluating the standard integral solution of the diffusion equation. By use of this procedure all the normal errors associated with finite difference schemes are avoided. Once $\theta(x,t)$ is known the values of the velocity $u(x,t)$ in the physical domain are obtained by using the inverse of the Cole-Hopf transformation. The effects of increase in Reynolds number simply add to the computation time required since the range of the quadrature

in finding $\theta(x,t)$ to the accuracy required is increased. The higher the Reynolds number the greater is the argument of the exponentials in the integrand of the integral for $\theta(x,t)$.

A detailed description of the spectral characteristics with time for an initial random signal having a Gaussian probability distribution has been made for two completely different initial spectra along with the detailed description of this wave characteristics in the physical domain. Numerical calculations for the random signal have been based corresponding to conditions in air at STP. The conflict between the nonlinear steepening effect and the viscous broadening effects is displayed and the results are found to be in agreement with those obtained by Cole(1951). At time $t > 0$ the nonlinear distortion resulting in the sudden population of energy into the high wavenumbers with a fall-off of $1/k^2$. It is shown that the number of zero crossings fall as $1/\sqrt{t}$ in agreement with Lighthill's theory for periodic random waves. At large times the waveform distorts and sawtooth like structures are formed. Beyond the 'shock formation time' these sawtooths merge according to Lighthill's ' bunching' phenomenon when the waves with large amplitude overtake the waves with smaller amplitude and the number of zero crossings is thereby reduced. At still larger times the viscous dissipation takes over with the wavenumber spectrum falling exponentially and the number of sawtooths being smaller in number. It follows that the waves at large time have a structure independent of the initial random wave. At still larger times, far greater than was possible in the present numerical work, it is expected that the wave will reduce to a single periodic sawtooth wave. This then becomes the initial condition for Cole's analytic solution where it is shown that ultimately all initial waves reduce to a single sine wave of vanishingly small amplitude.

The effects of nonlinear distortion with time found for the simple waves was also present in the case of the multiple sawtooth waves. As time increased the sum and difference mechanisms resulted in the changes in both lower and higher wavenumber spectra. There are changes in the wavenumber spectrum with increase in Reynolds number in the high wavenumber spectrum and the shock wave thickness decreases towards a near discontinuity. The effects of Reynolds number on shock thickness is found by noting the change in the Taylor microscale with increase in R. It is found that throughout the propagation the Taylor microscale Reynolds number remains approximately constant with $R_T \sim R$. For all complex wave distribution examined the Taylor microscale is evaluated at the commencement of propagation. For any complex wave it has been found that shocks quickly develop due to nonlinear steepening and that beyond the shock formation time the wave

evolves into an assemblage of sawtooths waves similar to those analysed by Gurbatov(1991) and Lighthill(1994) in cases where viscous effects are neglected. Thus the energy transfer into the high wavenumber region shows the wavenumber interactions arising from sum and difference mechanism. The sum wavenumber components form high wavenumbers and the difference wavenumber components form the low wavenumber region.

Although overall these changes have resulted in nonlinear steepening and viscous broadening of the initial profile, nevertheless it is shown that the energy transfer mechanism from the initial discrete spectrum to a near continuous and finally back towards a discrete spectrum is highly complex. The growth of higher harmonics of the spectrum due to the nonlinear effects resulting in the signal distortion and the gradual fall in the spectrum due to viscous dissipation at large times has been investigated.

Random noise signal of test case 2(i) and 2(ii)

In order to account for a substantial difference in the spectrum of the test case 1, test case 2(i), which is the exponential spectrum, was propagated. Test case 2 is different from test case 1 since however much nonlinear distortion tries to produce a $1/k^2$ spectrum in the high wavenumbers, $< U >^2$ falls immediately beyond $t = 0$ and hence the the spectrum falls more exponentially than $1/k^2$ in the high wavenumbers. Though the truncation wavenumber is more than the truncation in the test case 1, the rate of dissipation is lower than in test case 1. Thus the rate of dissipation is found to depend on the shape of the initial spectrum. Another version of the exponential decay [test case 2 (ii)] spectrum was computed in order to account for a substantial difference from test case 2(i) and to demonstrate the effect of the nonlinear distortion and viscous broadening of a small change in the low wavenumber region compared with a very large change (amounting to 60dB) in the high wavenumber end of the initial spectrum. Comparisons between these two exponential spectra showed that the case (ii) decayed faster than case 2 (i) and for large times the divergence increased in the high wave number region to more than their difference in the high wavenumber at time $t = 0$.

Effect of propagating a Gaussian signal with different phase values

When different initial phase were used to propagate the signal of test case 1 having Gaussian statistics it was found that for any time the spectral decay in the low and high wavenumber components was the same irrespective of the initial phase value. This phenomena was exemplified by propagating the initial signal of test case 1 for atleast 6 different initial phase values.

Spectra having same initial energy

When different initial waveforms having equal kinetic energy propagate to very large times it was found that ultimately at sufficiently large time they had almost the same kinetic energy. This phenomena was exemplified in the comparisons between test cases 1 and 2(i). More numerical experiment need to be performed for different initial spectra having equal initial energy to conclude on this result.

The effects of Taylor microscale

The effects of the nondimensional of the Taylor microscale, λ/L with time in the propagation of the complex finite amplitude acoustic wave have been studied. It is shown that the changes in λ/L reflect the statistical properties of the signal for the higher moments especially in the skewness and flatness. The Taylor microscale $\lambda(0)/L$ at time $t = 0$ for both test cases 1 and 2 has been computed where λ/L for test case 2 is smaller than λ/L for test case 1. For $t > 0$, the Taylor microscale has been computed for test case 1 only. The changes in λ/L also result in the change in the kinetic energy and the rate of dissipation with time. It is shown that λ is related to the shock wave thickness and is proportional to the average spacing between shocks. It is shown that the Taylor microscale, λ/L and the number of zero crossings, n_z are dependent on the skewness and flatness of the waveform and its derivatives and that a knowledge of the skewness and flatness alone cannot determine the joint pdf and the values of λ and n_z. The waveform, its derivative and λ can be determined from the 2-point velocity correlation function. It is shown that for an initial distribution corresponding to a given spectrum, λ/L can be determined. Its role in the wave distribution process is far more important than the relatively small changes in the peak wavenumber with time.

For test case 1 it is shown the value of λ/L first decreases up to the shock formation time and then increases approximately as $\sqrt{t}$.

Rate of dissipation The rate of dissipation for both test cases is described and shown that the rate of dissipation depends on the initial spectrum. The choice of the truncation wavenumber k_T affected the initial rate of dissipation and λ/L. Comparing the rate of dissipation ϵ for test case 1 and 2, it is shown that the rate of dissipation also depends on the initial shape of the spectrum.

The dependence of the rate of change of dissipation with time on the initial spectrum was studied. In test case 1, where the peak wavenumber $k_p = 32$, the rate of dissipation first increased by a small amount and then fell approximately as $1/t^2$. On the other hand

in test case 2(i), where $k_p = 1$, the rate of dissipation falls like $1/t^{1.5}$ from time $t = 0$. This results in the fall in kinetic energy for test case 2(i) immediately at $t > 0$ as $t^{-3/4}$ instead of $1/t$ observed in test case 1. In the case of test case 1, nonlinear distortion extends the $1/k^2$ spectrum upto the Nyquist wavenumber immediately at $t > 0$, thereby holding the kinetic energy almost constant upto the average shock formation time and then falls as $1/t$. Thus although during the early stages of propagation the total energy remains constant, the choice of the peak wavenumber and the truncation wavenumber and the initial shape of the spectrum controls the dissipation function, ϵ.

All studies on Burgers equation have shown that the dissipation mechanism, relate to thermo-viscous diffusion, creates the relevant increase in entropy in finite amplitude waves as required by the Rankine-Hugoniot relations. The sites of rises in entropy are restricted to the regions of large negative velocity gradients. Elsewhere the changes in entropy are small and negligible. As Reynolds number increases so the shock waves become closer to near discontinuities.

Statistical aspects of the random signal

Soon after this work was commenced, Gurbatov(1991) described an analytic method used to investigate the statistical theory of random waves in nonlinear acoustics. The numerical computations of the statistical evolution with time of a complex random waveform, which is initially Gaussian, have been performed and provide an alternative approach to that of Gurbatov. The present numerical studies consider the evolution of the high wavenumber spectrum resulting from the nonlinear propagation of random waves. It is found the initial Gaussian signal rapidly becomes skew(non-Gaussian) for both the test cases 1 and 2. The detailed processes by which the initial Gaussian signal is transformed into a non-Gaussian signal, as a result of nonlinear distortion and the changes in the dissipation rate with time as a function of Reynolds number, have been described. The evolution of the signal moments shows the increase in the skewness arises from nonlinear effects. The evolution of the bispectrum with time, which is important for investigating the sum and difference mechanism of the harmonic wave number components, has numerically been computed. The area under the bispectrum, which defines the skewness, shows the distribution becomes more and more skew with time. At large times the bispectrum is of lesser importance since the waveform gets simplified and has a lesser number of zero crossings. Clearly when this number is small it is no longer possible to continue a statistical analysis.

Comparison of the PDF's with Kraichnan's analytic work

The analogy between the distortion of finite amplitude acoustic waves and Burgers turbulence suggested a comparison be made between Kraichnan's analytic studies relating to Burgers turbulence and the current numerical work. In the latter work the skewed distribution of $\partial u/\partial x$ is in agreement with the work of Kraichnan, showing that an initial Gaussian noise signal becomes highly non-Gaussian in its first and higher derivative. The signal waveform also becomes non-Gaussian. It is found that when the initial random signal propagates to very large time the number of zero crossings becomes greatly reduced and the waveform evolves into a random sawtooth with a waveform far simpler in appearance to that of the initial complex signal.

Comparison of Gaussian and non-Gaussian initial signals

Special attention is given to the state of the initial signal and in particular when the initial probability distribution of the signal is Gaussian as opposed to non-Gaussian. This case had evoked comment in the literature of nonlinear acoustic waves. One application investigated here is Blackstock and Webster's discrepancy that arose between their analytic model and experiments. It was shown that when a distorted signal is re-randomised it causes the spectra to decay faster than the original signal. This is because re-randomising amounts to a significant change at the higher wavenumbers at later times . It is shown that re-randomising increases the number of zero crossings. It is shown that the phase distribution in the initial signal is important in the evolution of a random noise signal of finite amplitude. Re-randomising the signal with Gaussian statistics resulted in adding more dissipation due to increased 'bunching' which resulted from more zero crossings as given by Lighthill. Thus re-randomising the signal at $t > 0$ does not effect the total energy, but affects the dissipation and hence the high wavenumber are rapidly depopulated with time. In Webster and Blackstock's(1978) work it was suggested in a comparison between experiments and a computational model, based on plane wave propagation, that 'phase is not important in nonlinear propagation provided the noise is truly random'. In contrast it has been shown in this numerical work that the power spectrum of the evolving waveform depends critically on the phase statistics of the initial signal. The comparison with Blackstock's experimental results involves making an allowance for spherical wave propagation since the present numerical algorithm is for one dimensional plane waves only. It is found that the equivalent plane wave propagation deduced from Blackstock's experimental work

involving spherical waves is in good agreement with the present numerical results for plane waves and hence is a qualitatively comparison. This confirms the importance of phase distribution in the initial signal. It is shown that the decay is faster for a signal which is initially non-Gaussian and made Gaussian after a small time when the signal has suffered nonlinear distortion.

Comparison of the propagation of random noise with Lighthill's inviscid theory

An important objective of this investigation was to compare the numerical results obtained for a complex random waveform distortion at high Reynolds numbers with Lighthill's(1994) inviscid 'bunching' theory on the propagation of an assemblage of initially plane periodic sawtooth waves. An important first step was to summarise the energy decay laws for periodic and nonperiodic finite amplitude sawtooth waves as discussed by Lighthill's(1978).

The reason for the apparent paradox between the $1/t$ and the $1/\sqrt{t}$ amplitude decay laws for shock strength for the periodic sawtooth wave has been explained from this investigation where the average shock strength decreases not as $1/t$ but as $1/\sqrt{t}$ in agreement with Lighthills findings from his numerical example. This confirms that the shock strength decay as $1/\sqrt{t}$ holds in both cases of the periodic boundary and isolated boundary conditions. Thus from the numerical results for the propagation of an initial random noise signal for large value of R at $t > t_s$ were found to resemble an assemblage of sawtoothed waves described by Lighthill's(1994). The propagation of these sawtoothed waves follow a $1/t$ decay in energy in agreement with Lighthill's results for sawtoothed waves in inviscid medium.

Comparisons were then made for the propagation of an initial arbitrary random signal, which developed into a set of random sawtooth waves, with the results of Lighthill's inviscid calculations. It was found that the energy for test case 1 for a high Reynolds number decayed as $1/t$ as given by Lighthill. But for lower Reynolds the energy follows the $1/t$ law upto a sufficiently long time after which it diverged from it by a small amount. From these results it was shown that the positive velocity gradients slopes at any time were constant and the 'bunching' of waves was clearly observed in agreement with Lighthill theory. The number of zero crossings is greatly reduced with time and asymptotically the complex waveform reduces to a single sawtooth wave of reduced amplitude.

Effects due to Reynolds number for test case 1

It has been found that nonlinear steepening of the random wave distribution in the phys-

ical domain results in energising higher wavenumbers by the sum and difference mechanism. The process of thermoviscous broadening and resulting dissipation destroy the higher wavenumbers although such effects are confined predominantly to the vicinity of the shocks preventing them from being discontinuous. As Reynolds number is decreased the effects of thermoviscous dissipation increase and ultimately results in a decrease in the wave steepening. When the Reynolds number is increased the result is a change in the high wavenumber spectrum and in the physical domain such effects are confined to the shocks only, which become thinner. The low wavenumber spectrum almost remains invariant and the structure of the expansion waves remains almost independent of Reynolds number. For low Reynolds number the high wavenumber spectrum falls almost exponentially with time. The changes in the high wavenumber end of the spectrum at large times for different Reynolds number was shown by comparing results for $R = 600$ with $R = 100$. It was found that the spectra for both the high and low Reynolds number remained invariant in the low wavenumber region as discussed above. At very low Reynolds numbers viscous broadening greatly exceeded nonlinear steepening and the signal decayed linearly reducing it to a damped acoustic wave of small amplitude.

9.1 Further Research

The current investigation into the characteristics of the nonlinear propagation of complex plane waves of high Reynolds number in a uniform and homogeneous medium can be extended in two main directions.

(i) To develop the present numerical method to include spherical and cylindrical propagation. This will involve certain changes in the Convolution method algorithm required to handle the case of isolated wave propagation. It would be necessary to show that in the case of spherical spreading the amplitude of random wave will on average decay as $1/r\sqrt{\ln(r)}$ as given by Blackstock (1964*a*). Although the weak shock theory described by Pestorious(1974) goes to some extent in describing spherical spreading, it would be important to extend the Convolution method for studies on these waves and to make comparisons with the Pestorious algorithm. For such studies it would be more practical to treat radiation from a source rather than to investigate the initial value problem as investigated in the present work. This would involve a straight forward modification to

the present numerical programme and would not involve extra computation.

One of the cases that could be tackled would be the passage of a complex wave train passing through turbulence. In this case the turbulence would be frozen during the passage of the wave trains and it would be necessary to derive the frozen turbulence velocity distribution along a ray from known atmospheric statistical data. Once the frozen turbulent velocity distribution along a ray is specified the geometric acoustic equation can be solved by a step by step integration along the ray to find the evolved form of the acoustic wave train.

(ii) The general treatment of nonlinear nonplanar waves would be by the method of nonlinear geometric acoustics. This would involve the evaluation of the equivalent ray tube area first using the method of linear geometrical acoustics. A step by step method integrating along a ray could be developed to include atmospheric inhomogeneities such as absorption and variation in wind velocity.

References

Abramowitz M., Stegun I.A., 'Handbook of Mathematical functions ', Dover Publications Inc. NewYork, 1965.

Aanonsen S.I., Barkve T., 'Distortion and harmonic generation in the near field of a finite amplitude sound beam ', *J. Acoust. Soc. Am.* **75**:749-768, 1984.

Basdevant C., Deville M., 'Spectral and Finite difference solutions of the Burgers equation ', *Computers and Fluids* **141**:23-41, 1986.

Batchelor G.K., 'The theory of Homogeneous turbulence ', Cambridge University Press, 1956.

Bateman H., 'Some recent researches on the motion of fluids ' Mon Weather Rev **43**:163-170, 1915.

Beyer R.T., 'Parameter of Nonlinearity in Fluids', *J. Acoust. Soc. Am.* **32**:719-721, 1960.

Benton E.R., 'Some new exact, viscous, nonsteady solutions of Burgers nonlinear diffusion equations' *Phys. Fluids* **10**(21):13-19, 1967.

Benton E.R., Platzmann G.W., 'A table of solutions of one-dimensional Burgers equation ' *Qrtly Appl Math* **29**:195-212, 1972.

Blackstock D.T., 'Propagation of plane sound waves of finite amplitude in nondissipative fluids,' *J. Acoust. Soc. Am.* **34**(1):9-24, 1962.

Blackstock D.T.,(*a*) 'On plane, spherical and cylindrical waves of finite amplitude in lossless fluids.' *J. Acoust. Soc. Am.* **36**:217-219, 1964.

Blackstock D.T.,(*b*) 'Thermoviscous attenuation of plane,periodic finite amplitude sound waves,' *J. Acoust. Soc. Am.* **36**:534-542, 1964.

Blackstock D.T., 'Connection between the Fay and Fubini solution for plane sound waves of finite amplitude. ' *J. Acoust. Soc. Am.* **39**(6):1019-1026, 1965.

Blackstock D.T., 'Convergence of the Keck-Bayer perturbation solution for plane waves

of finite amplitude in a viscous fluid.' *J. Acoust. Soc. Am.* **39**(2):411-413, 1966.

Blackstock D.T., 'Transient solution for sound radiated into a viscous fluid.' *J. Acoust. Soc. Am.* **41**(5):1312-1319, 1967.

Blackstock D.T., 'History of nonlinear acoustics and a survey of Burgers and related equations', *Proceedings of a conference held at Applied Research Laboratories. The University of Texas* 3-27, 1969.

Blackstock D.T., 'A comparison between weak shock theory and Burgers equation in nonlinear acoustics ', Symposium on Aerodynamic noise 14th to 17th september. Loughborough University of Technology. Paper Number C.1, 1970.

Blackstock D.T., 'Nonlinear Acoustics(theoretical)',In Am. Inst.Phys. Handbook. (edited D.E. Gray), 3rd edn. New York McGraw-Hill, 1972.

Blokhintsev D.I., 'The propagation of sound in an inhomogeneous and moving medium.', *J. Acoust. Soc. Am.* **18**:322-328, 1946.

Box G.E, Tiao G.C., 'Bayesian inference in statistical analysis. ' Copyright Addison Wesley Publishing company, Inc, 1973.

Burgers J.M., 'A mathematical model illustrating the theory of turbulence ', *Advances in Applied Mathematics* **9**:25-226, 1951.

Carslaw H.S., Jaeger J.C.,'Operational methods in Applied Mathematics', Oxford, 1941.

Canuto C., Hussaini M.Y., 'Spectral methods in Fluid Dynamics ', Springer-Verlag, NewYork, 1987.

Cole J.D., 'On a Quasilinear Parabolic equation occurring in Aerodynamics ' *Quarterly of Applied Mathematics* **9**:225-236, 1951.

Crighton D.G., 'Model equations of nonlinear acoustics ' *Ann Rev. Fluid Mech*, 11-33, 1979.

Crighton D.G., Scott J.F., 'Asymptotic solutions of model equations in nonlinear acoustics ', *Phil Trans R Soc Lond* A **292**:107-134, 1979.

Crighton D.G., 'Acoustics as a branch of fluid mechanics', *J. Fluid Mech.* **106**:261, 1981.

Crighton D.G., 'Modern methods in Analytical Acoustics', *Lecture Notes Springer-Verlag London Limited* , 1992.

Cox T.J., Darlington P., 'Using Neural networks to model nonlinear acoustic propagation', *Acustica* **2**:95-99, 1994.

Earnshaw S.,'On the Mathematical Theory of Sound ', *Phil. Trans. R. Soc. Lond.*, **150**:133-148, 1859.

Euler L.,'General Principles of the Motion of Fluids ', (see Truesdell, ' Rational fluid mechanics', 1687-1765,') LXXXIV-LXXXIX, 1755.

Fay R.D., 'Plane Sound Waves of finite amplitude ', *J. Acoustic. Soc. Am.* **3**:222-241, 1931.

Fenlon F.H.,'A recursive procedure for computing the nonlinear spectral interactions of progressive finite amplitude waves in nondispersive fluids,' *J Acoust. Soc Am.* **50**:1299-1312, 1971.

Fubini-Ghiron E., 'Anomalies in Acoustic Wave Propagation of Large Amplitude ', *Alta Freq,* **4**:530-581, 1935.

Goldberg Z.A., 'On the Propagation of Plane Waves of Finite Amplitude ', *Sov. Phys Acoust*, **3**:329-347, 1957.

Gottlieb D. Orszag S.A., 'Numerical Analysis of spectral Methods: Theory and Applications ', SIAM Monograph no 26, SIAM, Philedelphia, U.S.A, 1977.

Guiraud J.P.,'Theorie du Bruit Ballistique,' ONERA Note Tech., **79**, 1964.

Gurbatov S.N., Malakhov A.N., and Pronchatovo-Rubtsov., 'Evolution of higher order spectra of nonlinear random waves ', *Radiophysics and Quantum Electronics* (Translated from Izvestiya Vysshikh Uchebnykh Zavednii') **29(6)**:523-528, 1986.

Gurbatov S.N., Malakhov A.N.,'Nonlinear random waves and turbulence in nondispersive media: waves, rays and particles ', Manchester Univ. Press, 1991.

Hamilton M.F., Blackstock D.T., 'Propagation of acoustic shock waves of large amplitude ', in *Frontiers in Nonlinear acoustics*' 141-146. Elsevier London, 1990.

Hayes W.D., 'Energy invariant for geometric acoustic in a moving medium ' , *Phys. Fluids* **11**:1654-1656, 1965.

Hammerton P.W., Crighton D.G., 'Overturning of nonlinear acoustic waves. Part 1 A General method ', *J. Fluid Mech.* **252**:585-599, 1993.

Hammerton P.W., Crighton D.G., 'Overturning of nonlinear acoustic waves. Part 2 Relaxing gas dynamics ', *J. Fluid Mech.* **252**:601-615, 1993.

Hinze J.O., 'Turbulence: An introduction to its mechanism and theory ', The Maple Press Company, York PA, 1959.

Hirsh C., 'Numerical Computation of internal and external flows ' , **1** Wiley and Sons, 1989.

Hopf E., 'The Partial differential equation $[u_t + uu_x = \mu uu_{xx}]$', *Comm Pure Appl. Math* **3**:201-203, 1951.

Howell G.P., 'Truncated Taylor series solution to a Generalized Burgers equation', *Jl of Sound and Vibration* **108**:1133-145, 1986.

Hugoniot H., 'On the Propagation of Movement through a Body and Especially through an Ideal Gas' ,*J. de l'Ecole Polytech* **58**:1-125, 1889.

Inoue Y., Yano T., 'Propagation of strongly nonlinear plane waves. ' *Jl. Acoust. Soc. Am.* **94**:1632-1642, 1993.

Jeng D.T., Forester S., Halland S., Meecham W.C., 'Statistical initial value problem for Burgers' model equation of Turbulence ', *Physics of Fluids* **9**(11):2114-2120, 1966.

Johnson D.R., Robinson D.W., 'The Subjective evaluation of sonic bangs', *Acustica* **18** Heft 5241, 1967.

Kac M., *Bell American Math. Soc.* **49**:314-320, 1944.

Kamakura T., Nakashima Y., Aoki S.,'Experiments on the degenerate parametric source in air', *J Acoust. Soc Jpn* **39**:247-252, 1983.

Khokhlova V.A., Rudenko O.V., Sapozhnikov O.A., ,'Sawtooth waves: One dimensional statistical ensembles and thermal self focusing of the beams', *Frontiers of Nonlinear Acoustics: Proc 12th ISNA* **39**:47-63, 1990.

Kim K.I., Powers E.J.,'Digital bispectral analysis of self-excited fluctuation spectra.', *Physics of Fluids* **21**(8):1452-1453, 1978.

Kraichnan.R.H., 'Models of Intermittency in Hydrodynamic Turbulence', *Physical Review Letter* **65**(5):575-578, 1990.

Kuha S., Private communication, 1995.

Lagerstrom P.A., Cole J.D., and Trilling L., 'Problems in the theory of the Viscous Compressible Fluids ', Calif. Inst. Technol. Guggenheim Aeronaut. Lab. Rep. Off. Nav. Res., 1949.

Lagrange J.L., 'Researches on the Nature and propagation of Sound ,' reprinted in *Oeuvres de Lagrange* **1**:39-48, 1759.

Landau L.D., 'On Shock waves at Large distances from the place of their Origin ' , *J.Phys* (USSR) **9**:496-500, 1945.

Lighthill M.J., 'Waves in fluids' C.U.P, 1978.

Lighthill M.J.,'Viscosity effects in sound waves of finite amplitude. In Surveys in Mechanics ', Cambridge University Press, 250-351, 1956.

Lighthill M.J., Some aspects of the aeroacoustics of high speed jets ' ICASE Report No. 93-20, 1993.

Lilley G.M., Organisation De Cooperation et de Development Economiques ' Conference Sur La Recherche en Matiere de bang sonique' Chateau de la Muette, Paris, 1970.

Lin Y.K., 'Probabilistic theory of structural dynamics ' , McGraw-Hill Book Company New York, 1967.

Mayer P.L., 'Introductory Probability and Statistical Applications ', Addison-Wesley, Reading, Mass, 1965.

Meecham W.C., Siegel A.,'Wiener-Hermite expansion in model turbulence at large Reynolds numbers', *The Physics of Fluids* **7**(8):1178-1190, 1964.

Mellen R.H., 'Numerical solution of Burgers diffusion equation for arbitrary waveforms'. 111th ASA meeting, 1986.

Mendousse J.S.,'Nonlinear dissipation distortion of progressive sound waves at moderate amplitudes', *J. Acoust. Soc. Am.* **25**:51-54, 1953.

Mitome H., 'An exact solution for finite amplitude plane sound waves in a dissipative fluid' *J Acoust. Soc. Am.* **86**(6):2334-2338, 1989.

Morfey C.L., and Howell G.P.,'Nonlinear propagation of aircraft noise in the atmosphere' *AIAA Journal* **19**(8):986-992, 1981.

Morfey C.L., 'Unpublished notes '., 1994.

Murdoch J., Barnes J.A., 'Statistical Tables for Science and Engineering Management and Business Studies ', Macmillan Press Ltd. Second edition, 1970.

Nakamura T., Nakamura A., Takeuchi R., 'Simulation of nonlinear propagation of finite amplitude sound wave through a circular pipe,'*Acustica* **38**:331-333, 1977.

Naugol'nykh K.A., Soluyan S.I., Khoklov R.V., Akust. Zhur. **9** 'English translation Soviet Physics. Acoust. **9**42-46, 1963.

Newland D.E., 'An Introduction to Random Vibrations and Spectral Analysis ' Second Edn, Longman, 1984.

Nikias C.L. and Mendel M.J., 'Signal Processing with Higher Order Spectra ', IEEE Signal Processing Magazine , 1993.

Novikov A.K., 'Bispectral Analysis of vibration and noise of ships machines as applied to diagnostic problems', Proceedings Transport Noise Conference St Petersburg 305-308, 1994.

Pernet,D.F. and Payne R.C., 'Nonlinear propagation of Signals in Air,' *J.Sound Vib*

17:383-396, 1971.

Pestorious F.M., 'Propagation of finite amplitude noise' *Symposium on Finite amplitude waves in fluids.* Programmes and Summaries, 1973.

Pestorious F.M.,Williams S.B., Blackstock D.T.,'Effects of nonlinearity on noise propagation' *Proceedings of the 2nd Interagency Symposium on University Research in Transport Noise* North Carolina State University. 448-459, 1974.

Pierce A.D., 'Acoustics An Introduction to Its Physical Principles and Applications', Copyright by Mcgraw-Hill Inc. All rights reserved, 1981.

Pierce A.D., 'Wave equation for sound in fluids with unsteady inhomogeneous flow ', *J. Acoustic. Soc. Am.* **87**(6):2292-2299, 1990.

Piersol D.E, Bendat J.S., 'Measurement and analysis of random data ' Copyright John Wiley and son, Inc., 1966.

Poisson S. D.,'Memoir on the Theory of Sound', *J. Ecole. Polytech.*, **7**:319-392, 1808.

Press W.H., Flannery B.P., Teukolsky S.A., Vetterling W.T., 'Numerical Recipes ', Cambridge University Press., 1986.

Punekar J.N., Ball G.J.,Morfey C.L., 'Numerical simulation of noise propagation', Proc. of International Conference on Acoustics. Lyon, France 91-94, 1994

Punekar J.N., Ball G.J., Lilley G.M., Morfey C.L., 'Numerical simulation of the nonlinear propagation of random noise', *Proc. of 15th Proc. International Congress on Acosutics.* Trondheim, Norway. **II**:153-156, 1995

Rankine W., 'On the Thermodynamic Theory of Waves of Finite Longitudinal Disturbance '*Phil Trans Roy Soc (London)* **160**:277 1870.

Rayleigh Lord, *Proc. Roy. Soc. A* **84**:247-284, 1910.

Rice S.O., 'Mathematical analysis of random noise', Pts III and IV. *Bell Syst. Tech. Jl* **XXIV**(1), 1945.

Riemann B., 'Abhandl. Ges. Wiss. Gottingen, Math.- physik Kl' **8**:43-65, 1858.

Roman D., Zoltogorski B., 'Multi-Dimensional transfer function for a Non-Dissipative Burgers' Equation', *Archives of Acoustics* 1990 **113**:253-259, 1986.

Rudenko O.V. Soluyan S.I.,'Theoretical Foundations of Nonlinear Acoustics'. Consultants Bureau, 1977.

Sinai Y.G., 'Statistics of shocks in solutions of inviscid Burgers equation.', *Commun. Math. Phys* **148**:601-621, 1992.

Scott J.F.,'Uniform asymptotics for spherical and cylindrical nonlinear acoustic waves

generated by a sinusoidal source', *Proc R Soc Lond A* **375**:211-230, 1981.

Scott J.F.,'The nonlinear propagation of acoustic noise', *Proc R Soc Lond A* **383**:55-70, 1982.

She Z., Aurell E., Frisch U.,'The inviscid Burgers Equation with initial Data of Brownian Type ,' *Commun. Math. Phys* **148**:623-641, 1992.

Sod G.A., 'Numerical Methods in fluid dynamics ', Cambridge University Press, 1985.

Sparrow V., 'A numerical method for general finite amplitude wave propagation in two dimensions and its applications to spark pulses ', *Jl. Acoust. Soc.Am.*, **90** (5), 1991.

Stokes G.G., 'On the theories of the Internal Friction of Fluids in Motion, and of the Equilibrium and Motion of Elastic Solids ', *Trans.Camb.Phil.Soc* **8**:287-319, 1845.

Taylor G.I., 'The conditions necessary for discontinuous motion in gases ', *J. Ec. Polytech*, **58**:1-125, 1889.

Trivett D.H., Van Buren A.L., 'Propagation of plane cylindrical and spherical finite amplitude waves ', *J. Acoust. Soc. Am.* **69**:943-949, 1981.

Van Buren A.L., 'Mathematical model for nonlinear standing waves in a tube,' *J. Sound Vib* **42**:273-280, 1975.

Watanabe Y.,Urabe Y.,'Experiments and algorithms of calculation concerning the propagation of finite amplitude waves- Nonlinear acoustics (3),' *J Acoust. Soc Jpn* **38**:105-112, 1982.

Webster J.C. and Blackstock D.T., 'Finite Amplitude Saturation of plane sound waves in air ' *J.Acoust.Soc.Am.* **62**:518-23, 1977.

Webster D.A, Blackstock D.T., 'Experimental investigation of outdoor propagation of finite amplitude noise' NASA Contractor Report 2992., 1978.

Whitham G.B., 'On the propagation of weak shock waves', *J. Fluid Mech* **1**:290-318, 1956.

Whitham G.B., 'Linear and nonlinear waves', New York : Wiley 636 1974.

Wu Jin-yuan, Shung Kirk K., 'Nonlinear energy exchange among harmonic modes and its application to nonlinear imaging' *Jl. Acoust. Soc. Am.*, **88**(6):2852-2858, 1990.

Yano T., 'The mean pressure and density in a strongly nonlinear plane acoustic wave', *J.Acoust.Soc.Am.* **100**(91):666-668, 1996.

Appendix A

Spectral method

The spectral method used to solve Burgers equation [see Chapter 3] is based on the method described by Canuto(1987). Time marching at every time step is carried out in the spectral domain using the Adams-Bashforth method for the convective term and Crank-Nicholson method for the diffusive term. The truncated Fourier series pair for periodicity in x, as defined in Canuto(1987), are as follows,

$$u(x_j) = \sum_{k=0}^{N} \tilde{u}_k e^{ikx_j} \qquad 0 \leq j \leq N-1 \tag{A.1}$$

$$\tilde{u}_k = \frac{1}{N} \sum_{j=0}^{N-1} u(x_j) e^{-ikx_j} \qquad 0 \leq k \leq N-1 \tag{A.2}$$

Differentiation for the first derivative $\partial u/\partial x$ is carried out in the spectral space, giving

$$\left(\frac{\partial \tilde{u}}{\partial x}\right)_k = -ik\tilde{u}_k \tag{A.3}$$

The second derivative is

$$\left(\frac{\partial^2 \tilde{u}}{\partial x^2}\right)_k = k^2 \tilde{u}_k \tag{A.4}$$

Aliasing: When products of the form $u\partial u/\partial x$ are transformed into the spectral domain, they generate high frequency components which, through a combination of the Fourier modes for a truncated Fourier transform will reappear as low frequency components. These spurious low frequency components alias the actual modes and destroy the solution. The nonlinear term can be written as

$$u\frac{\partial u}{\partial x} = \sum_{n=0}^{N} \sum_{m=0}^{N} im\tilde{u}_n \tilde{u}_m e^{i(n+m)x}$$

$$= \sum_{s=0}^{N} imP_s e^{isx}$$

where

$$P_s = \sum_{n+m=s}^{N} \tilde{u}_m \tilde{u}_n + \sum_{n+m=s+N}^{N} \tilde{u}_m \tilde{u}_n$$

The second term on the right hand side is the aliasing term.

Let f^n and f_1^n be $\left(\tilde{u}\frac{\partial \tilde{u}}{\partial x}\right)_k$ and $\left(\frac{\partial^2 \tilde{u}}{\partial x^2}\right)_k$ respectively.

The first time step is the backward Euler method.

$$\tilde{u}^{n+1} = u^n - \Delta t[f^n + f_1^n]$$

The second time step is the second order Adams-Bashforth for the convective and Crank-Nicholson for the viscous term.

$$\tilde{u}^{n+2} = \tilde{u}^{n+1} - \Delta t[\frac{3}{2}f^{n+1} - \frac{1}{2}[f^n) - \frac{\nu}{2}(f_1^{n+2} + f_1^{n+1})]$$

For all other time steps the third order AB for the convective and CN for the diffusive term is used.

$$\tilde{u}^{n+3} = \tilde{u}^{n+2} - \Delta t[\frac{15}{8}f^{n+2} - \frac{10}{8}f^{n+1} + \frac{3}{8}f^n + \frac{\nu}{2}(f_1^{n+2} + f_1^{n+1})]$$

At every time step an inverse transform of $\tilde{u}(k,t)$ gives the solution to the Burgers equation.

Appendix B

Spectral solution for the diffusion equation

In chapter 2 the solution to Burgers equation has been obtained using the Cole-Hopf transformation. This involves the solution to the linear one-dimensional unsteady diffusion equation satisfying initial and periodic boundary conditions.

It is shown by reference to standard textbooks [Carslaw and Jaeger(1941)] on the diffusion equation that the solution to

$$\frac{\partial \theta}{\partial t} + \nu \frac{\partial^2 \theta}{\partial x^2} = 0 \tag{B.1}$$

with initial conditions $\theta(x,0) = \theta_0(x)$ and periodic boundary conditions is found using a combination of Laplace and Fourier transform methods. Using first the Laplace transform method with the Laplace operator, p, equation B.1 reduces to the subsidiary equation

$$p\tilde{\theta} = \nu \frac{d^2\tilde{\theta}}{dx^2} + \theta_0(x) \tag{B.2}$$

where $\tilde{\theta}(x:p)$ is the Laplace transform of $\theta(x,t)$. This may be solved by the method of variation of parameters or by using Fourier transforms on x and t and writing $p = i\omega$. Then

$$\tilde{\theta}(\omega,k) = \int_{-\infty}^{\infty} \frac{e^{-ikx}\theta_0(x)}{(\nu k^2 - i\omega)} dx \tag{B.3}$$

and its inverse Fourier transform leads to

$$\theta(x,t) = \frac{1}{2\pi} \int_{-\infty}^{\infty} \theta_0(\xi) \int_{-\infty}^{\infty} e^{ik(x-\xi)} e^{-\nu k^2 t} dk d\xi \tag{B.4}$$

But

$$\int_{-\infty}^{\infty} \cos k(x-\xi) e^{-\nu k^2 t} dk = \sqrt{\frac{\pi}{4\nu t}} e^{-\frac{(x-\xi)^2}{4\nu t}} \tag{B.5}$$

so finally

$$\theta(x,t) = \frac{1}{\sqrt{4\pi\nu t}} \int_{-\infty}^{\infty} \theta_0(\xi) \exp - \frac{(x-\xi)^2}{4\nu t} d\xi \tag{B.6}$$

with

$$\frac{\partial \theta(x,t)}{\partial x} = - \frac{1}{\sqrt{4\pi\nu t}} \int_{-\infty}^{\infty} \theta_0(\xi) \frac{(x-\xi)}{2\nu t} \exp \left(\frac{-(x-\xi)^2}{4\nu t} \right) d\xi \tag{B.7}$$

as given in chapter 2.

Appendix C

Fast Fourier Transform (FFT) Method

Exact solutions to Burgers equation are obtained from the FFT method for moderate Reynolds number. This method uses the Cole Hopf transformation and solves the diffusion equation in the spectral domain. Time marching for the diffusion equation is carried out in the spectral domain using the Crank Nicholson semi implicit scheme. With variables x, t the Burgers equation is

$$\frac{\partial u}{\partial t} + u\frac{\partial u}{\partial x} = \nu\frac{\partial^2 u}{\partial x^2} \tag{C.1}$$

The non-dimensional form of the Burgers equation is

$\overline{u} = u/U$, $\overline{x} = x/l$, $\overline{t} = tU/l$ and $R = Ul/\nu$

the Burgers equation becomes

$$\frac{\partial \overline{u}}{\partial \overline{t}} + \overline{u}\frac{\partial \overline{u}}{\partial \overline{x}} = \frac{1}{R}\frac{\partial^2 \overline{u}}{\partial \overline{x}^2}$$

The Cole-Hopf transformation is

$$\overline{u} = -\frac{R}{2}\frac{\partial\theta/\partial\overline{x}}{\theta}$$

where θ satisfies the diffusion equation

$$\frac{\partial \theta}{\partial \overline{t}} = \frac{1}{R}\frac{\partial^2 \theta}{\partial \overline{x}^2}$$

with $0 \leq \overline{x} \leq 1$

The fully discretized equations in the spectral space are given as follows.

The first time step uses the Euler method.

$$\theta^{n+1} = \theta^n + \frac{\Delta\overline{t}}{R}[\theta_1^n]$$

$\Delta\bar{t}$ is the non-dimensional time step.

$\theta_1 = \partial^2\theta^n/\partial\bar{x}^2 = -k^2\tilde{\theta}^n$, k being the wavenumber . The second and subsequent time steps are

$$\theta^{n+2} = \theta^{n+1} + \frac{\Delta\bar{t}}{R}[\frac{\theta_1^{n+2}}{2} + \frac{\theta_1^{n+1}}{2}]$$

$$\theta^{n+2} - \frac{\Delta\bar{t}}{R}\frac{\theta_1^{n+2}}{2} = \theta^{n+1} + \frac{\Delta\bar{t}}{R}\frac{\theta_1^{n+1}}{2}$$

$$\theta^{n+2} - \frac{\Delta\bar{t}(-k^2)}{R}\frac{\theta^{n+2}}{2} = \theta^{n+1} + \frac{\Delta\bar{t}}{R}\frac{\theta^{n+1}(-k^2)}{2}$$

$$\theta^{n+2}[1 - \frac{\Delta\bar{t}(-k^2)}{2R}] = \theta^{n+1}[1 + \frac{\Delta\bar{t}(-k^2)}{2R}]$$

$$\theta^{n+2} = \frac{\theta^{n+1}[2R - \Delta\bar{t}k^2]}{[2R + \Delta\bar{t}k^2]}$$

the scheme is unconditionally stable. For every time step an inverse transform of $\tilde{\theta}(k,t)$ and its corresponding θ_1 gives the solution to the diffusion equation. Knowing $\theta(x,t)$ and $\partial\theta(x,t)/\partial x$ and using the Cole-Hopf transform, the solution to the Burgers equation $u(x,t)$ for any time can be obtained.

Appendix D

Newton's Raphson's Iterative Method for the Exact Solution

This section gives the numerical method used to solve the exact inviscid equation using an iterative technique. The solution is computed from the solution of the transcendental equation using the Newton Raphson's method and is described below.

The quasilinear parabolic equation which is the Burgers equation

$$\frac{\partial u}{\partial t} + u\frac{\partial u}{\partial x} = \nu\frac{\partial^2 u}{\partial x^2} \tag{D.1}$$

reduces to the hyperbolic equation

$$\frac{\partial u}{\partial t} + u\frac{\partial u}{\partial x} = 0 \tag{D.2}$$

when $\nu = 0$.

If $u(x,0) = f(x)$ then the solution to equation D.2 at any time t is

$$u(x,t) = f(x - u(x,t)t)$$

Thus if

$$y = x - u(x,t)t$$

then

$$u(x,t) = f(y)$$

and

$$y = x - tf(y)$$

Hence for any (x,t), y can be found with

$$u(x,t) = (x-y)/t$$

Consider a special test case when

$$u(x,0) = -sin(\pi x).$$

For $t > 0$

$$y(x,t) = x + tsin(\pi y)$$

which is a transcendental equation in y for a given (x,t)

This can be solved using the Newton Raphson iterative method.

Let the test function be

$$F = y - x - tsin(\pi y)$$

with

$$\frac{dF}{dy} = 1 - t\pi cos(\pi y)$$

then

$$y_{n+1} = y_n - \frac{F(y_n)}{\frac{dF}{dy}(y_n)}$$

this iteration continues until

$$|F(y(n))| < E_{rr}$$

where E_{rr} is a specified error.

Once $y(x,t)$ is known for a given (x,t) one can find

$$u(x,t) = \frac{x - y(x,t)}{t}$$

where the solution is only found in $0 < x < 1$ where the periodic wavelength is unity.

Then for any time t, $u(x,y)$ can be calculated.

It is noted that where $u(x,t)$ is zero so $y(x,t) = x$ for any time t.

The length 0 to l which is the period of the waveform is divided into N equispaced parts of length h so that

$$h = \frac{1}{N}$$

The solution is tripled valued for

$$x < 0 \text{ and } x > 2\pi.$$

The true solution discards the triple values and replaces them by a shock wave as found by Lighthill and Witham using the equal area rule. The shock formation time for the inviscid Burgers equation is given by

$$t_s = \left| -\frac{1}{\left(\frac{\partial u_(x,0)}{\partial x}\right)} \right|_{\min}$$

[see equation 2.41 in chapter 2] and in this case for $u(x,0) = -sin(x)$ the shock formation time

$$t_s = 1/\pi = 0.31$$

Thus the velocity distribution steepens between $t = 0$ and t_s and then quickly tends towards a ramp function or N wave with reduced amplitude.

Appendix E

Trapezoidal rule

This section contains the integration scheme used in the Convolution method. The evaluation of an integral

$$I = \int_b^a f(x)dx$$

defining the function $f(x)$ at known values x_i, and with

$$f(x_i) = f_i$$

$$I = h\sum f_i$$

can be regarded as the integral in equation 4.5 in chapter 4. There is a sequence of x_i's denoted by $x_0, x_1, ...x_N$ which are spaced apart by a constant step h, with

$$x_j = a + jh$$

where $j = 0, 1, 2, 3.....n$, $b = a + nh$ then

$$\int_b^a f(x)dx = \int_{x_0}^{x_1} f(x)dx + \int_{x_1}^{x_2} f(x)dx + ... \int_{x_{n-1}}^{x_n} f(x)dx$$

$$\int_b^a f(x)dx = \frac{h}{2}(f_0 + f_1) + ...\frac{h}{2}(f_{n-1} + f_n)$$

$$= \frac{h}{2}(f_0 + f_n) + h(f_1 + f_2 + ...f_{n-1})$$

is the trapezoidal rule. Hence the solution of the diffusion equation 4.5 and its derivative 4.6, was found using the Trapezoidal rule given above.

Appendix F

Method of Stationary Phase

The effects of Reynolds number on the solution of Burgers equation for test case 1 are described in chapter 8. It is shown that for high Reynolds numbers, the solution of Burgers equation requires the solution to the diffusion equation [see equation 2.52], $\theta(x,t) \rightarrow \theta_0$ for very small times. This can be proved using the method of stationary phases due to Stokes and Kelvin as described by Crighton(1979). The solution of the diffusion equation is [see equation 4.5 in chapter 4]

$$\theta(x,t) = \frac{1}{\sqrt{4\pi\nu t}} \int_{-\infty}^{\infty} \theta_0(\xi) exp(-(x-\xi)^2/4\nu t) d\xi \tag{F.1}$$

Let

$$G = \frac{1}{4\nu t}.$$

Here G is a large parameter, since t and ν are small quantities. With

$$h(\xi) = (2\xi x - \xi^2)$$

equation F.1 can be written as

$$\theta(x,t) = \sqrt{\frac{G}{\pi}} \int_{-\infty}^{\infty} \theta_0(\xi) \exp\left(-Gx^2\right) \exp\left(Gh(\xi)\right) d\xi$$

Consider

$$I = \int_{-\infty}^{\infty} \theta_0(\xi) \exp\left(Gh(\xi)\right) d\xi. \tag{F.2}$$

If θ_0 is a smooth function of ξ and provided $h(\xi)$ is twice differentiable, it is seen that the maximum contribution to the integrand comes from the region surrounding $h'(\xi) = 0$, where $\xi = \alpha$. But since

$$h(\xi) = 2x\xi - \xi^2 \tag{F.3}$$

$$h'(\xi) = 2x - 2\xi \tag{F.4}$$

$$h''(\xi) = -2 \tag{F.5}$$

Hence $h'(\xi) = 0$ when $\xi = x$, and so when $\alpha = x$, $h'(\alpha) = 0$. Near $\xi = \alpha$, a Taylor series expansion gives

$$h(\xi) = h(\alpha) + (\xi - \alpha)h'(\alpha) + \frac{(\xi - \alpha)^2}{2!}h''(\alpha) + ... \tag{F.6}$$

and since $h'(\alpha) = 0$

$$h(\xi) - h(\alpha) = \frac{(\xi - \alpha)^2}{2!}h''(\alpha).$$

Let

$$\lambda^2 = -\frac{(\xi - \alpha)^2}{2!}h''(\alpha)$$

with

$$\lambda = (\xi - \alpha)\sqrt{\frac{-h''(\alpha)}{2}}.$$

Therefore $\lambda = (\xi - \alpha)$, since $h''(\alpha) = 2$ and $d\xi/d\lambda = 1$, and

$$I = 2\theta_0(x)e^{G(x^2)} \int_0^\infty e^{(-G\lambda^2)}d\lambda. \tag{F.7}$$

But

$$\int_0^\infty \exp(-G\lambda^2)d\lambda = \frac{\sqrt{\pi}}{2\sqrt{G}}$$

Hence equation F.7 becomes

$$I = \frac{\sqrt{\pi}}{\sqrt{G}}e^{Gx^2}\theta_0(x)$$

and substituting into equation F.1, the result is

$$\theta(x, t \to 0) = \theta_0(x)$$

Appendix G

Derivation of the Energy Equation from the Burgers equation

The derivation of the energy equation from the Burgers equation is given below. It is required for the determination of the spectral behaviour of the energy in the wavenumber space. Burgers equation

$$\frac{\partial u}{\partial t} - \nu \frac{\partial^2 u}{\partial x^2} = -u \frac{\partial u}{\partial x} \tag{G.1}$$

can be transformed into the corresponding energy equation as given by Canuto et al (1987). Let us introduce the Fourier transform pairs $\tilde{u}$ and u defined by

$$\tilde{u}(\tilde{k}, t) = \frac{1}{2\pi} \int_{-\infty}^{\infty} e^{-i\tilde{k}x} u(x, t) dx \tag{G.2}$$

and

$$u(x, t) = \int_{-\infty}^{\infty} \tilde{u}(\tilde{k}, t) e^{i\tilde{k}x} dk \tag{G.3}$$

where the Fourier coefficient $\tilde{u}(\tilde{k}, t)$ is complex. If equation G.1 is multiplied by $e^{-i\tilde{k}x}/2\pi$ and integrate with respect to x from $-\infty$ to $+\infty$

$$\frac{1}{2\pi} \int_{-\infty}^{\infty} \frac{\partial u}{\partial t} e^{-i\tilde{k}x} dx - \frac{\nu}{2\pi} \int_{-\infty}^{\infty} \frac{\partial^2 u}{\partial x^2} e^{-i\tilde{k}x} dx = \frac{-1}{2\pi} \int_{-\infty}^{\infty} u \frac{\partial u}{\partial x} e^{-i\tilde{k}x} dx \tag{G.4}$$

hence or

$$\frac{\partial \tilde{u}(\tilde{k}, t)}{\partial t} + \nu \tilde{k}^2 \tilde{u}(\tilde{k}, t) = +i \int_{-\infty}^{\infty} (\tilde{k} - \tilde{k}') \tilde{u}(k') \tilde{u}(\tilde{k} - \tilde{k}') d\tilde{k}' \tag{G.5}$$

From equation G.5 it is seen that the last term in the LHS contributes to the linear damping with time, whereas the nonlinear term contributes to the distortion in both space. The

energy equation is found by multiplying equation G.5 by its conjugate,

$$\tilde{u}^* \frac{\partial \tilde{u}}{\partial t} + \nu \tilde{k}^2 \tilde{u}\tilde{u}^* = i\tilde{u}^*(k) \int_{-\infty}^{\infty} (\tilde{k} - \tilde{k}\prime)\tilde{u}(\tilde{k}\prime)\tilde{u}(\tilde{k} - \tilde{k}\prime)d\tilde{k}\prime.$$

$$\tilde{u} \frac{\partial \tilde{u}^*}{\partial t} + \nu \tilde{k}^2 \tilde{u}\tilde{u}^* = i\tilde{u}(k) \int_{-\infty}^{\infty} (\tilde{k} - \tilde{k}\prime)\tilde{u}^*(\tilde{k}\prime)\tilde{u}^*(\tilde{k} - \tilde{k}\prime)d\tilde{k}\prime.$$

But

$$E = \tilde{u}\tilde{u}*$$

is the spectral energy density and F is the nonlinear term. The energy equation is

$$(\partial/\partial t + 2\nu\tilde{k}^2)E(\tilde{k}, t) = F(\tilde{k}, t) \tag{G.6}$$

Appendix H

Statistical moments

The probability density function for a single random variable u with Gaussian statistics is written as

$$p(u) = \frac{1}{\sqrt{2\pi}\sigma} e^{\frac{-u^2}{2\sigma^2}} \tag{H.1}$$

The average, variance, skewness and kurtosis of u are related to the moments of p. However for both Gaussian and non-Gaussian statistics these quantities are defined below in the physical and spectral domain.

Average :

$$< u >= \frac{1}{N} \sum_{j=1}^{N} < u_j^2 >^{1/2} \tag{H.2}$$

When the velocity $u(x,t)$ is a zero-mean random process, the second moment is given by

Variance :

$$< u^2 >= \frac{1}{N} \sum_{j=1}^{N} (u_j)^2 = \sigma^2 \tag{H.3}$$

Standard deviation (σ) :

$$< u^2 >^{1/2} = \sqrt{\frac{1}{N} \sum_{j=1}^{N} (u_j)^2} \tag{H.4}$$

Skewness :

$$S_1 = \frac{1}{N} \sum_{j=1}^{N} \frac{(u_j)^3}{\sigma^3} \tag{H.5}$$

Flatness or Kurtosis :

$$F_1 = \frac{1}{N}\sum_{j=1}^{N}\frac{(u_j)^4}{\sigma^4} \tag{H.6}$$

Non-dimensional form of the moments and the PDF:

The zeroth moment of the power spectrum is $E(\tilde{k})$, where $\tilde{k}$ is the wavenumber. Since the non-dimensional form of $\tilde{k}$ is $\tilde{k}L = 2\pi k$ where k is an integer then the zeroth moment of $E(k)$ is given by

$$I_0 = \sum_{1}^{M} E(k) \tag{H.7}$$

and the second moment is

$$I_2 = \sum_{1}^{M} k^2 E(k) \tag{H.8}$$

Thus the variance $< U^2 >$, when u and x are non-dimensionalised with respect to u_{ref} and l_{ref} respectively is

$$< U^2 >= 2\pi I_0 \tag{H.9}$$

and

$$< \left(\frac{\partial U}{\partial X}\right)^2 >= (2\pi)^3 I_2 \tag{H.10}$$

The statistics of the derivatives of U are similarly defined. Thus for a variance of $< \left(\frac{\partial U}{\partial X}\right)^2 >$ the skewness is the found to be

$$S_2 = \frac{< \left(\frac{\partial U}{\partial X}\right)^3 >}{< \left(\frac{\partial U}{\partial X}\right)^2 >^{3/2}}. \tag{H.11}$$

and the flatness

$$F_2 = \frac{< \left(\frac{\partial U}{\partial X}\right)^4 >}{< \left(\frac{\partial U}{\partial X}\right)^2 >^2}. \tag{H.12}$$

The statistics of higher order derivatives are similarly defined. The joint probability density function of the two random variables U and $\frac{\partial U}{\partial X}$ is $p(U, \frac{\partial U}{\partial X})$ where

$$\int\int p\left(U, \frac{\partial U}{\partial X}\right) dU d\left(\frac{\partial U}{\partial X}\right) = 1. \tag{H.13}$$

If the variables of U and $\frac{\partial U}{\partial X}$ are statistically independent then

$$p\left(U, \frac{\partial U}{\partial X}\right) = p(U)p\left(\frac{\partial U}{\partial X}\right) \tag{H.14}$$

If $\dot{U} = \partial U/\partial X$ then

$$\frac{<\dot{U}^2>}{<U^2>} = \frac{\int_{-\infty}^{\infty} \dot{U}^2 p(\dot{U}) d\dot{U}}{\int_{-\infty}^{\infty} U^2 p(U) dU} = \frac{L^2}{\lambda^2} \tag{H.15}$$

where λ is the Taylor microscale. Thus λ is a function of the ratio of the pdf's of U and $\dot{U}$. The definition of λ arises from

$$\epsilon = \nu <\dot{U}>^2 = \nu \frac{U^2}{\lambda^2}$$

The number of zero crossings in a sample is related to the joint pdf. The number of zero crossings in a sample length of unity, when the statistics are Gaussian is given by Rice's(1945) formula

$$n_z = \sqrt{\frac{\sum_1^M k^2 E(k)}{\sum_1^M E(k)}}$$

and

$$\frac{\lambda}{L} = \sqrt{\frac{\sum_1^M E(\tilde{k})}{(2\pi)^2 \sum_1^M \tilde{k}^2 E(\tilde{k})}}.$$

Thus it is seen that n_z is inversely proportional to λ is clearly seen. The non-Gaussian form of the statistics of U and $\dot{U}$ is seen by the values of their skewness and flatness factors. These are S_1, S_2 and F_1, F_2 where in the case when the statistics are Gaussian $S_1 = S_2 = 0$ and $F_1 = F_2 = 3$. Hence the number of zero crossings and the Taylor microscale are dependent on S_1, S_2 and F_1, F_2. However a knowledge of the skewness and flatness alone cannot determine the joint PDF and the values of n_z or λ. As in the theory of turbulence, $<U>^2$, $<\dot{U}>^2$ and λ can be determined from the 2- point velocity correlation function.

When the distribution of U is given for $t = 0$ corresponding to a given spectrum and statistics, λ can be determined. For $t > 0$, λ initially decreases to a minimum near the average shock formation time which itself is related to λ at $t = 0$. Beyond the average shock formation time, where the wave degenerates into a series of random sawtooths λ^2 is found to increase proportional to t. Now $\left(\frac{\partial U}{\partial X}\right)_-$ is much greater than $\left(\frac{\partial U}{\partial X}\right)_+$ and near the shock formation time is nearly infinite. However as a result of the finite viscosity, the shocks are always of finite thickness and $\left(\frac{\partial U}{\partial X}\right)_-$ is also finite. Since

$$\lambda^2 = \frac{<U>^2}{<\dot{U}>^2}$$

the average thickness of the shocks is

$$\sqrt{\frac{<U>^2}{<\dot{U}>^2}} = \lambda.$$

But the number of shocks, n_z is also a function of λ as shown above and hence the distance, l, between shocks is also proportional to λ, although $l > \lambda$.

The average value of a function $F\left(U, \frac{\partial U}{\partial X}\right)$ is

$$\bar{F} = \int \int F\left(U, \frac{\partial U}{\partial X}\right) p\left(U, \frac{\partial U}{\partial X}\right) dU d\left(\frac{\partial U}{\partial X}\right) \tag{H.16}$$

where the integration is over all values of U and $\frac{\partial U}{\partial X}$. If the random process is Gaussian both $p(U)$ and $p(\frac{\partial U}{\partial X})$ are defined by equation H.1 and the integration of H.16 is simplified.

Appendix I

Estimating the Statistical properties of the Burgers Equation

Burgers Equation which is a one-dimensional quasi-linear parabolic equation is given by

$$\frac{\partial u}{\partial t} + u\frac{\partial u}{\partial x} = \nu\frac{\partial^2 u}{\partial x^2} \tag{I.1}$$

I.1 Estimation of the spatial average

The average with respect to x over the spatial domain 0 to L is

$$\frac{d}{dt}\int_0^L u dx + \int_0^L \frac{\partial u^2/2}{\partial x} dx = \nu \int_0^L \frac{\partial^2 u}{\partial x^2} dx \tag{I.2}$$

from which for periodic boundary conditions, the nonlinear term cancels and

$$\frac{d\overline{u}}{dt} = \nu[\frac{\partial u}{\partial x}(L) - \frac{\partial u}{\partial x}(0)] \tag{I.3}$$

where $\overline{u}$ is the average or the mean value and is given by

$$\overline{u} = \frac{1}{L}\int_0^L u dx$$

But if u is periodic then

$$\frac{\partial u}{\partial x}(L) = \frac{\partial u}{\partial x}(0) \tag{I.4}$$

and $\overline{u}$ = constent, independent of time. In the numerical experiments reported above $\bar{u} = 0$ at time $t = 0$ and is therefore zero for all time.

I.2 Estimation of the statistical properties for the inviscid BE

Equation I.1 reduces to the hyperbolic equation

$$\frac{\partial u}{\partial t} + u\frac{\partial u}{\partial x} = 0 \tag{I.5}$$

when $\nu = 0$. Multiplying equation I.5 by u and integrating with respect to x over the spatial domain 0 to L.

$$\frac{d}{dt}\int_0^L \frac{u^2}{2}dx + \int_0^L \frac{\partial u^3/3}{\partial x}dx = 0 \tag{I.6}$$

Under the periodic conditions $u(0,t) = u(l,t)$ the nonlinear term is zero. The remaining term is then

$$\frac{d}{dt}\int_0^L \frac{u^2}{2}dx = 0 \tag{I.7}$$

Integrating it

$$\overline{u^2} = \text{constant} \tag{I.8}$$

Integrating in a similar way for higher moments, which is obtained by multiplying the equation by u^2, u^3.....u^n and integrating the equation with respect to x gives

$$\overline{u^2},\ \overline{u^3}.....\overline{u^n} = \text{constant}.$$

Hence for the inviscid BE all moments, 0 to n do not change with time. When discontinuities such as shocks develop these relations no longer hold. The correct values can be obtained by including the viscous terms and finding the limiting values as $\nu \to 0$.

I.3 Estimation of the statistical properties for BE

Variance :

On multiplying equation I.1 by u and integrating with respect to x over the spatial domain 0 to l gives

$$\frac{d}{dt}\int_0^L \frac{u^2}{2}dx + \int_0^L \frac{\partial u^3/3}{\partial x}dx = \nu\int_0^L u\frac{\partial}{\partial x}\left(\frac{\partial u}{\partial x}\right)dx \tag{I.9}$$

Since the nonlinear term is zero for periodic boundary conditions equation I.9 becomes

$$\frac{d< u^2/2 >}{dt} = -\nu < \left(\frac{\partial u}{\partial x}\right)^2 > \tag{I.10}$$

[1] The Taylor microscale, λ defined in chapter 6 can be written as

$$\lambda^2 = \frac{< u^2 >}{< \left(\frac{\partial u}{\partial x}\right)^2 >}$$

Equation I.10 can be written as

$$\frac{d \ln < u^2 >}{dt} = -\frac{2\nu}{\lambda^2} \tag{I.11}$$

Skewness :

On multiplying the Burgers equation by u^2 and integrating with respect to x over the spatial domain 0 to L gives the 3rd moment equation

$$\frac{d}{dt}\int_0^L \frac{u^3}{3} dx + \int_0^L \frac{\partial u^4/4}{\partial x} dx = \nu \int_0^L u^2 \frac{\partial}{\partial x}\left(\frac{\partial u}{\partial x}\right) dx \tag{I.12}$$

Under periodic boundary conditions $u(0, L) = u(L, t)$ the nonlinear term is zero. Hence

$$\frac{d}{dt}\int_0^L \frac{u^3}{3} dx = \nu \left[u^2 \frac{\partial u}{\partial x}\right]_0^L - 2\nu \int_0^L u \left(\frac{\partial u}{\partial x}\right)^2 dx \tag{I.13}$$

which reduces to

$$\frac{d}{dt}\int_0^L \frac{u^3}{3} dx = -\frac{4\nu}{3}\int_0^L \left(\frac{\partial u^{3/2}}{\partial x}\right)^2 dx \tag{I.14}$$

or

$$\frac{d < u^3 >}{dt} = -4\nu \overline{\left(\frac{\partial u^{3/2}}{\partial x}\right)^2} \tag{I.15}$$

If the skewness of u is

$$S_1(t) = \frac{< u^3 >}{< u^2 >^{3/2}}$$

then it follows that

$$\frac{dS_1}{dt} + \frac{3S_1}{2}\frac{d \ln < u^2 >}{dt} = \frac{-4\nu < \left(\frac{\partial u^{3/2}}{\partial x}\right)^2 >}{< u^2 >^{3/2}} \tag{I.16}$$

[1] The corresponding relation in isotropic turbulence is different since turbulence is 3-dimensional and

$$\frac{d3 < u^2/2 >}{dt} = -15\nu < \left(\frac{\partial u}{\partial x}\right)^2 >$$

$$= \frac{-4\nu r_1}{\lambda^2} \tag{I.17}$$

where

$$r_1 = \frac{< \left(\frac{\partial u^{3/2}}{\partial x}\right)^2 >}{\sqrt{< u^2 >} < \left(\frac{\partial u}{\partial x}\right)^2 >}.$$

In Gaussian statistics $S_1 = 0$ and it is deduced from equation I.17 that $S(t)$ will change with time and the statistics will become non-Gaussian. The change in $< u^2 >$ with time determined from equation I.11 depends on the finite value of ν and similarly $S_1(t)$ in equation I.17 depends on the terms involving ν. The numerical work has determined the changes of $< u^2 >$ and S_1 with time. It is found S_1 changes rapidly from zero and quickly attains a value near -0.5. At later times its value only changes slightly. The changes in $S_1(t)$ are consistant with equation I.17. The general solution of equation I.17 can be written but its evaluation depends on the value of the correlation coefficients r_1 which has to be determined. It can be determined from the numerical data but the post processing has yet to be completed.

Flatness :

On multiplying the Burgers equation by u^3 and integrating with respect to x over the spatial domain 0 to L gives the 4th moment

$$\frac{d\overline{u}^4}{dt} = -12\nu u^2 < \left(\frac{\partial u^{3/2}}{\partial x}\right)^2 >= -3\nu < \left(\frac{\partial u^2}{\partial x}\right)^2 > \tag{I.18}$$

Let $F_1(t)$ be the flatness of the random variable, u, where

$$F_1(t) = \frac{< u^4 >}{< u^2 >^2}$$

then it follows that

$$\frac{dF_1}{dt} + 2F_1 \frac{d \ln < u^2 >}{dt} = \frac{3\nu r_2}{\lambda^2} \tag{I.19}$$

where

$$r_2 = \frac{< \left(\frac{\partial u^2}{\partial x}\right)^2 >}{< u^2 >< \left(\frac{\partial u}{\partial x}\right)^2 >}$$

For a Gaussian process at $t = 0$, $F_1(0) = 3$. From equation I.19 as well as I.17 it is seen that at time $t > 0$ the process becomes non-Gaussian with skewness and flatness different from the value of 0 and 3 respectively at $t = 0$. The numerical work has determined the changes of F_1 with time, and its values are consistant with solutions to the differential equations for $F_1(t)$ given by equation I.19.

The values of S_2 and F_2, which are respectively the skewness and flatness for the derivatives of u with respect to x, show far greater deviations from their Gaussian values than S_1 and F_1. The values of S_2 and F_2 have been obtained in the present numerical solutions of Burgers equation.

Appendix J

Derivation of the rate of dissipation

The rate of dissipation can be derived from the energy equation. Now Burgers equation is

$$\frac{\partial u}{\partial t} + u\frac{\partial u}{\partial x} = \nu_e \frac{\partial^2 u}{\partial x^2} \tag{J.1}$$

, where ν_e is the effective kinematic viscosity, and the energy equation is found by multiplying each term of J.1 by u and integrating with respect to x over the spatial domain 0 to L. It is found

$$\frac{d}{dt}\int_0^L \frac{u^2}{2}dx + \int_0^L \frac{\partial u^3/3}{\partial x}dx = \nu_e \int_0^L \frac{\partial^2 u^2/2}{\partial x^2}dx - \nu_e \int_0^L (\frac{\partial u}{\partial x})^2 dx \tag{J.2}$$

With the periodic boundary conditions at $x = 0$ and $x = L$ the nonlinear and viscous diffusion terms vanish, and the remaining terms are

$$\frac{d}{dt}\int_0^L \frac{u^2}{2}dx = -\nu_e \int_0^L \left(\frac{\partial u}{\partial x}\right)^2 dx \tag{J.3}$$

so if the kinetic energy,

$$K = \frac{1}{L}\int_0^L \frac{u^2}{2}dX = \frac{< u^2 >}{2}$$

$$\frac{dK}{dt} = -\epsilon \tag{J.4}$$

where ϵ is the rate of dissipation

$$\epsilon = \nu_e < \left(\frac{\partial u}{\partial x}\right)^2 > .$$

Since the energy spectrum function is $E(\tilde{k})$, where $\tilde{k}$ is the wavenumber, it is found that

$$< u^2 >= \int_0^\infty E(\tilde{k})d\tilde{k}$$

and

$$\frac{d}{dt}\int_0^\infty E(\tilde{k})d\tilde{k} = -2\nu_e\int_0^\infty \tilde{k}^2 E(\tilde{k})d\tilde{k} \tag{J.5}$$

where the total kinetic energy [1]

$$K(t) = \frac{1}{2}\int_0^\infty E(\tilde{k})d\tilde{k}.$$

The rate of dissipation, ϵ, is

$$\epsilon = -\frac{dK}{dt} = \nu_e\int_0^L (\frac{\partial u}{\partial x})^2 dx = 2\nu_e\int_0^\infty \tilde{k}^2 E(\tilde{k})d\tilde{k}. \tag{J.6}$$

In the solution of Burgers equation the initial energy is defined in terms of $< u^2(0) >$ and the initial rate of dissipation, $\epsilon = \nu_e < \left(\frac{\partial u}{\partial x}(0)\right)^2 >$. An initial Taylor microscale is also defined as

$$\lambda(0) = \frac{< u^2(0) >^{1/2}}{< \left(\frac{\partial u}{\partial x}(0)\right)^2 >^{1/2}}.$$

All initial values $< u^2(0) >$, $\lambda(0)$, and $< \left(\frac{\partial u}{\partial x}(0)\right)^2 >$ change rapidly with time $t > 0$ due to nonlinear distortion and correspond to the changes as the process becomes more non-Gaussian.

[1] In the theory of turbulence it is usual to define $E(\tilde{k})$ so that $K(t) = \int_0^\infty E(\tilde{k})d\tilde{k}$.

Appendix K

Derivation of the decay law for the shock strength

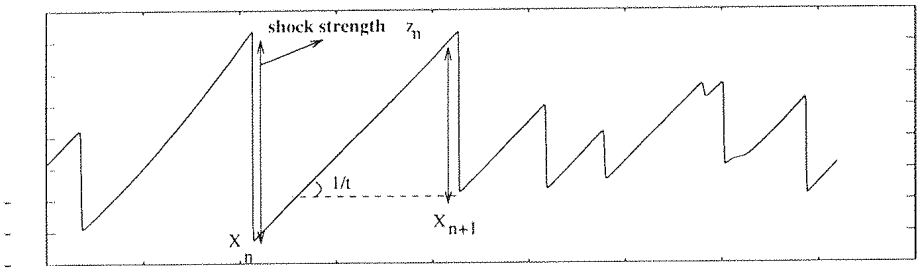

Figure K.1: A series of randomly spaced sawtooths.

It is illustrated in figure K.1 a series of randomly located sawtooth waves at a given time as obtained from one of the present numerical experiments. Following Lighthill(1994) the shock strength z_n at X_n is defined as the difference in the particle velocities ahead of and behind it. z_n is a positive quantity. Let X_n and X_{n+1} be the coordinates of the n^{th} and the $(n+1)^{th}$ shock respectively. Thus if v_n is the particle velocity at X_n and downstream of the shock,

$$v_{n-1} + \left(\frac{X_n - X_{n-1}}{t}\right) = v_n + z_n \tag{K.1}$$

and

$$v_n + \left(\frac{X_{n+1} - X_n}{t}\right) = v_{n+1} + z_{n+1} \tag{K.2}$$

It is assumed a large number of shocks exist over a length L and the distribution is periodic with L the periodic length. Then with periodic boundary conditions at $x = 0$ and $x = L$

, the sums of v_n over $n = 1$ to N vanish, and since

$$\sum_{n=1}^{N}(X_n - X_{n-1}) = L \tag{K.3}$$

it is found

$$\sum_{n=1}^{N(t)} z_n = \frac{L}{t} \tag{K.4}$$

as obtained by Lighthill, and where $N(t)$ the number of shocks in the period is a function of time. Thus

$$\frac{1}{N}\sum_{n=1}^{N} z_n =< z >= \frac{L}{N(t)t} \tag{K.5}$$

where $< z >$ is the average strength of the shock waves in the assemblage at time t. It appears that on average each shock decreases in strength as $1/t$, but this result can only hold when $N(t)$ is a constant. However due to the phenomenon of 'bunching' the number of shocks in the period $x = 0$ to $x = L$ decreases with time. It is found that $N \sim 1/\sqrt{t}$ for times large compared with the shock formation time so that on average

$$< z >\sim \frac{1}{\sqrt{t}} \tag{K.6}$$

and not proportional to $1/t$. Lighthill(1994) obtained a similar shock strength dependence on time using a different argument. Lighthill also found this law in a simple numerical experiment and this was further confirmed in the more detailed present numerical studies.

The $1/\sqrt{t}$ law obtained in equation K.6 only exists when a large number of shocks of random strength exist in a period. In the special case of an assemblage of equispaced sawtooths all of the same strength their number is invariant with time and their strength decays as $1/t$ since $N(t)$ is now a constant. The $1/\sqrt{t}$ law for plane waves also exists for the nonperiodic or isolated wavetrain, where the dominant example is that of the sonic boom plane wave propagation. In this case the phenomenon of 'bunching' also exists but is not so marked since the number of shocks of different strengths in the initial sample is small. Nevertheless the number of shocks decrease in time as the stronger engulf the weaker shocks although in this case the distance between the ends of the distribution increases with time. The $1/\sqrt{t}$ rule in this example of the propagation of an isolated shock wave train is easily established using the Lighthill-Whitham 'equal area rule'.

Appendix L

Shock formation time for the sine wave

Let the initial velocity distribution at $t = 0$ equal

$$u(x, 0) = A_1 \sin(k_0 x)$$

where A_1 is the maximum amplitude of the sine wave and k_0 is the discrete wavenumber. Then noting

$$\frac{\partial u}{\partial x} = k_0 A_0 \cos(k_0 x)$$
$$\left(\frac{\partial u}{\partial x}\right)_{\max} = k_0 A_0,$$

in the profile at $t = 0$. But the shock formation time is given by

$$t_s = \left| -\frac{1}{\left(\frac{\partial u(x,0)}{\partial x}\right)} \right|_{\min}$$

for the sine wave

$$t_s = \frac{1}{k_0 A_0} \tag{L.1}$$

In the random wave distribution $< \left(\frac{\partial u(0)}{\partial x}\right)^2 >$ is dominated by its peak values of $\frac{\partial u}{\partial x}$ positive or negative. In such cases an average shock formation time is defined as

$$\bar{t_s} = \frac{1}{< \left(\frac{\partial u(0)}{\partial x}\right)^2 >^{1/2}} = \frac{\lambda(0)}{< u_0^2 >^{1/2}} \tag{L.2}$$

where $\lambda(0)$ is the Taylor microscale at $t = 0$. Ofcourse $\bar{t_s} > t_s$ and for a sine wave

$$\bar{t_s} = \sqrt{2} t_s \tag{L.3}$$

Thus the shock formation time based on the Taylor microscale is $\sqrt{2}$ times the shock formation time based on the maximum amplitude of $\frac{\partial u}{\partial x}$ in the profile at $t = 0$.

Appendix M

Energy dependence on the peak wavenumber

Let k_p be the integer wavenumber corresponding to the peak and k_T be the truncation integer wavenumber for the energy spectrum of test case 1 defined in chapter 7, figure 6.3. a and b are constants used to define the non-dimensional energy spectrum as used in the numerical method. Thus the zeroth moment I_0, which is proportional to the total energy, is

$$I_0 = \int_0^\infty E(k)dk = \int_0^{k_p} ak^2 dk + \int_{k_p}^{k_T} \frac{b}{k^2} dk \tag{M.1}$$

where $b/a = k_p^4$. After integration it is found therefore for test case 1 described in chapter 6

$$I_0 = a\left(\frac{k_p^3}{3} + k_p^3 - \frac{k_p^4}{k_T}\right) \tag{M.2}$$

Thus when $a = 1$,

$$I_0 = \int_0^\infty E(k)dk = a\frac{4k_p^3}{3}\left(1 - \frac{3k_p}{4k_T}\right) \tag{M.3}$$

Thus from equation M.3, I_0 is equal to $4k_p^3/3$ when $k_p << k_T$, and $a = 1$.

The second moment I_2 is

$$I_2 = \int_0^\infty k^2 E(k)dk = \int_0^{k_p} ak^4 dk + \int_{k_p}^{k_T} bdk \tag{M.4}$$

and after integration

$$I_2 = ak_p^4 k_T\left(1 - \frac{4k_p}{5k_T}\right) \tag{M.5}$$

giving $I_2 = ak_p^4 k_T$ when $k_p << k_T$ and $a = 1$. It is also noted that as $k_T \to \infty$ so $I_2 \to \infty$ also. The rate of dissipation, ϵ, is proportional to $\nu_e I_2$ and hence as $k_T \to \infty$ for finite ν_e so $\epsilon \to \infty$. This is usually referred to as entropy catastrophe.

The result for I_0 and I_2 have been obtained from integral transforms. In the numerical method I_0 and I_2 have been evaluated using discrete transforms. The differences between these results have been checked and found to be small.

In chapter 6 it is found that the Taylor microscale, λ, can be obtained from

$$\lambda^2/L^2 = \frac{1}{(2\pi)^2} \frac{\int_0^\infty E(k)dk}{\int_0^\infty k^2 E(k)dk} = \frac{I_0}{(2\pi)^2 I_2} \tag{M.6}$$

Thus on substitution of I_0 and I_2 from equation M.3 and M.5

$$\frac{\lambda}{L} = \sqrt{\frac{4}{(2\pi)^2 3 k_T k_p} \frac{\left(1 - \frac{3k_p}{4k_T}\right)}{\left(1 - \frac{4k_p}{5k_T}\right)}} \tag{M.7}$$

It is seen from this relation between the Taylor microscale and the peak wavenumber given in equation M.7, that as the truncation wavenumber is increased so the Taylor microscale is decreased. For a given ratio of k_p/k_T, the Taylor microscale is inversely proportional to the peak wavenumber. The rate of dissipation, ϵ, is proportional to $\nu_e I_2$ and hence increases with increase in k_T.

Appendix N

Derivation of the non-dimensional parameters derived from the energy equation

The energy equation derived from the non-dimensional form of Burgers equation is [see equation I.10]

$$\frac{d < U^2 >}{dT} = -\frac{1}{R} < \left(\frac{\partial U}{\partial X}\right)^2 > . \tag{N.1}$$

where $U = u/u_{ref}$ is the non-dimensional velocity, $X = x/l_{ref}$, $T = tu_{ref}/l_{ref}$, and $R = u_{ref}l_{ref}/\nu_e$ is the reference Reynolds number. The definition of the Taylor microscale, λ, as given in equation 6.1 in chapter 6 is

$$\frac{\lambda}{L} = \sqrt{\frac{\int_0^\infty E(\tilde{k})d\tilde{k}}{\int_0^\infty \tilde{k}^2 E(\tilde{k})d\tilde{k}}} = \frac{< U^2 >^{1/2}}{< \left(\frac{\partial U}{\partial X}\right)^2 >^{1/2}}.$$

where the nondimensional wavenumber $\tilde{k} = 2\pi k$ where k is an integer, and hence

$$\lambda = \frac{L}{2\pi}\sqrt{\frac{I_0}{I_2}} \tag{N.2}$$

where I_0 and I_2 are the zeroth and the second moment of the power spectral density $E(k)$ respectively defined in Appendix H. The value of λ at $T = 0$,

$$\lambda(0) = \frac{L}{2\pi}\sqrt{\frac{I_0(0)}{I_2(0)}} \tag{N.3}$$

The Taylor microscale Reynolds number R_T at $t = 0$, with $< u^2(0) >=< u_0^2 >$,

$$R_T(0) = \frac{< u_0^2 >^{\frac{1}{2}} \lambda(0)}{\nu_e}. \tag{N.4}$$

At any time t

$$R_T(t) = \frac{< u^2 >^{1/2} \lambda(t)}{\nu_e}. \tag{N.5}$$

It is then possible to define other Reynolds numbers. These include

$$R_p = \frac{< u_0^2 >^{\frac{1}{2}} l_p}{\nu_e} \tag{N.6}$$

based on $< u^2(0) >^{1/2}$ and l_p, the wavelength corresponding to k_p, and

$$R_L = \frac{< u_0^2 >^{\frac{1}{2}} L}{\nu_e}, \tag{N.7}$$

based on the periodic length L, and both R_p and R_L are evaluated at $t = 0$ only. At any time T the energy equation reduces to

$$\frac{d \ln < U^2 >}{dT} = -\frac{1}{R_L} \frac{1}{\lambda^2/L^2}. \tag{N.8}$$

showing when $< U^2 > \sim 1/T$ then

$$\frac{\lambda}{L} = \frac{\sqrt{T}}{\sqrt{R}}. \tag{N.9}$$

The value of $R_T(T)$ can now be found from equation N.5 giving

$$R_T(T) = \frac{< u_0^2 >^{1/2} \lambda}{\nu_e} = \text{constant}. \tag{N.10}$$

Thus R_T remains constant during the decay for times $T >> T_S$. The constant value of R_T in the decay is not equal to R_T at $T = 0$ although it will be of similar magnitude. Thus R_T is an important characteristic parameter in the present study defining the relative importance of nonlinear steepening to viscous broadening.

For $T = 0$

$$< U_0^2 >= \frac{< u_0^2 >}{u_{ref}^2} \tag{N.11}$$

so

$$< u_0^2 >^{1/2} = u_{ref} < U_0^2 >^{1/2} = u_{ref} \sqrt{I_0(0)} \tag{N.12}$$

where $u_{ref} = R\nu_e/l_{ref}$. Also

$$< U^2 >^{1/2} = 2\pi \sum_{k=1}^{M} E(k) = 2\pi I_0 \tag{N.13}$$

and similarly

$$< \frac{\partial U}{\partial X} >^{1/2} = (2\pi)^{3/2} \sqrt{I_2} \tag{N.14}$$

with

$$\epsilon = \frac{1}{R} < \left(\frac{\partial U}{\partial X} \right)^2 >= \frac{< U^2 >}{R(\lambda/L)^2} \tag{N.15}$$

$$= \frac{(2\pi)^3}{R} \sum_{k=1}^{M} k^2 E(k) = \frac{(2\pi)^3}{R} I_2 \tag{N.16}$$

Hence,

$$\frac{\lambda^2}{L^2} = \frac{< U^2 >}{< \frac{\partial U}{\partial X} >^2}$$

and

$$\frac{\lambda}{L} = \frac{1}{2\pi} \sqrt{\frac{I_0}{I_2}}$$

as given above. The non-dimensional shock formation time is given by

$$T_s = \min \left| -\frac{1}{\frac{\partial U}{\partial X}} \right|$$

But for the random distribution at $T = 0$ typical of a high Reynolds number, the maximum value of $\partial U/\partial X$ are of same order as their average value and as discussed previously it can be assumed that for a random signal

$$\bar{T}_s = \frac{1}{< \left(\frac{\partial U}{\partial X} \right)^2_{t=0} >^{\frac{1}{2}}}$$

where $\bar{T}_s$ is the average shock formation time. But

$$< \left(\frac{\partial U}{\partial X} \right)^2 >= \int_0^\infty \tilde{k}^2 E(\tilde{k}) d\tilde{k}$$

$$= (2\pi)^3 I_2$$

so

$$\bar{T}_s = \frac{1}{(2\pi)^{3/2} \sqrt{I_2}}. \tag{N.17}$$

Now at $T = 0$

$$\frac{< U^2(0) >}{\lambda^2(0)/L^2} = \int_0^\infty \tilde{k}^2 E(\tilde{k}) d\tilde{k} = (2\pi)^3 \int_0^\infty k^2 E(k) dk$$

so

$$2\pi I_0(0) = (2\pi)^3 \frac{\lambda^2(0)}{L^2} I_2(0) \tag{N.18}$$

or

$$\sqrt{I_0(0)} = (2\pi) \frac{\lambda(0)}{L} \sqrt{I_2(0)} \tag{N.19}$$

and from equations N.17 and N.19 the average shock formation time is given by

$$\bar{T}_s = \frac{\lambda(0)/L}{\sqrt{I_0(0)} \sqrt{2\pi}}$$

showing the relation between λ/L and the non-dimensional shock formation time. The average dimensional shock formation time is

$$\bar{t}_s = \bar{T}_s \frac{l_{ref}}{u_{ref}} \tag{N.20}$$

where

$$\bar{T}_s = \frac{\lambda(0)/L}{< U_0^2 >^{1/2}} \tag{N.21}$$

The theoretical shock formation time is obtained strictly from inviscid calculations and is therefore independent of the Reynolds number. Equation N.17 gives a statistical or average value of the shock formation time, and is used for the present numerical calculations involving finite but large values of R, and including the cases where the shocks are of finite thickness.

Appendix O

Relation between R, R_p, R_T

In chapter 6 the Taylor microscale, λ, has been defined by

$$\lambda/L = \frac{1}{2\pi}\sqrt{\frac{\int_0^\infty E(k)dk}{\int_0^\infty k^2 E(k)dk}} = \frac{1}{2\pi}\frac{\sqrt{I_0}}{\sqrt{I_2}}$$

noting that the wavenumber $\tilde{k} = 2\pi k/L$. In the initial distribution $E(k)$ is specified and hence the value of λ/L at $T = 0$ can be determined. It is not a function of the Reynolds number. However it defines the initial rate of dissipation. Hence the Reynolds number based on the Taylor microscale at $T = 0$ is important in defining the relative importance of nonlinear distortion to viscous broadening as discussed previously.

The relation between the Reynolds numbers, R_p based on the wavelength, l_p, corresponding to the peak integer wavenumber, k_p, and the Taylor microscale Reynolds numbers, R_λ, based on the Taylor microscale λ is determined as follows. The rate of dissipation, ϵ, as defined in chapter 6, is given by

$$\epsilon = -\frac{dK}{dt} = \nu\int_0^L (\frac{\partial u}{\partial x})^2 dx = 2\nu\int_0^\infty \tilde{k}^2 E(\tilde{k})dk.$$

Dimensionally it is also proportional to $u_0^3/l_p$where the constant of proportionality is order unity. If this constant is equal to unity then

$$\nu_e\frac{u_0^2}{\lambda^2} = \frac{u_0^3}{l_p} \tag{O.1}$$

then

$$\frac{u_0 l_p}{\nu_e} = \left(\frac{l_p^2}{\lambda^2}\right) \tag{O.2}$$

Alternatively it can be written

$$\frac{u_0\lambda}{\nu_e} = \frac{l_p}{\lambda} = \sqrt{\frac{u_0 l_p}{\nu_e}} \tag{O.3}$$

Thus the Taylor microscale Reynolds number, $R_T(0) = \sqrt{R_p(0)}$, where $R_T(0) = \frac{u_0\lambda}{\nu_e}$. The relation between $R_T(t)$ and R, the Reynolds number used in the computations is as follows. From the definitions above

$$R_T = \frac{< u^2 >^{1/2} \lambda}{\nu_e} = \frac{u_{ref} l_{ref}}{\nu_e} = \frac{< U^2 >^{1/2} \lambda}{L}$$

since $l_{ref} = L$. Thus

$$R_T = R < U^2 >^{1/2} \frac{\lambda}{L}$$

$$= R \times \text{constant}$$

for $T > \bar{T}_s$, and hence the reference Reynolds number, R, used in the computations is directly proportional to R_T, which for $T > \bar{T}_s$ is a constant.